

# BUCKLING AND DYNAMIC BEHAVIOR OF NON-UNIFORMLY HEATED CYLINDRICAL PANELS

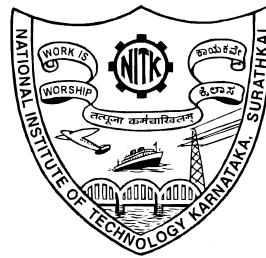
Thesis

Submitted in partial fulfillment of the requirements for the degree  
of

DOCTOR OF PHILOSOPHY

by

VINOD BHAGAT



DEPARTMENT OF MECHANICAL ENGINEERING  
NATIONAL INSTITUTE OF TECHNOLOGY  
KARNATAKA SURATHKAL, MANGALORE - 575025,  
INDIA

April, 2017



## DECLARATION

I hereby *declare* that the Research Thesis entitled **BUCKLING AND DYNAMIC BEHAVIOR OF NON-UNIFORMLY HEATED CYLINDRICAL PANELS** which is being submitted to the *National Institute of Technology Karnataka, Surathkal* in partial fulfillment of the requirements for the award of the Degree of *Doctor of Philosophy* is a *bonafide report of the research work carried out by me*. The material contained in this Thesis has not been submitted to any University or Institution for the award of any degree.

**Vinod Bhagat**  
Registration No.: 145071  
Dept. of Mechanical Engg.

Place: NITK - Surathkal

Date: 10-04-2017





## CERTIFICATE

This is to *certify* that the Research Thesis entitled **BUCKLING AND DYNAMIC BEHAVIOR OF NON-UNIFORMLY HEATED CYLINDRICAL PANELS**, submitted by **Vinod Bhagat** (Registration No.: 145071) as the record of the research work carried out by him, is *accepted* as the *Research Thesis submission* in partial fulfillment of the requirements for the award of degree of *Doctor of Philosophy*.

**Dr. P. Jeyaraj**  
Research Guide  
Assistant Professor  
Dept. of Mechanical Engg.  
NITK Surathkal - 575025

**Dr. S. M. Murigendrappa**  
Research Guide  
Associate Professor  
Dept. of Mechanical Engg.  
NITK Surathkal - 575025

**Chairman - DRPC**  
(Signature with Date and Seal)



## ACKNOWLEDGEMENTS

I express my sincere gratitude, regards and thanks to my research supervisors Dr. P. Jeyaraj, Assistant Professor and Dr. S. M. Murigendrappa, Associate Professor, Department of Mechanical Engineering, National Institute of Technology Karnataka, Surathkal, Mangalore, for their excellent guidance, invaluable suggestions and generous help at all the stages of my research work. It has been a privilege to have worked with them. I'm sure without their guidance this work would not have taken this final shape. Their interest and confidence in me was the reason for all the success I have made.

I sincerely thanks to the RPAC members, Dr. N. Gnanasekaran, Department of Mechanical Engineering and Dr. K. Vadivuzhezhian, Department of Applied Mechanics and Hydraulics for providing valuable suggestion and support extended to me on all occasion.

I wish to express my sincere thanks to Prof. K. V. Gangadharan, Department of Mechanical Engineering, National Institute of Technology Karnataka, Surathkal, Mangalore for his kind help in providing the facilities. I also thank Prof. Narendranath S, Head of Department, Department of Mechanical Engineering, National Institute of Technology Karnataka, Surathkal, Mangalore for his kind support.

The unfailing support of my colleagues had provided brilliant ideas, everlasting optimism and assistance. I would like to thank my friends Nivish, Karthik, Arun, Rajesh, Sunil and Shushanth for their selfless advice, assistance and contribution in this work.

I thank Almighty God for giving me the confidence and presence of mind throughout this endeavor and completing this work without any problem.

Lastly, I would like to immensely thank my parents, sisters and relatives, for their undying love, encouragement and support throughout my life and education. Without them and their blessings, achieving this goal would not have been possible.

(Vinod Bhagat)



# ABSTRACT

Today, curved panels especially cylindrical and conical are considered as a backbone of numerous engineering structures. Knowledge of buckling and dynamic behavior of structures over a range of temperature is essential for their better design. Most of the studies carried out on heated panels are based on uniform temperature distribution assumption. However, in real life application, the cylindrical panels employed in structures are exposed to non-uniform temperature variation due to the location of the heating source and thermal boundary conditions. In the present study, the thermal buckling strength of the non-uniformly heated metallic panel predicted numerically is validated experimentally using in-house developed experimental set-up. Further studies are extended to investigate the effect of non-uniform temperature variation on buckling strength and free vibration characteristics of metallic, laminated composite, and functionally graded carbon nanotube (FGCNT) reinforced polymer composite, cylindrical panels using the finite element method. Finally, the optimization of a non-uniformly heated laminated cylindrical panel against thermal buckling strength and fundamental natural frequency is also carried out.

Typical variation of temperature-deflection plot for different temperature fields is obtained experimentally and further, inflection point method is used to predict the critical buckling temperature from temperature-deflection plot. Experimental studies are further extended to analyze the influence of geometrical parameters and structural boundary constraints on critical buckling temperature. Experimentation results reveal that the location of the heat source and resulting non-uniform

temperature field influences the thermal buckling strength significantly. Among three cases examined in experimentation for the position of heat source, minimal buckling strength is observed when the heater is located at the center of the panel while maximum buckling strength is observed when the heater is located at the forefront curved edge. It is also found that aspect ratio and structural boundary constraints play a major role in deciding the buckling strength of the panel.

From the numerical studies carried out on non-uniformly heated panels, a relation known as magnification factor is established to evaluate the buckling strength of non-uniformly heated cylindrical panels knowing the buckling strength of uniformly heated panels. Among five cases investigated for the position of heat source, the highest magnification factor is observed for a panel with the heat source located at the forefront curved edge. It is observed that the free vibration mode shapes of the panel change significantly with increase in elevated temperature. The changes are observed in terms switching of modes with a significant change in modal indices. With the rise in temperature, nodal and anti-nodal positions of a particular free vibration mode shape are shifting towards the location where the intensity of the heat source is high and structural stiffness is low.

It is found that for a stiffer panel, the buckling strength of the laminated and FG-CNT composite panels with temperature-dependent elastic properties is significantly lesser than that of the panels with temperature independent elastic properties. Panel with maximum area exposed to a peak temperature of particular non-uniform temperature fields shows lowest buckling strength. Functional grading of CNTs with more amount of CNTs located close to top and bottom of the panel (FG-X) results in higher buckling strength and free vibration frequencies compared to those panel with maximum CNTs distribution near the mid-plane. Free vibration frequencies of non-uniformly heated FG-CNT panel with temperature dependent properties is observed to decrease drastically with elevated temperature compared to the panel with temperature independent properties. Variation

in frequencies observed in a pre-stressed panel with temperature dependent and independent properties is more significant in stiffer panels. Irrespective of temperature dependent and independent properties, shifting of nodal and anti-nodal lines and change of modal indices are also observed at elevated temperature.

Well-known and generally acknowledged optimization technique, particle swarm optimization is employed for the optimization of thermal buckling strength of laminated composite panels exposed to five different temperature fields. Two different optimization approach like single objective optimization approach and multi-objective optimization approach are employed. In single objective optimization, the panel is exposed known temperature field whereas, in multi-objective optimization, the panel is exposed to unknown temperature fields when in-service. It is found from the analysis that the variation in the optimum buckling strength of non-uniformly heated panels is more significant at lower curvature ratio. Whereas, variation in the optimum fiber orientation under different temperature fields is significant at higher curvature ratio. Multi-objective optimization approach has proved to be superior to that of single objective optimization approach when panels are exposed to the unpredictable thermal environment.

Further, studies are carried out on optimization of both thermal buckling strength and fundamental free vibration frequency of heated panels using particle swarm optimization in conjunction with the artificial neural network. Multi-objective design index (MODI) has been derived for the panel considering buckling strength and fundamental frequency as objectives for optimization. It is found that MODI of the cylindrical panels under thermal load is complex and significantly influenced by the temperature fields, lamination scheme, in-plane boundary constraints, elevated temperature and geometric parameters. It is also observed that the MODI of the panel can be maximized by optimizing laminate orientations. Further, it is observed that panel with lamination scheme of  $(\theta^\circ / -\theta^\circ / \theta^\circ / -\theta^\circ)_S$  gives higher value of MODI compared to other lamination schemes considered.

KEYWORDS: Non-uniform temperature, Thermal buckling, Free vibration,  
Finite element method, Particle swarm optimization, Artificial  
neural network





# TABLE OF CONTENTS

<b>ACKNOWLEDGEMENTS</b>	<b>ii</b>
<b>ABSTRACT</b>	<b>iv</b>
<b>LIST OF TABLES</b>	<b>xv</b>
<b>LIST OF FIGURES</b>	<b>xix</b>
<b>1 INTRODUCTION AND LITERATURE REVIEW</b>	<b>1</b>
1.1 Introduction . . . . .	1
1.2 Literature Review . . . . .	5
1.2.1 Thermal buckling . . . . .	5
1.2.2 Free vibration . . . . .	11
1.2.3 Free vibration under thermal load . . . . .	16
1.2.4 Optimization of thermal buckling and free vibration . . . . .	19
1.3 Closure . . . . .	22
1.4 Objective and Scope of study . . . . .	24
<b>2 METHODOLOGY</b>	<b>28</b>
2.1 Experimental investigation . . . . .	28
2.1.1 Working of experimental setup . . . . .	33
2.2 Numerical investigation on an isotropic panel . . . . .	35
2.3 Numerical Investigation on laminated panel with and without temperature dependent elastic properties . . . . .	43
2.3.1 Finite element formulation . . . . .	43

2.4	Optimization of buckling temperature and fundamental natural frequency . . . . .	52
2.4.1	Single objective optimization . . . . .	52
2.4.2	Multi-objective optimization . . . . .	55
2.5	Closure . . . . .	57
<b>3</b>	<b>EXPERIMENTAL INVESTIGATION</b>	<b>58</b>
3.1	Geometry of the cylindrical panel analyzed . . . . .	58
3.2	Structural boundary constraints . . . . .	59
3.3	Non-uniform temperature profiles . . . . .	59
3.4	Inflection point method . . . . .	60
3.4.1	Repeatability test of experiments . . . . .	61
3.5	Comparison of experimental and numerical results . . . . .	62
3.6	Closure . . . . .	71
<b>4</b>	<b>STUDY OF CYLINDRICAL PANEL WITH TEMPERATURE INDEPENDENT PROPERTIES</b>	<b>72</b>
4.1	Introduction . . . . .	72
4.2	Variation of temperature fields . . . . .	72
4.3	Structural boundary constraints . . . . .	73
4.4	Case study-I: Isotropic cylindrical panel . . . . .	76
4.4.1	Validation . . . . .	76
4.4.2	Results and discussion . . . . .	77
4.5	Case study-II: Laminated composite cylindrical panel . . . . .	91
4.5.1	Validation . . . . .	93
4.5.2	Results and discussion . . . . .	94
4.6	Closure . . . . .	109
<b>5</b>	<b>STUDY ON CYLINDRICAL PANEL WITH TEMPERATURE DEPENDENT PROPERTIES</b>	<b>110</b>
5.1	Introduction . . . . .	110

5.2	Variation of temperature fields . . . . .	110
5.3	Case study-I: Laminated composite cylindrical panel . . . . .	111
5.3.1	Results and discussion . . . . .	112
5.4	Case study-II: Functionally graded carbon nano-tubes reinforced composites cylindrical panel . . . . .	123
5.4.1	Validation Studies . . . . .	125
5.4.2	Results and discussion . . . . .	126
5.5	Closure . . . . .	143
<b>6</b>	<b>OPTIMIZATION STUDIES</b>	<b>148</b>
6.1	Introduction . . . . .	148
6.2	Optimization studies on buckling strength . . . . .	149
6.2.1	Problem Formulation . . . . .	149
6.2.2	Validation of optimum thermal buckling strength . . . . .	151
6.2.3	Results and discussion . . . . .	151
6.3	Optimization studies on buckling strength and fundamental fre- quency . . . . .	162
6.3.1	Problem formulation . . . . .	163
6.3.2	Results and discussion . . . . .	164
6.4	Closure . . . . .	172
<b>7</b>	<b>SUMMARY AND CONCLUSIONS</b>	<b>174</b>
7.1	Summary . . . . .	174
7.2	Conclusions . . . . .	175
7.3	Scope for future research . . . . .	178

## LIST OF TABLES

3.1	Adjustable small segment positions to simulate boundary constraints.	59
3.2	IR heater positions to simulate different temperature fields. . . .	60
3.3	Variation of temperature fields in a cylindrical panel computed using numerical approach. . . . .	61
3.4	Critical buckling temperature of panel-1 obtained from different set of experiments . . . . .	62
3.5	Comparison of critical buckling temperature, °C obtained experimentally and numerically . . . . .	67
3.6	Influence of aspect ratio on critical buckling temperature, °C .	68
3.7	Influence of boundary constraints on critical buckling temperature, °C of panel-2 . . . . .	71
4.1	Cylindrical panel with location of heat source . . . . .	74
4.2	Cylindrical panel with different structural boundary constraints.	75
4.3	Comparison of natural frequencies with Au and Cheung (1996) .	77
4.4	Magnification factor of first kind for CCCC isotropic panel . . .	79
4.5	Magnification factor of first kind for CCFC isotropic panel . . .	80
4.6	Magnification factor of second kind for SSSS isotropic panel . .	81
4.7	Effect of thickness ratio on fundamental buckling mode shape of CCCC isotropic panel . . . . .	86
4.8	Effect of thickness ratio on fundamental buckling mode shape of CCFC isotropic panel . . . . .	86
4.9	Effect of curvature ratio on fundamental buckling mode shape of CCCC isotropic panel . . . . .	87
4.10	Effect of curvature ratio on fundamental buckling mode shape of CCFC isotropic panel . . . . .	87
4.11	Effect of temperature fields on free vibration frequencies (Hz) of isotropic panel . . . . .	88

4.12	Effect of thermal load on free vibration frequency (Hz) and associated modal indices of an isotropic panel . . . . .	90
4.13	Effect of thermal load on the free vibration mode shapes of an isotropic panel . . . . .	92
4.14	Comparison of critical buckling temperature with Katariya and Panda (2016 <i>a</i> ) . . . . .	93
4.15	Magnification factor of first kind for CCCC laminated panel . . . . .	96
4.16	Magnification factor of first kind for CCFC laminated panel . . . . .	96
4.17	Effect of thickness ratio on fundamental buckling mode shape of CCCC laminated panel . . . . .	100
4.18	Effect of thickness ratio on fundamental buckling mode shape of CCFC laminated panel . . . . .	101
4.19	Effect of curvature ratio on fundamental buckling mode shape of CCCC laminated panel . . . . .	102
4.20	Effect of curvature ratio on fundamental buckling mode shape of CCFC laminated panel . . . . .	102
4.21	Effect of boundary constraints and temperature fields on the buckling temperature of laminated panel . . . . .	104
4.22	Effect of lamination schemes and temperature fields on the buckling temperature of CCCC laminated panel . . . . .	105
4.23	Effect of lamination schemes and temperature fields on the buckling temperature of CCFC laminated panel . . . . .	105
4.24	Effect of thermal load and boundary constraints on free vibration frequencies (Hz) and associated modal indices of laminated panel . . . . .	107
4.25	Effect of thermal load and boundary constraints on the free vibration mode shapes of laminated panel . . . . .	108
5.1	Different temperature fields in cylindrical panel . . . . .	111
5.2	Influence of different lamination schemes on the buckling temperature of the panel with TID and TD properties . . . . .	117
5.3	Influence of thickness ratio on the fundamental buckling mode of the panel with TD properties . . . . .	118
5.4	Influence of curvature ratio on the fundamental buckling mode of the panel with TD properties . . . . .	118

5.5	Effect of buckling temperature( $T_{cr}$ ) on free vibration frequencies of laminated composite panel . . . . .	120
5.6	Effect of elevated temperature ( $T_o=300^{\circ}\text{C}$ ) on free vibration frequencies of laminated composite panel . . . . .	121
5.7	Effect of buckling temperature( $T_{cr}$ ) on free vibration modes of laminated composite panel . . . . .	122
5.8	Comparison of buckling strength of the FGM panel with TD properties . . . . .	126
5.9	Comparison of Non-dimensional natural frequencies with Zhang <i>et al.</i> (2014a) . . . . .	127
5.10	Influence of CNTs volume fraction, CNTs grading patterns and temperature fields on the buckling temperature . . . . .	137
5.11	Influence of structural boundary constraints, CNTs grading patterns and temperature fields on the buckling temperature . . . . .	138
5.12	Influence of CNTs grading patterns on the fundamental buckling mode of CCCC cylindrical panel . . . . .	139
5.13	Influence of CNTs volume fraction on the fundamental buckling mode of CCCC cylindrical panel . . . . .	139
5.14	Influence of thermal load and CNTs grading patterns on the fundamental frequencies(Hz) of cylindrical panel with TID properties . . . . .	144
5.15	Influence of thermal load and CNTs grading patterns on the fundamental frequencies(Hz) of cylindrical panel with TD properties . . . . .	145
5.16	Influence of thermal load on the free vibration modes of cylindrical panel with TD and TID properties . . . . .	146
6.1	Comparison of optimum laminate orientation with Topal and Uzman (2008) . . . . .	151
6.2	Effect of curvature ratio on the optimum laminate orientation( $\theta_{opt}^{\circ}$ ) of CCCC panel . . . . .	154
6.3	Effect of thickness ratio on the optimum laminate orientation( $\theta_{opt}^{\circ}$ ) of CCCC panel . . . . .	155
6.4	Effect of boundary constraints on the optimum buckling strength of CCCC panel . . . . .	156
6.5	Effect of aspect ratio on the optimum laminate orientation( $\theta_{opt}^{\circ}$ ) of CCCC panel . . . . .	158

6.6	Effect of thickness ratio on the optimum laminate orientation( $\theta_{opt}^{\circ}$ ) and the buckling strength, of CCCC panel. . . . .	159
6.7	Effect of curvature ratio on the optimum laminate orientation( $\theta_{opt}^{\circ}$ ) and the buckling strength, of CCCC panel . . . . .	160
6.8	Effect of aspect ratio on the optimum laminate orientation( $\theta_{opt}^{\circ}$ ) and the buckling strength, of CCCC panel . . . . .	162
6.9	Influence of weighting factor and temperature fields on $MODI_{max}$	167
6.10	Influence of weighting factor and temperature fields on the optimum laminate orientation( $\theta_{opt}^{\circ}$ ) . . . . .	167
6.11	Influence of lamination schemes and temperature fields on the optimum laminate orientation( $\theta_{opt}^{\circ}$ ) . . . . .	168
6.12	Influence of lamination schemes and temperature fields on $MODI_{max}$	168
6.13	Influence of thickness ratio and temperature fields on $MODI_{max}$	170
6.14	Influence of thickness ratio and temperature fields on the optimum laminate orientation( $\theta_{opt}^{\circ}$ ) . . . . .	170
6.15	Influence of curvature ratio and temperature fields on $MODI_{max}$	171
6.16	Influence of curvature ratio and temperature fields on the optimum laminate orientation( $\theta_{opt}^{\circ}$ ) . . . . .	171
6.17	Influence of boundary constraints and temperature fields on $MODI_{max}$	172
6.18	Influence of boundary constraints and temperature fields on the optimum laminate orientation( $\theta_{opt}^{\circ}$ ) . . . . .	172



## LIST OF FIGURES

2.1	Experimental setup (i) Line diagram (ii) Actual setup . . . . .	29
2.2	Panel considered for experimental investigation (A= width; B= length; R= curvature radius) . . . . .	30
2.3	Schematic of the fixture: (i) Name of the parts (ii) Assembled fixture and (iii) Photograph . . . . .	32
2.4	Schematic of LabVIEW program used in experimentation . . . . .	36
2.5	Geometry of the cylindrical panel . . . . .	37
2.6	Eight noded shell element used to modeled isotropic cylindrical panel . . . . .	39
2.7	Flow chart of numerical investigation methodology . . . . .	42
2.8	Prediction of temperature fields through experiments . . . . .	42
2.9	Flow chart to illustrate the numerical investigation . . . . .	43
2.10	Laminated cylindrical panel analyzed . . . . .	44
2.11	Eight-noded shell element used to modeled laminated composite cylindrical panel . . . . .	49
2.12	A scheme of numerical analysis followed for buckling temperature optimization . . . . .	53
2.13	A scheme of numerical analysis followed for the multi-objective optimization . . . . .	56
2.14	Neural network scheme employed for the analysis . . . . .	57
3.1	Inflection point method to obtain critical buckling temperature .	61
3.2	Temperature-deflection plot measured nearer to the heat source in panel-2 with temperature fields of type, (i) Case(a), (ii) Case(b) and (iii) Case(c) . . . . .	63
3.3	Comparison of numerical results with experimentation for CCCC cylindrical panel-1 with temperature fields of type, (i) Case(a), (ii) Case(b) and (iii) Case(c) . . . . .	65

3.4	Comparison of numerical results with experimentation for CCCC cylindrical panel-2 with temperature fields of type, (i) Case(a), (ii) Case(b) and (iii) Case(c) . . . . .	66
3.5	Influence of aspect ratio on temperature-deflection plots obtained for panels with temperature fields of type, (i) Case(a), (ii) Case(b) and (iii) Case(c) . . . . .	69
3.6	Influence of boundary constraints on temperature-deflection plots obtained for panel-2 with temperature fields of type, (i) Case(a), (ii) Case(b) and (iii) Case(c) . . . . .	70
4.1	Influence of thickness ratio and temperature fields on buckling temperature of isotropic panel with boundary constraints, (i) CCCC and (ii) CCFC . . . . .	83
4.2	Influence of curvature ratio and temperature fields on buckling temperature of isotropic panel with boundary constraints, (i) CCCC and (ii) CCFC . . . . .	83
4.3	Influence of temperature fields on buckling mode shape of an isotropic panel with boundary constraints, (i) CCCC and (ii) CCFC . . . . .	85
4.4	Comparison of non-dimensional fundamental natural frequency of panel under thermal load . . . . .	94
4.5	Influence of thickness ratio and temperature fields on buckling temperature of laminated panel with boundary constraints, (i) CCCC and (ii) CCFC . . . . .	97
4.6	Influence of curvature ratio and temperature fields on buckling temperature of laminated panel with boundary constraints, (i) CCCC and (ii) CCFC . . . . .	98
4.7	Influence of aspect ratio and temperature fields on buckling temperature of laminated panel with boundary constraints, (i) CCCC and (ii) CCFC . . . . .	100
4.8	Effect of laminate orientation on buckling temperature of CCCC laminated panel . . . . .	103
5.1	Influence of thickness ratio on the buckling temperature of the panel with TID and TD properties . . . . .	113
5.2	Influence of curvature ratio on the buckling temperature of the panel with TID and TD properties . . . . .	114

5.3	Influence of aspect ratio on the buckling temperature of the panel with TID and TD properties . . . . .	115
5.4	Configurations of different FG-CNTs reinforced panels . . . . .	123
5.5	Effect of thickness ratio and temperature fields on buckling strength of CCCC cylindrical panel with CNTs pattern (i) UD, (ii) FG-X, (iii) FG-O, and (iv) FG-V . . . . .	130
5.6	Effect of curvature ratio and temperature fields on buckling strength of CCCC cylindrical panel with CNTs pattern (i) UD, (ii) FG-X, (iii) FG-O, and (iv) FG-V . . . . .	132
5.7	Effect of thickness ratio and temperature fields on buckling strength of CCCC cylindrical panel with CNTs volume fraction (i) 0.12, (ii) 0.17, and (iii) 0.28 . . . . .	133
5.8	Effect of curvature ratio and temperature fields on buckling strength of CCCC cylindrical panel with CNTs volume fraction (i) 0.12, (ii) 0.17, and (iii) 0.28 . . . . .	135
5.9	Effect of CNTs volume fraction on fundamental frequencies of CCCC cylindrical panel with temperature fields (i) Case(a), (ii) Case(b), (iii) Case(c), (iv) Case(d) and (v) Case(e) . . . . .	141
5.10	Effect of CNTs grading patterns on fundamental frequencies of CCCC cylindrical panel with temperature fields (i) Case(a), (ii) Case(b), (iii) Case(c), (iv) Case(d) and (v) Case(e) . . . . .	142
6.1	Effect of curvature ratio on the optimum buckling strength of CCCC laminated panel with (i) Symmetric and (ii) Un-symmetric . . . . .	153
6.2	Effect of thickness ratio on the optimum buckling strength of CCCC laminated panel with (i) Symmetric and (ii) Un-symmetric . . . . .	155
6.3	Effect of aspect ratio on the optimum buckling strength of CCCC laminated panel with (i) Symmetric, (ii) Un-symmetric . . . . .	157
6.4	Comparison of buckling strength of panels using single and multi-objective optimization approach with curvature ratio, (i) $R/S=1$ and (ii) $R/S=2.5$ . . . . .	161
6.5	Comparison of optimum buckling strength using single and multi-objective optimization approach with aspect ratio, (i) $L/S=1$ and (ii) $L/S=1.5$ . . . . .	162
6.6	Influence of weighting factors on MODI of CCCC panel with temperature fields of type (i) Case(a), (ii) Case(b), (iii) Case(c) , (iv) Case(d) and (v) Case(e) . . . . .	166

6.7 Influence of lamination schemes on MODI of CCCC panel with temperature fields of type (i) Case(a), (ii) Case(b), (iii) Case(c) , (iv) Case(d) and (v) Case(e) . . . . . 169

# CHAPTER 1

## INTRODUCTION AND LITERATURE REVIEW

### 1.1 Introduction

Curved panels are defined as a thin or a thick structure composed of single or multilayer of an isotropic or composite material. They are classified based on its curvature such as a panel with both of its radius is zero is called as a flat panel, a panel with one of its radius is zero is cylindrical, whereas both radii are zero is spherical, and one radius is zero and another varies linearly with the axial length is conical. Curved panels especially cylindrical and conical forms a backbone of numerous engineering structures mainly because of their lucrative properties such as high stiffness, containment of space, high strength to weight ratio and excellent load-carrying capability. They are considered to have high membrane stiffness than that of the bending stiffness, thus can withstand a large amount of membrane strain energy without large deformations. They have a wide area of application in all engineering fields which includes turbine disks, oil storage tanks, piping systems, nuclear vessels and pressure vessels. Further their usage in aviation and marine industries is just incomparable.

Aluminum being lightweight and strong is best suited for aircraft manufacture. It is considered roughly a third the weight of steel reducing the dead weight of the aircraft, thus permitting it to take more load. Furthermore, its high corrosion resistance property enhances the safety of the aircraft and its passengers. Aluminum panels are also being used in many engineering applications where the weight of the structures is given more preference. The late 90s, aluminum materials have

been slowly replaced by advanced materials like composites and nanocomposites in many industrial sectors. The use of composite materials in automotive, marine and aviation industries has increased greatly in recent years. This is largely due to their ability to be tailored to meet design requirements of strength and stiffness. Composite materials possess excellent properties such as its volume to its weight ratio, low coefficient of thermal expansion, outstanding elastic properties and good corrosion and chemicals resistant, thus grabbed the attention of numerous researcher(Rogers (1968), Ramakrishna *et al.* (2001), Eide *et al.* (2003), Meistring *et al.* (2006), Koronis *et al.* (2013), Tang (2014), Balaji *et al.* (2014)).

Composites material are made from two or more constituent materials having distinct physical or chemical properties. It offers an excellent combination of properties which are different from the individual parent materials and are also lighter in weight. Composite is mainly composed of two constituent elements viz fiber and matrix. The fibers are employed in contemporary composites due to its high specific mechanical properties, thus acts as the primary load carrying constitutes. Since the last few decades, graphite and carbon are considered as best fiber materials. Matrix surrounds the fibers and protects it from extraneous damage, thus acts as a bonding element. Metal, ceramic and polymer are the commonly employed matrix constituents. Bonding interface between the matrix and reinforcement decides the effectiveness of transformation of the load. Whereas, bonding mainly depends on the types of reinforcement and matrix and the fabrication method that has been employed. Laminated composite panels are made of laminae and each laminae comprising of fibers (e.g. graphite, boron, glass) enclosed in a matrix material (e.g. metal, epoxy, resin). In recent decades laminated composites have been employed in numerous engineering applications due to their tailor-made thermal and mechanical properties. Due to a sudden change in the material properties at the interface between two different materials, results in stress concentration which leads to material failure. Cracks are more likely to initiate at the interface and then propagates into the weaker section. Further, residual stress is also observed

in laminates due to the difference in thermal coefficient of the materials.

Analysts from Japan in the mid-1980s (Niino *et al.* (1988), Hirano *et al.* (1988), Sasaki *et al.* (1989)) observed that the impact of inter-laminar stresses generated due to an abrupt change in material properties can be significantly diminished by continuous grading of material properties. Functionally graded material replaces sharp interface by gradient interface, thus gives a smooth transition from one material to the other. Functionally graded materials (FGMs) have picked up a parcel of consideration from a few specialists and thus considered as a progressive material. FGMs decreases the interfacial stresses without sacrificing the structural strength and ductility. Future applications necessitate materials having exceptional mechanical, chemical and thermal properties which must maintain the distinctive environmental conditions and at the same time accessible effectively at sensible costs.

Carbon nanotubes (CNTs) have grabbed a lot of consideration as of late because of their excellent thermal, electrical and mechanical properties. For instance, their Young's moduli are higher than 1TPa with the density of just  $1.3 \text{ g/cm}^3$  which is better than all carbon fibers. Because of such intriguing features, CNTs are chosen as a promising possibility to reinforce the composites. Unique features of CNTs and FGMs may be accomplished together through the functionally graded distribution of CNTs. Functionally graded carbon nanotube reinforced composites (FG-CNTRC) were initially presented by Shen (2012). An examination by Shen (2012) demonstrated that bending moment in a composite plate might be diminished extensively through a nonuniform dissemination of CNTs over the thickness of a plate. (Thermal buckling of temperature dependent FG-CNT reinforced composite conical shells). The functionally graded carbon nanotubes reinforced composite (FGCNTRC) materials is relied upon to be the new era material having an extensive variety of unexplored potential applications in various technological areas, for example, aviation, automotive, pharmaceutical, defense, vitality, chemical

and structural. They can also be utilized as gas adsorbents, actuators, catalyst supports, probes, chemical sensors, nano pipes, nanoreactors and so forth.

As of late, part of the consideration is given in decreasing the weight of the engineering structural components which are utilized in automotive, nuclear plants, military, special storage tanks and aviation ventures. As a result of weight reduction, the majority of the structural components result as slender members which offer less resistance to the compressive load. In most of the engineering applications, structural components like curved panels are exposed to the hostile thermal environment during their operation thus, develops thermal stress in it. Stresses set up due to thermal load may lead to buckling failure and affects the dynamic behavior of the panel. So, it is very important to investigate the buckling and vibration behavior of panels under thermal load. In practice, because of un-symmetric geometric variation and the nature of heat source, most of the panels are exposed to arbitrarily varying non-uniform temperature fields. Structures used in aerospace vehicles such as high-speed aircraft, car panels located close to the engine, components of rockets and missiles, electronic circuit board, columns of the heating furnace and nuclear vessels are typical examples of structures exposed to non-uniform heating during their service. Thin curved panels under non-uniform temperature distribution are more susceptible to thermal buckling. As a whole, the non-uniform thermal load plays a vital role in determining and monitoring the structural design. Further, stresses developed due to non-uniform thermal load significantly influences the free vibration behavior of the structures.

The investigation of free vibration gets to be distinctly one of the vital factors in the design of curved panel because the panels utilized in various disciplines of engineering have less thickness contrasted with its lateral dimensions. In practice, most of the structures are exposed to dynamic loads henceforth it turns out to be imperative to find the natural frequency of the structure in order to prevent the phenomenon of resonance. When the same structure is operated under thermal



load, it is essential to examine its dynamic behavior where it is altogether influenced by the thermal pre-stress due to change in the structural stiffness with the thermal load.

## 1.2 Literature Review

### 1.2.1 Thermal buckling

Buckling behavior of uniformly heated, simply supported and clamped cylindrical panels was analyzed by Chen and Chen (1987) using Galerkin's method. They found that buckling temperature was significantly influenced by the aspect ratio, fiber alignment, modulus ratio, boundary conditions and panel curvature. Thangaratnam *et al.* (1989) made use of finite element method to investigate the buckling behavior of laminated composite cylindrical and conical shells under thermal environment. It was found that the buckling behavior of laminated shell is different under thermal and mechanical load with respect to fiber orientation. Thermal buckling of simply supported antisymmetric angle-ply laminated cylindrical shells exposed to uniform temperature was studied by Jeng-Shian and Wei-Chong (1991) using finite element method based on the higher order displacement functions. They found that thermal buckling temperature predicted by higher order theory is overestimated by first order theory which thus evokes the higher order displacement theory in the analysis of thermal buckling for a laminated shell. To predict thermal buckling of laminated composite circular cylindrical shells, Ma and Wilcox (1991) developed an analytical method. They found that, buckling temperature decrease with the increase in radius to thickness ratios and lamination angles. They also observed that for an antisymmetric laminate the coupling effect between bending and compression disappears as the number of layers increase. Birman and Bert (1993) employed the equilibrium equations to analyze the influence of high temperature on the buckling behavior of the unstiffened re-

inforced composite cylindrical plates and shells. Plates and shells subjected to thermal and axial load were considered for analysis. Gotsis and Guptill (1994) examined the angle-ply laminated thin shells in a hot environment to study the effect of various parameters on the buckling behavior. They investigated the influence of length to thickness ratio of the cylinder, fiber volume fractions, different layup configurations and through thickness temperature profiles on the buckling strength of the panel. Eslami and Javaheri (1999) analyzed the buckling behavior of laminated circular cylindrical shells by employing Donnell and improved Donnell equations. Shell considered was exposed to mechanical and thermal loads with simply supported boundary conditions. For thermal load, uniform temperature rise and radial temperature difference were assumed. Noticeable differences was found for a critical load computed for long cylinders based on the Donnell and improved Donnell theories.

Shahsiah and Eslami (2003) estimated the thermal buckling strength of simply supported functionally graded cylindrical shells employing equations based on the Sanders kinematic relations, the Donnell stability equations, and the first-order shell theory. Shells analyzed was assumed to have through thickness linearly varying material properties. They found that buckling strength of cylindrical shells under through thickness linear temperature variation was lower than the cylindrical shell under nonlinear temperature difference. Patel *et al.* (2004) studied the thermal buckling behavior of laminated cross-ply oval cylindrical shells using finite element approach based on higher-order displacement model. They noticed that buckling behavior of the cylindrical shells was significantly influenced by ovality parameter value, shell geometry, nominal circumferential wave number, and lay-up. Functionally graded cylindrical shells exposed to three different thermal loads was analyzed by Wu *et al.* (2005). Simply supported cylindrical shell with the material properties varies in the thickness direction was investigated by using Donnell's shell theory. Further, they also found that the buckling temperature was influenced by the aspect ratio, the functionally graded index, and the rel-

ative thickness. Matsunaga (2007) employed a global higher-order shell theory to determine the buckling strength of simply supported cross-ply laminated composite shallow shells under thermal load. Patel *et al.* (2007) considered angle-ply laminated elliptical cylindrical shells to analyze thermo-elastic buckling behavior under uniform thermal load. They studied the effects of elliptical cross-sectional parameter, radius-to-thickness, and length-to-radius ratios, and ply- angles on the critical buckling temperature and associated mode shapes. They also found that the shells are highly sensitive to non-circularity in the optimum ply-angle range whereas less sensitivity away from the optimum ply-angle range. Roh *et al.* (2008) have numerically investigated the thermal buckling characteristics for composite conical shell structures. The structural modeling of composite conical shell panels was done by using layerwise displacement theory. The governing equations were obtained by using the Hamilton's principle. The influences of geometric parameters like the semi-vertex angle, subtended angle, radius to thickness ratio, and length to thickness ratio, on the natural frequency and the critical buckling temperature of the composite conical shells was presented. Finite element method was used by Darvizeh *et al.* (2010) to investigated the effect of important structural parameters such as cut-out at the apex on the thermal buckling of composite shells with selected boundary condition along with uniform and linearly varying thermal load. Hafezalkotob and Eslami (2010) have studied the thermo-mechanical buckling behavior of simply supported shallow spherical shells made of functionally graded material. Properties of shell panel change gradually through the shell thickness direction from pure metal on the inner surface to pure ceramic on the outer surface and its temperature dependent. First-order shear deformation theory and element-free kp-Ritz method were employed by Zhao and Liew (2010) to analyze the buckling behavior of functionally graded cylindrical shells subjected to a thermal and mechanical load. Material properties were calculated in terms of a power-law equation of the volume fraction of the panel constituents. Thermal buckling and post-buckling behavior of a functionally graded carbon nanotubes

(FG-CNT) exposed to in-plane temperature variation were studied by Shen and Zhang (2010). Molecular dynamics simulation was used to compute temperature-dependent material properties of SWCNTs. It was observed from the analysis that buckling strength of the plate can be enhanced by altering the pattern of functional grading.

State space approach was employed by Khdeir (2012) to obtain exact solutions for the thermoelastic behavior of cross-ply cylindrical, spherical and doubly curved shells exposed to arbitrary temperature field with different boundary conditions. Composite cylindrical shells reinforced by carbon nanotubes was analyzed by Shen (2012) under uniform temperature rise. The governing equations based on higher order shear deformation theory was used to study the buckling and post-buckling behavior. It was found that buckling and post-buckling strength of the shell under thermal load can be increased by functionally graded reinforcement. Thermal buckling behavior of deep imperfect FGM spherical shells was analyzed by Jahanbakhsh *et al.* (2012) using the Wan-Donnell geometrical imperfection model. Influence of different temperature fields and the magnitude of initial geometric imperfection on the thermal buckling strength of the shell was examined. Topal (2013) maximized the thermal buckling strength of the laminated composite plates using extended layerwise approach. The first order shear deformation theory (FSDT) was employed to obtain the finite element solution and extended layerwise approach for optimization. Later, the buckling behavior of laminated shell panel in the thermal environment was analyzed by Panda and Singh (2013). They investigated the influence of different modular ratios, thickness ratios, stacking sequences, amplitude ratios, symmetric and unsymmetrical lamination schemes (cross-ply and angle-ply), on buckling and post-buckling behavior of the panel. The buckling behavior of functionally graded cylindrical panels under thermal load was studied by Kar and Panda (2014). The effect of different parameters such as power-law index, thickness ratio, curvature ratio and aspect ratio on buckling strength were analyzed for both temperature independent and dependent

material properties of each constituent. It was observed that buckling temperature of the panels can be enhanced by increasing the power-law indices and aspect ratios. A higher value of buckling temperature was noted for the higher value of temperature rise. Finite element method was used by Aubad (2014) to analyze the thermal buckling of multi-layered composite spheroidal spherical shells with clamped boundary condition under uniform temperature. It was found that the critical buckling temperature of the panel was highly influenced by the spherical angle, fiber orientation, number of layers of composite shell and radius to thickness ratio. Asadi *et al.* (2016) investigated the laminated composite cylindrical shells with shape memory alloy fibers to understand the thermal bifurcation behavior. They found that buckling strength of shells can be improved by using proper shape memory alloy. Kandasamy *et al.* (2016a) employed finite element method to investigate the thermal buckling and free vibration behavior of moderately thick functionally graded material (FGM) structures including plates, cylindrical panels and shells under thermal environments. Sun *et al.* (2015) investigated the buckling behavior of the temperature dependent FGM cylindrical shells exposed to an axial compression in thermal environment using Reddy's high-order shear deformation theory and then they compared results with the classical Donnell's theory. Katariya and Panda (2016b) developed a mathematical model for a laminated curved structure to compute in-plane and out of plane shear strains and stress using higher order shear deformation theory. Further, they also predicted thermal buckling temperature of uniformly heated laminated structures using Green-Lagrange type nonlinear strains. Mirzaei and Kiani (2016b) employed first order shear deformation theory to investigate the thermal buckling of FG-CNTs reinforced composite plates with temperature dependent thermo-mechanical properties. It was observed that FG-X pattern of the CNTs distribution gives higher critical temperature compared to other patterns. Ahmadi and Pourshahsavari (2016) analyzed the buckling strength of FG cylindrical panels using differential quadrature method. Panels were analyzed for three different thermal loads i.e. uniform temperature

rise and non-uniform temperature rise in the axial and radial direction. It was found that buckling temperature predicted using three-dimensional buckling equations were more accurate than Donnell shell theory. It was also noticed that for the higher thickness of panel Donnell's theory overestimates the buckling temperature. Cylindrical shell with FGM coating was investigated by Han *et al.* (2017) to analyze its buckling behavior analysis under thermal load.

However, very few research work was done experimentally to study the buckling behavior of the plate and shell when exposed to heat. Murphy and Ferreira (2001) investigated thermal buckling of a uniformly heated plate experimentally. They compared the experimental results with the analytical results, obtained based on Von-Karman plate theory. Digital image correlation (DIC) was implemented by Jin *et al.* (2014*b*) and Jin *et al.* (2015) to determine the buckling strength of an Aluminum circular plate and laminated composite plate under uniform temperature distribution. With the help of DIC, they also obtained the buckling mode shapes. Further, George *et al.* (2016) investigated the thermal buckling behavior of beam subjected to non-uniform thermal load experimentally and then compared with numerically obtained values. Sahoo *et al.* (2016) employed three point bend test and modal analysis to study the static, free vibration and the transient behavior of the laminated composite flat/curved panels. Experimental results were compared to the numerical results obtained using two higher-order mid-plane kinematics. Sahoo *et al.* (2017) analyzed the static and free vibration behavior of laminated woven glass/epoxy composite plate experimentally and validated through numerical approach. The laminated composite shear deformable plate was modelled by employing higher-order kinematic theories. Mehar and Panda (2017) investigated the deflection behavior of carbon nanotube-reinforced composite plate experimentally using three-point bending setup. Further experimentation results was compared with the results obtained numerically using finite-element method.

### 1.2.2 Free vibration

Soldatos (1984) analyzed the free vibration of thin elastic cross-ply laminated circular cylindrical panels using theoretical formulation. Later, he also compared the numerical values of vibration obtained for simply supported cylindrical panels using closed form solution with most of the thin shell theories. Sanders shell theory was modified by Reddy and Liu (1985) to develop a higher-order shear deformation shell theory for laminated orthotropic shells. Developed theory accounts for the parabolic distribution of through thickness transverse shear strains and tangential stress-free boundary conditions on the boundary surfaces of the shell. They also gave solution for bending and natural vibration of simply supported cylindrical and spherical shells. Finite element solution was given by Narita *et al.* (1993) to analyze the free vibration of cross-ply laminated, closed cylindrical shells using classical lamination theory based on the energy expressions. They also investigated the influence of different composite stacking sequences and material constants on the free vibration behavior. Chakravorty *et al.* (1995) studied free vibration behavior of point supported laminated composite cylindrical shells by using finite element analysis based on first order shear deformation theory. Wherein they made use of an eight-noded curved quadrilateral isoparametric elements. Lam and Loy (1995) analyzed thin orthotropic laminated cylindrical shells to know the influence of boundary constraints and fiber orientation on the fundamental frequencies. For which they developed a simple method of analysis based on Love's first approximation theory and Ritz's procedure. They found that fundamental frequencies are highly influenced by fiber orientation and boundary constraints. Dasgupta and Huang (1997) made use of finite element method to analyze the free vibration of thick composite spherical panels. The layer-wise laminated shell theory was employed to encounter the shortcoming of conventional shear deformable plate theories because the gradient of the deformation field was not necessarily continuous through the thickness, due to the discontinuity of material properties

at layer interfaces. Singh (1999) employed Rayleigh-Ritz method to study the free vibration behavior of doubly curved deep sandwich panels. Further, they used the same approach to obtain results for cylindrical, circular and spherical sandwich panels with different boundary conditions. Three-dimensional theory of elasticity was employed by Loy and Lam (1999) to study the vibration behavior of isotropic cylindrical shell under simply supported and clamped boundary conditions. In the analysis, a thick cylindrical shell was divided into an arbitrary number of thin layers in the thickness direction. They also compared the frequency behavior of thick shell with that of the thin shell. Lam and Qian (2000) employed first order shear deformation theory to analyze the free vibration of thick symmetric angle-ply laminated composite cylindrical shells. The frequency characteristics of thick symmetric angle-ply and cross-ply laminated composite cylindrical shells were compared under different  $h/R$  and  $L/R$  ratios. Further, the influence of a number of lamination layers and fiber orientation on the frequency with simply supported boundary condition was investigated.

Finite element analysis based on first order shear deformation theory was employed by Sahu and Datta (2002) to investigate the vibration and parametric resonance characteristics of laminated composite doubly curved shells under different in-plane static and periodic loadings. They also investigated the influence of a number of layers, side to thickness ratio, static load factor, boundary conditions, the degree of orthotropic, ply orientations and various load parameters on the principal instability regions of doubly curved panels. Ram and Babu (2002) investigated the free vibration of composite spherical shell cap with and without cutout by employing finite element method derived from higher-order shear deformation theory. Wherein an eight-noded isoparametric shell element with nine degrees of freedom at each node was used for the analysis. They observed that the fundamental frequency of composite spherical panels increases with the increase in cut-out size except in the case of simply supported orthotropic spherical shell cap having fibers along the meridional direction. Ganapathi *et al.* (2002)



used higher-order shear deformation theory to investigate the dynamic behavior of laminated cross-ply composite non-circular thick cylindrical shells subjected to a thermal/mechanical load. Shell response was predicted by using finite element approach in conjunction with direct time integration technique. The formulation used in the analysis accounts for the variation of in-plane and transverse displacements through the thickness. The influence of natural frequencies of spherical shells was studied by Buchanan and Rich (2002) using a nine-node Lagrange finite element with three different boundary conditions namely free, simply supported and fixed. It was found that frequency of free vibration can be controlled by adjusting boundary condition definition. Zhao *et al.* (2004) examined the effects of different curved edge boundary conditions on the frequency characteristics of cylindrical panels. Mesh free kp-Ritz method was employed to analyze the influence of various curved-edge boundary constraints on the frequency characteristics of cylindrical panels. Finite element analysis of multi-layered, doubly curved, laminated composite shells having spherical and ellipsoidal shapes was improved by Sk and Sinha (2005) using Koiter's shell theory and Mindlin's hypotheses. They found that proposed method predicts better free vibration frequency with a relatively small number of elements. Nguyen-Van *et al.* (2008) analyzed laminated plate/shell structures based on first order shear deformation theory with a stabilized nodal- integrated quadrilateral element. They demonstrated the capability, efficiency and simplicity of the developed element through several numerical examples. Lee (2009) used the pseudo-spectral method to analyze the free vibration of axisymmetric and asymmetric spherical caps. Chebyshev polynomials and Fourier series were employed to express the displacements and rotations. He presented some numerical examples to demonstrate free vibration behavior under clamped, hinged and free boundary conditions. Panda and Singh (2009) investigated the free vibration behavior of doubly curved composite spherical shell panel under uniform temperature. They employed nonlinear finite element method based on higher order shear deformation theory. Influence of different parameters such

as lamination scheme, modular ratio, amplitude ratio, thickness ratio, curvature ratio, aspect ratio and various support conditions, were examined. R-function theory and variational methods based on first order shear deformation theory were employed by Kurpa *et al.* (2010) to analyze the vibration behavior of laminated composite shells. They also have analyzed the influence of different parameters like curvature, geometry, ply orientation and boundary conditions, on the dynamic behavior of the shallow shell.

Superposition-Galerkin approach was employed by Mochida *et al.* (2012) to study the dynamic behavior of the double curved shallow shell with a different combination of simply supported and clamped edges. They considered the different curvature ratio, aspect ratio, and boundary conditions, to study the natural frequency of thin shells. Hosseini-Hashemi *et al.* (2012) investigated the free vibration of Levy-type FGM cylindrical panels to know the validity range of Donnell and Sanders shell theories. Material properties of the panel were assumed to vary through thickness according to power law distribution. Under various boundary conditions, the influence of different geometry and material parameters on the validity range of above theories were analyzed. Yas *et al.* (2013) used the three-dimensional theory of elasticity to determine the vibrational characteristics of functionally graded carbon nanotubes composite cylindrical panels. The panel analyzed was assumed to have carbon nanotube (CNT) fraction varying smoothly in the radial direction. They observed that natural frequency of the shell was significantly influenced by kind of distribution and volume fraction of CNT and highest frequency was noted when CNTs were oriented at  $2\pi$  and  $\pi/6$ . Further, they also found that the natural frequency decreases with increasing L/R ratio for short cylindrical panels and remains unaltered for long cylindrical panels. Alibeigloo (2013) employed the three-dimensional theory of elasticity to analyze free vibration behavior of functionally graded carbon nanotube-reinforced composite (FG-CNTRC) cylindrical panel embedded in piezoelectric layers with simply supported boundary conditions. He also found the influence of volume fraction of

CNT, piezoelectric layer thickness, CNTs distribution, modes number and mid-radius to thickness ratio on the vibration behavior. Haar wavelet based approach is presented by Jin *et al.* (2014a) for the analysis of free vibration of functionally graded (FG) cylindrical shell. It was found that approach employed offers advantages such as simplicity, fast convergence, low computational cost and high precision. Lei *et al.* (2014) analyzed the free Vibration of functionally Graded Carbon Nanotube-Reinforced Composite Cylindrical Panels under static and periodic axial force by implementing the element-free kp- Ritz method. Micromechanical model based on the Eshelby-Mori-Tanaka approach was used to estimate the effective material properties. Detailed parametric studies were carried out to know the influence of edge-to-radius ratio, the volume fraction of carbon nanotubes and radius-to-thickness ratio on dynamic stability responses of FG-CNTR cylindrical panels. Zhang *et al.* (2014b) employed the mesh-free kp-Ritz to predict free vibration and flexural strength of functionally graded carbon nanotube-reinforced composite (FG-CNTRC) cylindrical panels. Proposed formulations were based on the first-order shear deformation shell theory. CNTs were assumed to be graded in thickness direction symmetric about the middle surface of the cylindrical panel. A micromechanical model based on the Eshelby Mori Tanaka approach was employed to compute the effective material properties. Size-dependent equations of motion for functionally graded cylindrical shell were developed by Beni *et al.* (2015) using shear deformation model and rotation inertia. Material properties of the shell were assumed to varying continuously along the thickness. Tornabene *et al.* (2015) investigated the free vibration behavior of single and multilayered isotropic, composite and sandwich cylindrical and spherical shell panels using different theories. Further, they compared the solution obtained using classical two-dimensional (2D) and three-dimensional (3D) finite elements (FEs), classical and refined 2D generalized differential quadrature (GDQ) methods and an exact three-dimensional solution. Fantuzzi *et al.* (2016) investigated free vibration behavior of simply supported spherical and cylindrical shells with the functionally

graded material (FGM). A two-dimensional computational model was compared with three-dimensional exact shell models in terms of frequencies and vibration modes. The variation in 2D numerical results and 3D exact results depends on thickness ratio, lamination sequence, materials and geometry of the structure. Mirzaei and Kiani (2016a) investigated the free vibration characteristics of single-walled carbon nanotubes reinforced composite plates. Refined rule of mixtures approaches that involves the efficiency parameters was employed to calculate the properties of the composite material. Further, they found that frequencies of the panel can be enhanced by increasing the volume fraction of carbon nanotubes. Brischetto *et al.* (2016) compared a three-dimensional (3D) exact solution with several two-dimensional (2D) numerical solutions like classical 2D finite elements (FEs), and classical and refined 2D generalized differential quadrature (GDQ) solutions. They also investigated vibration modes for the comparison of results obtained by the 2D numerical methods with that of 3D exact solution.

### 1.2.3 Free vibration under thermal load

Studies related to free vibration behavior of heated cylindrical panels are not available in the open literature so, free vibration studies carried out on heated plates and cylindrical shell are grouped and reported in this section. Jones *et al.* (1980) studied the linear behavior of plates at elevated temperatures. They presented a mathematical formula to relate the fundamental frequency of vibration to the critical buckling temperature and the corresponding frequency of the unheated plate. Finite element method was employed by Rao and Ganesan (1985) to investigate free vibration behavior of isotropic plates placed in the hot fluids. They determined natural frequencies of plates immersed in hot water with six types of temperature distributions. They found that natural frequency of the plate reduces with increase in temperature when it is exposed to elevated temperature. Semiloof finite element formulation was presented by Dhanaraj *et al.* (1990) to

analyze the free Vibrational characteristics of composite laminates under thermal stress. Angle-ply and cross-ply rectangular laminates with simply supported and clamped edge conditions were considered for the analysis. The behavior of fundamental modes of vibration of initially stressed composite laminated plates was studied under uniform temperature rise. They found that the change in frequencies with initial stresses depends on the aspect ratio of the plate, orthotropy ratio and also on the angle of fiber orientation. Ram and Sinha (1992) studied the influence of temperature and moisture on the free vibration of laminated composite plates. They considered quadratic isoparametric element in finite element analysis which accounts for transverse shear deformation. It was found that for symmetric and antisymmetric laminates with simply supported and clamped boundary conditions, natural frequency decreases with the increase in temperature and uniform moisture concentration. Parabolic shear deformation theory was used by Bhimaraddi and Chandrashekhara (1993) to compute nonlinear vibrations of heated anti-symmetric angle-ply laminated plates using the Von Karman type large deflection model. They analyzed simply supported plate to know the influence of the temperature loading and initial imperfections on the response characteristics. Lee and Lee (1997) investigated the thermal post-buckling and natural vibration of thermally post-buckled plates by using the finite element method based on the first-order shear deformable plate theory (FSDT) and Von Karman strain-displacement relation. The influence of fiber orientation and aspect ratio on post-buckling and vibration behaviors were analyzed for simply supported laminated plates exposed to uniform temperature rise.

The functionally graded cylindrical panel was studied by Yang and Shen (2003) to investigate the free vibration and dynamic instability, exposed to combined static and periodic axial forces under thermal environment employing Galerkin technique and Bolotin's method. Material properties analyzed was assumed to be temperature dependent. Mead (2003) investigated modes and frequencies of a free rectangular Kirchoff plate exposed to in-plane stresses developed due to

stated non-uniform surface temperature distributions. He employed Rayleigh-Ritz method for the analysis and shown that natural frequencies and flexural modes change dramatically due to thermal load. Park *et al.* (2004) investigated the vibration behavior of the thermally buckled composite plate embedded with shape memory alloy (SMA) fibers. For the analysis of a composite plate with embedded SMA fibers, the nonlinear finite element equations based on the first-order shear deformation plate theory was formulated. Shiau and Kuo (2006) concluded that if the shape of a free vibration mode is similar to the plate buckling mode then the natural frequency of that mode will drop to zero when the temperature reaches buckling temperature. Vibration behavior of uniformly heated laminated composite skew plates with small amplitude was studied by Singha *et al.* (2006) by employing a shear deformable finite element. They analyzed first three natural frequencies in the pre- and post-buckled states till the point of secondary bifurcation. They also found that with an increase in temperature the fundamental frequency changes to a form corresponding to next higher mode. Finite element method was employed by Vangipuram and Ganesan (2007) to investigate the free vibration and damping characteristics of a plate composing of composite stiff layers and isotropic viscoelastic core under uniform temperature rise. The temperature-dependent viscoelastic core properties and influence of pre-stress was considered for investigation. They conducted different parametric studies and observed shifting of modes with temperature rise. Jeyaraj (2013) investigated buckling and free vibration characteristics of isotropic plates under arbitrarily varying temperature distributions using finite element method under different boundary conditions. It was found that nodal and anti-nodal position of the free vibration modes changes with the rise in temperature. It was also found that frequencies of the panel decrease with the increase in temperature close to buckling temperature. Panda and Mahapatra (2014) investigated nonlinear free vibration characteristics of laminated composite shallow shell exposed to uniform temperature load. The mid-plane kinematics of the laminated shell was calculated based on higher order shear

deformation theory to account out of plane shear stresses and strains accurately. The nonlinearity in geometry was considered in a Green-Lagrange sense due to the thermal load. They also analyzed the influence of curvature ratio, thickness ratio, thermal expansion coefficient, modular ratio, support condition, amplitude ratio and lamination scheme on free vibration response. Kar and Panda (2015) analyzed free vibration behavior of functionally graded single/doubly curved panels exposed to uniform, linear and nonlinear temperature fields. They used higher order shear deformation theory to investigate the mid-plane kinematics of panel geometry and the governing equation of the panel was derived from Hamilton's principle. Kandasamy *et al.* (2016*b*) investigated the free vibration and thermal buckling behavior of moderately thick functionally graded material (FGM) plates, cylindrical panels and shells under thermal environments by employing first-order shear deformation theory (FSDT). Song *et al.* (2016) analyzed the vibration characteristics of CNT-reinforced functionally graded composite closed cylindrical shells considering thermal effect employing high-order shear deformation theory. Ghadiri and Safarpour (2017) studied the free vibration behavior of a functionally graded (FG) porous cylindrical microshell exposed to a thermal environment using first-order shear deformation shells and the modified couple stress theories. The material properties are assumed to be temperature dependent and are graded in the thickness direction. Mehar and Kumar Panda (2017) studied the vibration behavior of carbon nanotube reinforced sandwich curved shell panel exposed to elevated thermal environment using the higher-order shear deformation theory. The sandwich panel analyzed was assumed to have temperature-dependent properties.

#### **1.2.4 Optimization of thermal buckling and free vibration**

Walker *et al.* (1997) optimized the thermal buckling temperature for symmetrically laminated plates. To maximize the buckling temperature of the plate, finite element method in conjunction with an optimization routine was employed. They

analyzed panel for different parameters, boundary conditions, and various thermal loadings. It was found that boundary conditions and temperature distribution has a major impact on the optimal ply angle. Spallino and Thierauf (2000) optimized the thermal buckling strength of laminated composite plates exposed to uniform temperature profile using guided random search method. The buckling temperatures of Graphite/Epoxy laminated composite plates were maximized by Singha *et al.* (2000) for a given total thickness taking relative thicknesses of layers and fiber directions as design variables. Wherein they employed finite element method for thermal buckling analysis and genetic algorithm (GA) for optimization. Further, they found that buckling loads can be increased significantly with appropriately orienting the fiber directions and varying the thickness of different layers. Fares *et al.* (2005) considered the multi-objective problem of laminated composite plates to maximize thermal buckling and to minimize post-buckling dynamic response with laminate thickness and control energy as constraints. The problem formulation was based on a shear deformation theory inculcating the von-Karman nonlinearity. Wherein, they found that the optimization over the layer thickness is less effective than optimization over the orientation. Adali and Duffy (1990) maximized the buckling temperature by optimizing the fiber orientations and layer thicknesses of antisymmetric with a constraint of equal mass or equal thickness. Laminated plate analyzed was constructed by using a sandwich hybrid structure with outer layers of high-modulus fiber composite material and inner layers of low-modulus fiber composite material. Abouhamze and Shakeri (2007) used multi-objective optimization approach to maximize the first natural frequency and critical buckling load of laminated cylindrical panels under mechanical load by optimal stacking sequence method. They employed genetic algorithm in combination with artificial neural networks for optimization. Topal and Uzman (2007) presented the optimal design of simply supported laminated composite plates exposed to in-plane static loads. The objective function formulated was to maximize the buckling load capacity of laminated plates with fiber orientation as a design



variable. Finite element analysis was based on first-order shear deformation theory similarly optimization was on modified feasible direction method. The influence of geometrical parameters, the number of layers, load ratios, material anisotropy and functionally graded materials on the optimum results were analyzed. Later, same optimization method was employed by Topal and Uzman (2008) to optimized thermal buckling strength of laminated plates exposed to uniformly distributed temperature load. They formulated problem by taking an objective function as maximization of the critical buckling temperature of laminated plates and the fiber orientation as a design variable. Topal (2009) further extended their work of optimization on to symmetrically laminated cylindrical shells exposed to uniform thermal load. They investigated the influence of length-to-radius ratio, a number of layers, and boundary constraints on the optimum results. Topal and Uzman (2009) optimized the frequency of symmetrically laminated composite plates by varying fiber orientation. The first-order shear deformation theory was considered for vibration analysis of laminated folded plates and the modified feasible direction (MFD) method for the optimization. Gharib and Shakeri (2010) used a genetic algorithm (GA) in combination with artificial neural networks (ANN) to maximize the natural frequency and buckling load of the laminated cylindrical shell by optimizing the stacking sequence of the shell. Artificial neural network models were formed to estimate the buckling load and natural frequency of the structure. Vibration study was based on three-dimensional elasticity equations. Wang *et al.* (2010) modified Ant Colony Algorithm (ACA) known as multi-city-layer ant colony algorithm (MCLACA) to optimize the buckling strength of the laminated composite panel. They compared MCLACA method with ACA and genetic algorithm (GA) and found that MCLACA method gives better computational efficiency and robustness. Buckling temperature of laminated composite skew plates was optimized by Malekzadeh *et al.* (2012a) using differential quadrature method in conjunction with the genetic algorithms. The temperature dependent material properties were assumed for the analysis and the governing equa-

tions were based on the first-order shear deformation plate theory. Influence of the boundary conditions, the temperature dependence of the material properties, the number of layers, length-to-thickness ratio and skew angle on the optimum buckling temperature of the laminated skew plates were presented. Vosoughi and Nikoo (2015) employed the combination of differential quadrature method, Young bargaining model, and non-dominated sorting genetic algorithm to optimize fundamental natural frequency and thermal buckling strength of laminated composite plates. Kamarian *et al.* (2016) maximized the critical buckling temperature of laminated composite plates by optimizing the stacking sequence of the laminates using a powerful meta-heuristic algorithm called firefly algorithm (FA) depends on the flashing behavior of fireflies. They found that it is more efficient optimization technique compared other optimization techniques. Unified Particle Swarm Optimization (UPSO) method was employed by Sreehari and Maiti (2016) to enhance the buckling load capacity of composite plates having damage under hygrothermal environment. For optimization, fiber orientation was taken as a design variable. Further, they carried out analysis on different aspect ratios, ply orientations, and boundary conditions.

### 1.3 Closure

Based on the literature survey, it was found that most of the researchers have analyzed beams or plates that were exposed to a uniform temperature above ambient and in some cases through the thickness temperature variation using numerical and analytical approach. Wherein, it was found that the temperature variation field, thickness ratio, aspect ratio and structural boundary conditions significantly influences the critical buckling temperature and dynamic behavior of the shells. Limited experimental work has been observed in the area of buckling strength of the structure exposed to uniform temperature distributions. Considering the significance of the non-uniform temperature field in the practical applications,

it is vital to investigate the thermal buckling strength of non-uniformly heated structures experimentally.

Literature survey also revealed that in-depth analysis on combined buckling and free vibration behavior of isotropic and laminated cylindrical panel under non-uniform thermal load has not been reported which is critical from the practical point of view. However, few literature reports on cylindrical shells under thermal environment were limited to either uniform or vary in, one-dimension or, in the thickness direction. In practice, because of un-symmetric geometric variation and the nature of heat source, most of the panels are exposed to arbitrarily varying non-uniform temperature fields. Structures used in aviation, marine, storage tanks, nuclear vessels etc. are typical examples of structures exposed to non-uniform heating during their service. Thin cylindrical shells under non-uniform temperature distribution are more susceptible to thermal buckling. As a whole, the non-uniform thermal load plays a vital role in determining and monitoring the structural design. Further, stresses developed due to non-uniform thermal load significantly influences the free vibration behavior of the structures.

Further, it is also seen from presented literature that, laminated and functionally graded carbon nanotubes reinforced composites(FG-CNTRC) cylindrical panel with temperature dependent properties has not been analyzed for its detailed study on combined buckling and free vibration behavior under non-uniform thermal load, which is crucial from the practical viewpoint. However, some literature reports on cylindrical shells under thermal environment were confined to either uniform or vary in the thickness direction with temperature independent material properties.

It is also found that most of the researchers have optimized the thermal buckling load of uniformly heated plates, cylindrical shells, and panels. Optimization of buckling strength and the fundamental frequency of non-uniformly heated laminated cylindrical panel is yet to be investigated. The behavior of non-uniformly

heated laminated composite cylindrical panels is different from the uniformly heated panels, thus it is important to optimize thermal buckling strength and the fundamental frequency of cylindrical panels with different non-uniform temperature fields.

## 1.4 Objective and Scope of study

A literature review revealed that the several researchers investigated thermal buckling of structures under uniform temperature rise above ambient. But in real life, most of the structures such as high-speed aircraft's, car panels located close to the engine, components of rockets and missiles, electronic circuit board, columns of the heating furnace and nuclear vessels are exposed to non-uniform temperature variation field. The behavior of structures subjected to non-uniform temperature field may be different from that of the uniform temperature field. Thus there is a need to carry out a detailed investigation on the behavior of the structures when exposed to non-uniform inplane temperature distributions. Most of the structures employed in engineering application are in the form of cylindrical panels, thus present analysis focuses on cylindrical panels. A detailed experimental investigation needs to be conducted on the buckling behavior of the cylindrical panel exposed to non-uniform temperature variations. Stresses developed due to non-uniform temperature distribution can influence the buckling and free vibration behavior of the structures. Thus, in-depth analysis on combined buckling and free vibration behavior of the cylindrical panel under non-uniform temperature variation fields needs to addressed and the present study focuses on these aspects. Later, the variation of buckling and free vibration behavior of the panels with temperature dependent and temperature independent properties of materials are also addressed in the present study. Further, it is also found from the literature that buckling strength and fundamental natural frequency of the laminated composite panel can be enhanced by optimizing the fiber orientation. Thus, laminated com-

posite cylindrical panel exposed to non-uniform temperature field is optimized for its buckling temperature and fundamental natural frequency by employing a well-known optimization approach particle swarm optimization in conjunction with an artificial neural network. Based on this, the following objectives are formulated.

- To investigate the buckling behavior of non-uniformly heated isotropic cylindrical panels by finite element approach and validation through experimentation.
- To analyze the buckling and free vibration behavior of non-uniformly heated isotropic, laminated and FG-CNT reinforced composite panels by finite element approach.
- To optimize the buckling strength and fundamental natural frequency of non-uniformly heated laminated cylindrical panel using optimization techniques viz particle swarm optimization (PSO) and artificial neural network(ANN).

Each chapter in the thesis composed of an introduction, problem formulation followed by results and discussion. At the end, the conclusion of the research work is presented to show the critical and significant outcomes. Various section of the thesis is organized and presented in the following manner.

Chapter 2 focuses on the methodology adopted to analyze the buckling behavior of non-uniformly heated cylindrical panel experimentally and numerically. Construction and working of in-house developed experimental setup are discussed in detail. The various heating position used to simulate three different non-uniform temperature variation field is also presented in this chapter. Finite element approach used to measure critical buckling temperature of the non-uniformly heated cylindrical panel is also discussed in detail. The methodology adopted to investigate the buckling and free vibration behavior of non-uniformly heated laminated cylindrical panel with and without temperature-dependent elastic properties using finite element method is also discussed in this chapter. An optimization approach to maximize the buckling strength and fundamental frequency of the panel are presented. The detailed algorithm of well-known optimization technique, particle swarm optimization, and artificial neural network are presented.

Execution of experimental setup to measure the buckling strength of the non-uniformly heated cylindrical panel is presented in chapter 3. LabVIEW program is used to control the total experimental setup and to obtain temperature-deflection data which is used to estimate critical buckling temperature. Finite element approach discussed in the previous chapter is also implemented in this section to capture temperature-deflection plot numerically. Further, temperature-deflection plot obtained experimentally and numerically are compared. This chapter also focuses on the influence of different geometrical parameters, non-uniform temperature fields and structural boundary constraints on the critical buckling temperature of the cylindrical panels.

Chapter 4 focuses on the detailed investigation on combined buckling and free vibration behavior of non-uniformly heated cylindrical panel with temperature independent properties by employing the finite element approach. Two different materials are analyzed in this chapter, namely isotropic and laminated composite. Further, the influence of different geometric parameters, structural boundary constraints and non-uniform temperature fields on buckling and free vibration behavior are studied. A factor to predict the buckling temperature of the cylindrical panel with non-uniform temperature field is also established in this chapter. Critical outcomes of the buckling and free vibration analysis of non-uniformly heated cylindrical panel are also discussed and presented in this chapter.

Studies on buckling and free vibration behavior of the non-uniformly heated cylindrical panel has been extended further in Chapter 5 with temperature dependent properties. Finite element approach is implemented to investigate the combined buckling and free vibration behavior of non-uniformly heated panel. In this chapter, two different materials are analyzed namely laminated composite and functionally graded carbon nanotubes reinforced composite. Influence of temperature dependent properties, different geometric parameters, structural boundary constraints and non-uniform temperature fields on buckling and free vibration

behavior are analyzed in this chapter. Further, chapter 5 also presents important outcomes of the buckling and free vibration analysis of non-uniformly heated cylindrical panel with temperature dependent properties.

Optimization of buckling temperature and fundamental natural frequency of non-uniformly heated laminated composite cylindrical panels are presented in chapter 6. Two different cases are discussed in this chapter, the first case focuses on optimization of buckling temperature using particle swarm optimization. Whereas the second case deals with the multi objective optimization of buckling temperature and fundamental natural frequency using particle swarm optimization in conjunction with artificial neural networks. Laminate orientation is considered as a design variable for optimization. Influence of different geometric parameters, structural boundary constraints and non-uniform temperature fields on optimum buckling strength and fundamental natural frequency are also investigated in this chapter.

The research work and significant conclusions are summarized in Chapter 7

# CHAPTER 2

## METHODOLOGY

The methodology followed to predict the critical buckling temperature through the experimental method and its comparison with finite element based numerical method is discussed in the present chapter. Further, this chapter also focuses on the methodology adopted in the numerical investigation of buckling and free vibration characteristics of the non-uniformly heated cylindrical panel with and without temperature-dependent elastic properties. At the end of this chapter, the methodology adopted in optimizing the thermal buckling load and the fundamental frequency is presented.

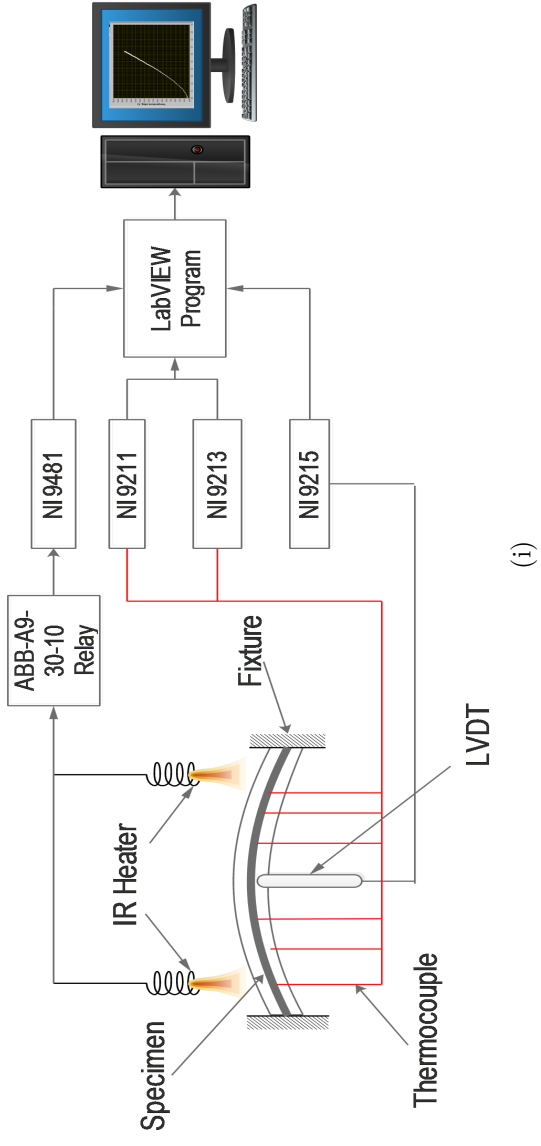
### 2.1 Experimental investigation

The critical buckling temperature of the cylindrical panel exposed to three types of non-uniform temperature fields is computed by using in-house developed experimental set-up shown in Fig. 2.1. Cylindrical panel considered for the analysis is shown in Fig. 2.2

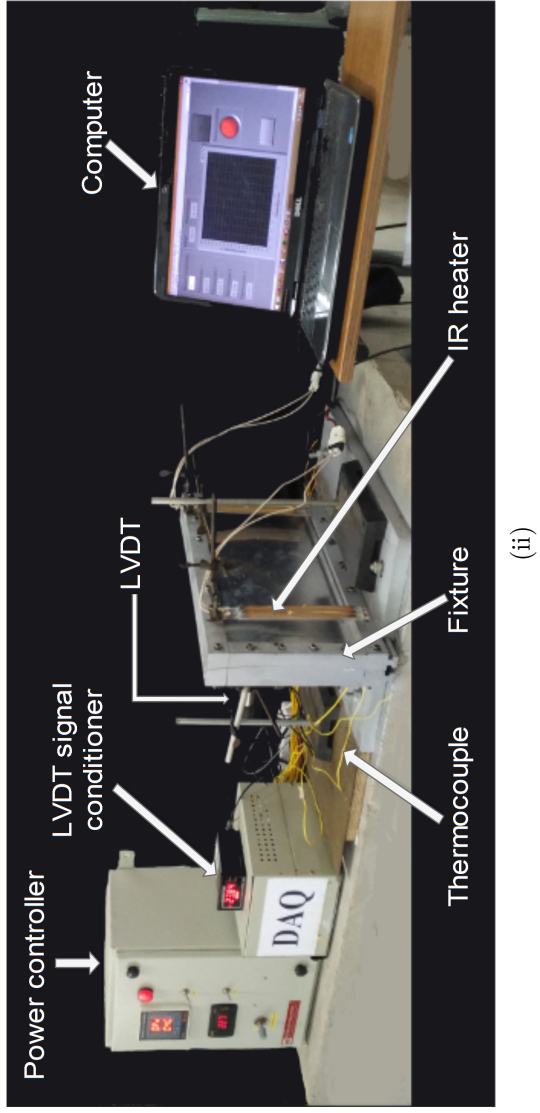
The different components that are employed in the experimental test rig are listed below along with their specification.

- **Fixture:** The in-house developed fixture is used for the conduction of experimentation. The fixture of typically a portal frame structure contains a pair of base plates, open portal frames and adjustable short segments as shown in Fig. 2.3. The dimensions of the base plates are  $0.55\text{m} \times 0.2\text{m} \times 0.025\text{m}$  with a T-slot to accommodate open portal frames of the fixture. Computerized





(i)



(ii)

Figure 2.1: Experimental setup (i) Line diagram (ii) Actual setup

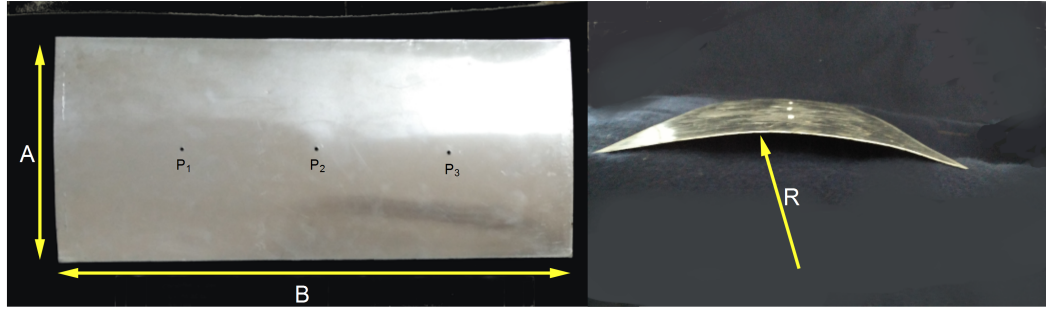


Figure 2.2: Panel considered for experimental investigation ( $A$ = width;  $B$ = length;  $R$ = curvature radius)

numerical control (CNC) machining is used to make precise T-slot. The base plates are provided with four holes for bolting it on the strong foundation base for proper fixation condition. Holes are specifically designed to allow the fixture to set for linear movement as and when required depending upon the specimen configuration. The base plates also provides sufficient space to mount Linear variable displacement transducer (LVDT) and heater stand. Open portal frames of the fixture are specially designed for a cylindrical panel with curvature ratio of 5. Dimensions of the open portal frame are length (0.55m)  $\times$  width(0.04m)  $\times$  height(0.29m). About the construction, the bottom of the open portal frames is provided with a T projection which fits in the T-slot provided in the base plates. They are also provided with a rectangular slot which runs up to 0.4m thus, allows some linear movement to the adjustable short segment. This linear movement of the adjustable short segments helps in carrying out experiments on test specimens with different aspect ratio. There were total 18 holes of diameter 0.006m equally spaced provided on the frames for the Allen bolts, which holds specimen firmly results in clamped edge boundary conditions. An adjustable short segment having rectangular projection is fitted in the rectangular slot of an open portal frame. Projection in the adjustable short segments ensures the zero rotational moments with a firm grip on the test specimen. Assembly of the fixture is done in the following manner, initially, the base plates are fixed

to the foundation with the help foundation bolts. Open portal frames of the fixture are then placed with push fit through T-slot provided for the same. Finally, adjustable short segments are fastened with the help of fasteners in the rectangular slot as per the required aspect ratio.

- **K-Type Thermocouple:** In order to measure temperature variation across the surface of the specimen of a typical cylindrical panel, thin K-type thermocouples with a sensitivity of  $41 \mu\text{V}/^\circ\text{C}$  and maximum temperature range of  $1260^\circ\text{C}$  are employed. K-type thermocouples offer certain advantages like high corrosion resistance, accurate, reliable and a wide temperature range thus used in the present study. Thermocouple welding machine is used to make bead for the K-type wire. Wherein wires are cut to the required size and then with the help of thermocouple bead making machine, a bead is made.
- **Linear Variable Differential Transducer (LVDT):** To measure the transverse displacement of the specimen at the required location, Honeywell made MVL7 LVDT with a stroke range of  $\pm 1$  inch and with an operating temperature range of  $-50^\circ\text{C}$  to  $+125^\circ\text{C}$  is employed. It is connected to the specimen with the help of small attachment made of Teflon bar to avoid the direct exposure of LVDT to high temperature.
- **Infra Red (IR) Heater:** A twin tube short wave infrared heater is used in the present study to obtain different non-uniform temperature fields. The heater is provided with gold plating which acts as reflector thus prevents heat loss from the backside and thus efficiently transfer heat onto the specimen. Heaters used are of  $3000\text{W}/240\text{V}$  with  $230\text{mm}$  of overall length and capable of producing heat up to  $900^\circ\text{C}$ .
- **Data Acquisition (DAQ):** Data in the form of temperature and displacement is recorded in a computer with the help of data acquisition systems.

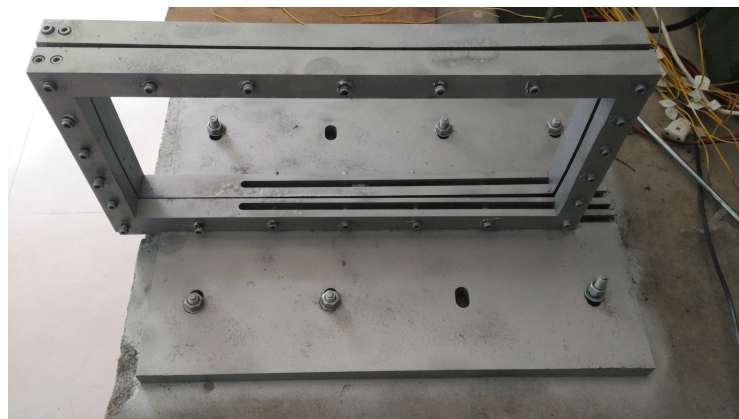
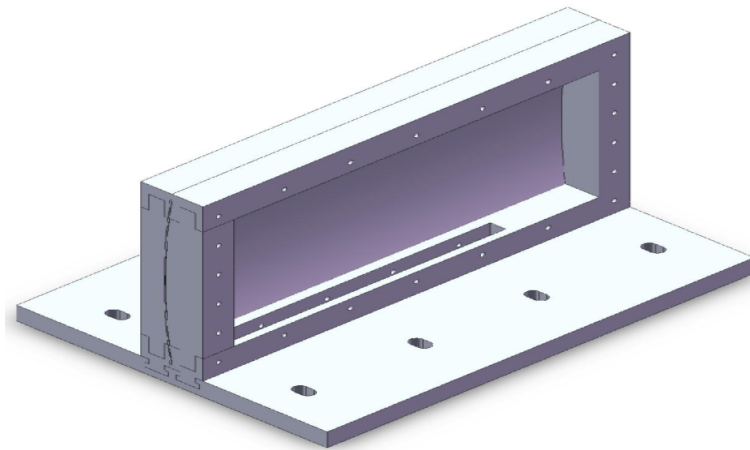
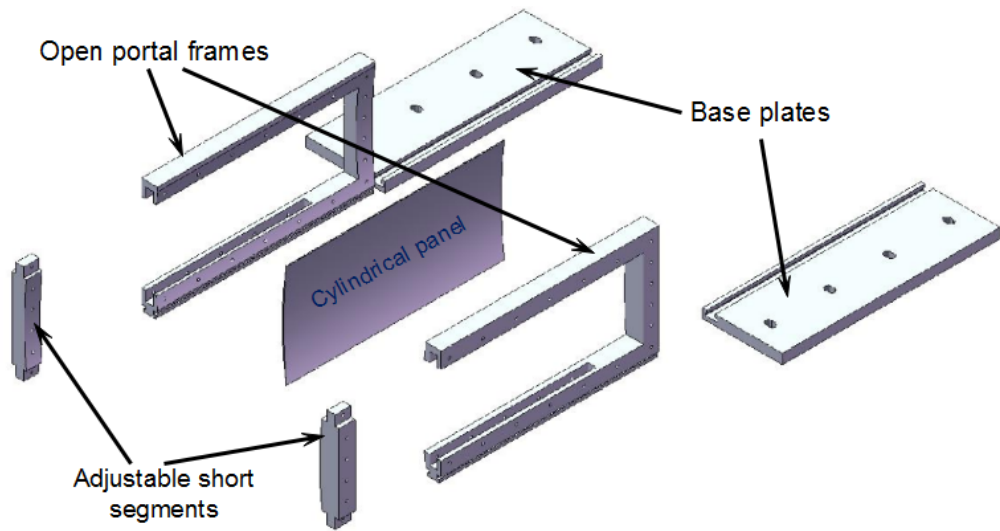


Figure 2.3: Schematic of the fixture: (i) Name of the parts (ii) Assembled fixture and (iii) Photograph

Similarly, it is also employed to control the relay used in the experimental setup. Four different Data Acquisition Modules from National Instruments(NI) that are used in setup are listed below

- **NI 9211 (Temperature measurement)**: 4-channel thermo-couple DAQ, used to measure temperature output from K type thermocouples at four different location.
- **NI 9213 (Temperature measurement)**:16-channel thermo-couple DAQ, used to measure temperature output from K type thermocouples at sixteen different location.
- **NI 9215 (Deflection measurement)**: The DAQ was used to record the displacement of the LVDT. It has four channel module which takes analog output voltage of the LVDT and the data obtained then processed further using LabVIEW software for the analysis.
- **NI 9481 (Temperature control)**: The DAQ was used to switch on/off the industrial relay which in-turn controls the IR heaters. It is typical 4-channel, single pole, single throw digital output module that gives the digital ON/OFF signal based on the LabVIEW program which triggers the industrial relay.

### 2.1.1 Working of experimental setup

Working principle of the in-house developed experimental setup used to obtain the critical buckling temperature is presented in this section.

Initially, the panels of required dimension are cut from a flat sheet and then with the help of a rolling machine, panels with required curvature ratio are prepared. An inspection is made to check the profile of the specimen and presence of any surface crack. The grid is prepared for the panel and temperature is measured at

the different grid points. Different temperature values recorded along the surface of the panel are used to obtain temperature profile for numerical investigation. Three holes of 3mm diameter are drilled onto the panel wherein, two holes are located at a distance of 100mm away from the center line while other at the center. These holes are used to fix LVDT onto the specimen with the help of nut and bolt. Adjustable short segments of the fixture are adjusted as per the required length. As mentioned before, the panels are held in the fixture by using Allen bolts. LVDT stand is placed on the base plate of the fixture and height is adjusted as per requirements. LVDT is adjusted to set the initial reading equal to zero. Infrared heaters are held in their stand mounted on the base plate of the fixture. The IR heaters can be placed at any position along the length to obtain different non-uniform temperature fields. The voltage regulator is used in the present set-up especially to control the intensity of heat radiated from the heater. DAQs are connected to a personal computer with the help of LabVIEW program. Graphical user interface of the LabVIEW is designed in such a way that, the total setup can be controlled easily with some input parameters. The experimental setup developed in-house and used to predict the buckling strength of the panels under non-uniform heating is as shown in Fig. 2.1(ii).

Once the total setup is complete then the following procedure is adopted to perform experiments:

Initially, the cylindrical panels are heated to the desired temperature by a controller supported by LabVIEW program. The IR heaters used to heat the panels through radiation and are operated till it attains the desired temperature. The temperature of the panels are then recorded with the help of K-type thermocouple. A provision is made in the fixture to accommodate cylindrical panels with different lengths and structural boundary conditions. This is achieved by adjusting the location of adjustable short segments of the fixture. Due to heating and restriction to the in-plane movements, thermal stress develops in the panels makes it to deflect out-of-plane direction and are recorded with the help of LVDT. The

variation between temperature and deflection is obtained using a LabVIEW tool till the temperature of the panels reaches to pre-set value. Once the temperature on the panel reaches the pre-set temperature an industrial relay unit switches off the heater. However, a provision also made in the program for an emergency exit. Thus, the experimental setup is operated through a LabVIEW program is as shown in Fig. 2.4. Temperature-deflection plot obtained through experiments is used to predict the critical buckling temperature.

Features of the LabVIEW program developed for the present study to record, store and process the data. A "Comparator" palette is used to compare the temperature on the panel with the pre-set temperature specified initially and accordingly gives binary output. Further, binary output from the comparator is used to switch the case structure, which then activates the NI 9481 DAQ, thus controls the ON/OFF position of the heater. LVDT data extracted from the NI 9215 is converted to root mean square value using "Statistics" palette available in LabVIEW software. "X-Y Graph" palette is used to plot data from temperature and the displacement array. There is a provision made in the program using "Write to Measuring Files" palette which saves data in a Microsoft® excel file. Once the experiment is completed, inflection point method is used to determine the critical buckling temperature from the temperature-deflection plot. At the inflection point change in concavity is observed in the temperature-deflection plot and the corresponding coordinate of the inflection point on the temperature axis determine the critical buckling temperature.

## 2.2 Numerical investigation on an isotropic panel

Cylindrical panel as shown in Fig. 2.5 with thickness ( $h$ ), mean radius of curvature ( $R$ ), length ( $B$ ) and width ( $A$ ) analyzed in the present study. An orthogonal curvilinear coordinate system ( $x, y, z$ ) is set at  $h/2$ . The in-plane displacements

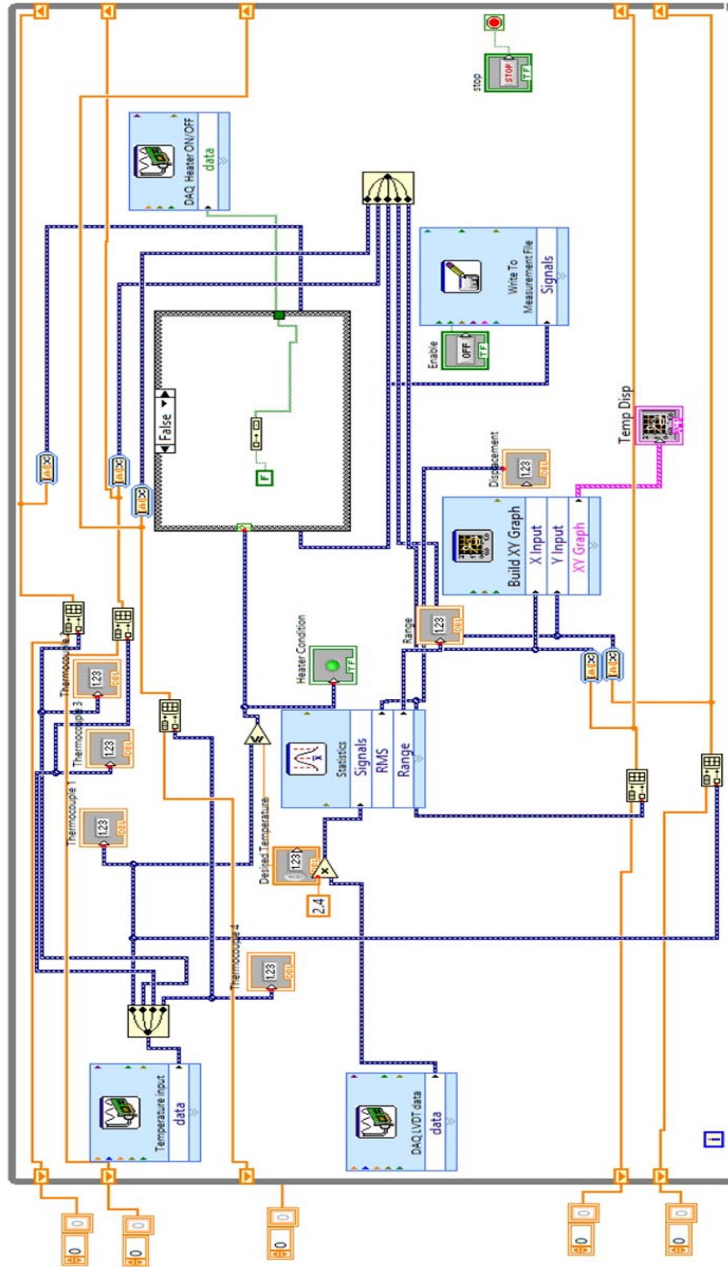


Figure 2.4: Schematic of LabVIEW program used in experimentation



are functions of  $x$ ,  $y$  and  $z$  coordinates and referred as  $u$ ,  $v$  and  $w$ . Similarly,  $\phi_x$  and  $\phi_y$  denotes the rotations about  $x$ - and  $y$ - directions. To complete, finite

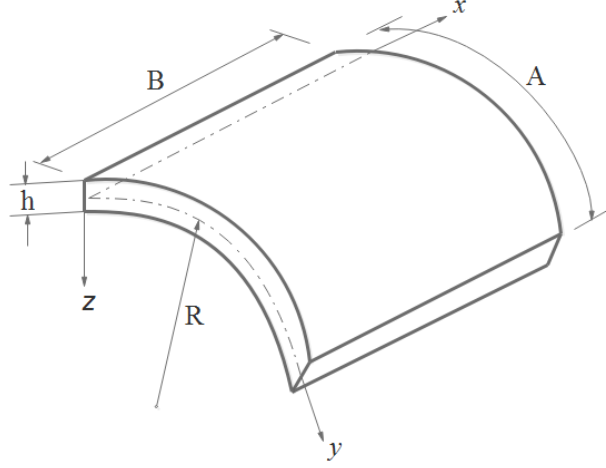


Figure 2.5: Geometry of the cylindrical panel

element formulation given by Khdeir (2012) is presented here. At any point the displacement fields  $u$ ,  $v$  and  $w$  are given by

$$\begin{aligned} u(x, y) &= u^0(x, y) + z\phi_x(x, y) \\ v(x, y) &= v^0(x, y) + z\phi_y(x, y) \\ w(x, y) &= w^0(x, y) \end{aligned} \quad (2.1)$$

where  $u^0$ ,  $v^0$  and  $w^0$  are the mid-plane displacements,  $\phi_x$  and  $\phi_y$  are rotational displacements. Strains at any point along the thickness are given by

$$\begin{Bmatrix} \varepsilon_x \\ \varepsilon_y \\ \gamma_{xy} \end{Bmatrix} = \begin{Bmatrix} \varepsilon_x^0 \\ \varepsilon_y^0 \\ \varepsilon_{xy}^0 \end{Bmatrix} + z \begin{Bmatrix} k_x \\ k_y \\ k_{xy} \end{Bmatrix} \quad (2.2)$$

where,  $\{\epsilon\}$ ,  $\{\epsilon^o\}$  and  $\{\kappa\}$  denotes the strain vector, mid-surface strain vector and curvature vector, respectively.

$$\begin{Bmatrix} \epsilon_x^0 \\ \epsilon_y^0 \\ \epsilon_{xy}^0 \end{Bmatrix} = \begin{Bmatrix} \frac{\partial u^0}{\partial x} \\ \frac{\partial v^0}{\partial y} + \frac{w}{R} \\ \frac{\partial u^0}{\partial y} + \frac{\partial v^0}{\partial x} \end{Bmatrix} \quad (2.3)$$

$$\begin{Bmatrix} k_x \\ k_y \\ k_{xy} \end{Bmatrix} = \begin{Bmatrix} \frac{\partial \phi_x}{\partial x} \\ \frac{\partial \phi_y}{\partial y} \\ \frac{\partial \phi_x}{\partial y} + \frac{\partial \phi_y}{\partial x} \end{Bmatrix} \quad (2.4)$$

The constitutive relations for an isotropic cylindrical panel considering thermal effects are related as

$$\begin{Bmatrix} \sigma_x \\ \sigma_y \\ \tau_{xy} \end{Bmatrix} = [Q] \begin{Bmatrix} \epsilon_x - \alpha \Delta T(x, y) \\ \epsilon_y - \alpha \Delta T(x, y) \\ \gamma_{xy} \end{Bmatrix} \quad (2.5)$$

where,  $[Q]$  represents stiffness matrix and  $\{\sigma_x, \sigma_y, \tau_{xy}\}^T$  represents the stress vector obtained using constitutive relations. In-plane stress resultant and moment resultant are defined as

$$N = \begin{Bmatrix} N_x \\ N_y \\ N_{xy} \end{Bmatrix} = \int_{-h/2}^{h/2} \begin{Bmatrix} \sigma_x \\ \sigma_y \\ \tau_{xy} \end{Bmatrix} dz \quad (2.6)$$

$$M = \begin{Bmatrix} M_x \\ M_y \\ M_{xy} \end{Bmatrix} = \int_{-h/2}^{h/2} \begin{Bmatrix} \sigma_x \\ \sigma_y \\ \tau_{xy} \end{Bmatrix} z dz \quad (2.7)$$

The thermal stress resultant  $\{N^T\}$  and thermal moment resultant  $\{M^T\}$  vector

generated due to the temperature gradient  $\Delta T(x, y)$  are given by

$$N^T = \begin{Bmatrix} N_x^T \\ N_y^T \\ N_{xy}^T \end{Bmatrix} = \int_{-h/2}^{h/2} [Q] \begin{Bmatrix} \alpha \Delta T(x, y) \\ \alpha \Delta T(x, y) \\ 0 \end{Bmatrix} dz \quad (2.8)$$

$$M^T = \begin{Bmatrix} M_x^T \\ M_y^T \\ M_{xy}^T \end{Bmatrix} = \int_{-h/2}^{h/2} [Q] \begin{Bmatrix} \alpha \Delta T(x, y) \\ \alpha \Delta T(x, y) \\ 0 \end{Bmatrix} z dz \quad (2.9)$$

Problem is evaluated by “ $n$ ” numbers of shell element with eight nodes per element with each nodes having six degree-of-freedom. The displacement components,  $\{U\}$  are approximated by the product of shape function matrix  $[N_i]$  and nodal displacement vector  $\{u_i\}$ .

$$\{U\} = \sum_{i=1}^8 [N_i] \{u_i\} \quad (2.10)$$

Shape functions for the 8-noded shell element as shown in Fig. 2.6 are given by

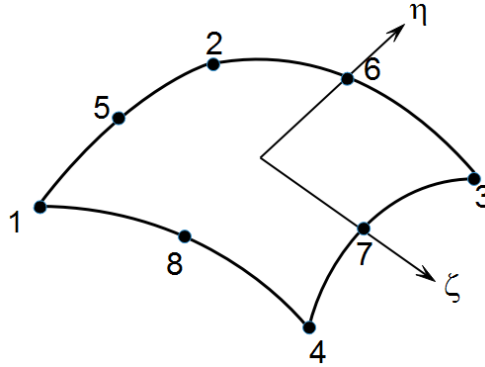


Figure 2.6: Eight noded shell element used to modeled isotropic cylindrical panel

$$\begin{aligned}
N_1 &= \frac{1}{4}(1 - \zeta)(1 - \eta)(-\zeta - \eta - 1) & N_5 &= \frac{1}{2}(1 - \zeta^2)(1 - \eta) \\
N_2 &= \frac{1}{4}(1 - \zeta)(1 - \eta)(\zeta - \eta - 1) & N_6 &= \frac{1}{2}(1 + \zeta)(1 - \eta^2) \\
N_3 &= \frac{1}{4}(1 + \zeta)(1 + \eta)(\zeta + \eta - 1) & N_7 &= \frac{1}{2}(1 - \zeta^2)(1 + \eta) \\
N_4 &= \frac{1}{4}(1 - \zeta)(1 + \eta)(-\zeta + \eta - 1) & N_8 &= \frac{1}{2}(1 - \zeta)(1 - \eta^2)
\end{aligned} \tag{2.11}$$

By implementing the standard finite element approach, structural stiffness matrix and geometric stiffness matrix are evaluated. Due to non-uniform thermal load and structural boundary constraints, membrane compressive load is developed in the cylindrical shell panel which is computed by static analysis. Static analysis is executed by applying the structural stiffness matrix  $[K]$ , the nodal displacement vector,  $\{u\}$  and the load vector due to rise in temperature,  $\{F\}$ .

$$[K]\{u\} = \{F\} \tag{2.12}$$

where, the structural stiffness matrix  $[K]$  is given by

$$[K] = \iint [B]^T [D] [B] dx dy \tag{2.13}$$

$$\{F\} = \iint [B]^T \begin{bmatrix} N^T \\ M^T \end{bmatrix} dx dy \tag{2.14}$$

where,  $[B]$  is the linear strain displacement matrix and  $[D]$  the constitutive matrix. The geometric stiffness matrix  $[K_\sigma]$  which accounts for stress developed due to thermal load is calculated from the static analysis using Eq. (2.42)

$$[K_\sigma] = \iint [G]^T \begin{bmatrix} N_{xx} & N_{xy} \\ N_{xy} & N_{yy} \end{bmatrix} [G] dx dy \tag{2.15}$$

where,  $[G]$  is evaluated from shape function by appropriate differentiation and the critical buckling temperature and its corresponding mode shape are obtained by linear buckling analysis using the structural stiffness matrix and geometric stiffness

matrices as follows

$$\left( [K] + \lambda_i [K_\sigma] \right) \{ \psi_i \} = 0 \quad (2.16)$$

where,  $\lambda_i$  and  $\psi_i$  are the  $i^{th}$  eigenvalue and associated eigenvectors, respectively. Critical buckling temperature,  $T_{max}$ , is stated as the product of the first eigenvalue,  $\lambda_1$  and the equivalent rise in temperature above reference temperature,  $\Delta T$ , i.e.  $T_{max} = \lambda_1 \Delta T$ . Physically,  $T_{max}$  is said to be the peak temperature of a particular temperature field at which any structure loses its structural stability due to thermal stresses generated in it. Fundamental buckling mode shape obtained from the eigenvalue buckling analysis used to take into account an initial geometric imperfection to perform the non-linear static structural analysis. In the present work, numerical investigations are carried out with the help of commercially available finite element software, ANSYS. A flowchart employed to carry out the numerical investigation is depicted in Fig. 2.7.

After, linear buckling analysis, a non-linear static structural analysis is performed by considering the geometric non-linearity of the panel and finally, a temperature-deflection curve is obtained. To account for geometric imperfection in the non-linear static structural analysis, buckling mode shapes found from eigenvalue buckling analysis is incorporated. In the non-linear analysis, the panel is modeled with imperfection as discussed earlier. Then temperature field obtained from the experiment is given to the panel as a thermal load in the non-linear static structural analysis. In order to do so, data obtained from the thermocouple is processed and converted to temperature by using LabVIEW software. MATLAB<sup>®</sup> curve fitting tool is used to obtain a relation between nodal coordinates and corresponding temperature which is then fed into ANSYS to perform non-linear static structural analysis as depicted in Fig. 2.8. The non-linear static structural analysis is carried out using following equation.

$$[K(u)] \{u\} = \{F\} \quad (2.17)$$

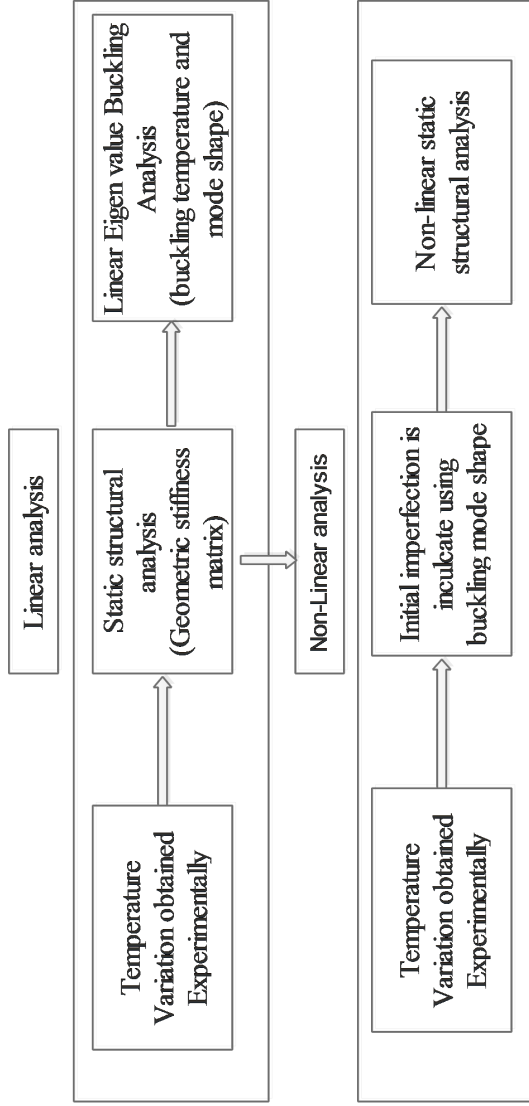


Figure 2.7: Flow chart of numerical investigation methodology

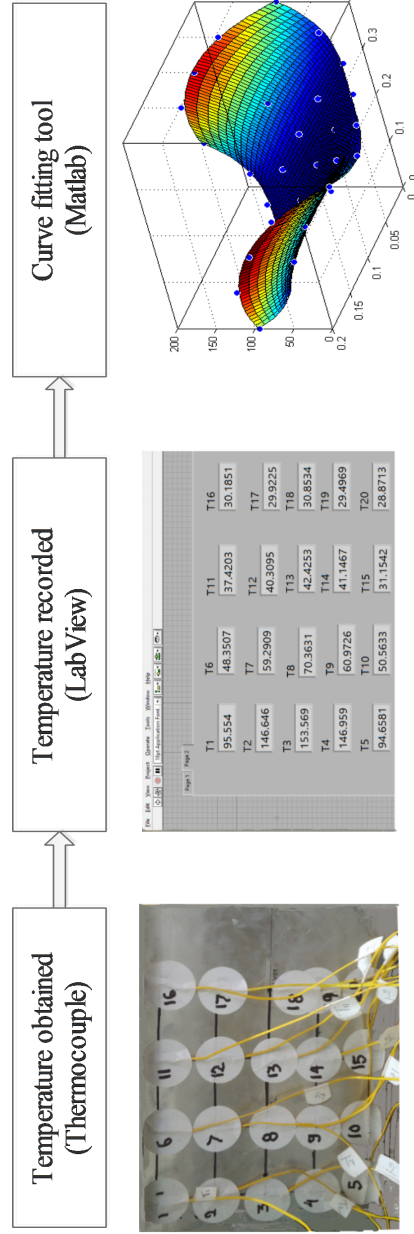


Figure 2.8: Prediction of temperature fields through experiments

where,  $[K(u)]$  is the updated stiffness matrix for each load step.

## 2.3 Numerical Investigation on laminated panel with and without temperature dependent elastic properties

In this section, the methodology followed to evaluate the buckling strength and free vibration behavior of non-uniformly heated cylindrical panel is presented. The approach comprises of three portions as shown in Fig. 2.9, in the first portion, heat transfer analysis is carried out to compute the non-uniform temperature fields. The second portion consists of static analysis wherein stress developed due to non-uniform temperature field is obtained and the last portion consists of buckling and pre-stressed modal analysis to predict the critical buckling temperature and free vibration characteristics respectively. Mathematical modeling and finite element formulation are presented in the preceding sections.

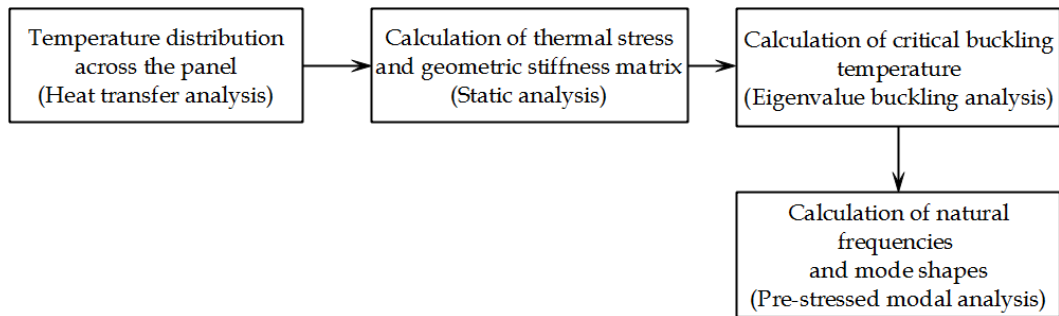


Figure 2.9: Flow chart to illustrate the numerical investigation

### 2.3.1 Finite element formulation

A cylindrical panel of width ( $S$ ), length ( $L$ ), thickness ( $h$ ) and radius ( $R$ ) measured from the mid depth of thickness shown in Fig. 2.10 is considered. An orthogonal

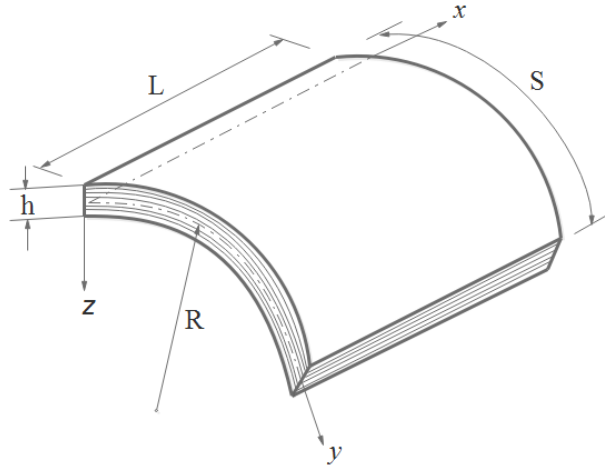


Figure 2.10: Laminated cylindrical panel analyzed

curvilinear coordinate system  $(x, y, z)$  is placed at  $h/2$  and  $L$  and  $S$  are measured along the  $x$  and  $y$  axes, respectively. The surface generated by  $x$ - $y$  is the reference surface ( $z=0$ ) and  $z$  is normal to the  $x$ - $y$  surface. In-plane displacements denoted by  $u$ ,  $v$  and  $w$  are functions of  $x$ -,  $y$ - and  $z$ -coordinates. Similarly,  $\phi_x$  and  $\phi_y$  are the rotations about  $x$ - and  $y$ - directions.

### Heat transfer analysis

For a two-dimensional differential equilibrium equation of laminated composites under steady-state heat conduction in the absence of heat generation is of the form:

$$k_{xx} \frac{\partial^2 T}{\partial x^2} + k_{yy} \frac{\partial^2 T}{\partial y^2} = 0 \quad (2.18)$$

where  $k_{xx}$  and  $k_{yy}$  are thermal conductivity in longitudinal and transverse direction, respectively, and  $T$  is the temperature. For isotropic cylindrical panel thermal conductivity in longitudinal and transverse direction is same i.e.  $k_{xx} = k_{yy}$ . The variational form of the governing Eq. (2.18) is given by

$$I = \frac{1}{2} \int_a \{\Delta T\}^T [K_c] \{\Delta T\} da + \frac{1}{2} \int_{S_1} h_1 T^2 dS - \int_{S_1} h_1 T_\infty dS - \int_{S_2} q T dS \quad (2.19)$$



where  $h_1$ ,  $\Delta T$ ,  $q$ ,  $T_\infty$ ,  $S_1$  and  $S_2$  represent the convection heat transfer coefficient, temperature gradient vector, heat flux, ambient temperature, convection heat transfer boundary and heat flux specified boundary, respectively. Heat transfer in the panel is through conduction mode, thus, Eq. (2.19) reduces to

$$I = \frac{1}{2} \iint \{\Delta T\}^T [K_c] \{\Delta T\} dx dy \quad (2.20)$$

By imposing the minimization condition to Eq. (2.20), yields

$$[K_c] \{T_e\} = \{0\} \quad (2.21)$$

where  $T_e$  is the nodal temperature vector and  $[K_c]$  is the conduction matrix. With the help of Eq. (2.21), temperature field on the cylindrical panel is obtained as per the temperature boundary constraints specified along the edges of the panel. In heat transfer analysis, the cylindrical panel under uniform and non-uniform temperature field is modeled by using an 8-noded isoparametric thermal shell element (SHELL 132). Subsequent to this, the structural analysis is carried out to get the geometrical stiffness matrix which consists of in-plane thermal stress components.

### Structural analysis

For laminated cylindrical panel, structural analysis is carried out by employing formulation which is discussed in this section.

The displacement fields  $u$ ,  $v$  and  $w$ , at any point in a shell element are given by

$$\begin{aligned} u(x, y, z) &= u_0(x, y) + z\phi_x(x, y) \\ v(x, y, z) &= v_0(x, y) + z\phi_y(x, y) \\ w(x, y, z) &= w_0(x, y) \end{aligned} \quad (2.22)$$

where  $u_0$ ,  $v_0$  and  $w_0$  are the mid-plane displacements and the linear strain-displacement relations at the mid-plane ( $z=0$  plane) are given by

$$\begin{pmatrix} \varepsilon_{xx} \\ \varepsilon_{yy} \\ \gamma_{xy} \end{pmatrix} = \{\varepsilon_0\} + z \{\kappa\} \quad (2.23)$$

$$\begin{pmatrix} \gamma_{yz} \\ \gamma_{xz} \end{pmatrix} = \{\gamma_0\} \quad (2.24)$$

where,  $\{\varepsilon_0\}$ ,  $\{\kappa\}$  and  $\{\gamma_0\}$  are the linear strain vector, curvature vector and shear strains vector respectively given by

$$\varepsilon_0 = \begin{pmatrix} \frac{\partial u_0}{\partial x} \\ \frac{\partial v_0}{\partial y} + \frac{w}{R} \\ \frac{\partial u_0}{\partial y} + \frac{\partial v_0}{\partial x} \end{pmatrix} \quad (2.25)$$

$$\kappa = \begin{pmatrix} \frac{\partial \phi_x}{\partial x} \\ \frac{\partial \phi_y}{\partial y} \\ \frac{\partial \phi_x}{\partial y} + \frac{\partial \phi_y}{\partial x} \end{pmatrix} \quad (2.26)$$

$$\gamma_0 = \begin{pmatrix} \phi_y + \frac{\partial w_0}{\partial y} - \frac{v}{R} \\ \phi_x + \frac{\partial w_0}{\partial x} \end{pmatrix} \quad (2.27)$$

The stress-strain relations for a laminated cylindrical panel considering thermal

effects are as follows:

$$\begin{pmatrix} \sigma_{xx} \\ \sigma_{yy} \\ \tau_{xy} \\ \tau_{xz} \\ \tau_{yz} \end{pmatrix} = \begin{bmatrix} Q_{11} & Q_{12} & 0 & 0 & 0 \\ Q_{21} & Q_{22} & 0 & 0 & 0 \\ 0 & 0 & Q_{66} & 0 & 0 \\ 0 & 0 & 0 & Q_{44} & 0 \\ 0 & 0 & 0 & 0 & Q_{55} \end{bmatrix} \begin{pmatrix} \varepsilon_{xx} - \alpha_{xx}\Delta T(x, y) \\ \varepsilon_{yy} - \alpha_{yy}\Delta T(x, y) \\ \gamma_{xy} \\ \gamma_{yz} \\ \gamma_{xz} \end{pmatrix} \quad (2.28)$$

where symbols used in the matrix are defined by

$$Q_{11} = \frac{E_{11}}{1 - \nu_{12}\nu_{21}}; Q_{22} = \frac{E_{22}}{1 - \nu_{12}\nu_{21}}; Q_{12} = \frac{\nu_{21}E_{11}}{1 - \nu_{12}\nu_{21}}$$

$$Q_{66} = G_{12}; Q_{44} = G_{23}; Q_{55} = G_{13}$$

$\Delta T(x, y)$  is the temperature variation along the panel surface.  $E_{11}$  and  $E_{22}$  are Young's moduli of laminated cylindrical panel in the principal material coordinates,  $\alpha_{11}$  and  $\alpha_{22}$  are coefficient of thermal expansion,  $\nu_{12}$  and  $\nu_{21}$  are Poisson's ratios and  $G_{12}$ ,  $G_{13}$  and  $G_{23}$  are the shear moduli.

The relation between stress resultants and strain obtained using usual assumptions of first order shear deformation theory is given by

$$\begin{pmatrix} N \\ M \\ Q_s \end{pmatrix} = \begin{bmatrix} A & \bar{B} & 0 \\ \bar{B} & D & 0 \\ 0 & 0 & A^S \end{bmatrix} \begin{pmatrix} \varepsilon_0 \\ \kappa \\ \gamma_0 \end{pmatrix} - \begin{pmatrix} N^T \\ M^T \\ 0 \end{pmatrix} \quad (2.29)$$

Wherein in-plane stress resultant(N), moment resultant(M) and transverse stress resultant( $Q_s$ ), respectively defined as

$$N = \begin{Bmatrix} N_{xx} \\ N_{yy} \\ N_{xy} \end{Bmatrix} = \int_{-h/2}^{h/2} \begin{Bmatrix} \sigma_{xx} \\ \sigma_{yy} \\ \tau_{xy} \end{Bmatrix} dz \quad (2.30)$$

$$M = \begin{Bmatrix} M_{xx} \\ M_{yy} \\ M_{xy} \end{Bmatrix} = \int_{-h/2}^{h/2} \begin{Bmatrix} \sigma_{xx} \\ \sigma_{yy} \\ \tau_{xy} \end{Bmatrix} z dz \quad (2.31)$$

$$Q_s = \begin{Bmatrix} Q_{xx} \\ Q_{yy} \end{Bmatrix} = \int_{-h/2}^{h/2} \begin{Bmatrix} \tau_{yz} \\ \tau_{xz} \end{Bmatrix} dz \quad (2.32)$$

The thermal stress resultant  $N^T$  and thermal moment resultant  $M^T$  are given by

$$N^T = \int_{-h/2}^{h/2} \begin{bmatrix} \alpha_{11} & \alpha_{22} & 0 \end{bmatrix} (Q_{11} + Q_{12}) \Delta T(x, y) dz \quad (2.33)$$

$$M^T = \int_{-h/2}^{h/2} \begin{bmatrix} \alpha_{11} & \alpha_{22} & 0 \end{bmatrix} (Q_{11} + Q_{12}) \Delta T(x, y) z dz \quad (2.34)$$

The extensional stiffness matrix ( $A$ ), extension-bending coupling matrix ( $\bar{B}$ ), bending stiffness matrix ( $D$ ) and transverse shear stiffness matrix ( $A^S$ ), are given by

$$\begin{pmatrix} A_{ij} & \bar{B}_{ij} & D_{ij} \end{pmatrix} = \int_{-h/2}^{h/2} Q_{ij} \begin{pmatrix} 1 & z & z^2 \end{pmatrix} dz \quad (2.35)$$

$$\left( A_{ij}^S \right) = \chi \int_{-h/2}^{h/2} Q_{ij} dz \quad (2.36)$$

where  $A_{ij}$ ,  $\bar{B}_{ij}$  and  $D_{ij}$  are defined for  $i, j=1, 2, 6$  and  $i, j= 4, 5$  in  $A_{ij}^S$ .  $\chi$  denotes the shear correction factor.

Layered structural shell element (SHELL 281) with eight nodes and six degree

of freedom per node is used. The displacement components,  $\{U\}$  are approximated by the product of shape function matrix  $[N_i]$  and nodal displacement vector  $\{q_i\}$ .

$$\{U\} = \sum_{i=1}^8 [N_i] \{q_i\} \quad (2.37)$$

Shape functions for the 8-noded shell element shown in Fig. 2.11 are as follows

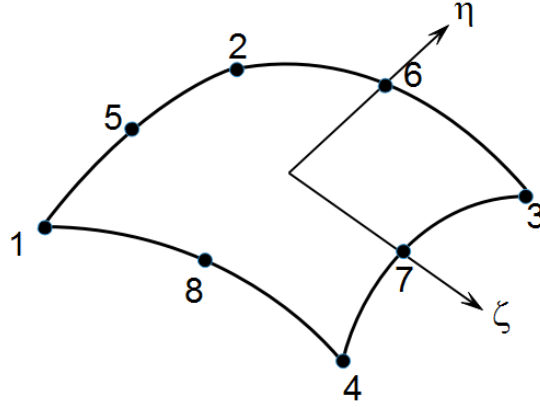


Figure 2.11: Eight-noded shell element used to modeled laminated composite cylindrical panel

$$\begin{aligned} N_1 &= \frac{1}{4}(1 - \zeta)(1 - \eta)(-\zeta - \eta - 1) & N_5 &= \frac{1}{2}(1 - \zeta^2)(1 - \eta) \\ N_2 &= \frac{1}{4}(1 - \zeta)(1 - \eta)(\zeta - \eta - 1) & N_6 &= \frac{1}{2}(1 + \zeta)(1 - \eta^2) \\ N_3 &= \frac{1}{4}(1 + \zeta)(1 + \eta)(\zeta + \eta - 1) & N_7 &= \frac{1}{2}(1 - \zeta^2)(1 + \eta) \\ N_4 &= \frac{1}{4}(1 - \zeta)(1 + \eta)(-\zeta + \eta - 1) & N_8 &= \frac{1}{2}(1 - \zeta)(1 - \eta^2) \end{aligned} \quad (2.38)$$

By following the usual finite element procedure, structural stiffness matrix, geometric stiffness matrix and mass matrix can be obtained (Jeng-Shian and Wei-Chong (1991)). The governing equation of the whole panel for static analysis is given by

$$[K] \{U\} = \{F\} \quad (2.39)$$

where  $[K]$  is the structural stiffness matrix,  $\{F\}$  is the thermal load vector and  $\{U\}$  is the nodal displacement vector. The structural stiffness matrix and thermal

load vector are given by

$$[K] = \iint [B]^T [C] [B] dx dy \quad (2.40)$$

$$\{F\} = \iint [B]^T \begin{bmatrix} N^T \\ M^T \end{bmatrix} dx dy \quad (2.41)$$

where  $[B]$  is the strain displacement matrix and  $[C]$  is the constitutive matrix which states the stress-strain relation of the material. Similarly, the geometric stiffness matrix  $[K_\sigma]$  determined from work done by the membrane forces developed due to thermal load and is given by

$$[K_\sigma] = \iint [G]^T \begin{bmatrix} N_{xx} & N_{xy} \\ N_{xy} & N_{yy} \end{bmatrix} [G] dx dy \quad (2.42)$$

where  $N_{xx}$ ,  $N_{yy}$  and  $N_{xy}$  are the membrane stresses developed due to thermal load and matrix  $[G]$  is obtained from the derivatives of shape functions. Buckling analysis are carried out on panels with temperature dependent and temperature independent properties.

### **Evaluating buckling temperature of panel with temperature independent properties:**

Buckling analysis for a panel with temperature independent properties is performed by solving the following governing equation.

$$([K] + \lambda_i [K_\sigma]) \{\psi_i\} = 0 \quad (2.43)$$

where  $\lambda_i$  is the eigenvalue and  $\{\psi_i\}$  is the corresponding eigenvector for  $i^{th}$  buckling mode. The product of the temperature rise  $\Delta T$  (above ambient temperature) and the lowest eigenvalue,  $\lambda_i$  gives the critical buckling temperature,  $T_{cr}$  (i.e.,  $T_{cr} =$

$\lambda_1 \Delta T$ ).

### Evaluating buckling temperature of panel with temperature dependent properties

Buckling analysis for a panel with temperature dependent properties is performed by using following iterative process (Malekzadeh *et al.* (2012b)).

- Step 1 Obtain the buckling temperature ( $\Delta T_{cr}$ ) of the panel with temperature-independent material properties at reference temperature  $T_0$  using Eq.(2.43).
- Step 2 Update stiffness matrix  $[K]$  by changing the property values at  $T = T_0 + \Delta T_{cr}$  to evaluate a new buckling temperature.
- Step 3 Repeat Step 2 till the thermal buckling temperature converges to a prescribed error tolerance. In the iteration process, error tolerance is given by the relative difference between the two consecutive values.

$$\varepsilon = \left| \frac{\Delta T_{cr}^{(i+1)} - \Delta T_{cr}^{(i)}}{\Delta T_{cr}^{(i)}} \right| \leq 10^{-4} \quad (2.44)$$

### Free vibration frequencies under thermal load

In order to find the effect of thermal stress on the natural frequencies and its associated mode shapes at a particular elevated temperature, pre-stressed modal analysis is carried out by using Eq. (2.45).

$$\left( ([K] + [K_\sigma]) - \omega_k^2 [M] \right) \{ \phi_k \} = 0 \quad (2.45)$$

where,  $\omega_k$  is the natural frequency of the pre-stressed structure,  $\{ \Phi_k \}$  the corresponding mode shape and  $[M]$  is the structural mass matrix defined by

$$[M] = \iint [N]^T [\rho] [N] dx dy \quad (2.46)$$

where  $[N]$  is shape function matrix and  $[\rho]$  is the inertia matrix. For static analysis panel has been modeled using an 8-noded isoparametric structural shell element (SHELL 281).

## 2.4 Optimization of buckling temperature and fundamental natural frequency

### 2.4.1 Single objective optimization

Numerical investigation on buckling of the non-uniformly heated laminated cylindrical panel is carried out to optimize its thermal buckling strength. Fig. 2.12 shows the scheme of numerical approach followed in the present work. A heat transfer analysis is initially performed to get the temperature field in accordance with the nature of thermal boundary condition, then static analysis is carried out to capture the stress field under thermal load, and finally, the eigenvalue buckling analysis is used to compute the critical buckling temperature as shown in Fig. 2.12. The present study uses particle swarm optimization (PSO) method to optimize the buckling strength of the non-uniformly heated laminated cylindrical panel. PSO code is used through the MATLAB<sup>®</sup> environment integrating it with ANSYS parametric design language (APDL) code for the optimization of thermal buckling strength. Wherein a design variable generated in PSO algorithm is written to the text file and given as an input to the APDL code. After executing the APDL code, generated result file is then imported in PSO algorithm. MATLAB<sup>®</sup> is used as an interface between APDL code and the PSO algorithm, thus it provides a way to transfer data which is in the form of input and output results.



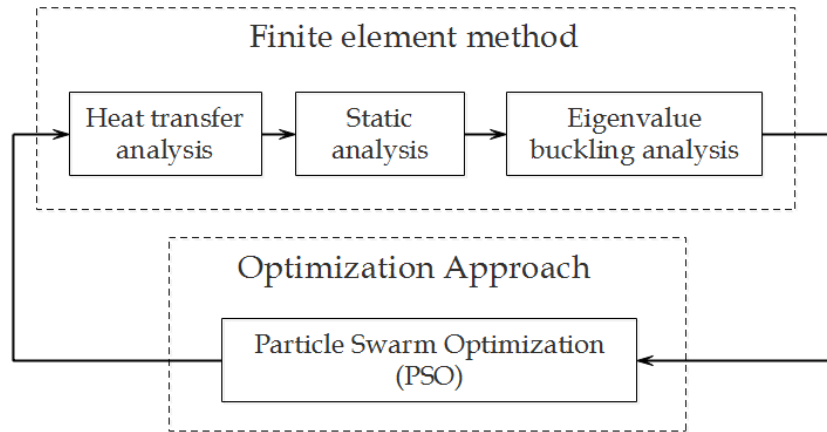


Figure 2.12: A scheme of numerical analysis followed for buckling temperature optimization

### Finite element analysis

A cylindrical panel with length ( $L$ ), thickness ( $h$ ), mean radius of curvature ( $R$ ) and width ( $S$ ) as shown in Fig. 2.10 is considered for the optimization studies. Mid-surface of the panel is used as a reference to locate an orthogonal curvilinear coordinate system ( $x, y, z$ ). As discussed in the earlier chapter, 8-noded layered isoparametric thermal shell element (SHELL 132) is employed to perform the heat transfer analysis to obtain the temperature field. Later, static structural analysis is performed by importing nodal temperature obtained through the heat transfer analysis. An 8-noded layered isoparametric structural shell element (SHELL 281) is used to perform the static analysis followed by linear eigenvalue buckling analysis which computes critical buckling temperature of the panel.

### Particle Swarm Optimization

Eberhart and Kennedy (1995) proposed a powerful evolutionary computation technique to solve optimization problems known as particle swarm optimization (PSO) method. Swarming behavior observed in schools of fish, flocks of birds, or swarms of bees is incorporated in the PSO method. PSO is simple in concept, faster in

convergence rate and easy to implement as very few parameters needs to be adjusted (Rini *et al.* (2011)). Bai (2010) given detailed algorithm of PSO method is as follows

Particle swarm optimization algorithm:

Step 1 Set PSO parameters like self-confidence factor ( $c_1$ ), swarm confidence factor( $c_2$ ), maximum iterations( $I_{max}$ ) (Shi and Eberhart (1998)).

Step 2 Initialize population of particles having positions X.

$$X_i = X_{\min} + r(X_{\max} - X_{\min})$$

where,  $X_{max}$ , upper and  $X_{min}$ , lower bounds on the design variables values and r, uniformly distributed random variable.

Step 3 Set iteration k=1

Step 4 Evaluate the fitness of each particle and the index of the best particle “b” is located.

$$F_i^k = f(X_i^k)$$

Step 5 Select the best position of each particle over time,  $P_i^k = X_i^k$  and the best global value in the swarm,  $P_g^k = X_b^k$ .

Step 6 Compute constriction factor ( $\chi$ ) to regulate the exploration and exploitation tradeoff and to ensure convergence behavior.

$$\chi = \frac{2}{|2 - \varphi - \sqrt{\varphi^2 - 4\varphi}|}$$

where  $\varphi = c_1 + c_2$

Step 7 Update velocity and position of particles using given Equations

$$v_i^{k+1} = \chi(v_i^k + c_1 r_1(p_i^k - X_i^k) + c_2 r_2(p_g^k - X_i^k))$$

where  $r_1$  and  $r_2$  are uniformly distributed random variables (0~1).

$$X_i^{k+1} = X_i^k + v_i^{k+1} \Delta t$$

where  $\Delta t$  is considered to be of a unit value.

Step 8 Evaluate fitness  $F_i^{k+1} = f(X_i^{k+1})$ ;  $\forall i$  and the index of the best particle “b<sub>1</sub>” is determined.

- Step 9 Update best position of each particle,  $p_i$  of population  $\forall i$ . If  $F_i^{k+1} < F_i^k$  then  $p_i^{k+1} = X_i^{k+1}$  else  $p_i^{k+1} = p_i^k$
- Step 10 Update best global value in the swarm,  $p_g$  of population. If  $F_{b1}^{k+1} < F_b^k$  then  $p_g^{k+1} = p_{b1}^{k+1}$  and set  $b = b_1$  else  $p_g^{k+1} = p_g^k$
- Step 11 If  $k < I_{max}$ , then  $k = k + 1$  and go to step 7 else go to step 12.
- Step 12 Print optimum solution.

## 2.4.2 Multi-objective optimization

The numerical scheme shown in Fig. 2.13 is implemented in the present study for the optimization of thermal buckling strength and the fundamental frequency of a non-uniformly heated laminated cylindrical panel. As depicted in the Fig. 2.13, numerical scheme starts with the heat transfer analysis to obtain the temperature field. Further, static analysis is performed to evaluate the stress field developed due to thermal load, and finally, an eigenvalue buckling analysis is carried out to find the critical buckling temperature. Modal analysis is also carried out on the heated panel to get its fundamental frequency. For optimizing, the present approach uses the artificial neural network(ANN) in conjunction with particle swarm optimization. A code is developed in the MATLAB<sup>®</sup> environment to integrate ANN with ANSYS parametric design language (APDL) code. Wherein ANN develops an effective network from the input and output values generated by finite element method. After successful completion of training and verification of neurons, finite element method is replaced by ANN for predicting buckling temperature and fundamental frequency for a given inputs. Replacement of finite element method by ANN ensures the reduction of computational time significantly. Particle swarm optimization (PSO) method is implemented in the present study to optimize the multi-objective problem. Wherein a design variable generated in PSO is given to ANN to extract desired output from it and fed back to PSO using MATLAB<sup>®</sup> interface. Since PSO is an iterative process, input and output data transfer from PSO to ANNs and vice versa is continuous until the optimum value is reached.

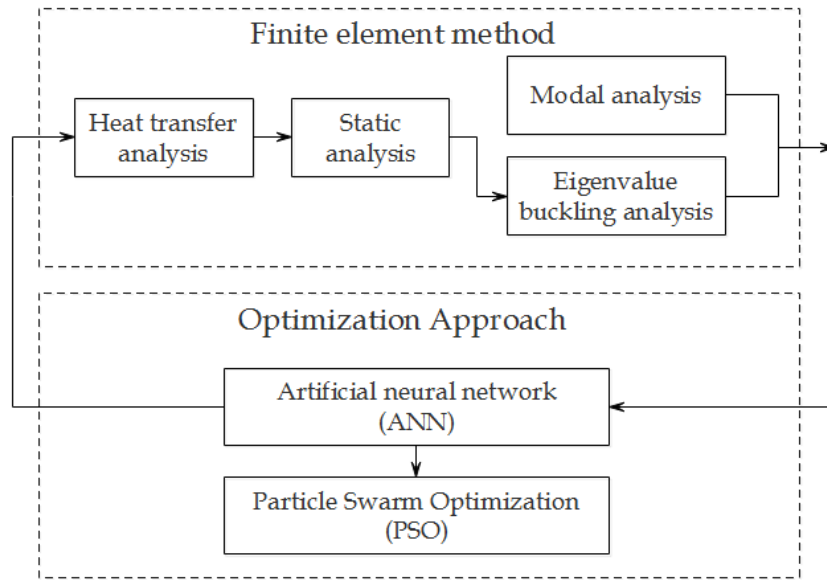


Figure 2.13: A scheme of numerical analysis followed for the multi-objective optimization

### Artificial Neural Network

Artificial Neural network(ANN) is a computing system comprising of multiple nodes, which replicates the biological neurons of the human brain. ANNs are normally arranged in layers which are composed of numerous interconnected nodes. Neurons interact with one another by connected links. Input data is given to the nodes where it is processed with simple operations and transferred to other neurons. Basically, ANNs try to gain information from previous results in order to construct a scheme of neurons that learn how to predict solution to a newly examined problem by adjusting the strength of the links between nodes. The neural networks scheme implemented in the present study is shown in Fig. 2.14. The feed-forward neural network always passes information from the first layer(input nodes) to the last layer(output nodes) through a hidden layer. Back-propagation learning algorithm, a supervised learning method is employed as a training method in the present study. Artificial neural network is implemented by using commercially available software, MATLAB®.

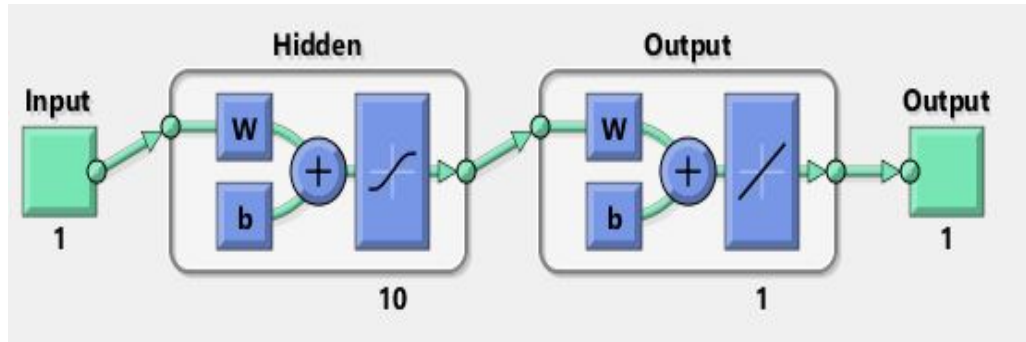


Figure 2.14: Neural network scheme employed for the analysis

## 2.5 Closure

First two section of this chapter focuses on the methodology adopted to compute critical buckling temperature of non-uniformly heated cylindrical panel experimentally and numerically. For experimentation, in-house experimental setup is developed and further, construction and working of the experimental set-up is illustrated in detail. To simulate different non-uniform temperature fields, heaters are placed at a different location along the length of the panel is presented in the form of figures. In the case of a numerical method, governing equations required to compute the critical buckling temperature are also presented. Further, the non-linear static structural analysis is employed to consider imperfection in the materials and same has been represented with the help of a flowchart. Later, the methodology followed to investigate buckling and free vibration behavior of non-uniformly heated cylindrical panel with temperature dependent and temperature independent properties are discussed with the mathematical formulation. This chapter also presents a methodology employed to optimize the buckling and fundamental natural frequency of non-uniformly heated cylindrical panel. Wherein well-known techniques like artificial neural network and particle swarm optimization are discussed. The methodology discussed in the present chapter are employed to investigate buckling and free vibration behavior in the following subsequent chapters.

## CHAPTER 3

### EXPERIMENTAL INVESTIGATION

A detailed description of the experimental setup developed in-house and the methodology followed for experimental and numerical investigation on buckling behavior of non-uniformly heated cylindrical panels are briefly discussed in the previous chapter. While present chapter discusses the experimental investigation carried out on an aluminum cylindrical panels subjected to non-uniform heating.

#### 3.1 Geometry of the cylindrical panel analyzed

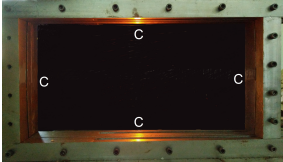
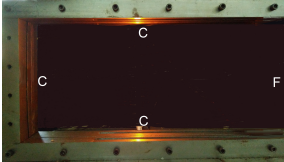
Considering the design constraints associated with the fixture developed for the experimental investigation, cylindrical panels with thickness ( $h$ )=2mm, thickness ratio ( $A/h$ )=100, and curvature ratio ( $R/A$ )=5 are prepared. Further to investigate the influence of aspect ratio on the buckling behavior, panels with two different aspect ratios ( $B/A$ )= 2 and 2.5 are considered. Panel with an aspect ratio of 2 is represented as panel-1 whereas the panel with an aspect ratio of 2.5 is represented as panel-2. Aluminum, being light weight and considering its potential applications in aerospace industries, the cylindrical panels made up of aluminum are considered for the investigation. Mechanical properties are as follows; Young's modulus ( $E$ )=69 GPa, Poisson's ratio ( $\mu$ )=0.3 and coefficient of thermal expansion ( $\alpha$ )= $22.5 \times 10^{-6}$  / $^{\circ}\text{C}$ . To prepare cylindrical panel with prescribed curvature, the manual rolling machine is used. The cylindrical panel considered for the investigation is shown in Fig. 2.2. Small holes are drilled through the panels at three different positions to know the influence of non-uniform temperature fields on buckling behavior at a different location of the panel. In Fig 2.2,  $P_1$ ,  $P_2$  and  $P_3$

indicates three different locations of the small holes drilled on the panel to obtain temperature-deflection plot.

### 3.2 Structural boundary constraints

Results obtained based on the numerical investigation presented in open literature, shown that the thermal buckling strength of cylindrical panels is significantly influenced by nature of structural boundary constraints. However, the corresponding experimental results are very limited. In order to analyze the influence of structural boundary constraints experimentally, panels are investigated under CCCC and CCFC (C-clamped edge and F-free edge) boundary constraints. The first letter in these boundary constraints is related to forefront curved edge at  $x=0$  in order. CCCC panels are analyzed to investigate the effect of complete restriction to in-plane expansion due to heating while CCFC panels are analyzed to investigate the effect of free expansion on buckling due to heating. Fixture developed can be used to simulate both CCCC and CCFC boundary constraints by adjusting its adjustable small segments as shown in Table 3.1.

Table 3.1: Adjustable small segment positions to simulate boundary constraints.

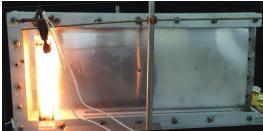
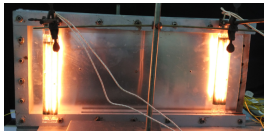
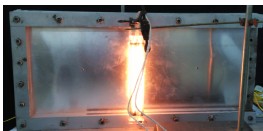
CCCC	CCFC
	
Adjustable small segment at right edge	Adjustable small segment at right edge is removed

### 3.3 Non-uniform temperature profiles

As discussed earlier, in real life applications most of the structures are exposed to non-uniform temperature field while in service. To analyze the influence of nature

of non-uniform temperature field on the buckling behavior, three different non-uniformly varying in-plane temperature fields are considered in the present study. Temperature variation fields are achieved by keeping the infra-red(IR ) heaters at different locations as given in Table 3.2. Depending on the location of IR heaters, three different temperature fields as shown in Table 3.2 are obtained: Case(a)-decreasing trend in temperature field; Case(b)-decreasing and increasing trend in temperature field; and Case(c)-increasing and decreasing trend in temperature field. The temperature field for Case(a) is obtained experimentally by placing the IR heaters at the left edge of the panel ( $x = 0$ ), whereas, temperature field for Case(b) is obtained by placing IR heater on the left and right edges of the panel ( $x = 0$  and  $x = B$ ) and Case(c) is obtained by keeping the IR heater at the center of the panel ( $x = B/2$ ). Measured temperatures at different locations on the panel are input to the curve fitting program developed using MATLAB<sup>®</sup> which is processed further to obtain different non-uniform temperature fields. Non-uniform temperature fields obtained using MATLAB<sup>®</sup> curve fitting tool are shown in Table 3.3 and are used for numerical investigation

Table 3.2: IR heater positions to simulate different temperature fields.

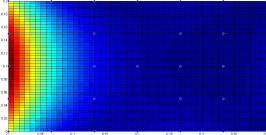
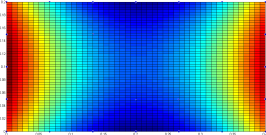
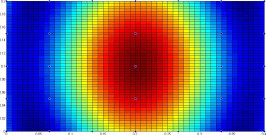
Case(a)	Case(b)	Case(c)
		
Heater position at left edge ( $x = 0$ )	Heaters position at left and right edge ( $x = 0; x = B$ )	Heater position at the center ( $x = \frac{B}{2}$ )

### 3.4 Inflection point method

In the present study, temperature deflection plots obtained through experiments are used to determine the critical buckling temperature of the panels. To determine the critical buckling temperature from temperature deflection plot, inflection



Table 3.3: Variation of temperature fields in a cylindrical panel computed using numerical approach.

Case(a)	Case(b)	Case(c)
		
Heater at left edge ( $x = 0$ )	Heater at left and right edge ( $x = 0; x = B$ )	Heater at the center ( $x = \frac{B}{2}$ )
Note: Dark-red: peak temperature, dark-blue: minimum temperature and other: in-between		

point method (Shariyat (2007), Czapski and Kubiak (2015)) is being employed. Sudden change in the slope of the temperature-deflection plot obtained for non-uniformly heated panels denotes critical buckling temperature. Fig. 3.1 depicts the computation of critical buckling temperature from the temperature-deflection plot recorded for a panel-2 at  $P_2$  exposed to Case(c) temperature field.

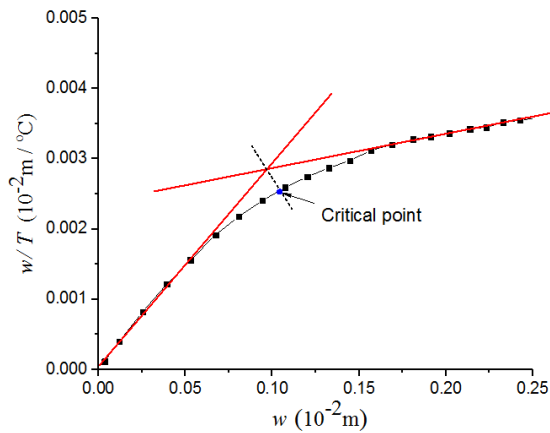


Figure 3.1: Inflection point method to obtain critical buckling temperature

### 3.4.1 Repeatability test of experiments

In order to check the repeatability of experiments, a number of trials of experiments are performed for a particular heating condition and for every trial untested specimen is used. Temperature-deflection plots for the three trials and correspond-

ing buckling temperature are compared to check the repeatability of experiments. For this purpose, the panel-2 with CCCC boundary constraints is analyzed and temperature-deflection plots are obtained at location  $P_1$  for case(a) and case(b) temperature field and at  $P_2$  for case(c) temperature field. Temperature-deflection plots obtained for non-uniformly heated cylindrical panels under three different trials are shown in Fig. 3.2. From Fig. 3.2, it is clear that, for a given temperature fields, the trend of temperature-deflection plots are almost identical for all the three different trials under identical conditions. It is also observed that the variations between three different trials are not significant. Similarly, critical buckling temperature obtained from the temperature-deflection plots using inflection point method for different trials are compared in Table 3.4. As expected, critical buckling temperature obtained for different experimental trials performed under identical conditions matches very well with each other.

Table 3.4: Critical buckling temperature of panel-1 obtained from different set of experiments

Temperature fields	Critical buckling temperature, °C		
	Exp. 1	Exp. 2	Exp. 3
Case(a)	45.65	47.43	46.68
Case(b)	43.20	44.22	45.12
Case(c)	38.45	43.43	40.21

### 3.5 Comparison of experimental and numerical results

Panels (panel-1 and panel-2) with CCCC boundary constraints, subjected to three types of temperature fields are considered for the comparison of experimental and numerical results. For the numerical investigation, the cylindrical panels are modeled using an 8-noded, structural shell element, SHELL281, present in ANSYS. SHELL281 has six degrees of freedom (three translation and three rotational) at

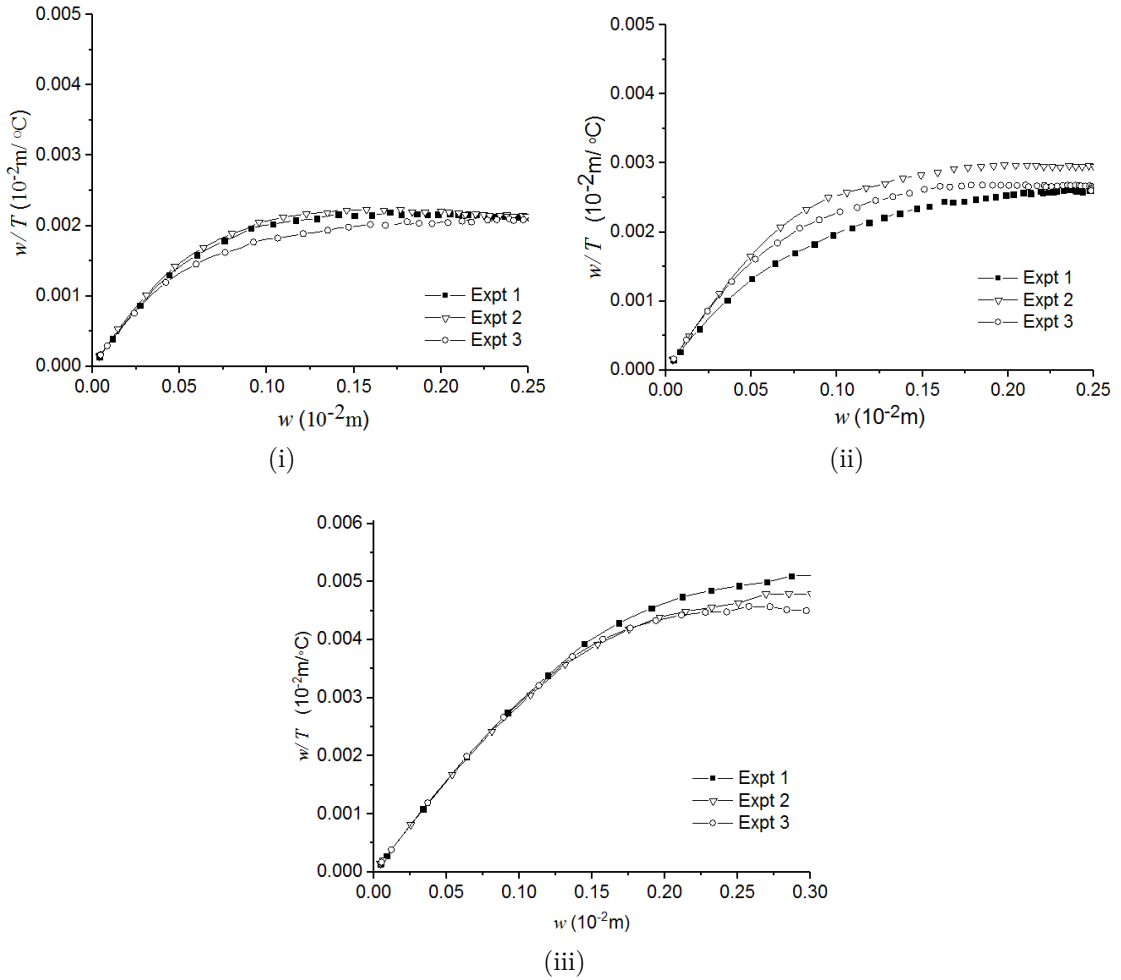


Figure 3.2: Temperature-deflection plot measured nearer to the heat source in panel-2 with temperature fields of type, (i) Case(a), (ii) Case(b) and (iii) Case(c)

each node. Temperature data corresponding to a particular type of heating are obtained from the experiment using thermocouple and LabVIEW program are given to the curve fitting tool available in MATLAB®. This temperature field is given as an input to the numerical analysis. Then the linear static structural analysis is performed to evaluate the thermal pre-stress. Then the linear eigenvalue buckling analysis is used to obtain the critical buckling temperature (lowest eigenvalue) and buckling mode shape (lowest eigenvector). Finally, the non-linear static structural analysis is carried out considering the imperfection of  $(1/n)^{th}$  of each buckling mode shape, where  $n$ , is the number of buckling modes extracted in linear buckling analysis. This ensures the elimination of the biased situation associated with first buckling mode shape.

Temperature-deflection plots obtained from a CCCC panel-1 exposed to non-uniform temperature fields using experimental approach is compared with the numerical approach as shown in Fig. 3.3. It is clear that experimentally obtained temperature-deflection plot matches very well with that of the numerically predicted plot. In order to confirm the numerical validation further, panel-2 with CCCC boundary constraint is also investigated and results are compared in Fig. 3.4. It is found that the plots obtained numerically and experimentally are in good agreement. It is also found that deflection obtained with the rise in temperature increases nonlinearly irrespective of temperature fields due to thermal stress.

Inflection point method is employed to find critical buckling temperature from the temperature-deflection plot and results are given in Table 3.5. It is observed that numerical results matches very well with that experimental results. It is also noted that critical buckling strength of the panel-2 is lower than the panel-1 due its lower stiffness. Further, significant variation in the buckling strength is noted for panels exposed to different temperature fields, thus it is concluded that nature of temperature variation influences thermal buckling strength of the

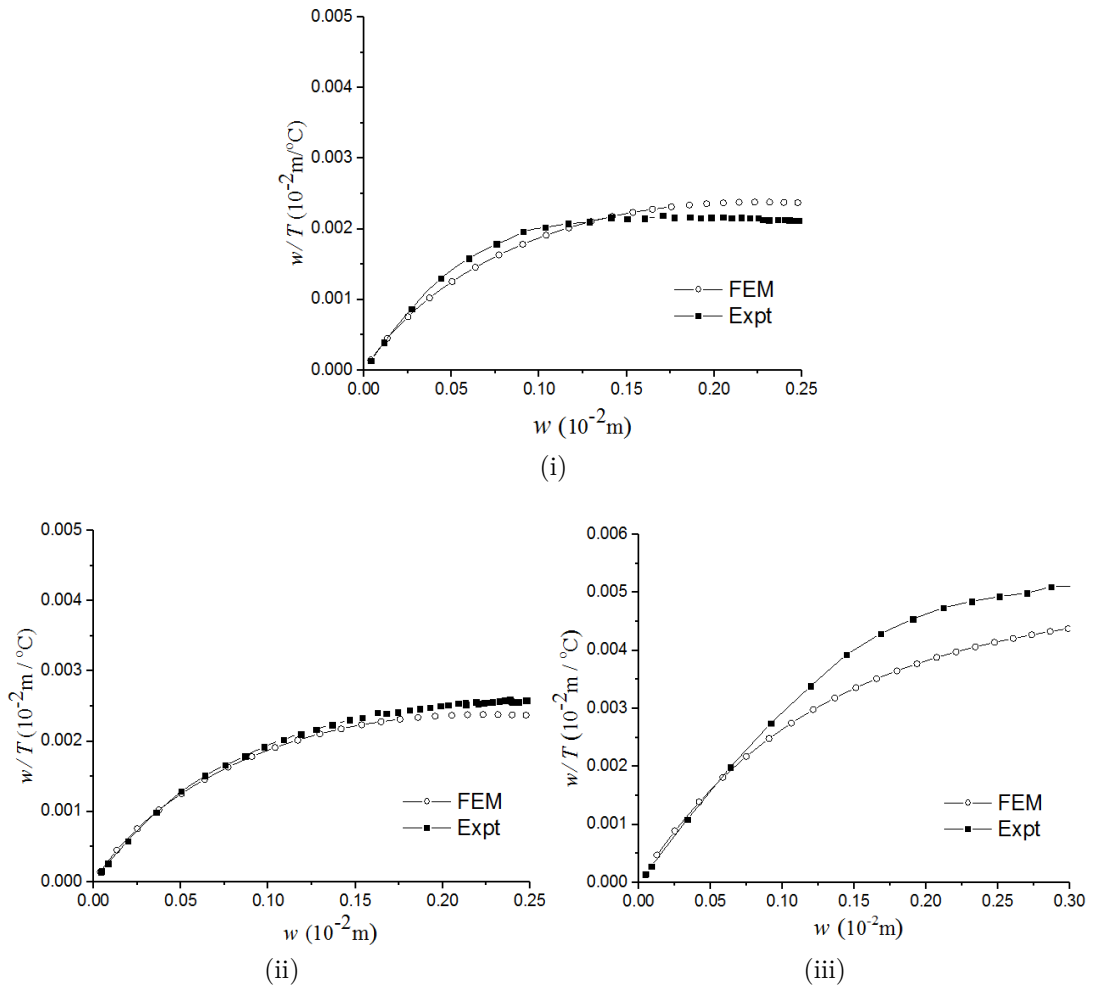


Figure 3.3: Comparison of numerical results with experimentation for CCCC cylindrical panel-1 with temperature fields of type, (i) Case(a), (ii) Case(b) and (iii) Case(c)

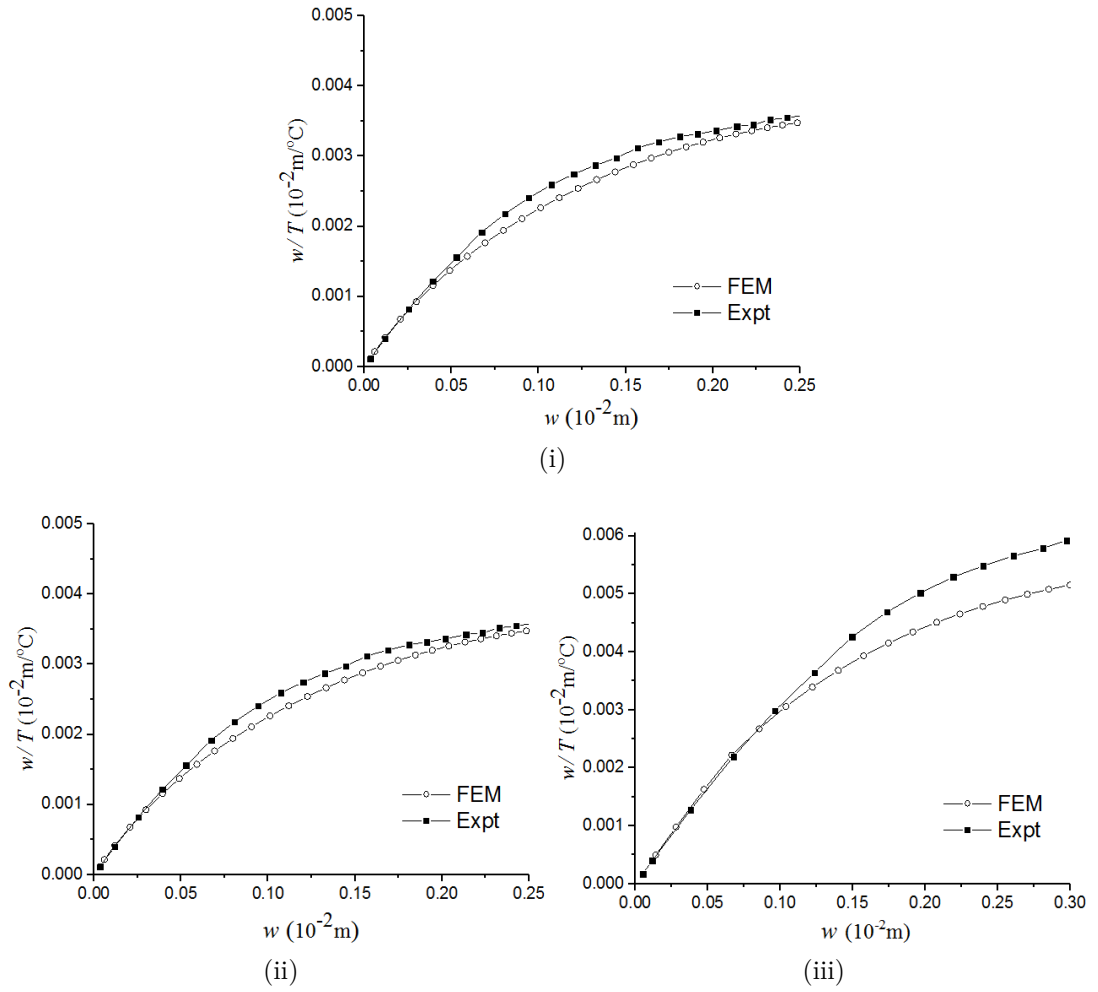


Figure 3.4: Comparison of numerical results with experimentation for CCCC cylindrical panel-2 with temperature fields of type, (i) Case(a), (ii) Case(b) and (iii) Case(c)

panels. Panels exposed to case(c) temperature field are observed to have lowest buckling strength irrespective of the aspect ratio. Whereas panels under case(a) temperature field are noted to have highest buckling strength. The panels under case(c) temperature field has a heat source located exactly at the less stiff area (at the center of the panel) thus, requires less membrane force to buckle. Whereas, the panel with case(a) has a heat source located at the more stiff area (close to clamped edge) thus found to have high buckling strength. Further, buckling strength of the panels with case(b) temperature field lies between the buckling strength of panels with case(a) and case(c). Case(b) temperature field has two heaters located at clamped edges (more stiff area) of the panel. Presence of two heaters in case(b) temperature field, develops more membrane forces compared to one heater in case(a) temperature field, thus panel under case(b) temperature field is observed to have low buckling strength compared to case(a) temperature field. Since both the heaters are located at a more stiffer area, case(b) temperature field has high buckling strength compared to case(c) temperature field. Data from Table 3.5 confirms the importance of heating source location and resulting temperature fields in deciding the buckling strength of the panels.

Table 3.5: Comparison of critical buckling temperature, °C obtained experimentally and numerically

Temperature field	Panel-1			Panel-2		
	FEM	Experiment	Diff.(% )	FEM	Experiment	Diff.(% )
Case(a)	47.43	48.75	2.70	40.38	42.01	3.88
Case(b)	44.22	46.59	5.09	35.48	37.33	4.95
Case(c)	40.21	42.30	4.94	34.33	35.25	2.60

Influence of aspect ratio of the panels on temperature-deflection plot associated with CCCC panel with different temperature fields is shown in Fig. 3.5. From Fig. 3.5 it is clear that panels with higher aspect ratio (panel-2) result in higher deflection compared to panel-1 which has relatively lower aspect ratio. This can be attributed to variation in structural stiffness with the aspect ratio of the panel. The panels under case(a) temperature field are noted to have less deflection

compared to other temperature fields. Under case(a), less amount of membrane compressive forces is developed as less amount of portion of the panel exposed to the higher intensity of heat as the heater is located at one edge of the panel with case(a) temperature field. Whereas for case(b) temperature field, the heat source is located on either edge of the panels, thus generates the high amount of membrane compressive force. Case(a) and case(c) temperature fields have only one heating source thus amount of compressive force generates is same in both cases, still, the panel under case(c) deflects more compared to case(a). This indicates that along with the intensity of the heating source, the location of the heat source also plays an important role in deciding the thermal buckling strength of the panel under non-uniform thermal load.

Table 3.6 shows the influence of aspect ratio on the critical buckling temperature of panel-2 exposed to non-uniform temperature fields. It is seen from Table 3.6 that panel-2 has lower buckling strength compared to panel-1 irrespective of temperature fields which mainly due to low stiffness associated with it. Further, panels exposed to case(c) temperature field gives the least buckling strength whereas highest buckling strength is observed with case(a) temperature field.

Table 3.6: Influence of aspect ratio on critical buckling temperature, °C

Temperature fields	Aspect ratio	
	B/A=2	B/A=2.5
Case(a)	47.43	40.38
Case(b)	44.22	35.48
Case(c)	40.21	34.33

Structural boundary constraints play a significant role in developing membrane forces along with the nature of temperature fields. Fig. 3.6 shows the influence of structural boundary constraints on the deflection of the panel-2 exposed to non-uniform temperature field. Two boundary constraints are considered in the present study namely, CCCC and CCFC. Panel-2 under case(a) temperature field is observed to have the same deflection under both CCCC and CCFC bound-



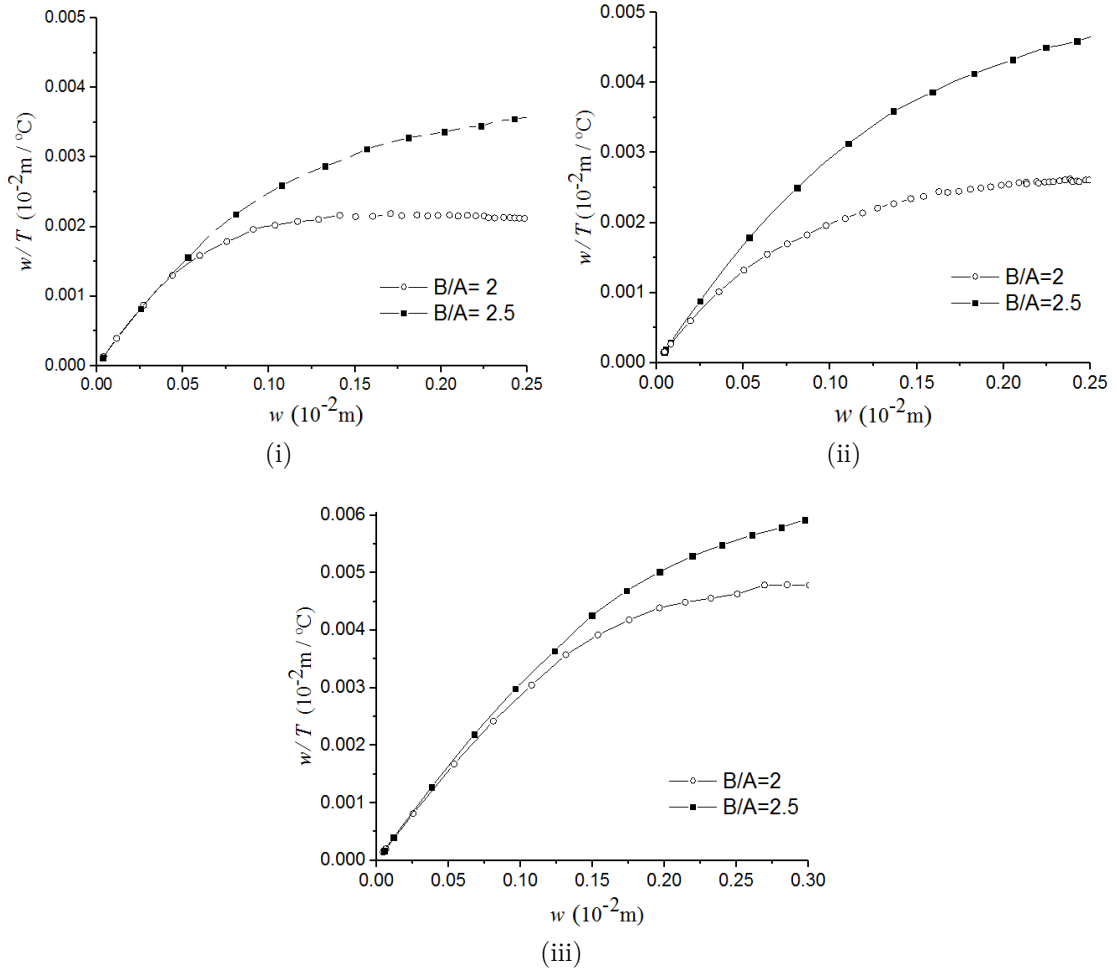


Figure 3.5: Influence of aspect ratio on temperature-deflection plots obtained for panels with temperature fields of type, (i) Case(a), (ii) Case(b) and (iii) Case(c)

ary constraints. Influence of free edge on the panel-2 is negligible under case(a) temperature field due to the location of heat source at the edge opposite to the free edge. For the CCFC panel compressive force generated at the heating, edge vanishes as it moves away from the heat source. Panel-2 exposed to case(b) temperature field is noted to have less deflection under CCFC boundary constraint compared to CCCC. As expected, panel-2 exposed to case(b) temperature field, some of the thermal stress generated releases from the free edge. Heating source under case(c) temperature field is closer to the free edge compared to case(a), decrements in the deflection are noticed under CCFC boundary constraint. It is

concluded that temperature fields along with boundary constraints, significantly influences the buckling behavior of the panel.

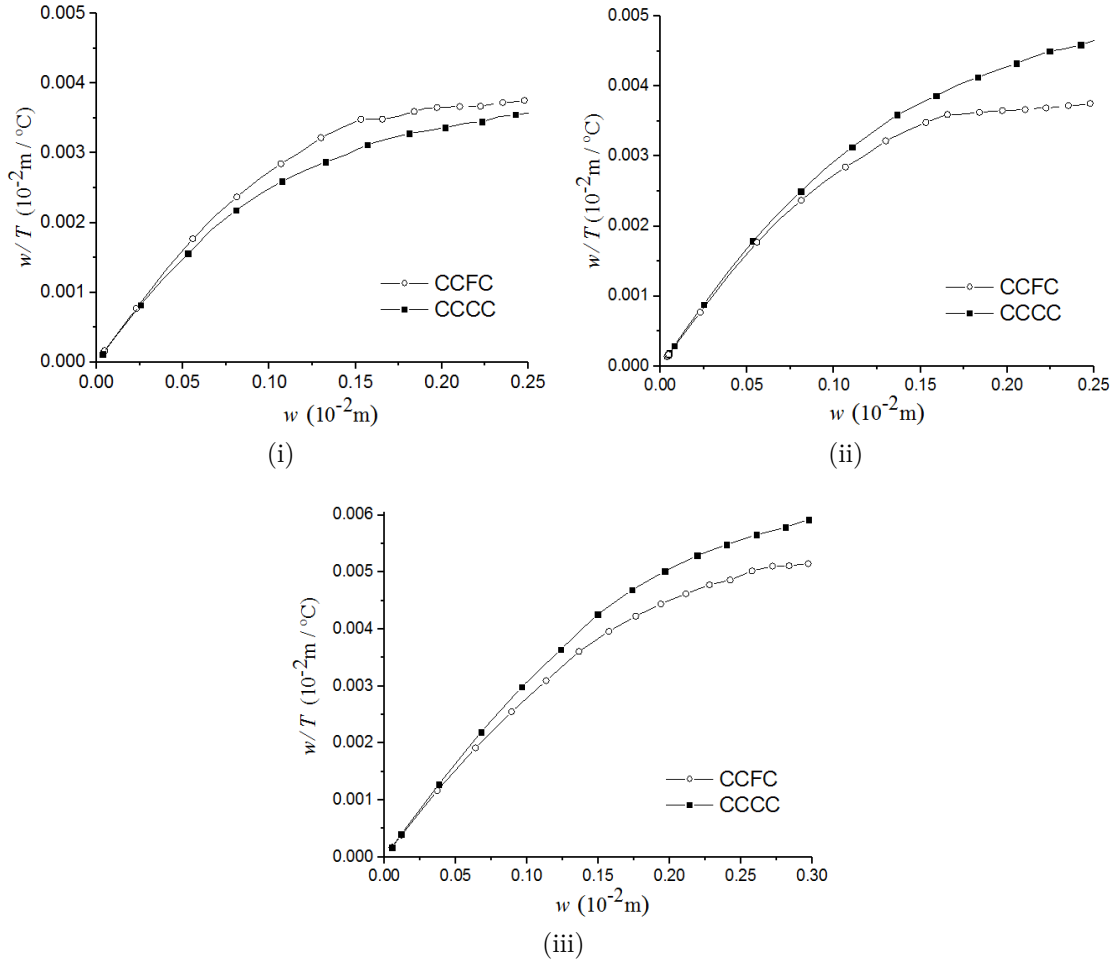


Figure 3.6: Influence of boundary constraints on temperature-deflection plots obtained for panel-2 with temperature fields of type, (i) Case(a), (ii) Case(b) and (iii) Case(c)

Table 3.7 shows the influence of structural boundary constraints on critical buckling temperature of panel-2 exposed to non-uniform temperature field. It is seen from Table 3.7 that, panel-2 with CCFC boundary constraints has high buckling strength compared to the panel with CCCC boundary constraint. This is mainly due to relaxation of thermal stress from the free edge which develops less membrane forces. Further, it is noted that panel exposed to Case(c) temperature field has low buckling strength wherein heat source is located at a center of the

panel having low stiffness.

Table 3.7: Influence of boundary constraints on critical buckling temperature, °C of panel-2

Temperature fields	Boundary constraints	
	CCCC	CCFC
Case(a)	40.38	41.17
Case(b)	35.48	38.17
Case(c)	34.33	37.08

### 3.6 Closure

Buckling behavior of non-uniformly heated aluminum cylindrical panel is investigated experimentally. The numerical results predicted based on finite element method are in good agreement with the experimentally predicted values. Cylindrical panels with two different aspect ratios namely panel-1 and panel-2 are analyzed. Effect of three different non-uniform temperature fields on buckling temperature are analyzed. Inflection point method is employed to evaluate critical buckling temperature from temperature deflection plot obtained through experimental method. It is also noted that critical buckling strength of the panel-2 is lower than the panel-1 due its higher aspect ratio thus results in lower stiffness. Results revealed that non-uniform temperature fields significantly influence the buckling behavior of the panel thus play a significant role in deciding the buckling strength. Panels exposed to Case(c) temperature field are observed to have lowest buckling strength whereas panels under Case(a) temperature field are noted to have highest buckling strength. Buckling behavior at three different location of the panels has also been investigated and it is found that deflection of the panels does changes with the location. Further, effects of structural boundary constraints on the buckling behavior are also analyzed experimentally. Buckling temperature noted for CCFC boundary constraints is higher than the CCCC.

## **CHAPTER 4**

# **STUDY OF CYLINDRICAL PANEL WITH TEMPERATURE INDEPENDENT PROPERTIES**

### **4.1 Introduction**

Experimental investigation revealed that, the buckling behavior of the non-uniformly heated cylindrical panel is significantly influenced by the nature of temperature fields and the geometrical parameters. Considering this behavior of the panel, studies have been further extended, to investigate the influence of non-uniform temperature fields on free vibration behavior of the cylindrical panel. Considering the difficulties associated with the experimental investigation for different sets of experiments, all further investigation are carried out using numerical approach. Free vibration behaviors of the cylindrical panel play a vital role in the design stage of the structures. Present chapter deals with the in-depth analysis on combined buckling and free vibration behavior of the cylindrical panel under non-uniform temperature fields. Studies are carried out on isotropic and laminated composite cylindrical panels.

### **4.2 Variation of temperature fields**

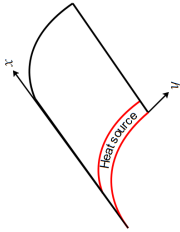
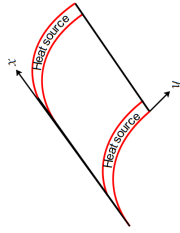
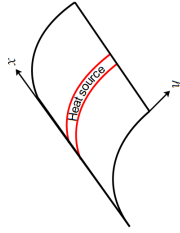
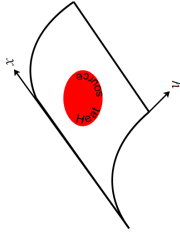


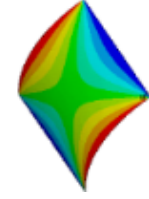
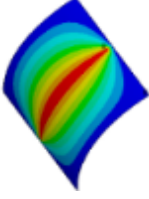
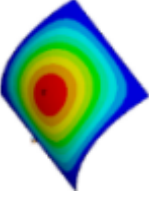
Depending on the assumed location of the temperature source, four variants of non-uniform in-plane temperature fields are considered in the present study. Further,

the panel is also analyzed under uniform temperature field for the comparison purpose. In the present study, different temperature fields considered are as follows; Case(a)-uniform temperature field; Case(b)- decreasing trend in temperature field; Case(c)- decreasing and increasing trend in temperature field; Case(d)-increasing and decreasing trend in temperature field and Case(e)-Camel hump trend in temperature field. Table 4.1 shows a cylindrical panel with the position of the heat source, associated temperature fields, and thermal boundary constraints.

### 4.3 Structural boundary constraints

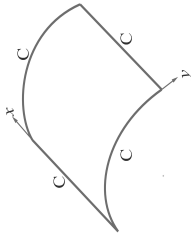
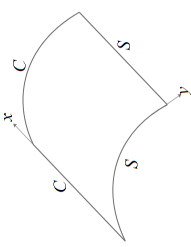
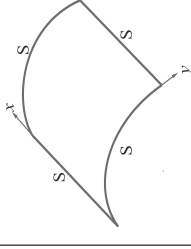
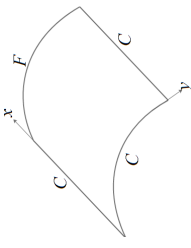
As noticed from the analysis carried out in the preceded section, buckling behavior of the panel is significantly influenced by structural boundary constraints. It is difficult to predict the boundary constraints associated with the structures in real life applications, thus to simulate real life situation cylindrical panel is investigated under four different structural boundary constraints namely CCCC, SSCC, SSSS and CCFC (where C- clamped edge, S-simply supported edge and F-free edge). First letter in these boundary constraints is related to forefront curved edge at  $x=0$  in order(Table 4.2). To understand the influence of complete restriction of in-plane expansion on the buckling strength of cylindrical panel, CCCC boundary constraint is considered. In order to investigate the effect of relaxed boundary constraints, SSSS panel is considered and SSCC panel is considered to investigate the effect of combined relaxed and completely constrained boundary constraint. The behavior of a heated panel which allows in-plane free expansion will be different from that of a panel with restriction of in-plane free expansion. So, CCFC panel which allows free expansion along the heating direction is also considered.

Table 4.1: Cylindrical panel with location of heat source

Description	Variation of temperature fields $T(x, y)$				
	Case(a)	Case(b)	Case(c)	Case(d)	Case(e)
Position of heat source	Uniform				
Temperature distribution					
Boundary constraints	$T(x,y) = 1^{\circ}C$	$T=0^{\circ}C$ at $y=0; y=S$ $T=1^{\circ}C$ at $x=0$ $T=0^{\circ}C$ at $x=L$	$T=0^{\circ}C$ at $y=0; y=S$ $T=1^{\circ}C$ at $x=0; x=L$	$T=0^{\circ}C$ at $y=0; y=S$ $x=0; x=L$ $T=1^{\circ}C$ at $x=L/2$	$T(x, y) = \sin(\pi y/S) \times \sin(\pi x/L)$

Note: Blue-ambient temperature; Red-  $1^{\circ}C$  above ambient temperature

Table 4.2: Cylindrical panel with different structural boundary constraints.

Structural boundary constraints			
CCCC	SSCC	SSSS	CCFC
			
$y=0, S; u=v=w=0$ $\theta_x = \theta_y = 0$	$y=S; v=w=0; \theta_x=0$ $y=0; u=v=w=0$ $\theta_x = \theta_y = 0$	$y=0, S; v=w=0$ $\theta_x = 0$	$y=0, S; u=v=w=0$ $\theta_x = \theta_y = 0$
$x=0, L; u_0=v_0=w_0=0$ $\theta_x = \theta_y = 0$	$x=0; u=w=0; \theta_y=0;$ $x=L; u=v=w=0$ $\theta_x = \theta_y = 0$	$x=0, L; u=w=0$ $\theta_y = 0$	$x=0; u=v=w=0$ $\theta_x = \theta_y = 0$

## 4.4 Case study-I: Isotropic cylindrical panel

A cylindrical panel with thickness ( $h$ ), width ( $S$ ), length ( $L$ ) and radius ( $R$ ) with following geometrical parameters:  $h = 1$  mm, thickness ratio ( $S/h$ ) =150, curvature ratio ( $R/S$ ) =2, aspect ratio  $L/S=1$  and angle of curvature ( $\theta$ ) = $45^\circ$  is considered for the investigation. Cylindrical panel is assumed to be made of mild steel with following properties; Young's modulus ( $E$ ) = 210GPa, Poisson's ratio ( $\mu$ ) = 0.3, coefficient of thermal expansion ( $\alpha$ ) =  $12.6 \times 10^{-6}/^\circ\text{C}$ , and density ( $\rho$ ) = 7850 kg/m<sup>3</sup>. The cylindrical panel is examined for two different dimension parameter ratio namely thickness ratio and curvature ratio along with five different temperature fields and three structural boundary constraints, in order to investigate buckling and free vibration characteristics of non-uniformly heated cylindrical panel.

### 4.4.1 Validation

#### Thermal buckling

Thermal buckling behavior of a fully clamped cylindrical panel examined by Al-Khaleefi (2004) has been considered for the validation. The dimensions of the panel are  $h= 1$ mm,  $S/h= 40$ ,  $R/S = 10$  and  $L/S = 1$  with following properties; Young's modulus ( $E$ ) = 40GPa, Poisson's ratio ( $\nu$ ) = 0.25, coefficient of thermal expansion ( $\alpha$ ) =  $79 \times 10^{-6}/^\circ\text{C}$ . Wherein, Al-Khaleefi (2004) has used first-order shear deformation shell theory based analytical approach to obtain the critical buckling temperature of a uniformly heated cylindrical panel. Present work used commercial finite element software ANSYS to obtain the critical buckling temperature. Critical buckling temperature evaluated using present approach is  $32^\circ\text{C}$  and matches well with that of the results reported by Al-Khaleefi (2004) which is  $25.28^\circ\text{C}$ .



Table 4.3: Comparison of natural frequencies with Au and Cheung (1996)

Mode	Natural frequencies, Hz	
	Au and Cheung (1996)	Present study
1	869	869
2	957	957
3	1287	1287
4	1363	1363

### Free vibration

Free vibration frequencies of a cylindrical panel with all edge clamped investigated by Au and Cheung (1996) is considered for the validation. Au and Cheung (1996) obtained natural frequencies of the cylindrical panel using isoparametric spline finite strip method, while the present method uses commercial FEA tool, ANSYS. The panel is made of aluminum with the following mechanical properties; Young's modulus ( $E$ ) = 68.9GPa, Poisson's ratio ( $\nu$ ) =0.33 and density ( $\rho$ ) =2657 kg/m<sup>3</sup>. The dimensions of the panel are  $\theta=0.133$  rad,  $h= 0.33$ mm,  $S=76.2$  mm,  $L/S = 1$  and  $R = 762$  mm. The results obtained using present study matches well with that of results reported in Au and Cheung (1996) as given in Table 4.3.

## 4.4.2 Results and discussion

### Buckling of cylindrical panel under thermal load

Buckling behavior of isotropic cylindrical panel exposed to different temperature fields is investigated in this section. Wherein a relation has been established to co-relate the buckling temperature of the panel obtained for non-uniform and uniform temperature field. Further, panels are also analyzed to study the influence of different geometrical parameters, temperature fields and structural boundary constraints on critical buckling temperature and corresponding mode. An investigation carried out on buckling behavior of the panel has been discussed in detail.

The relation between buckling temperature under uniform and non-uniform temperature fields known as Magnification factor of the first kind denoted by ( $\eta$ ) (Ko (2004)) is evoked in the present study.

$$\eta = \frac{[T_o]_{cr}}{[T_c]_{cr}} \quad (4.1)$$

where  $[T_o]_{cr}$  is the critical buckling temperature under non-uniform temperature field and  $[T_c]_{cr}$  is critical buckling temperature under uniform temperature field. In this study, peak temperature ( $T_o$ ) of  $1^\circ\text{C}$  above ambient is used and the heat sink temperature ( $T_s$ ) is allowed to vary in the range of ( $T_s / T_o = 0$  to  $1$ ) and the relation is then established for different temperature cases. From this relation it is easy to get critical buckling temperature of the panel under non-uniform temperature field, knowing the buckling temperature of the uniform temperature field. Table 4.4 shows the magnification factor of the first kind for different non-uniform temperature fields under CCCC boundary constraints. In Table 4.4,  $T_s / T_o = 0$  indicates that heat sink is at ambient temperature with peak temperature of  $1^\circ\text{C}$  above ambient temperature, in other words, panel is subjected to non-uniform temperature field with higher temperature difference while  $T_s / T_o = 1$  indicates both heat- sink and peak temperature are at  $1^\circ\text{C}$  above ambient temperature which indicates that the panel is subjected to uniform temperature variation field. From Table 4.4, it is clear that thermal buckling strength is significantly influenced by the nature of temperature variation as indicated by the values of the magnification factor of the first kind. It can be observed from Table 4.4 that the critical buckling temperature under Case(a) temperature field has to be magnified by 2.6 to get critical buckling temperature under Case(b) temperature field. Similarly, it has to be magnified by 1.49, 2.31 and 1.68 to get the critical buckling temperature of Case(c), Case(d) and Case(e), respectively. Thermal buckling strength is found to be minimum when a major portion of the panel is exposed to a maximum temperature of the particular temperature variation field. From the study, it has been

found that Case(c) and Case(e) temperature field has the lowest magnification factor compared to others. This indicates that more the panel surface is exposed to relatively higher temperatures in the variation, more the thermal stress will be developed and this will induce more membrane force in the panel which in turn reduces the critical buckling temperature.

Table 4.4: Magnification factor of first kind for CCCC isotropic panel

$T_s/T_o$	Case(b)	$\eta$	Case(c)	$\eta$	Case(d)	$\eta$	Case(e)	$\eta$
0	431	2.60	247	1.49	383	2.31	279	1.68
0.2	333	2.01	226	1.36	304	1.83	248	1.49
0.4	268	1.61	208	1.25	252	1.52	221	1.33
0.6	224	1.35	192	1.16	215	1.30	200	1.20
0.8	191	1.15	178	1.07	189	1.14	182	1.10
1	166	1.00	166	1.00	166	1.00	166	1.00

Panel with a free edge, which allows in-plane free expansion when exposed to thermal load will behave differently from the panel without a free edge, so CCFC cylindrical panel is analyzed to investigate the effect of free edge on buckling behavior. Table 4.5 shows the magnification factor of the first kind for CCFC cylindrical panel. From Table 4.5, it is observed that critical buckling strength of CCFC panel is also influenced by the nature of temperature variation. However, the variation of the buckling strength of CCFC cylindrical panel with nature of temperature variation is not similar to the CCCC panel. Unlike the CCCC panel, buckling strength of CCFC panel is influenced by the level of temperature at the free edge of a particular temperature field. When the free edge is exposed to the highest temperature of the variation, the panel experiences lowest buckling strength as observed for Case(d) in Table 4.5. It can be observed from Table 4.5 that buckling temperature under Case(a) has to be magnified by 2.12, 1.69, 2.3 and 1.98 to get buckling temperature under Case(b), Case(c), Case(d) and Case(e) temperature field respectively. It can be clearly seen from Table 4.4 and Table 4.5 that CCCC cylindrical panel has lowest critical buckling temperature compared to CCFC panel. This can be attributed to the free expansion due to heating

associated with the CCFC panel which allows some stress to relieve from the panel and thus produces less membrane force compared to CCCC panel.

Table 4.5: Magnification factor of first kind for CCFC isotropic panel

$T_s/T_o$	Case(b)	$\eta$	Case(c)	$\eta$	Case(d)	$\eta$	Case(e)	$\eta$
0	514	2.12	411	1.69	560	2.30	482	1.98
0.2	426	1.75	368	1.51	460	1.89	421	1.73
0.4	361	1.49	330	1.36	384	1.58	366	1.51
0.6	312	1.28	296	1.22	325	1.34	318	1.31
0.8	273	1.12	268	1.10	279	1.15	277	1.14
1	243	1.00	243	1.00	243	1.00	243	1

In most of the real cases, the panel under thermal load tries to expand under heating but its free expansion is prevented by the cooler boundary (heat sinks). This constraint due to non-uniform temperature will produce membrane compressive forces in the panel which results in thermal buckling. As the boundaries are heated up, constraints due to cooler boundaries will gradually relaxed, resulting in higher buckling temperature. In order to find out the influence of non-uniform temperature fields and heat sink temperature on the buckling temperature of the panel with free in-plane motion, a study has been carried out on a cylindrical panel with simply supported boundary constraints with in-plane motions. Magnification factor of the second kind denoted by  $\xi$  (Ko (2004)) is employed to relate the critical buckling temperature of a non-uniform temperature field obtained for an unheated boundary heat sink and for a boundary heat sinks when heated up.

$$\xi = \frac{[(T_o)_{cr}]_{(T_s \neq 0)}}{[(T_o)_{cr}]_{(T_s = 0)}} \quad (4.2)$$

where  $[(T_o)_{cr}]_{(T_s \neq 0)}$  indicates the critical buckling temperature when heat sink temperature is not equal to zero whereas,  $[(T_o)_{cr}]_{(T_s = 0)}$  indicates the critical buckling temperature when heat sink temperature is zero. Simply supported cylindrical panel with free in-plane motion is considered for the analysis along with two temperature distribution cases (Case(d) and Case(e)), as in both the cases heat

source is fully surrounded by cooler boundaries, hence the buckling behavior due to non-uniform temperature can be studied. Table 4.6 shows the magnification factor of second kind for SSSS cylindrical panel. It can be clearly observed from Table 4.6 that, Case(e) has lower buckling strength compared to Case(d) due to the fact that, in former the heat is applied in the region where the panel is less stiff. Results in Table 4.6 indicates that buckling temperature increases with heat sink temperature and becomes infinity when temperature distribution is uniform throughout the panel. The panel experiences uniform temperature rise above ambient temperature when  $T_s$  equals to  $T_o$ . SSSS panel analyzed allows free in-plane expansion and for the uniform temperature rise, the panel does not experience any membrane compressive forces required for buckling. When the temperature distribution becomes non uniform, thermal stresses will be generated which will set up the required membrane force in the panel.

Table 4.6: Magnification factor of second kind for SSSS isotropic panel

$T_s/T_o$	Case(d)	$\xi$	Case(e)	$\xi$
0	264	1.00	144	1.00
0.2	331	1.25	180	1.25
0.4	441	1.67	240	1.67
0.6	661	2.50	361	2.51
0.8	1323	5.01	721	5.01
1	$\infty$	$\infty$	$\infty$	$\infty$

To analyze the influence of the different dimensional parameter on the critical buckling temperature, a cylindrical panel with four different thickness ratio and curvature ratio have been considered. Fig. 4.1 indicates the influence of thickness ratio and temperature fields on the buckling strength of the panel under CCCC and CCFC boundary constraints. Similarly, Fig. 4.2 indicates the effect of curvature ratio and temperature fields on the thermal buckling strength of the cylindrical panel under CCCC and CCFC boundary constraints. From Fig. 4.1 and Fig. 4.2 it can be noticed that both thickness ratio and curvature ratio is inversely proportional to the buckling temperature. As the thickness ratio and

curvature ratio increases, the stiffness of the panel decreases which in turn decreases the buckling strength of the panel. Similarly, it can also be observed from the results that resistance to the thermal buckling decreases with the increase in curvature ratio and it attains minimum value when the curvature ratio tends to infinity. This is due to the fact that moment of inertia decreases with increase in curvature ratio which reduces the bending stiffness of the panel and hence the buckling strength of the panel irrespective of temperature fields. One can observe that under CCCC boundary constraint, Case(b) has the highest buckling temperature while for CCFC boundary constraint, Case(d) has the highest buckling temperature. However, Case(a) temperature field gives lowest buckling strength for both CCCC and CCFC boundary constraints. Data obtained from Fig. 4.1(i) and Fig. 4.2(i) shows that, under CCCC boundary constraints, Case(b) has the highest buckling temperature due to the fact that the heat source is located at the clamped supports and the membrane compressive forces generated due to heat is balanced by support reactions, hence more heat is required to produce sufficient membrane compressive forces in order to overcome the reaction forces and to cause buckling. Similarly, for the CCCC panel exposed to Case(d) has lower buckling strength than Case(b) as the heat source is located away from the supports where the reaction forces are less and the panel is less stiff. Furthermore, the CCCC panel under Case(e) temperature variation field has lower buckling strength compared to Case(d) due to the location of the heat source. Compared to other temperature fields discussed above Case(c) has lower buckling strength as it gets heat from two sides which produce more membrane compressive forces. Whereas Case(a) has lowest buckling temperature compared to all cases, as the entire cylindrical panel is exposed to heat. Under CCFC boundary constraint, all the temperature field is found to have higher buckling strength compared to respective temperature field with CCCC boundary constraint. There is a small variation in the buckling strength order has been observed in CCFC boundary constraint compared to CCCC. In the case of CCFC boundary constraints Case(d)

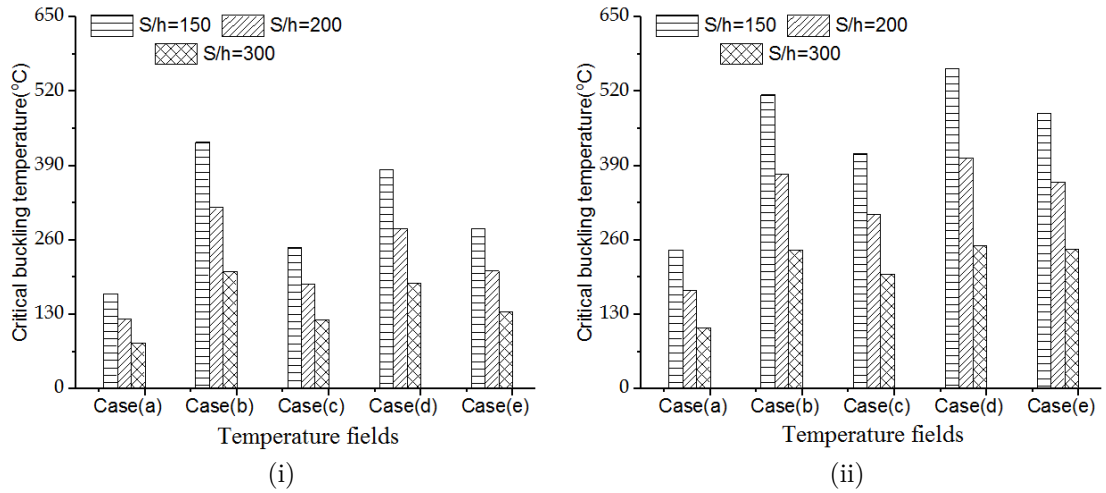


Figure 4.1: Influence of thickness ratio and temperature fields on buckling temperature of isotropic panel with boundary constraints, (i) CCCC and (ii) CCFC

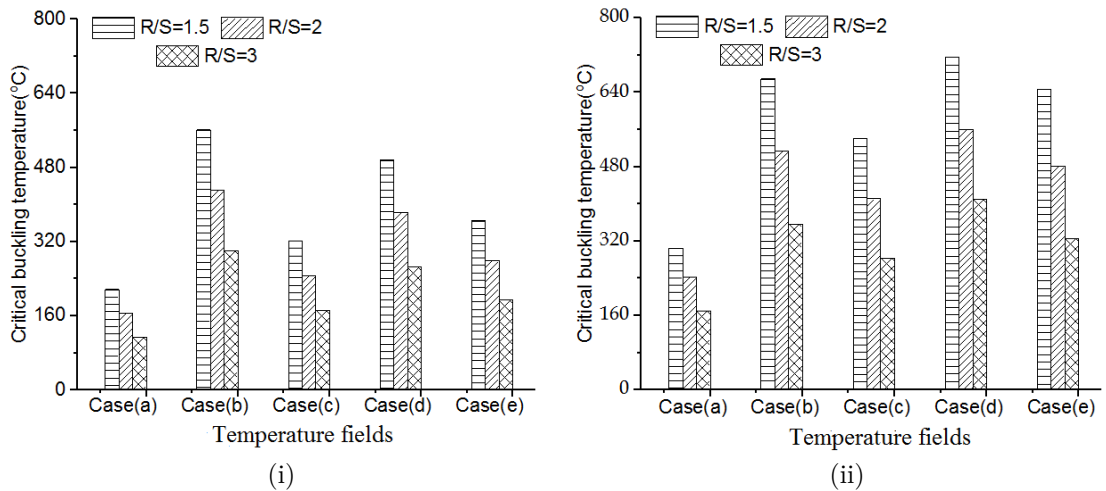


Figure 4.2: Influence of curvature ratio and temperature fields on buckling temperature of isotropic panel with boundary constraints, (i) CCCC and (ii) CCFC

has highest buckling temperature compared to other temperature fields due to the fact that heat source is located close to the free edge thus some of the thermal stress will be relieved from the free edge thus produce less membrane force.

Bending amplitude of the fundamental buckling mode associated with the center line of the cylindrical panel along the longitudinal direction ( $x$ - axis) is obtained to analyze the influence of temperature variation on the buckling mode

shape. Fig. 4.3(i) shows the influence of nature of temperature variation on buckling mode shape of CCCC panel. A panel with a thickness ratio of 150 and a curvature ratio of 2 with a thickness of 1mm has been considered for the investigation. From Fig. 4.3(i), one can observe that the influence of temperature field on the buckling mode shape and its amplitude is significant. Bending amplitude of the buckling mode observed for CCCC panel with Case(b) temperature field has a high peak towards the heat source location and it decreases as they move away from heat source. Similarly, the CCCC panel under Case(a), bending amplitude of the buckling mode remains constant for all peaks due to the fact that the total area is exposed to the same temperature. The maximum amplitude of the buckling mode under Case(c) and Case(e) temperature field occurs at the center of the panel where the area is less stiff and for Case(d) there is not much variation in the amplitude of the peaks. It is noticed that for all temperature fields except Case(b) the behavior of peaks is symmetric about the central line of the panel. This can be attributed to the un-symmetric temperature variation associated with the Case(b) temperature field. Fig. 4.3(ii) shows the non-dimensional bending amplitude associated with the buckling mode shape of CCFC panel. Compared to the CCCC panel, the influence of nature of temperature fields on buckling mode shapes of CCFC panel is significant as seen in Fig. 4.3(ii). Panel with CCFC boundary constraints has their highest amplitude peak away from the free edge irrespective of the temperature fields. It is also observed that the amplitude of the peaks is negligible in the region close to the free edge as it allows thermal stress to relieve from the free edge. Under CCFC boundary constraints Case(c) has the highest bending amplitude compared to others. The buckling mode shape pattern observed in CCFC panel with Case(b) field follows the same trend as observed in CCCC boundary constraints with slight variation in amplitude due to the fact that the effect of free edge on panel with Case(b) temperature field is minimum as the heat source is located far away from the free edge. However, for other cases, the trend is changing significantly with peak amplitude moving towards the



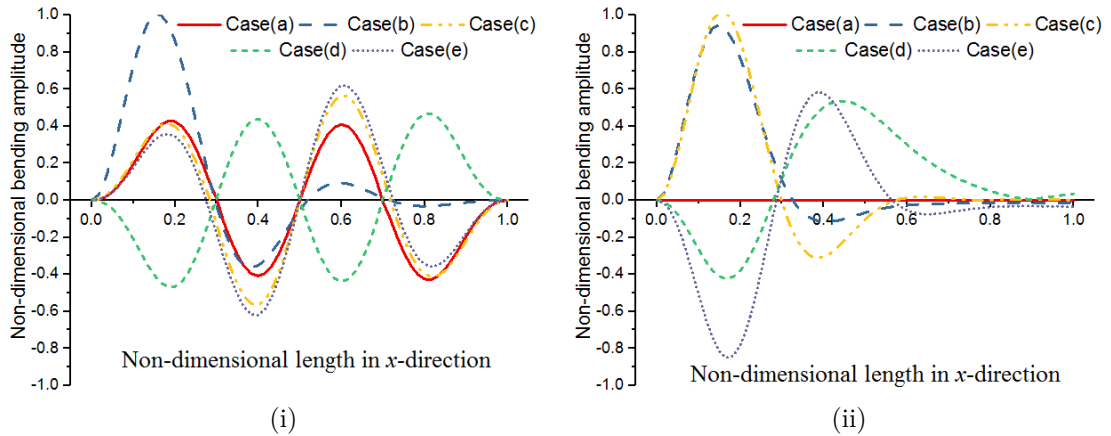


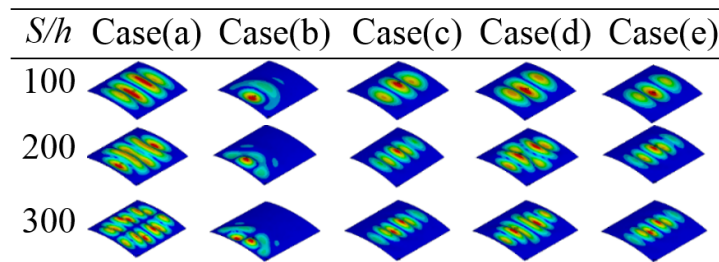
Figure 4.3: Influence of temperature fields on buckling mode shape of an isotropic panel with boundary constraints, (i) CCCC and (ii) CCFC

clamped edge due to un-symmetric boundary constraints. It can also be noted from Fig. 4.3(ii) that maximum amplitude always occurs nearer to the edge opposite to the free edge. This is due to the fact that at the free edge there won't be any reaction forces which opposes the membrane forces, but at clamped edge, there will be reaction forces which induce stress in the panel and thus making it buckle.

Influence of thickness ratio and temperature field on the buckling mode shape of the CCCC and CCFC panels are shown in Table 4.7 and Table 4.8 respectively. It can be clearly seen from Table 4.7 and Table 4.8 that thickness ratio has a significant effect on the buckling mode shape as stiffness changes with the thickness ratio irrespective of the temperature fields. From Table 4.7 one can observe that the CCCC panel under Case(b) temperature field has buckling mode shapes with maximum bending amplitude towards the edge exposed to the peak temperature of Case(b) and the edge opposite to this experiences least bending amplitude. When the CCCC panel is exposed to Case(c), Case(d) and Case(e) temperature fields, there is no significant variation in buckling mode shapes while modal indices of the buckling mode shapes along the longitudinal ( $x$ ) direction increases with the thickness ratio. When the CCCC panel exposed to Case(a) temperature field,

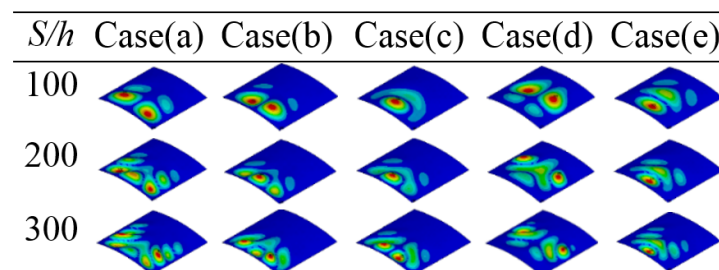
modal indices along the longitudinal ( $x$ ) direction increases with thickness ratio as seen for Case(c), Case(d) and Case(e). However, when the thickness ratio is 300, buckling mode shape has modal indices of two along the circumferential ( $y$ ) direction. It is observed from Table 4.8 that CCFC panel under Case(d) temperature field has buckling mode shape with a maximum bending amplitude at the mid-portion of the panel which is exposed to peak temperature while the free edge experience least bending amplitude. Whereas for buckling mode shapes under other heating conditions, the maximum bending amplitude is found to occur away from the free edge. It is also observed that under all temperature fields bending amplitude of buckling mode shape is found to be minimum at the free edge.

Table 4.7: Effect of thickness ratio on fundamental buckling mode shape of CCCC isotropic panel



Note: Red- max. displacement, Blue- min. displacement and others-inbetween

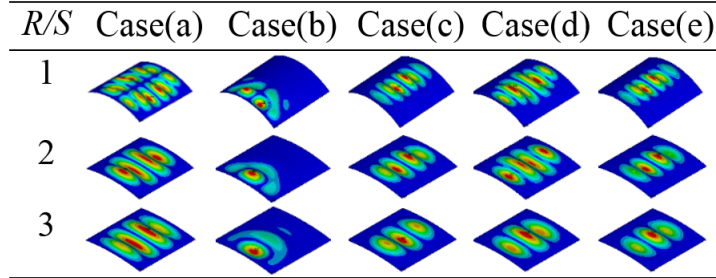
Table 4.8: Effect of thickness ratio on fundamental buckling mode shape of CCFC isotropic panel



Note: Red- max. displacement, Blue- min. displacement and others-inbetween

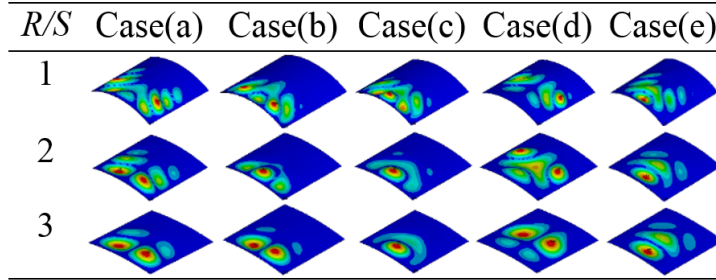
Effect of curvature ratio and temperature variation on the buckling mode shapes of CCCC and CCFC cylindrical panels are shown in Table 4.9 and Ta-

Table 4.9: Effect of curvature ratio on fundamental buckling mode shape of CCCC isotropic panel



Note: Red- max. displacement, Blue- min. displacement and others-inbetween

Table 4.10: Effect of curvature ratio on fundamental buckling mode shape of CCFC isotropic panel



Note: Red- max. displacement, Blue- min. displacement and others-inbetween

ble 4.10 respectively. Influence of curvature ratio on the buckling mode shape is significant due to change in moment of inertia with the curvature ratio. As the curvature ratio increases, the maximum bending amplitude of the buckling mode of the CCCC panel is moving towards the center of the panel where the panel is less stiff being Case(b) temperature field as exceptional. CCFC panel under all temperature fields except Case(d) has maximum bending amplitude of buckling mode shape at the fixed edge opposite to free edge as seen in Table 4.10. For Case(d) temperature field, the maximum bending amplitude of buckling mode occurs at a central portion of the panel which is subjected to maximum heat. It can also be noted that as the curvature ratio increases modal indices of buckling modes along the longitudinal ( $x$ ) direction decreases.

### Free vibration behavior under thermal load

The pre-stressed modal analysis is carried out on the cylindrical panel exposed to some elevated temperature as a function of critical buckling temperature, to understand the behavior of free vibration and its mode shapes subjected to various temperature fields under different boundary constraints. Further, to analyze the effect of heat sink temperature and non-uniform temperature fields on the behavior of natural frequencies, cylindrical panel exposed to two different temperature fields (Case(d) and Case(e)) under simply supported boundary constraint which allows in-plane motion is considered. Table 4.11 shows the effect of non-uniform temperature on free vibration frequencies of the simply supported cylindrical panel with free in-plane motion. For the analysis, cylindrical panel subjected to a non-uniform temperature field with a peak temperature ( $T_o$ ) of 100°C above ambient temperature is considered and the heat sink temperature ( $T_s$ ) is allowed to vary over the range of 0°C to 100°C above ambient temperature in the steps of 20°C with no external in-plane boundary constraints. From Table 4.11, it is clear that free vibration frequency is minimum when the sink temperature is at 0°C above ambient temperature and it increases with increase in sink temperature.

Table 4.11: Effect of temperature fields on free vibration frequencies (Hz) of isotropic panel

Mode	Ambient temp	$T_s/T_o$ (Case(d))						$T_s/T_o$ (Case(e))					
		0	0.2	0.4	0.6	0.8	1*	0	0.2	0.4	0.6	0.8	1*
1	177	156	161	165	169	173	177	130	146	157	165	171	177
2	210	196	199	202	205	207	210	192	196	200	204	207	210
3	303	288	292	295	298	301	303	292	297	299	301	302	303
4	334	321	324	327	329	331	334	307	313	320	325	330	334

\*Case(a) temperature field

To study the effect of thermal load on natural frequencies, cylindrical panel exposed to the different temperature fields under clamped boundary constraints is considered. Table 4.12 shows the effect of thermal load on free vibration frequencies of the cylindrical panel under CCCC boundary constraints. It is observed that free vibration frequencies under ambient temperature decrease with an increase

in temperature irrespective of temperature fields due to a reduction in structural stiffness caused by thermal stress. To analyze the combined effect of free edge and thermal load on the free vibration frequencies, CCFC panel is also investigated. There is not much variation can be noticed in the free vibration frequencies of CCFC cylindrical panel subjected to a different thermal load. Free vibration mode shape also plays an important role while designing a thin structure of cylindrical panels as it gives the nodal and anti-nodal position of the particular mode through which mode can be excited. Hence it is very important to know the mode shape variation under thermal load along with the frequency.

From Table 4.13, it is clear that changes in free vibration mode shapes with the increase in temperature are significant for all the temperature fields. Moving of nodal and anti-nodal positions and shifting of modes are commonly observed for the different temperature fields. For example, mode 1 of CCFC panel having modal indices of (1,2) at ambient temperature changes to (1,3) at 95% of the critical buckling temperature under Case(b) temperature field as seen in Table 4.13. A similar trend has been observed for other free vibration modes also. From Table 4.13 it can also be observed that for CCFC panel, the anti-nodal position of modes is moving towards the clamped edge with an increase in temperature. For example, under Case(c) temperature field at ambient temperature, free vibration modes under mode 1 and mode 3 is found to occur at the free edge, but with the increase in temperature, it is found to occur at fixed edge. This is due to the fact that with the increase in temperature, panel becomes soft at the free edge, thus making the vibration modes to shift towards the stiffer side of the panel. The influence of nature of temperature fields on free vibration modes of the CCCC cylindrical panel is also shown in Table 4.13. Compared to CCFC panel, a variation of free vibration mode shapes of CCCC panel with temperature variation is less. This can be attributed to the symmetric structural boundary constraints associated with the CCCC cylindrical panel. For CCCC panel under Case(b), modal indices changes from (1,2) to (1,3) whereas for other cases it changes to

Table 4.12: Effect of thermal load on free vibration frequency (Hz) and associated modal indices of an isotropic panel

Boundary constraints	Modes	Temperature fields											
		At ambient temp.		Case(a)		Case(b)		Case(c)		Case(d)		Case(e)	
		50% $T_{cr}$	95% $T_{cr}$	50% $T_{cr}$	95% $T_{cr}$	50% $T_{cr}$	95% $T_{cr}$	50% $T_{cr}$	95% $T_{cr}$	50% $T_{cr}$	95% $T_{cr}$	50% $T_{cr}$	95% $T_{cr}$
CCCC	1	1359 (1,2)	1206 (1,2)	793 (4,1)	1246 (1,2)	738 (1,3)	1234 (1,2)	812 (4,1)	1191 (1,2)	801 (4,1)	1224 (1,2)	789 (4,1)	
	2	1479 (1,3)	1331 (1,3)	851 (4,2)	1370 (1,3)	825 (2,2)	1359 (1,3)	922 (3,1)	1298 (1,3)	847 (4,3)	1339 (1,3)	862 (3,1)	
	3	2071 (2,3)	1640 (2,3)	916 (3,2)	1713 (2,3)	1117 (1,2)	1681 (2,3)	1107 (1,2)	1695 (2,3)	865 (3,2)	1683 (2,3)	1080 (1,2)	
	4	2075 (2,2)	1659 (2,2)	945 (5,1)	1732 (2,2)	1236 (1,3)	1706 (2,2)	1213 (2,3)	1697 (2,2)	979 (3,3)	1719 (2,2)	1182 (1,3)	
CCFC	1	894 (1,2)	836 (1,2)	749 (2,3)	857 (2,2)	733 (1,3)	837 (1,2)	734 (1,3)	838 (1,1)	654 (2,3)	841 (1,2)	748 (3,3)	
	2	1253 (1,3)	1203 (1,3)	754 (2,2)	1223 (1,3)	777 (2,2)	1187 (1,3)	751 (1,2)	1200 (1,3)	713 (1,2)	1199 (1,3)	772 (1,2)	
	3	1597 (2,2)	1432 (2,2)	771 (3,2)	1459 (2,2)	823 (2,2)	1429 (2,2)	858 (2,2)	1420 (2,2)	1005 (3,3)	1408 (2,3)	960 (2,3)	
	4	1615 (2,3)	1441 (2,3)	1059 (3,3)	1472 (2,3)	1175 (1,3)	1433 (2,3)	986 (1,3)	1421 (2,32)	1092 (3,3)	1413 (2,2)	1083 (2,3)	

Note:  $T_{cr}$  - Critical buckling temperature associated with temperature field

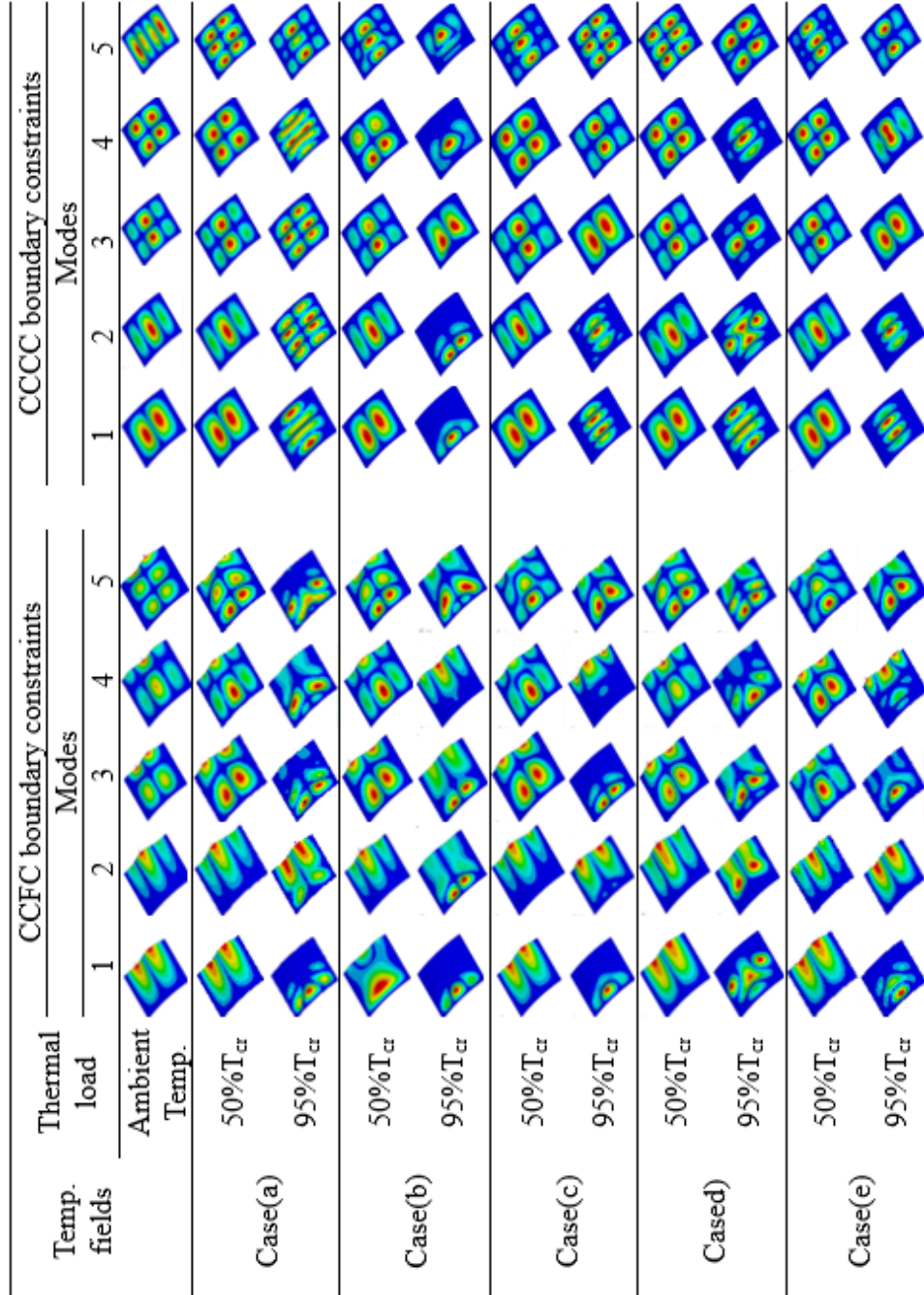
(4,1) which shows that temperature has a significant effect on vibration mode shapes.

## 4.5 Case study-II: Laminated composite cylindrical panel

Buckling and free vibration behavior of a laminated composite cylindrical panel under non-uniform heating is analyzed in this section. Effect of different geometrical parameters on the buckling behavior of the panel exposed to different temperature fields is analyzed along with the effect of boundary constraints. Similarly, the effect of different temperature fields on the free vibration behavior is also investigated. In the present study, a cylindrical panel with thickness ( $h$ ), width ( $S$ ), length ( $L$ ) and radius ( $R$ ) with following geometrical parameters: ( $h$ ) =0.001m, thickness ratio ( $S/h$ ) =100, aspect ratio ( $L/S$ ) =1 and curvature ratio ( $R/S$ ) =5 has been considered otherwise it is mentioned. Panel is assumed to be made of orthotropic material with following properties;  $E_{11}$ =181GPa,  $E_{22}$ =10.3GPa,  $E_{33}$ =10.3GPa,  $G_{12}$ = $G_{13}$ =7.17GPa,  $G_{23}$ =2.39GPa,  $\nu_{12}$ = $\nu_{13}$ = $\nu_{23}$ =0.28,  $\rho$ =1603kg/m<sup>3</sup>,  $\alpha_1/\alpha_2$ = 0.02/22.5,  $k_1/k_2$ =4.62/0.72,  $\alpha_0$  =10<sup>-6</sup>/°C. Where  $E$ ,  $G$ ,  $\nu$ ,  $\alpha$  and  $K$  denote Young's modulus, Shear modulus, Poisson's ratio, coefficient of thermal expansion and thermal conductivity, respectively. The subscripts 1, 2, and 3 refer to the on-axis material coordinates. Four layered laminated cylindrical panel with the lamination scheme of [0/90/90/0] is considered for the investigation. Five different in-plane temperature fields and four different structural boundary constraints CCCC, SSCC, SSSS and CCFC discussed in the preceded section has been considered.

Non-dimensional critical buckling temperature( $T_{cr}^*$ ) given by Katariya and Panda, 2016 (Eq.4.3) is used to represent the critical buckling temperature in

Table 4.13: Effect of thermal load on the free vibration mode shapes of an isotropic panel



Note: Red- max. displacement, Blue- min. displacement and others-inbetween



the present work.

$$T_{cr}^* = \alpha_0 \times T_{cr} \times 10^3 \quad (4.3)$$

### 4.5.1 Validation

#### Thermal buckling

The thermal buckling temperature of simply supported laminated panel [15/-15]<sub>3</sub> exposed to uniform temperature rise examined by Katariya and Panda (2016a) is considered for validation. The panel is made of six layers with the lay up of [15/-15]<sub>3</sub> and  $R/S=5$  and  $L/S = 1$  with following elastic properties;  $E_1/E_0=21$ ,  $E_2/E_0=1.7$ ,  $E_2/E_3=1$ ,  $G_{12}/E_0= 0.65$ ,  $G_{23}/E_0= 0.639$ ,  $G_{12}/G_{13}=1$ ,  $\nu_{12}=\nu_{13}=\nu_{23}=0.21$ ,  $\alpha_1/\alpha_0=-0.21$ ,  $\alpha_2/\alpha_0= \alpha_3/\alpha_0=16$ ,  $\alpha_0=10^{-6}/\text{in}/\text{in}/^\circ\text{F}$ . Where  $E$ ,  $G$ ,  $\nu$  and  $\alpha$  denote Young's modulus, Shear modulus, Poisson's ratio and coefficient of thermal expansion respectively, and the subscripts 1, 2, and 3 refer to the on-axis material coordinates. Katariya and Panda (2016a) used higher order displacement functions based finite element method, while present method used FSDT based finite element method. Critical buckling temperature predicted using the present method matches well with the results reported by Katariya and Panda (2016a) as seen in Table 4.14.

Table 4.14: Comparison of critical buckling temperature with Katariya and Panda (2016a)

$S/h$	Non-dimensional critical buckling temperature $T_{cr}^*$		Difference in %
	Katariya and Panda (2016a)	Present study	
40	0.854	0.877	2.6
100	0.547	0.568	3.8

## Free vibration frequency

A conical panel investigated by Jooybar *et al.* (2016) to analyze the free vibration behavior under thermal load has been considered for the validation. They obtained non-dimensional fundamental frequency of the conical panel using finite element method based on FSDT. However, the present method uses layered structural shell element SHELL 281 available in commercial finite element software ANSYS. The panel is made of ceramic ( $\text{Si}_3\text{N}_4$ ) with the following mechanical and thermal properties;  $E= 348.43\text{GPa}$ ,  $\nu= 0.24$  and  $\rho= 2370 \text{ kg/m}^3$ ,  $k= 9.19\text{W/mK}$ ,  $\alpha= 5.8723 \times 10^{-6}/\text{K}$ . The dimensions of the panel are  $L/R_1 = 1$ ,  $h/R_1= 0.1$ ,  $\beta= 60^\circ$  and  $\theta= 120^\circ$ . Non-dimensional natural frequency ( $\bar{\omega} = 2 \times \pi \times \frac{L^2}{h} \times \sqrt{\frac{\rho}{E}}$ ) under thermal load obtained using present study shows good agreement with that of results reported in Jooybar *et al.* (2016) as shown in Fig. 4.4.

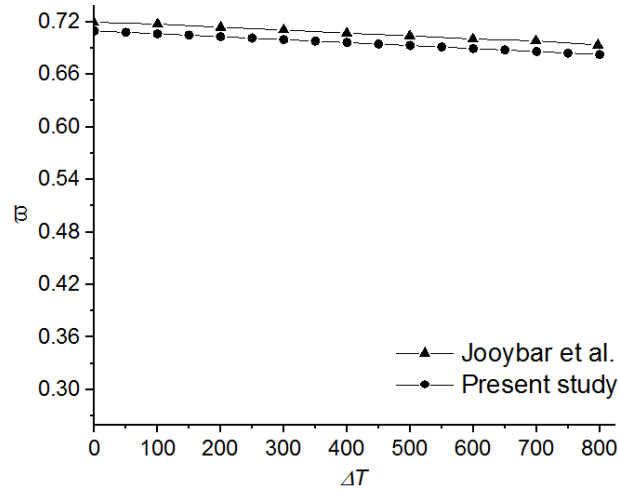


Figure 4.4: Comparison of non-dimensional fundamental natural frequency of panel under thermal load

## 4.5.2 Results and discussion

Buckling strength of a symmetric cross-ply laminated cylindrical panel exposed to non-uniform heating is presented here. Effect of thickness ratio, aspect ratio, curvature ratio and structural boundary constraints on critical buckling temperature

and associated mode shape are investigated in detail. The magnification factor of the first kind for different non-uniform temperature fields is given in Table 4.15, for CCCC panel.  $T_s/T_o = 0$  in Table 4.15 shows that, the panel is subjected to a peak temperature of  $1^\circ C$  above ambient while heat sink is maintained at ambient temperature, which in other words, states that panel is subjected to non-uniform temperature field across the panel surface with a temperature variation of  $1^\circ C$  to  $0^\circ C$  above ambient. Panel with both heat-sink and peak temperature at  $1^\circ C$  above ambient is indicated by  $T_s/T_o = 1$  which means that panel is subjected to uniform temperature variation field. From the values indicated by  $\eta$ , it can be clearly seen that nature of temperature variation has a significant impact on the thermal buckling strength of the panel. Table 4.15 reveals that the critical buckling temperature of a panel under Case(b) temperature field can be obtained by magnifying the Case(a) temperature field with a factor of 3.10. Similarly, critical buckling temperature of a panel under Case(c), Case(d) and Case(e) temperature fields can be obtained by a magnifying factor of 1.56, 2.21, 1.72 respectively. Table 4.15 also shows that among all non-uniform temperature field, Case(c) has the lowest buckling temperature as in Case(c) temperature field more portion of the panel is exposed to the peak temperature of the temperature fields. It is also noted that Case(e) has relatively less buckling strength compared to Case(b) and Case(d). From the above observation, it can be concluded that the thermal stress developed will be more when the major portion of the panel surface is exposed to a peak temperature of the non-uniform temperature field and the resulting membrane force reduces the buckling strength of the panel.

As the panels with free edge behave differently from the all edges clamped panel under thermal load, a CCFC cylindrical panel is analyzed. Table 4.16 depicts the magnification factor of the first kind for CCFC panel. It is clear from Table 4.16 that the buckling strength of panel is influenced by the nature of temperature variation irrespective of its edge conditions. However, the buckling behavior of the CCFC panel with the nature of temperature variation is not similar

Table 4.15: Magnification factor of first kind for CCCC laminated panel

$T_s/T_o$	Case(b)		Case(c)		Case(d)		Case(e)	
	$T_{cr}^*$	$\eta$	$T_{cr}^*$	$\eta$	$T_{cr}^*$	$\eta$	$T_{cr}^*$	$\eta$
0	1.47	3.10	0.74	1.56	1.05	2.21	0.82	1.72
0.2	1.04	2.19	0.67	1.44	0.85	1.78	0.72	1.51
0.4	0.8	1.68	0.6	1.25	0.71	1.49	0.63	1.34
0.6	0.65	1.37	0.55	1.19	0.61	1.28	0.57	1.2
0.8	0.55	1.15	0.51	1.06	0.53	1.12	0.52	1.09
1.0*	0.47	1	0.47	1	0.47	1	0.47	1

to the CCCC panel. Unlike the CCCC panel, the level of temperature at the free edge for a given temperature variation determines the buckling strength of CCFC panel. From Table 4.16 it is found that the buckling temperature for Case(b), Case(c), Case(d) and Case(e) temperature fields can be obtained by magnifying the buckling temperature under Case(a) with a factor of 2.09, 1.75, 1.95 and 1.89 respectively. It can be clearly seen from Table 4.15 and Table 4.16 that CCCC cylindrical panel has poor buckling strength compared to the CCFC panel. It is anticipated, as CCFC boundary constraint, the panel is allowed to expand freely along the direction of the free edge, thus the amount of stress developed in CCFC panel is less than the CCCC panel. However, membrane forces developed due to thermal stress is less in CCFC panel making it to buckle at a higher temperature.

Table 4.16: Magnification factor of first kind for CCFC laminated panel

$T_s/T_o$	Case(b)		Case(c)		Case(d)		Case(e)	
	$T_{cr}^*$	$\eta$	$T_{cr}^*$	$\eta$	$T_{cr}^*$	$\eta$	$T_{cr}^*$	$\eta$
0	3.68	2.09	3.09	1.75	3.43	1.95	3.32	1.89
0.2	3.05	1.73	2.70	1.53	3.21	1.83	3.18	1.81
0.4	2.59	1.47	2.39	1.36	2.87	1.63	2.77	1.57
0.6	2.24	1.27	2.14	1.22	2.42	1.37	2.33	1.33
0.8	1.97	1.12	1.93	1.10	2.04	1.16	2.01	1.14
1.0*	1.76	1.00	1.76	1.00	1.76	1.00	1.76	1.00

The effect of thickness ratio on the buckling strength of the panel subjected to different temperature fields is shown in Fig. 4.5(i) and Fig. 4.5(ii) respectively, for CCCC and CCFC edge conditions. It is clearly seen from Fig. 4.5 that buckling

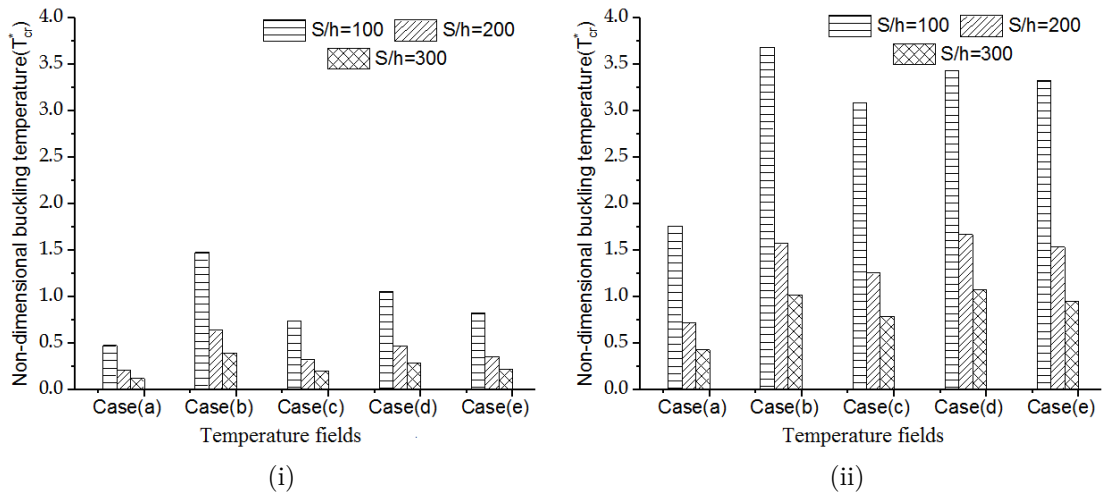


Figure 4.5: Influence of thickness ratio and temperature fields on buckling temperature of laminated panel with boundary constraints, (i) CCCC and (ii) CCFC

temperature decreases with increase in thickness ratio. This behavior of the panel indicates that the stiffness of the panel decreases with the increase in thickness ratio making it to buckle at low temperature. It can be well observed from Fig. 4.5(i) and Fig. 4.5(ii) that the variation in the buckling strength of panel for different temperature cases is significantly influenced by the thickness ratio at lower values whereas the variation is minimal at higher values of thickness ratio. At higher values of thickness ratio, the width of the cylindrical panel is found to be more which increases the non-supporting area of the panel thus making it very less stiff. Due to this low stiffness, small amount of membrane forces is sufficient to cause thermal buckling. It is also noted that the CCFC panel always has better buckling strength compared to CCCC panel due to free edge associated with it. From Fig. 4.5(i) and Fig. 4.5(ii), it is also observed that, panels exposed to Case(a) temperature field has a poor buckling strength while Case(b) temperature field results in better buckling strength it is due to amount of membrane forces generated by thermal load is more in Case(a) temperature field compared to Case(b) temperature field.

Fig. 4.6(i) and Fig. 4.6(ii) shows the influence of curvature ratio on the buckling

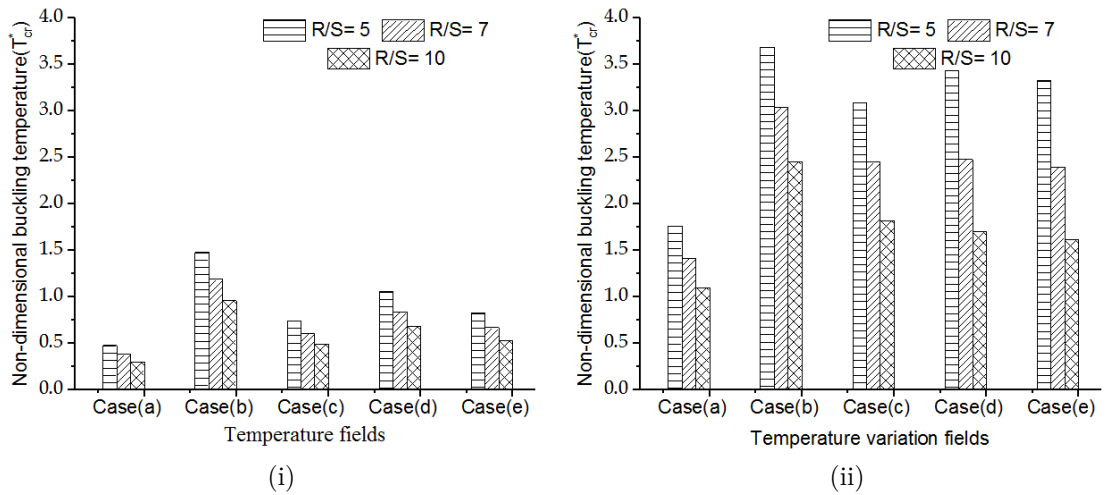


Figure 4.6: Influence of curvature ratio and temperature fields on buckling temperature of laminated panel with boundary constraints, (i) CCCC and (ii) CCFC

temperature of the panel under CCCC and CCFC boundary constraints. Influence of curvature ratio on the buckling temperature of the panel is similar to that of thickness ratio wherein buckling temperature decreases with the increase in curvature ratio. This behavior of the panel is mainly due to change in moment of inertia with the curvature ratio. At a lower curvature ratio, variation in the buckling temperature for different temperature fields is more significant. Under Case(b) temperature field, the location of the heat source is close to the fixed support and the membrane forces developed due to temperature variation is well poised by support reactions. Thus panel under Case(b) requires more amount of heat to develop sufficient membrane force that causes buckling. Since the heat source is located away from the fixed support where the panel is less stiff, the panel under Case(d) and Case(e) temperature fields is observed to have less buckling strength than the panel with Case(b) temperature field. Along with the location of the heat source, the amount of heat supplied play an important role in determining the buckling strength of the panel. The panel under Case(c) temperature field has a heating source at the fixed supports where it is stiffer, but still, produces high membrane forces due to the amount of heat given is more in Case(c) tem-

perature field compared to Case(b), Case(d) and Case(e). Furthermore, the panel under Case(a) is fully exposed to uniform heat, making it to buckle at a lower temperature compared to all other temperature fields.

Effect of aspect ratio on the buckling temperature of CCCC and CCFC panels under different temperature fields is shown in Fig. 4.7(i) and Fig. 4.7(ii) respectively. It is interesting to know that the panel behaves differently under different temperature fields with the change in aspect ratio. It can be noted from Fig. 4.7(i), that as the aspect ratio increases buckling strength of the CCCC panel under Case(a) and Case(e) temperature fields decreases whereas for other temperature fields buckling strength increases. The stiffness of the panel decreases with the increase in aspect ratio, thus the amount of heat applied and its location decides the buckling strength of the panel under different aspect ratio. Under Case(a) temperature field, the CCCC panel is exposed to uniform temperature rise, making it to buckle at a lower temperature with the increase in aspect ratio. Similarly, for the CCCC panel under Case(e) temperature field, the highest temperature of the variation is applied at the less stiff area thus buckles at a lower temperature. However, for other temperature fields membrane forces generated due to heat, decreases with the increase in aspect ratio, which thus increases the buckling strength of the panel. Unlike CCCC panel, CCFC panel under Case(b), Case(c) and Case(d) behaves similar to the Case(a) and Case(e) temperature fields as shown in Fig. 4.7(ii). Wherein buckling strength of the CCFC panel decreases with the aspect ratio of the panel under all temperature fields. Along with the aspect ratio, the free edge of the CCFC panel adds in lowering the stiffness of the panel which thus decreases the buckling strength of the panel.

Influence of thickness ratio and temperature fields on fundamental buckling mode shape of the CCCC panel and CCFC panel are given in Table 4.17 and Table 4.18, respectively. From Table 4.17, it is clear that the buckling mode shape of the CCCC panel is highly influenced by the thickness ratio, while it

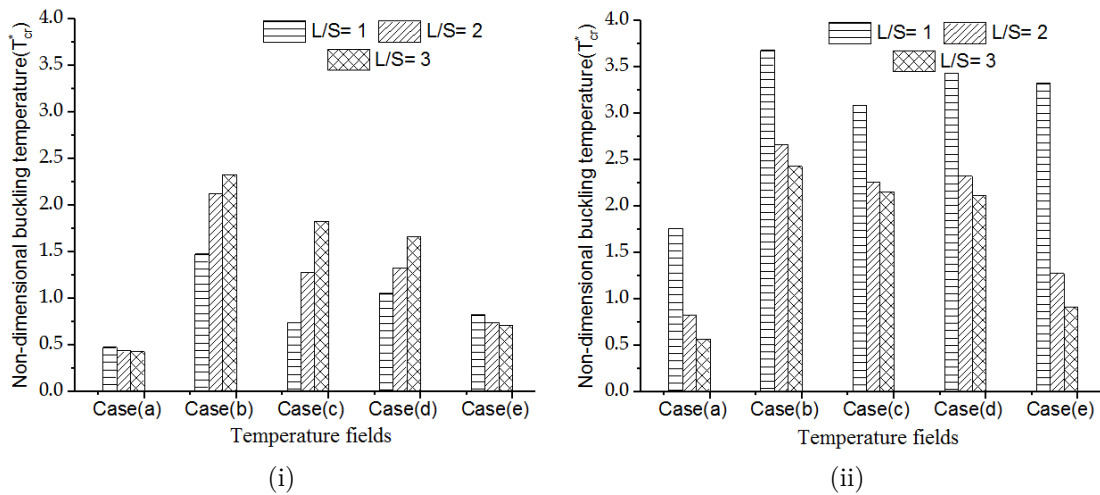
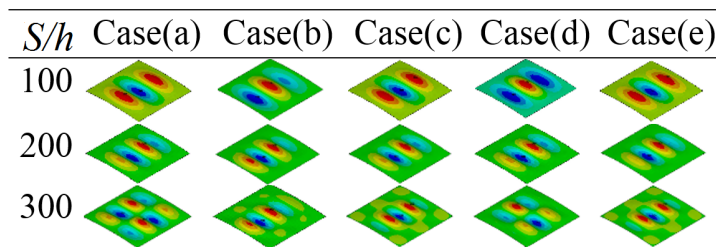


Figure 4.7: Influence of aspect ratio and temperature fields on buckling temperature of laminated panel with boundary constraints, (i) CCCC and (ii) CCFC

is not much influenced by the nature of temperature fields. Change in buckling mode shape with an increase in thickness ratio can be attributed to decrease in structural stiffness with increase in thickness ratio. Table 4.17 also reveals that the CCCC panel with Case(b) temperature field is observed to have maximum bending amplitude where the panel area is exposed to a peak temperature of Case(b). For the CCCC panel subjected to Case(b), Case(c), and Case(e), buckling mode shapes do not change significantly with the increase in thickness ratio but their modal indices along longitudinal direction increase with the thickness ratio.

Table 4.17: Effect of thickness ratio on fundamental buckling mode shape of CCCC laminated panel

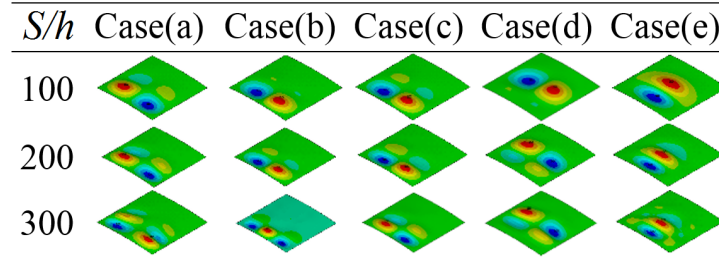


Note: Red- max. displacement, Blue- min. displacement and others-inbetween

Further for the CCCC panel under Case(a) and Case(d) temperature fields, at a



Table 4.18: Effect of thickness ratio on fundamental buckling mode shape of CCFC laminated panel



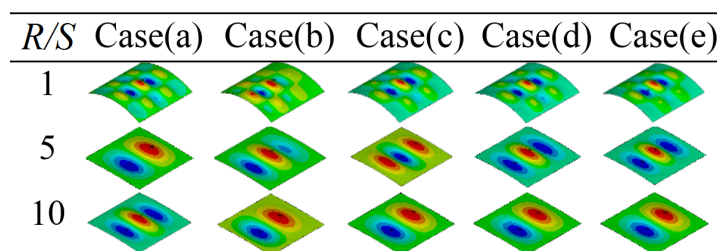
Note: Red- max. displacement, Blue- min. displacement and others-inbetween

higher value of thickness ratio, modal indices of the buckling mode shapes changes in both longitudinal and circumferential direction. From Table 4.18, it is clear that buckling mode shapes and its indices observed under CCFC panel are totally different from that of CCCC panel. Buckling mode shape of the CCFC panel is influenced by both the thickness ratio and the nature of temperature variation. CCFC panel under Case(d) and Case(e) temperature fields has a heat source at the central location where the structural stiffness is minimum. Thus maximum bending amplitude of the buckling mode shape occurs around the central location. However, for all other temperature fields, the maximum bending amplitude of buckling mode shape occurs at a location away from the free edge.

Influence of temperature variation and curvature ratio on the buckling mode shape is shown in Table 4.19- Table 4.20 for CCCC and CCFC panels respectively. It is known that the moment of inertia changes with the curvature ratio and its effect can be seen in the buckling mode shape and associated modal indices. Table 4.19 reveals that the modal indices associated with the buckling mode for a given temperature field are highly influenced by the curvature ratio of the CCCC panel. It is also observed that at higher curvature ratio, there is not much variation in the bending amplitude and the modal indices of the CCCC panel for different temperature fields. However, the variation of buckling mode shape of CCFC panel with curvature ratio and non-uniform temperature field is different compared to

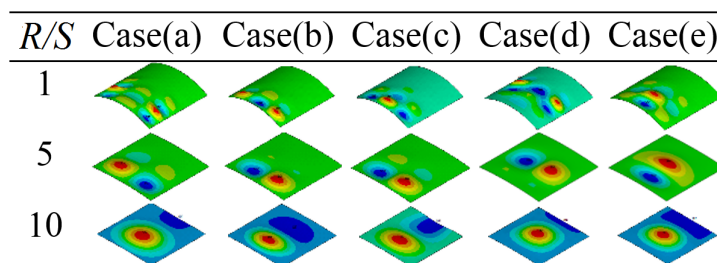
the CCCC panel as seen in Table 4.20. Table 4.20 also clearly indicates that nodal and antinodal lines of a buckling mode occur where the highest temperature of a particular temperature field occurs. The study also shows that modal indices of the buckling modes decrease with the increase in curvature ratio along the longitudinal and transverse direction.

Table 4.19: Effect of curvature ratio on fundamental buckling mode shape of CCCC laminated panel



Note: Red- max. displacement, Blue- min. displacement and others-inbetween

Table 4.20: Effect of curvature ratio on fundamental buckling mode shape of CCFC laminated panel



Note: Red- max. displacement, Blue- min. displacement and others-inbetween

CCCC cylindrical panel having symmetric angle laminate  $[\theta/-\theta/-\theta/\theta]$  is considered to analyze the effect of laminate orientation on critical buckling temperature. The value of  $\theta$  is varied from  $0^\circ$  to  $90^\circ$  in a step of  $5^\circ$  for various cases and results are given in Fig. 4.8. It is observed from Fig. 4.8 that the buckling temperature of the panel is significantly influenced by the laminate orientation. This can be attributed to change in stiffness of the panel due to change in elastic constants and thermal coefficient with the laminate orientation. It can be noted that buckling

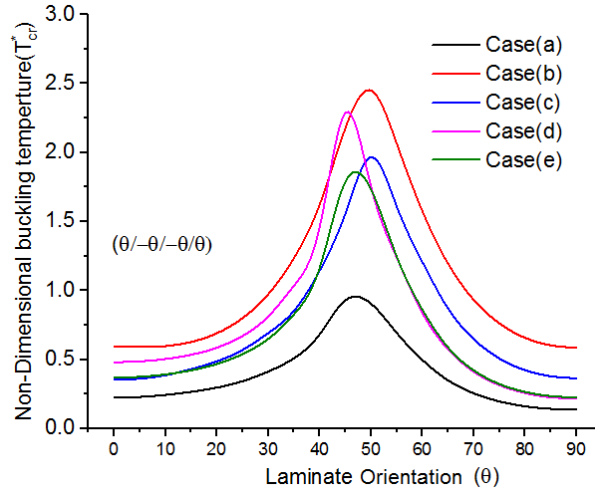


Figure 4.8: Effect of laminate orientation on buckling temperature of CCCC laminated panel

temperature of the panel increases with the laminate orientation and attains the maximum value around  $45^\circ$  to  $50^\circ$  and it reduces with further increase in laminate angle. Similarly, CCCC panel exposed to Case(b) temperature field has a better thermal buckling strength while Case(a) temperature field results in poor buckling strength. From Fig. 4.8 it is observed that the laminate orientation can be effectively used to tailor the thermal buckling strength of the laminated composite panel.

Structural boundary constraints of the panel are considered as the highly influencing factor in developing the thermal stress. To investigate this, a study is carried out on the panel with four different structural boundary constraints and results are given in Table 4.21. It is noted from Table 4.21 that CCCC panel has the lowest buckling strength compared to others. The panel under CCCC boundary constraints does not allow any free expansion at the edges which lead to the development of high thermal stresses. Whereas CCFC panel allows free expansion along one of its edge hence CCFC panel buckles at a higher temperature than CCCC panel. The panel under SSSS boundary constraints is observed to have highest buckling strength as panel don't allow any in-plane motion but

allow rotation, which makes a panel to relieve some stress through rotation thus produces less membrane forces. Panel with Case(a) temperature field has the minimum buckling strength under all boundary constraints. Similarly, panel under Case(b) temperature field has the lowest buckling temperature. It is also noted that panel under Case(d) temperature field has the highest buckling temperature than the Case(c) under CCCC, SSCC and CCFC boundary constraints due to the amount of heat supplied to the panel under Case(d) are less than the Case(c) temperature field. Whereas panel under SSSS boundary constraints, Case(c) has the highest strength than Case(d) and this can be attributed to the amount of stress generated mainly due to non-uniform temperature variation is more in Case(d) than in Case(c) temperature field. The panel under SSCC boundary constraints follows combined trend of CCCC and SSSS boundary constraints, thus buckling temperature recorded for SSCC panel lies between the CCCC and SSSS panel.

Table 4.21: Effect of boundary constraints and temperature fields on the buckling temperature of laminated panel

Boundary constraints	Temperature fields				
	Case(a)	Case(b)	Case(c)	Case(d)	Case(e)
CCCC	0.47	1.48	0.74	1.05	0.82
SSCC	1.43	5.37	2.58	2.87	2.55
SSSS	3.27	6.31	5.90	4.59	4.35
CCFC	1.76	3.68	3.09	3.43	3.32

The present study also focuses on the effect of the lamination scheme on the buckling temperature of the panel with different temperature fields and the same has been shown in Table 4.22 and Table 4.23 for CCCC and CCFC panels respectively. It can be seen from Table 4.22 that buckling temperature changes with the lamination scheme and similar trend has been observed for all the temperature fields. The stiffness of the panel is highly influenced by the lamination scheme used for the preparation of the panel. Symmetric cross-ply laminate [0/90/90/0] is observed to have minimum buckling strength while un-symmetric angle ply has the maximum buckling strength under CCCC boundary constraints. Compared to

all lamination schemes considered in the analysis, panel under Case(b) temperature field has the highest buckling temperature whereas Case(a) has the minimum value. Under CCFC boundary constraints symmetric cross-ply panel is found to have maximum buckling strength when subjected to Case(a), Case(b) and Case(c), as shown in Table 4.23. However, under Case(d) and Case(e) temperature fields, un-symmetric cross-ply panel records the maximum buckling strength wherein the location of heating source plays a major role in it. Similarly, the symmetric angle-ply panel records minimum buckling strength under Case(a), Case(d), and Case(e), temperature fields.

Table 4.22: Effect of lamination schemes and temperature fields on the buckling temperature of CCCC laminated panel

Lamination scheme	Temperature fields				
	Case(a)	Case(b)	Case(c)	Case(d)	Case(e)
0/90/90/0	0.47	1.47	0.74	1.05	0.82
0/90/0/90	0.69	1.99	1.10	1.68	1.23
45/-45/-45/45	0.74	1.76	1.28	1.61	1.36
45/-45/45/-45	0.92	2.17	1.55	2.28	1.78
0/45/-45/90	0.61	1.35	0.86	1.57	1.14

Table 4.23: Effect of lamination schemes and temperature fields on the buckling temperature of CCFC laminated panel

Lamination scheme	Temperature fields				
	Case(a)	Case(b)	Case(c)	Case(d)	Case(e)
0/90/90/0	1.76	3.68	3.09	3.43	3.32
0/90/0/90	1.48	3.07	1.72	3.64	3.37
45/-45/-45/45	0.84	1.77	1.5	1.79	1.55
45/-45/45/-45	1.08	2.2	1.83	2.52	2.06
0/45/-45/90	0.94	1.55	1.22	2.02	1.52

### Free vibration under thermal load

In order to study the influence of nature of temperature variation on the free vibration frequencies and its mode shape, a pre-stressed modal analysis has been carried out on a cylindrical panel exposed to five different temperature fields.

Cylindrical panel with a lamination scheme  $[0/90/90/0]$  is considered for the detailed investigation and the results are given in Table 4.24. Table 4.24 presents the influence of thermal load on the natural frequencies of the panel. Irrespective of structural boundary constraints and nature of temperature fields, the natural frequencies reduce with increase in temperature, as observed by (Ganesan and Pradeep (2005), Jeyaraj (2013)). This happens due to a reduction in structural stiffness with increase in thermal stress. Further, studies have been carried out to investigate the influence of temperature fields and structural boundary constraints on the free vibration mode shapes.

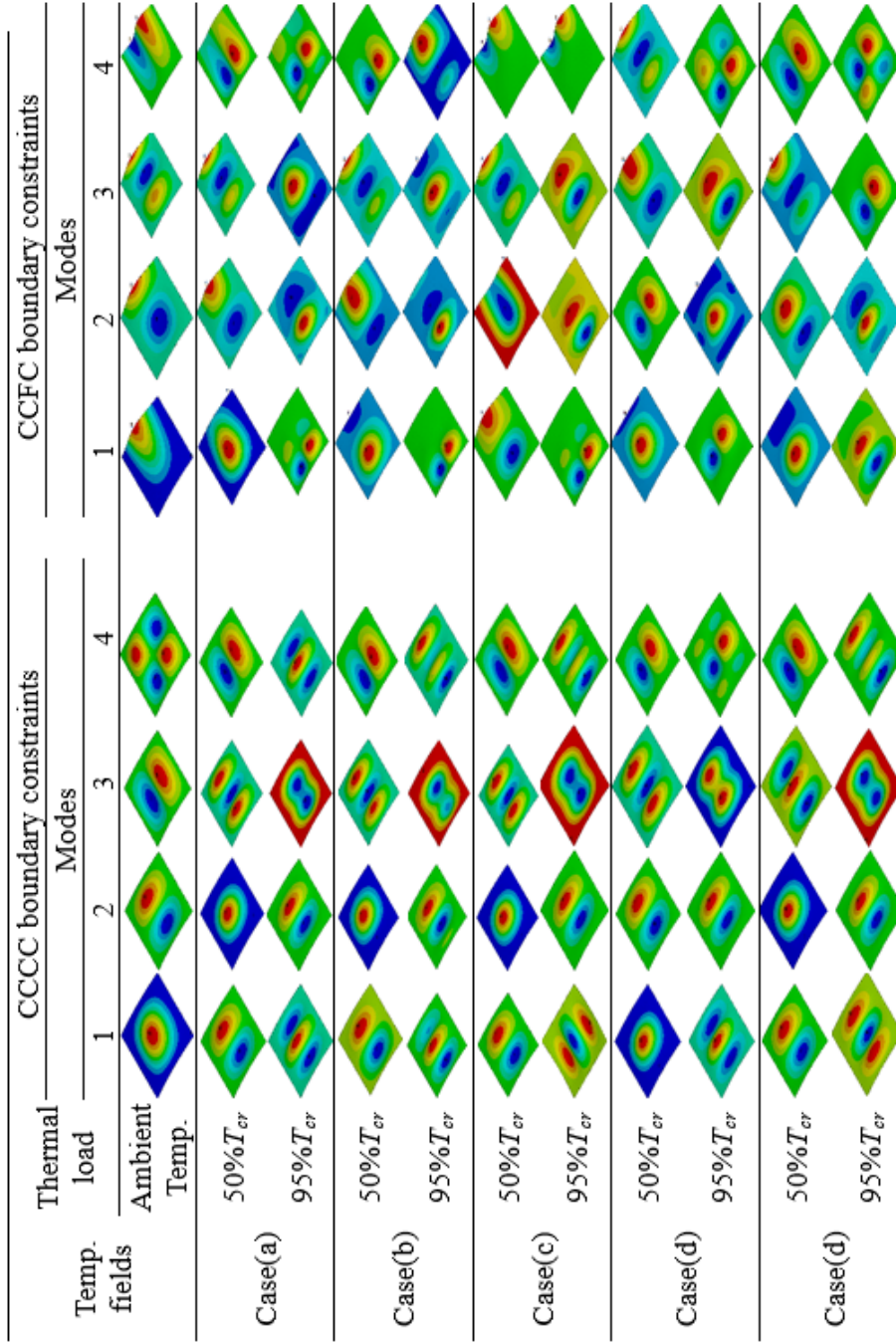
Variation in free vibration mode shapes of the panel with the increase in temperature is shown in Table 4.25. It is found that the free vibration mode shapes are significantly influenced by the level of temperature under all the temperature fields considered in the present study. Shifting of modes and moving of nodal and anti-nodal positions are commonly observed for the panel under different temperature fields. For example, mode 1 of CCCC panel having modal indices of (1,1) at ambient temperature changes to (3,1) at 95% of the critical buckling temperature under Case(a), Case(b), Case(d) and Case(e) temperature field whereas it changes to (1,3) for Case(c) temperature field as seen in Table 4.25. It is also observed that for the CCFC panel, with an increase in temperature, the anti-nodal position of modes is moving towards the fixed edge. For example, under Case(a), Case(b) and Case(c) temperature field, free vibration modes at ambient temperature under mode 1 are found to occur at the free edge but it shifts towards the fixed edge with the increase in temperature. This is due to the fact that; panel becomes soft at the free edge with the increases in temperature, thus making the vibration modes to shift towards the stiffer side of the panel. From Table 4.25 it is also revealed that free vibration mode shapes of the panel exposed to a temperature near the critical buckling temperature are similar to its buckling mode shape.

Table 4.24: Effect of thermal load and boundary constraints on free vibration frequencies (Hz) and associated modal indices of laminated panel

Boundary constraints	Modes	At ambient temp.	Temperature fields											
			Case(a)		Case(b)		Case(c)		Case(d)		Case(e)			
			50% $T_{cr}$	95% $T_{cr}$	50% $T_{cr}$	95% $T_{cr}$	50% $T_{cr}$	95% $T_{cr}$	50% $T_{cr}$	95% $T_{cr}$	50% $T_{cr}$	95% $T_{cr}$		
CCCC	1	2325 (1,1)	2067 (2,1)	789 (3,1)	2077 (2,1)	785 (3,1)	2076 (2,1)	784 (1,3)	2082 (1,1)	779 (3,1)	2072 (2,1)	795 (3,1)		
	2	2664 (2,1)	2119 (1,1)	1096 (2,1)	2139 (1,1)	1154 (2,1)	2135 (1,1)	1117 (2,1)	2091 (2,1)	1138 (2,1)	2107 (1,1)	1050 (2,1)		
	3	2876 (1,2)	2510 (3,1)	1978 (2,1)	2522 (3,1)	2002 (2,1)	2512 (3,1)	2011 (2,1)	2545 (3,1)	1975 (2,1)	2533 (3,1)	1978 (2,1)		
	4	3304 (2,2)	2667 (1,2)	2151 (3,1)	2713 (1,2)	2190 (3,1)	2726 (1,2)	2140 (3,1)	2603 (1,2)	2105 (1,2)	2677 (1,2)	2233 (3,1)		
CCFC	1	2260 (1,1)	2110 (1,1)	882 (1,2)	2157 (2,1)	930 (1,2)	2058 (2,1)	928 (1,2)	2031 (1,1)	759 (1,2)	1980 (2,1)	746 (2,1)		
	2	2354 (2,1)	2138 (2,1)	1728 (2,1)	2236 (2,1)	1537 (3,1)	2128 (1,1)	1055 (2,1)	2211 (1,2)	1576 (3,1)	2049 (2,1)	1094 (3,1)		
	3	2705 (3,1)	2352 (3,1)	1925 (1,1)	2373 (2,1)	2041 (3,1)	2178 (3,1)	1627 (2,1)	2226 (2,1)	1888 (2,1)	2271 (3,1)	1669 (1,2)		
	4	2771 (1,2)	2386 (1,2)	1952 (1,2)	2541 (1,2)	2219 (2,1)	2366 (1,2)	1803 (1,2)	2403 (3,1)	2216 (2,2)	2358 (1,2)	1797 (2,2)		

Note:  $T_{cr}$ - Critical buckling temperature associated with temperature field

Table 4.25: Effect of thermal load and boundary constraints on the free vibration mode shapes of laminated panel



Note: Red- max. displacement, Blue- min. displacement and others-in-between



## 4.6 Closure

This chapter deals with the investigation of buckling and free vibration behavior of cylindrical panels exposed to different temperature fields. The study has been carried out by using a numerical approach with the help of finite element tool. The material of the cylindrical panel considered for the analysis is assumed to have temperature independent properties. Two different cases have been analyzed, the first case is on isotropic cylindrical panel whereas the second case is on the laminated cylindrical panel. The panel has been analyzed for different geometrical parameters, temperature fields, and structural boundary constraints. The outcomes of the analysis indicate that the buckling and free vibration behavior of the cylindrical panels under thermal load are complex and significantly influenced by the temperature fields, in-plane boundary constraints, elevated temperature and geometric parameters. Magnification factors are established to predict the buckling temperature of the panel under non-uniform temperature fields knowing the buckling temperature under uniform temperature field. It is found from both the case studies that geometrical parameters such as thickness ratio, curvature ratio, and aspect ratio, play a dominant role in deciding the buckling strength of panels. Further, buckling temperature is inversely proportional to thickness and curvature ratio. Effect of non-uniform temperature fields on the buckling temperature of the panel is more prominent on the stiffer panel. It is also noticed that free vibration frequencies of the panel analyzed in both case studies decrease with the thermal load and variation is more significant at a thermal load close to buckling temperature. Shifting of nodal and anti-nodal lines and changing of modal indices with the rise in temperature has been observed through the present analysis. Further, jumping of free vibration modes is also noticed at a temperature close to the buckling temperature.

## CHAPTER 5

# STUDY ON CYLINDRICAL PANEL WITH TEMPERATURE DEPENDENT PROPERTIES

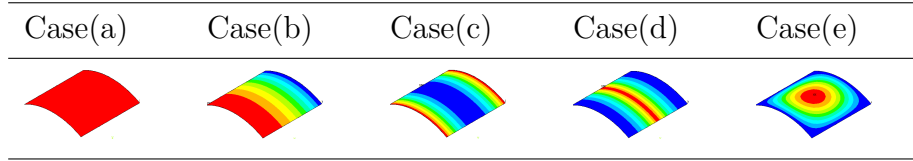
### 5.1 Introduction

As reported in preceding chapter the buckling and free vibration behavior of the cylindrical panel is highly influenced by the nature of in-plane temperature fields, geometrical parameters, and structural boundary constraints. The panel analyzed in preceding chapter was assumed to have temperature independent (TID) material elastic properties. But, elastic properties of polymer composite material are influenced by the elevated temperature. So, it is important to investigate the influence of temperature dependent (TD) elastic properties of the composite material on buckling and free vibration characteristics of the panel along with the nature of temperature fields and geometric parameters. The present chapter focuses on the buckling and the free vibration behavior of the cylindrical panel with temperature dependent(TD) properties using numerical approach. Two different case studies in terms of materials of the panel are analyzed in this chapter. The first case study focuses on the laminated composite cylindrical panel, whereas second case study is on functionally graded carbon nanotubes reinforced composites (FG-CNTRC) cylindrical panel.

### 5.2 Variation of temperature fields

Temperature-dependent heat transfer coefficient values of laminated composite and FG-CNTs reinforced composite panel was not found in the open literature.

Table 5.1: Different temperature fields in cylindrical panel



Note: Blue-ambient temperature, Red- peak temperature and others in-between

Thus instead of heat transfer analysis, in the present study, temperature fields are simulated using, three types of 1-D temperature field along the length and a 2-D in-plane variation. The panel, under uniform temperature field, is also investigated, so that influence of a change in the temperature field from uniform to non-uniform can be studied. Different temperature fields analyzed are shown in Table 5.1. Temperature fields with peak temperature,  $T_{max}$  are expressed in mathematical expression as given below,

Case(a): Uniform temperature field,  $T(x) = T_{max}$

Case(b): Decreasing temperature field,  $T(x) = T_{max}[1 - (\frac{x}{L})^2]$

Case(c): Decrease and increase temperature fields,  $T(x) = T_{max}[1 - (1 - abs(1 - \frac{2x}{L}))^2]$

Case(d): Increase and decrease temperature fields,  $T(x) = T_{max}[1 - abs(1 - \frac{2x}{L})^2]$

Case(e): Camel hump temperature field,  $T(x, y) = T_{max}[\sin(\frac{\pi y}{S}) \times \sin(\frac{\pi x}{L})]$

### 5.3 Case study-I: Laminated composite cylindrical panel

Analysis carried out on buckling and free vibration behavior of non-uniformly heated laminated composite cylindrical panel with TD properties are presented in this section. The analysis is carried out on a cylindrical panel with thickness ( $h$ ), width ( $S$ ), length ( $L$ ) and radius ( $R$ ) with following geometrical parameters:

( $h$ ) =0.001m, thickness ratio ( $S/h$ ) =200 and curvature ratio ( $R/S$ ) =5 if otherwise mentioned. The panel is assumed to be made of orthotropic material and its properties are assumed to be linear functions of the elevated temperature( $T$ ) (Shariyat (2007)).

$$\begin{aligned}
E_1(T) &= E_{10}(1 + E_{11}T) \\
E_2(T) &= E_{20}(1 + E_{21}T) \\
G_{12}(T) &= G_{120}(1 + G_{121}T) \\
G_{13}(T) &= G_{130}(1 + G_{131}T) \\
G_{23}(T) &= E_{230}(1 + E_{231}T) \\
\alpha_1(T) &= \alpha_{10}(1 + \alpha_{11}T) \\
\alpha_2(T) &= \alpha_{20}(1 + \alpha_{21}T)
\end{aligned} \tag{5.1}$$

where  $E_{10}/E_{20}=40$ ,  $G_{120}/E_{20} = G_{130}/E_{20}= 0.5$ ,  $E_{230}/E_{20}=0.2$ ,  $\nu_{12}=0.25$ ,  $\alpha_{10} = 10^{-6}/^{\circ}C$ ,  $\alpha_{20} = 10^{-5}/^{\circ}C$ ,  $E_{11}=-0.5 \times 10^{-3}$ ,  $E_{21} = G_{121} = G_{131} = G_{231} = -0.2 \times 10^{-3}$ ,  $\alpha_{11} = \alpha_{11} = 0.5 \times 10^{-3}$

Non-dimensional buckling temperature,  $T_{cr}^*$  is given by

$$T_{cr}^* = T_{cr} \times \alpha_{10} \times 10^3 \tag{5.2}$$

Non-dimensional frequency,  $\omega^*$  is given by

$$\omega^* = 2\pi \times f \times \frac{S^2}{h} \sqrt{\frac{\rho}{E_{20}}} \tag{5.3}$$

### 5.3.1 Results and discussion

#### Buckling behavior

The panel is analyzed to investigate the influence of different geometric parameters, temperature dependent(TD) properties and temperature fields on its buckling and free vibration behavior. A cylindrical panel with three different thickness ratio, aspect ratio, and curvature ratio are considered for investigation. Fig. 5.1

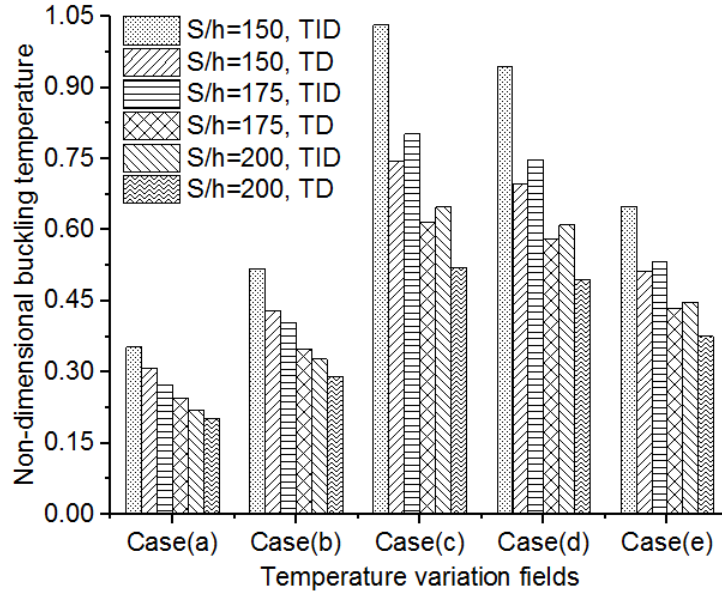


Figure 5.1: Influence of thickness ratio on the buckling temperature of the panel with TID and TD properties

shows the influence of the thickness ratio on the buckling temperature. In Fig. 5.1, TD indicates results obtained from a panel with temperature-dependent elastic properties and TID indicate results obtained from temperature-independent properties. As observed in previous analyses, buckling strength of the panel decrease with the increase in thickness ratio, this is due to the fact that the stiffness of the panel decrease with the increase in thickness ratio. This behavior is observed for the panel with both TD and TID properties. Panel exposed to Case(a) temperature field is observed to have low thermal buckling strength irrespective of thickness ratio and TD properties. Similarly, panel exposed to Case(c) temperature field is noticed to have high buckling strength. Further, it is also noticed that the difference in buckling temperature due to TD properties is highly significant at lower thickness ratio and it decreases with the increase in thickness ratio. Panel with a thickness ratio of 150, when exposed to Case(c) temperature field, exhibits the high buckling temperature difference between TD and TID properties compared to other temperature fields. Which indicates that the influence of TD properties is more significant at higher buckling temperature.

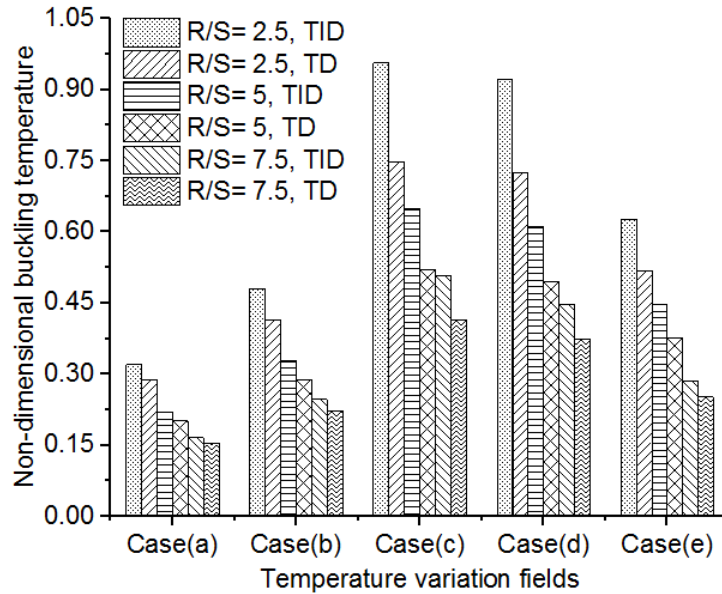


Figure 5.2: Influence of curvature ratio on the buckling temperature of the panel with TID and TD properties

The curvature ratio of the panel plays an important role in deciding the buckling strength of the panel. Panel with three different curvature ratio 2.5, 5 and 10 are considered for the investigation. As observed in the preceding chapter, the buckling strength of the panel decreases with the increase in curvature ratio and similar behavior is observed for a panel with TD properties also. Moment of inertia of the panel changes with the curvature ratio, which changes the stiffness of the panel. Panel with TD properties shows lower buckling strength compared to the panel with TID properties. Further influence of TD properties is more significant at lower curvature ratio and as expected it decreases with the rise in curvature ratio. Panel with different curvature ratio, when exposed to Case(c) temperature field, is observed to have high buckling strength whereas for the panel under Case(a) it is observed to have lower buckling strength. It is clearly seen from the analysis that, the influence of TD properties on buckling temperature is more significant on stiffer panels.

Fig. 5.3 shows the influence of aspect ratio and TD properties on the buckling temperature of the panel with different temperature fields. The panel is investi-

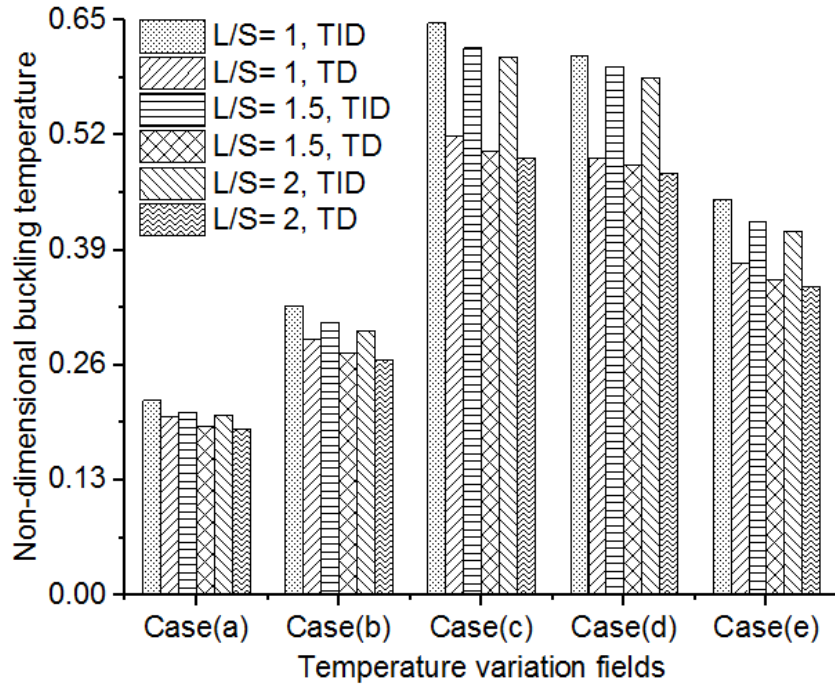


Figure 5.3: Influence of aspect ratio on the buckling temperature of the panel with TID and TD properties

gated with three different aspect ratio 1, 1.5 and 2 whereas thickness and curvature ratio are 150 and 5 respectively. It is observed from Fig. 5.3 that the buckling strength of the panel decrease with the increase in aspect ratio. As the aspect ratio increases, the length of the panel increases, which in turn decrease the stiffness of the panel. It is also observed that the influence of aspect ratio on the buckling strength is not so significant as compared to the thickness and curvature ratio analyzed in the preceded section. Further, the influence of TD material properties on buckling temperature is also observed for a panel with different aspect ratio. Among the different non-uniform temperature fields analyzed, Case(b) shows minimum buckling strength as a larger portion of the panel is exposed to peak temperature and hence develops more membrane forces.

Mechanical behavior of a laminated composite material is significantly influenced by the nature of the lamination scheme (lay-up) used. In order to investigate the effect of lamination schemes on the buckling temperature, eight layer laminated

panel with four different laminate schemes  $((0/90/0/90)_S, (0/90/0/90)_2, (45/-45/45/-45)_S$  and  $(45/-45/45/-45)_2$ ) is considered. Influence of different lamination schemes and TD properties on the buckling temperature is shown in Table 5.2. Angle ply lamination scheme results in higher buckling strength compared to cross-ply laminates as angle-ply laminate exhibit better properties in both transverse and longitudinal direction. Further, it is also noted that the symmetric lamination scheme gives less buckling strength compared to un-symmetric laminate. Panels exposed to Case(a) temperature field is observed to have lowest buckling strength while Case(c) with highest buckling temperature irrespective of the lamination scheme. Effect of TD properties on the buckling strength is significant for angle-ply lamination scheme compared to cross-ply.

Table 5.3 depicts the influence of thickness ratio on the fundamental buckling mode shape of the panel with different temperature fields. From Table 5.3, it is clear that the buckling mode shape of the panel changes significantly with the thickness ratio and the nature of non-uniform heating. Change in fundamental buckling mode shape with an increase in thickness ratio can be attributed to decrease in structural stiffness with increase in thickness ratio. Panel exposed to Case(b) temperature field is noted to have high bending amplitude in the area subjected to peak temperature, whereas section opposite to it experiences least bending amplitude as shown in Table 5.3. With the change in thickness ratio, buckling mode shapes observed for a panel with Case(e) does not change significantly but their modal indices increases along the circumferential direction. Similar behavior of the buckling modes is observed for a panel with Case(a), Case(b), Case(c) and Case(d), temperature fields.

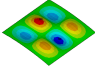
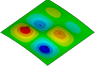
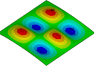
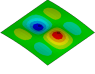
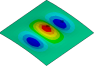
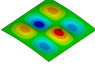
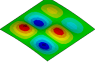
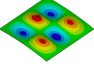
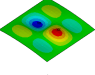
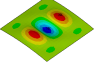
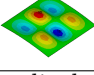
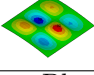
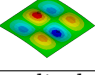
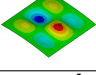
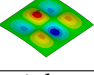
Influence of curvature ratio and temperature fields on the buckling mode shape is depicted in Tables 5.4. As expected, the moment of inertia of the panel changes with the curvature ratio and its effect can be seen in the buckling mode shape and its modal indices. Table 5.4 reveals that the modal indices associated with



Table 5.2: Influence of different lamination schemes on the buckling temperature of the panel with TID and TD properties

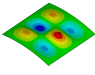
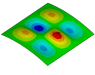
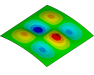
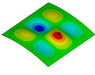
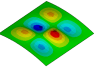
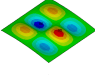
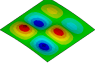
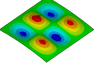
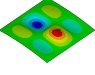
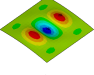
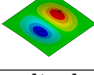
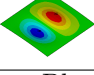
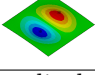
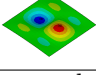
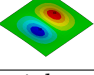
Temperature field	$(0/90/0/90)_s$		$(0/90/0/90)_2$		$(45/-45/45/-45)_s$		$(45/-45/-45/45)_2$		% Diff.
	TID	TD	TID	TD	TID	TD	TID	TD	
Case(a)	0.220	0.201	0.232	0.212	0.552	0.440	0.582	0.457	20.4
Case(b)	0.328	0.289	0.343	0.301	0.621	0.489	0.683	0.524	21.3
Case(c)	0.648	0.519	0.718	0.566	1.201	0.812	1.366	0.872	32.4
Case(d)	0.610	0.495	0.623	0.499	1.451	0.905	1.474	0.913	37.6
Case(e)	0.448	0.376	0.473	0.398	1.341	0.800	1.391	0.817	40.3

Table 5.3: Influence of thickness ratio on the fundamental buckling mode of the panel with TD properties

Thickness ratio	Temperature fields				
	Case(a)	Case(b)	Case(c)	Case(d)	Case(e)
$S/h=150$					
$S/h=200$					
$S/h=300$					

Note: Red- max. displacement, Blue- min. displacement and others-inbetween

Table 5.4: Influence of curvature ratio on the fundamental buckling mode of the panel with TD properties

Curvature ratio	Temperature fields				
	Case(a)	Case(b)	Case(c)	Case(d)	Case(e)
$R/S=2.5$					
$R/S=5$					
$R/S=10$					

Note: Red- max. displacement, Blue- min. displacement and others-inbetween

the buckling mode for different temperature fields are highly influenced by the curvature ratio of the panel. It is also observed that at higher curvature ratio, there is not much variation in the bending amplitude and the modal indices. Further, it is seen that the modal indices of the buckling modes decrease with the increase in curvature ratio along the longitudinal and circumferential direction irrespective of temperature fields.

### Free vibration under thermal load

The pre-stressed modal analysis is carried out to investigate the influence of thermal load on free vibration behavior and associated modes of a cylindrical panel with TD and TID properties, exposed to five different temperature fields. A

cylindrical panel with a lamination scheme of  $[0^\circ/90^\circ/0^\circ/90^\circ]_S$  is considered for the detailed investigation and the results are shown in Table 5.5. To demonstrate, the effect of the thermal load as a function of critical buckling temperature on free vibration characteristics, the panel is investigated at 50% and 95% of the critical buckling temperature,  $T_{cr}$ . As expected, irrespective of nature of temperature fields, the natural frequencies decrease with an increase in temperature. This happens due to a reduction in structural stiffness with increase in thermal stress. Reduction in the natural frequencies due to thermal load is observed for a panel with both TID and TD properties.

It is difficult to compare the results of free vibration frequencies under thermal load carried out for a panel with both TD and TID properties. As the thermal load considered for the investigation is a function of buckling temperature which is different for both TD and TID properties. Further, it is also observed that influence of temperature fields on natural frequencies of the panel cannot be compared as buckling temperature varies with the temperature fields also. Thus, panel exposed to different temperature fields with a constant thermal load is investigated. Panel exposed to  $300^\circ\text{C}$  is considered for this purpose and results are given in Table 5.6. It is clear from Table 5.6 that the natural frequencies of the panel decrease drastically for a panel with TD properties compared to TID properties. Reduction in material properties with increase in temperature results in significant reduction of natural frequencies and this effect is severe for a panel whose major area is exposed to peak temperature. Among different non-uniform temperature fields analyzed, a panel with Case(b) temperature field experiences the highest reduction in natural frequencies.

As reported in the previous chapter, significant changes in free vibration modes of the cylindrical panel with TD properties is observed when the thermal load is close to buckling temperature. Knowing this behavior, panel with TD properties is investigated to study the influence of TD properties on the free vibration modes.

Table 5.5: Effect of buckling temperature( $T_{cr}$ ) on free vibration frequencies of laminated composite panel

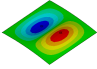
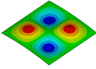
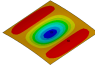
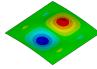
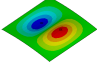
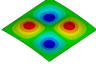
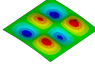
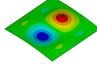
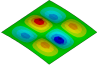
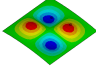
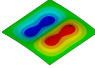
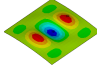
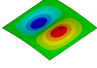
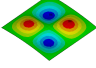
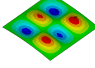
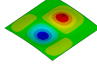
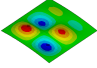
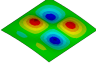
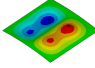
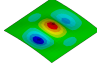
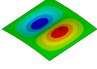
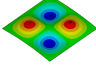
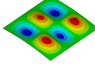
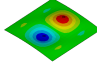
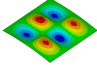
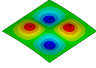
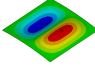
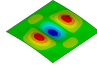
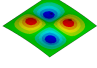
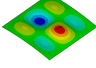
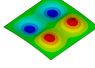
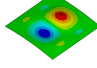
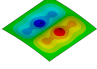
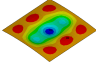
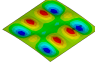
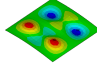
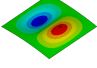
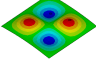
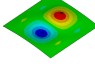
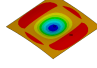
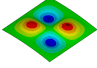
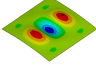
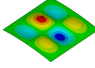
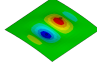
Cases	Modes	Temperature fields																
		At ambient temp.		Case(a)			Case(b)			Case(c)			Case(d)			Case(e)		
		50% $T_{cr}$	95% $T_{cr}$	50% $T_{cr}$	95% $T_{cr}$	50% $T_{cr}$	95% $T_{cr}$	50% $T_{cr}$	95% $T_{cr}$	50% $T_{cr}$	95% $T_{cr}$	50% $T_{cr}$	95% $T_{cr}$	50% $T_{cr}$	95% $T_{cr}$	50% $T_{cr}$	95% $T_{cr}$	
TID with pre-stress	1	0.092	0.082	0.036	0.082	0.034	0.085	0.036	0.085	0.036	0.041	0.027	0.081	0.038				
	2	0.114	0.085	0.040	0.085	0.043	0.086	0.049	0.086	0.049	0.044	0.054	0.086	0.039				
	3	0.128	0.113	0.075	0.114	0.074	0.112	0.079	0.112	0.079	0.074	0.104	0.113	0.041				
	4	0.141	0.119	0.084	0.119	0.085	0.120	0.084	0.120	0.084	0.089	0.113	0.115	0.057				
TD with pre-stress	1	0.092	0.080	0.035	0.079	0.033	0.079	0.034	0.079	0.034	0.050	0.004	0.078	0.038				
	2	0.114	0.084	0.039	0.084	0.041	0.083	0.043	0.083	0.043	0.059	0.045	0.084	0.040				
	3	0.128	0.113	0.071	0.113	0.068	0.110	0.067	0.110	0.067	0.072	0.089	0.110	0.040				
	4	0.141	0.117	0.079	0.116	0.078	0.113	0.070	0.113	0.070	0.091	0.094	0.112	0.053				

Table 5.6: Effect of elevated temperature ( $T_o=300^\circ\text{C}$ ) on free vibration frequencies of laminated composite panel

Cases	Modes	At ambient temp.	Temperature fields														
			Case(a)			Case(b)			Case(c)			Case(d)			Case(e)		
			50% $T_o$	95% $T_o$	95% $T_o$	50% $T_o$	95% $T_o$	95% $T_o$	50% $T_o$	95% $T_o$	95% $T_o$	50% $T_o$	95% $T_o$	95% $T_o$	50% $T_o$	95% $T_o$	95% $T_{cr}$
TID with pre-stress	1	0.092	0.071	0.065	0.083	0.050	0.089	0.086	0.082	0.050	0.085	0.075	0.078	0.078	0.078	0.078	0.078
	2	0.114	0.078	0.079	0.088	0.059	0.102	0.090	0.088	0.058	0.096	0.078	0.096	0.096	0.096	0.096	0.096
	3	0.128	0.092	0.109	0.118	0.077	0.125	0.119	0.119	0.076	0.122	0.100	0.122	0.122	0.122	0.122	0.100
	4	0.141	0.109	0.124	0.121	0.095	0.132	0.123	0.121	0.097	0.124	0.103	0.124	0.124	0.124	0.124	0.103
TD with pre-stress	1	0.092	0.064	0.041	0.079	0.018	0.085	0.078	0.078	0.024	0.081	0.063	0.078	0.078	0.078	0.078	0.063
	2	0.114	0.072	0.052	0.082	0.033	0.097	0.080	0.082	0.027	0.091	0.068	0.082	0.082	0.082	0.082	0.068
	3	0.128	0.083	0.070	0.111	0.067	0.120	0.104	0.111	0.066	0.116	0.084	0.111	0.111	0.111	0.116	0.084
	4	0.141	0.102	0.074	0.114	0.072	0.126	0.110	0.114	0.073	0.117	0.086	0.114	0.114	0.114	0.117	0.086

Table 5.6 shows the influence of thermal load on a panel exposed to different temperature fields with TD properties. As expected, it is observed from the analysis that free vibration modes of a panel with the thermal load changes even with TD properties. Further, change in nodal and anti-nodal position of modes with the thermal load close to buckling temperature is also observed.

Table 5.7: Effect of buckling temperature( $T_{cr}$ ) on free vibration modes of laminated composite panel

Temperature fields	Thermal load	Modes			
		1	2	3	4
	At ambient temp				
Case(a)	50% $T_{cr}$				
	95% $T_{cr}$				
Case(b)	50% $T_{cr}$				
	95% $T_{cr}$				
Case(c)	50% $T_{cr}$				
	95% $T_{cr}$				
Case(d)	50% $T_{cr}$				
	95% $T_{cr}$				
Case(e)	50% $T_{cr}$				
	95% $T_{cr}$				

Note: Red- max. displacement, Blue- min. displacement and others-inbetween

## 5.4 Case study-II: Functionally graded carbon nano-tubes reinforced composites cylindrical panel

Carbon nanotubes reinforced polymer nano-composite cylindrical panel with TD properties under non-uniform heating is considered for the investigation. The single-walled carbon nanotube (SWCNT) reinforcement is either functionally graded (FG) or uniformly distributed (UD) through the thickness direction. Three types of through thickness functionally graded distribution of carbon nanotubes (CNTs) namely, FG-O, FG-V, and FG-X are considered in the present study and for comparison, uniform distribution (UD) of CNTs is also considered. The configuration of different CNTs distribution is shown in Fig. 5.4. Effective material proper-

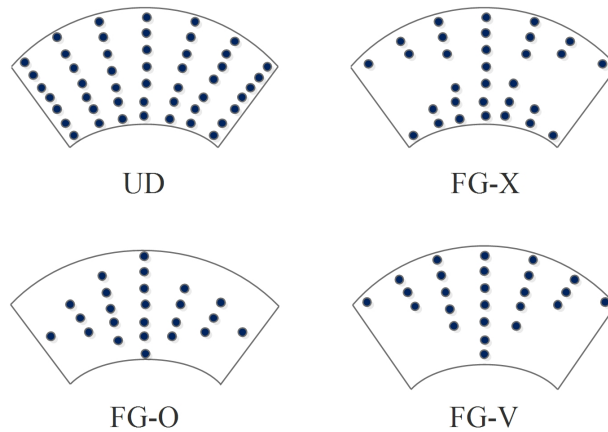


Figure 5.4: Configurations of different FG-CNTs reinforced panels

ties of Carbon nanotubes reinforced composite (CNTRC), are calculated based on Mori-Tanaka scheme (AU Shi *et al.* (2004)) or the rule of mixture (Fidelus *et al.* (2005)). The rule of mixture is identified as a simple model and also convenient to use while predicting the overall material properties. Consequently, in the present study, effective material properties of the reinforced composite panel are obtained by employing the rule of mixtures approach. Rule of mixtures approach which in-

incorporates the efficiency parameters is employed to obtain the elastic properties of FG-CNTRC cylindrical panel. The effective shear modulus and Young's modulus of the panel can be extracted by employing Eq. (5.4) (Shen (2011)).

$$\begin{aligned}
 E_{11} &= \eta_1 V_{CNT} E_{11}^{CNT} + V_M E^M \\
 \frac{\eta_2}{E_{22}} &= \frac{V_{CNT}}{E_{22}^{CNT}} + \frac{V_M}{E^M} \\
 \frac{\eta_3}{G_{12}} &= \frac{V_{CNT}}{G_{12}^{CNT}} + \frac{V_M}{G^M}
 \end{aligned} \tag{5.4}$$

In Eq. (5.4),  $\eta_1$ ,  $\eta_2$  and  $\eta_3$  are the efficiency parameters introduced to obtain the size dependent material properties of the FG-CNTRC cylindrical panel and are considered to fit the data collected from the conventional rule of mixtures approach with those of molecular dynamics simulation (Han and Elliott (2007)). Besides, in Eq. (5.4), the Young modulus and shear modulus of SWCNTs are denoted by  $E_{11}^{CNT}$ ;  $E_{22}^{CNT}$  and  $G_{12}^{CNT}$ , respectively. Furthermore, properties of the isotropic matrix are given by  $E^M$  and  $G^M$ .  $V_{CNT}$  and  $V_M$  represents the volume fraction of CNTs and matrix, respectively and follows the relation

$$V_{CNT} + V_M = 1 \tag{5.5}$$

In the present study, FG-CNTRC panel with four different types of CNTs distributions (Zhu *et al.* (2012)) through thickness directions has been analyzed. The volume fraction of CNTs in each lamina as a function of thickness coordinate for the three different types of CNTs distributions are as follows (Zhu *et al.* (2012)).



$$V_{CNT}(Z) = \begin{cases} V_{CNT}^* & (UD) \\ 2\left(1 - \frac{|2z|}{h}\right)V_{CNT}^* & (FG - O) \\ 2\left(\frac{2|z|}{h}\right)V_{CNT}^* & (FG - X) \\ \left(1 + \frac{2z}{h}\right)V_{CNT}^* & (FG - V) \end{cases} \quad (5.6)$$

$$V_{CNT}^* = \frac{W_{CNT}}{W_{CNT} + (\rho^{CNT}/\rho^m) - (\rho^{CNT}/\rho^m)W_{CNT}} \quad (5.7)$$

where, mass fraction and mass density of the CNTs are given by  $W_{CNT}$  and  $\rho^{CNT}$  respectively, whereas mass density of the isotropic matrix is given by  $\rho^m$ . The thermal expansion coefficients in longitudinal and transverse directions are denoted by  $\alpha_{11}$  and  $\alpha_{22}$ , respectively. The Poisson's ratio  $\nu_{12}$  and the overall mass density  $\rho$  are as given below.

$$\nu_{12} = V_{CNT}\nu_{12}^{CNT} + V_M\nu^m \quad (5.8)$$

$$\rho = V_{CNT}\rho^{CNT} + V_M\rho^m \quad (5.9)$$

$$\alpha_{11} = V_{CNT}\alpha_{11}^{CNT} + V_M\alpha^m \quad (5.10)$$

$$\alpha_{22} = (1 + \nu_{12}^{CNT})V_{CNT}\alpha_{22}^{CNT} + V_M\alpha^m - \nu_{12}\alpha_{11} \quad (5.11)$$

### 5.4.1 Validation Studies

#### Critical buckling temperature evaluation

Cylindrical shell made of functionally graded materials, investigated by Boroujerdy *et al.* (2014) for the thermal buckling strength with TD properties is considered for the validation. Material analyzed was  $\text{Si}_3\text{N}_4/\text{SUS}_{304}$  with proportionate dimensions of the panel are  $L = \sqrt{300Rh}$ ,  $R/h = 400$ . Boroujerdy *et al.* (2014) used an

analytical method, while present method uses commercial finite element software, ANSYS. An eight noded layered structural shell element formulated based on first order shear deformation theory. SHELL 281 available is used. Critical buckling temperature evaluated using the present method shows good agreement with that of Boroujerdy *et al.* (2014) as seen in Table 5.8.

Table 5.8: Comparison of buckling strength of the FGM panel with TD properties

Volume fraction index	Critical buckling temperature ( $K$ )		
	Boroujerdy <i>et al.</i> (2014)	Present	%diff.
0	392.79	393.95	0.29
0.2	402.31	401.86	0.11
0.5	412.55	411.09	0.35
1	424.15	421.61	0.60

### Evaluation of Free Vibration Frequencies

CNTs reinforced cylindrical panel analyzed by Zhang *et al.* (2014a) for its static and dynamic behavior has been considered for the validation. The dimension of the panel investigated are  $h=0.002\text{m}$ ,  $h/R=0.002$ ,  $L/R=0.1$  and  $\theta =0.1\text{rad}$ . For comparison, two types of CNTs distribution, namely UD and FG-X are considered with 0.12 of CNTs volume fraction. The present method uses an FEA tool, whereas Zhang *et al.* (2014a) used an approach based on first order shear deformation theory. Extracted non-dimensional natural frequency for a simply supported cylindrical shell, using present study matches very well with that of results reported by Zhang *et al.* (2014a) as shown in Table 5.9. Non-dimensional natural frequency is given by  $\hat{\omega} = \omega(\frac{S^2}{h})\sqrt{\frac{\rho^M}{EM}}$ .

### 5.4.2 Results and discussion

CNTRC cylindrical panel under non-uniform heating is studied to predict the buckling and dynamic characteristics. Influence of various geometric parameters,

Table 5.9: Comparison of Non-dimensional natural frequencies with Zhang *et al.* (2014a)

Modes	UD			FG-X		
	Zhang <i>et al.</i> (2014a)	Present	%Diff.	Zhang <i>et al.</i> (2014a)	Present	%Diff.
1	17.85	17.79	0.33	21.24	21.56	1.51
2	22.07	22.76	3.12	25.10	26.08	3.90
3	33.29	34.79	7.74	35.94	37.76	5.06
4	51.77	53.98	4.26	54.54	57.11	4.71
5	65.12	63.80	2.02	76.76	75.95	1.06

structural boundary constraints, and nature of temperature field on the buckling and free vibration behaviors of the panel are analyzed. Similarly, the free vibration behavior of the panel with TD properties, exposed to the thermal environment is also addressed. A cylindrical panel with thickness ( $h$ ), width ( $S$ ), length ( $L$ ) and radius ( $R$ ) with following geometrical parameters:  $h = 0.001\text{m}$ , thickness ratio ( $S/h$ ) = 100 and curvature ratio ( $R/S$ ) = 2 is considered for investigation in the present study otherwise it is mentioned. For the present simulation, Poly Methyl Methacrylate, referred to as PMMA, is chosen as the matrix with material properties  $E_m = (3.52 - 0.0034T)$  GPa,  $\nu_m = 0.34$  and  $\alpha_m = 45(1 + 0.0005\Delta T)10^{-6}/\text{K}$ . In the calculation of elasticity modulus of matrix  $T = T_0 + \Delta T$  where  $T_0 = 300\text{K}$  is the reference temperature. For reinforcement, (10, 10) armchair single-walled carbon nanotube (SWCNT) is selected. Poisson's ratio, shear modulus, elasticity modulus and thermal expansion coefficient of SWCNTs are assumed to be TD. To carry out an investigation on a panel with TD properties, the thermo-mechanical properties of (10, 10) armchair SWCNTs is predicted as a function of temperature using a third order interpolation (Mirzaei and Kiani (2015)). Change in thermo-mechanical properties of (10, 10) armchair SWCNTs with temperature for a range of  $300\text{K} \leq T \leq 700\text{K}$  are as follows:

$$\begin{aligned}
E_{11}^{CNT}(T)[Tpa] &= 6.3998 - 4.338417 \times 10^{-3}T + 7.43 \times 10^{-6}T^2 - 4.458333 \times 10^{-9}T^3 \\
E_{22}^{CNT}(T)[Tpa] &= 8.02155 - 5.420375 \times 10^{-3}T + 9.275 \times 10^{-6}T^2 - 5.5625 \times 10^{-9}T^3 \\
G_{12}^{CNT}(T)[Tpa] &= 1.40755 + 3.476208 \times 10^{-3}T - 6.965 \times 10^{-6}T^2 + 4.479167 \times 10^{-9}T^3 \\
\alpha_{11}^{CNT}(T) &= (-1.12515 + 0.02291688T - 2.887 \times 10^{-5}T^2 + 1.13625 \times 10^{-8}T^3) \times \alpha_0 \\
\alpha_{22}^{CNT}(T) &= (5.43715 + 9.84625 \times 10^{-4}T - 2.9 \times 10^{-7}T^2 + 1.25 \times 10^{-11}T^3) \times \alpha_0 \\
\alpha_0 &= 10^{-6}/K \\
\nu_{12}^{CNT} &= 0.175
\end{aligned} \tag{5.12}$$

Present analysis mainly focuses on four different configurations of CNTs distribution (UD, FG-X, FG-O and FG-V) with three different volume fractions (0.12, 0.17, 0.28) to investigate the influence of functional grading and volume fraction of CNTs on the buckling and free vibration characteristics of non-uniformly heated CNTRC cylindrical panel. In Figure 5.4, UD represents the uniform distribution of CNTs, FG-X represent volume fraction of CNTs increasing symmetrically from the mid-plane and FG-O represents volume fraction of CNTs decreasing symmetrically from the mid-plane. To know the effect of un-symmetry associated with CNTs distribution, FG-V is considered. The CNTs efficiency parameters,  $\eta_i$  for different volume fractions are  $\eta_1 = 0.137$  and  $\eta_2 = 1.022$  for  $V_{CNT}^* = 0.12$ ,  $\eta_1 = 0.142$  and  $\eta_2 = 1.626$  for  $V_{CNT}^* = 0.17$  and  $\eta_1 = 0.141$  and  $\eta_2 = 1.585$  for  $V_{CNT}^* = 0.28$  and  $\eta_2 = \eta_3$ . The panel is analyzed with five different in-plane temperature fields and three different boundary constraints (CCCC, SSSC, and CCFC).

Non-dimensional critical buckling temperature used to represent the critical buckling temperature is  $T_{cr}^*$  is given by

$$T_{cr}^* = T_{cr} \times \alpha_0 \times 10^{-3} \tag{5.13}$$

## Buckling Behaviour

The influence of thickness ratio and the in-plane temperature fields on the buckling strength is carried out on a panel with different thickness ratio. Fig. 5.5 shows the effect of the thickness ratio on the buckling strength of the CNTRC panel. It is observed that the buckling strength of the panel decreases with the increase in thickness ratio and a similar trend is noticed for all in-plane temperature fields. This behavior of the panel is observed due to change in stiffness and the developed membrane force of the panel with the thickness ratio. The panel, under Case(a) temperature field, has the lowest buckling strength compared to all other temperature fields considered in the analysis. This is due to the fact that the panel under Case(a) temperature field produces more membrane forces as the total area is exposed to peak temperature. In addition, it is observed that panel loses its buckling strength under TD properties. Material properties of the panel deteriorate with the temperature, thus buckling strength of the panel decreases. Variation in the buckling strength of the panel with TID and TD properties is more significant at lower thickness ratio and the variation ceases out with the increase in thickness ratio. Further, it is also observed that the buckling strength of the panel is influenced by the CNTs distribution. The panel with the FG-X pattern is observed to have highest buckling strength compared to the panels with other patterns of CNTs distribution (UD, FG-V, and FG-O). This is due to the fact that the stiffness of the panel with the FG-X pattern is high compared to other patterns considered here. Panel with the FG-V pattern is found to have better buckling strength than the FG-O pattern which indicates that CNTs distribution away from the mid-plane has the better effect on the stiffness of the panel.

The curvature of the cylindrical panel plays an important role in deciding the buckling strength of the panel. Fig. 5.6 Shows the influence of the curvature ratio and in-plane temperature fields on the buckling strength of the panel. It is seen from Fig. 5.6 that, the buckling strength is inversely proportional to the

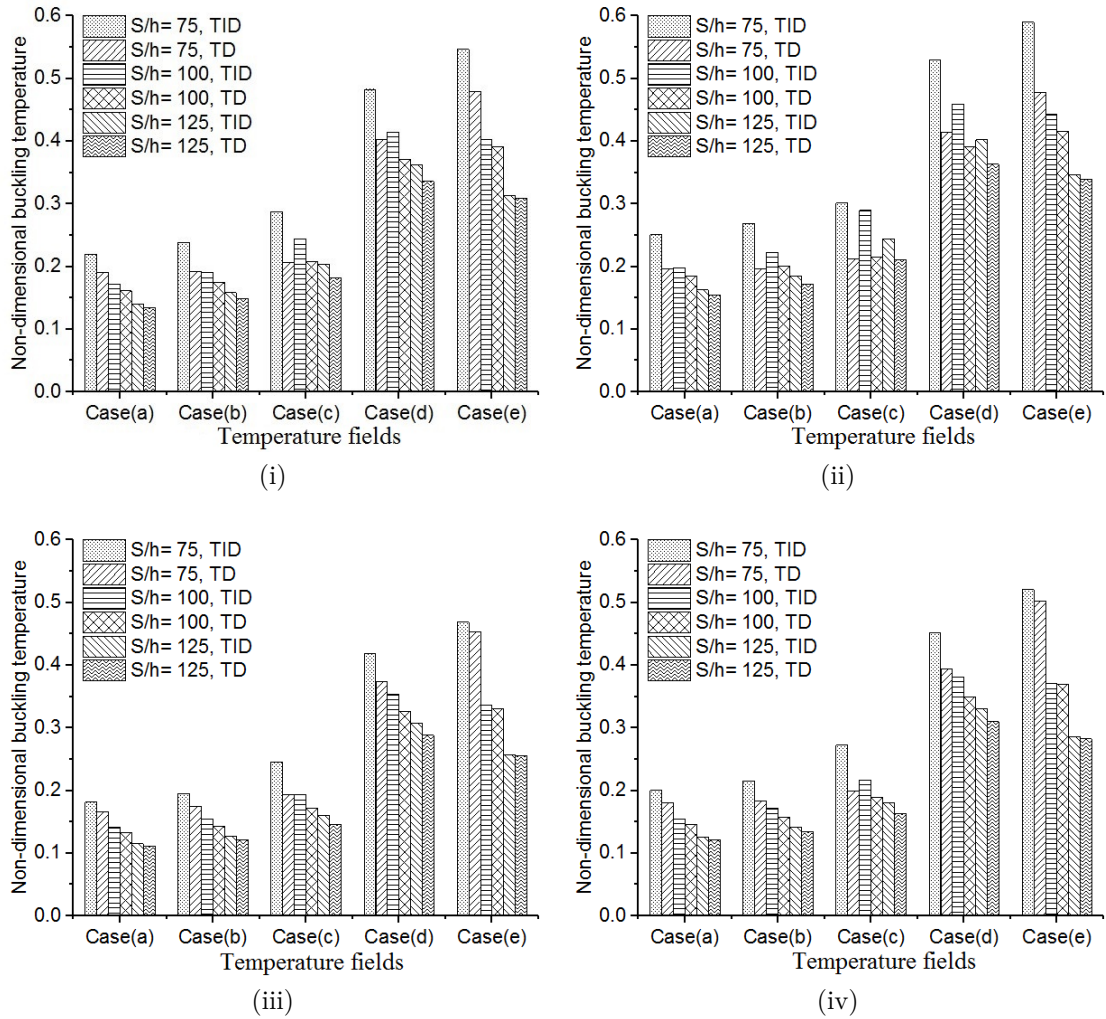


Figure 5.5: Effect of thickness ratio and temperature fields on buckling strength of CCCC cylindrical panel with CNTs pattern (i) UD, (ii) FG-X, (iii) FG-O, and (iv) FG-V

curvature ratio. As the curvature ratio increases, the moment of inertia of the panel decreases thus decreases the bending resistance of the panel. The buckling strength of the panel is influenced by the in-plane temperature fields irrespective curvature ratio. Case(d) and Case(e) temperature fields are observed to have a high buckling temperature due to the lower value of thermal stress generated. As seen before, TD properties of the panel influence the buckling strength and are found to be more significant at lower curvature ratio. At a lower curvature ratio, the panel has high buckling temperature and thus it affects the elastic properties significantly. Compared to different CNTs distributions pattern, the FG-X pattern is observed to have more buckling strength than others, whereas FG-O has low buckling strength.

Influence of volume fraction on the buckling strength of the panel along with the thickness ratio is investigated and for this, a panel with the FG-X pattern is considered. Again, it is observed from Fig. 5.7 that irrespective of the temperature fields and CNTs volume fraction, buckling strength of the panel decreases with the increase in thickness ratio. The buckling behavior of the panel with different temperature fields is observed to be same irrespective of CNTs volume fractions. Wherein panel under Case(a) and Case(e) temperature fields is observed to have a minimum and the maximum buckling strength of the panel. This indicates that the amount of area exposed to maximum temperature influences the buckling strength of the panel significantly. It is also observed from Fig. 5.7 that the buckling strength of the panel is enhanced by increasing the volume fraction of the CNTs. Thus volume fraction of 0.28 is observed to have a highest buckling temperature irrespective of temperature fields analyzed. Further, it is noted that the reduction in buckling strength due to TD properties is found to be more significant at a higher volume fraction and lower thickness ratio. To study the influence of curvature ratio and CNTs volume fraction, on the buckling strength, the panel with three different CNTs volume fraction is analyzed. Fig. 5.8 depicts the influence of volume fraction and curvature ratio on the buckling strength

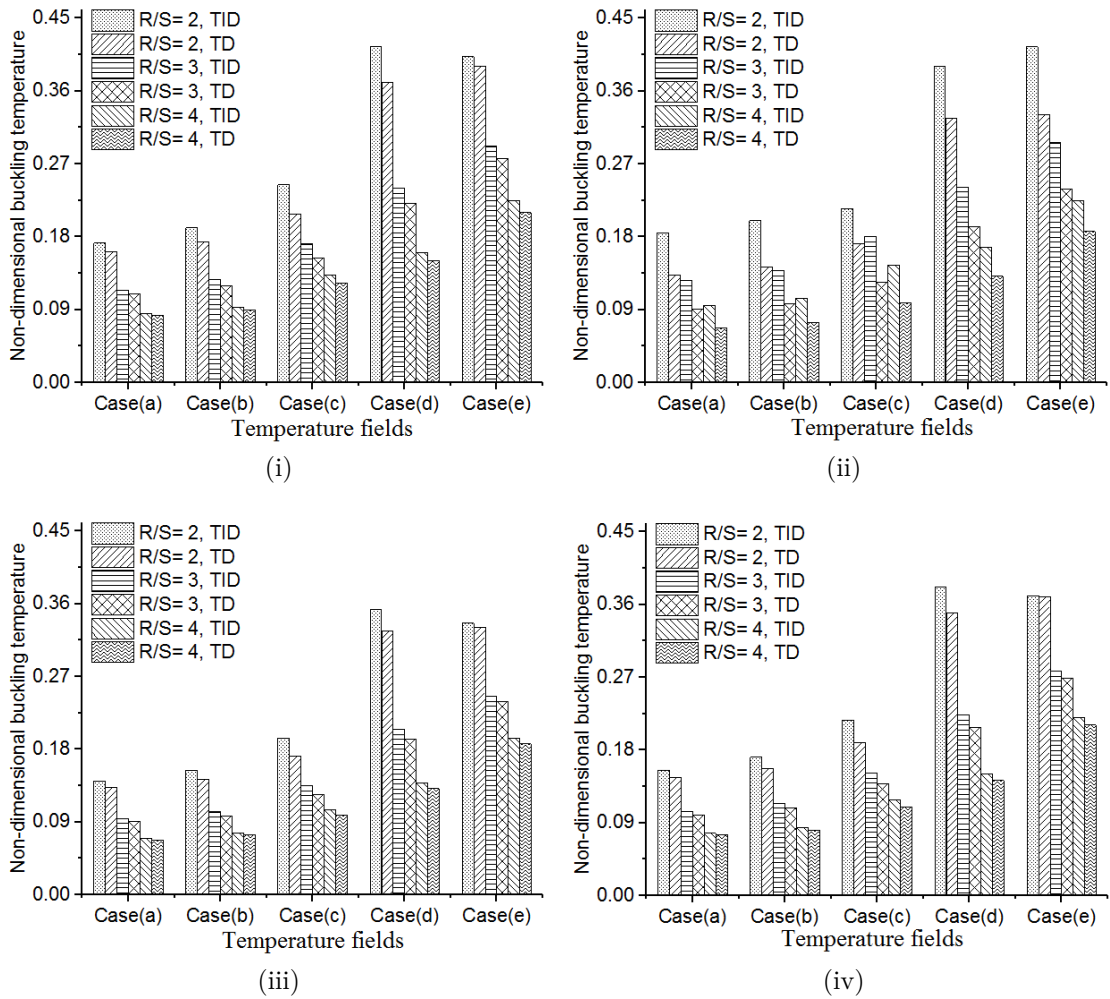


Figure 5.6: Effect of curvature ratio and temperature fields on buckling strength of CCCC cylindrical panel with CNTs pattern (i) UD, (ii) FG-X, (iii) FG-O, and (iv) FG-V



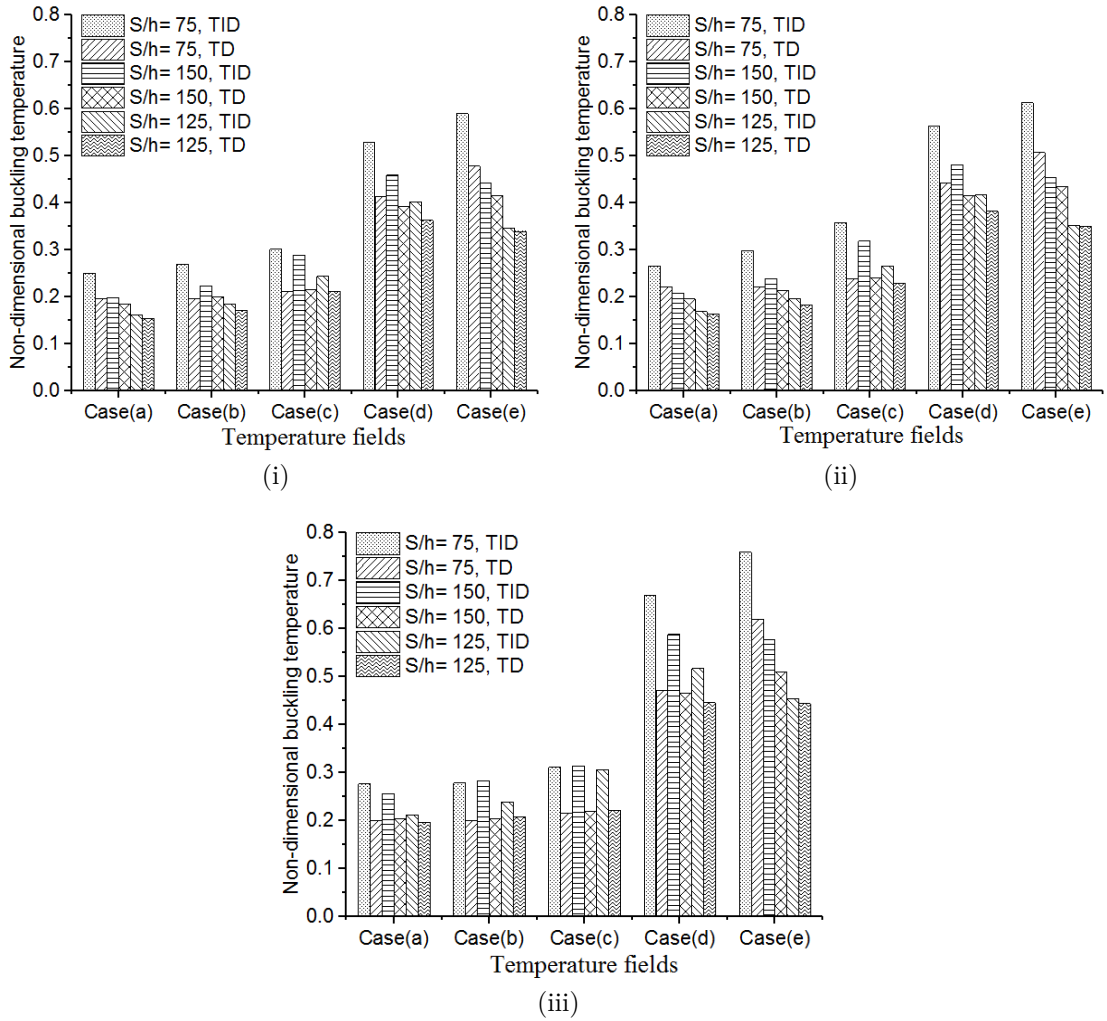


Figure 5.7: Effect of thickness ratio and temperature fields on buckling strength of CCC cylindrical panel with CNTs volume fraction (i) 0.12, (ii) 0.17, and (iii) 0.28

of the panel exposed to different temperature fields. As seen before, buckling strength of the panel decreases with the increase in curvature ratio irrespective of CNTs volume fraction. Variation in the buckling strength of the panel observed in the different temperature fields decreases with the increase in curvature ratio. Similarly, a reduction in the buckling strength due to TD properties of the panel reduces with the increase in curvature ratio. Further, it is seen that buckling strength of the panel increases with the CNTs volume fraction irrespective of the temperature fields and curvature ratio. Improvement of the buckling strength with the CNTs volume fraction is high at lower curvature ratio and vice-versa. It is also noticed that the influence of TD properties is more significant at higher CNTs volume fraction. This is due to the fact that the addition of CNTs, makes the panel stiffer thus increases the buckling temperature and because of this high temperature, material properties of the panel deteriorates significantly.

Table 5.10 shows the combined effect of functional grading pattern, CNTs volume fraction and TD properties, on the buckling strength of the panel with temperature fields. As observed in earlier studies, buckling strength of the panel increases with the CNTs volume fraction irrespective of functional grading patterns and nature of temperature fields. This indicates that reinforcement of CNTs enhances the structural stiffness of the composite and hence increases its buckling strength. Panel with FG-X pattern and volume fraction of 0.28 is observed to have maximum buckling strength irrespective of the temperature fields analyzed. Higher volume fraction with efficient distribution of CNTs makes panel much stiffer compared to other combination that is analyzed. Panel exposed to Case(a) and Case(d) temperature fields is observed to have lowest and highest buckling strength respectively. This correspondence to the development of membrane forces due to thermal load which is high in case of Case(a) and low in case of Case(d). Table 5.10 also shows the percentage difference of the buckling strength of the panel with TID and TD properties. It is noticed that higher percentage difference is observed for the FG-X pattern at a higher volume fraction.

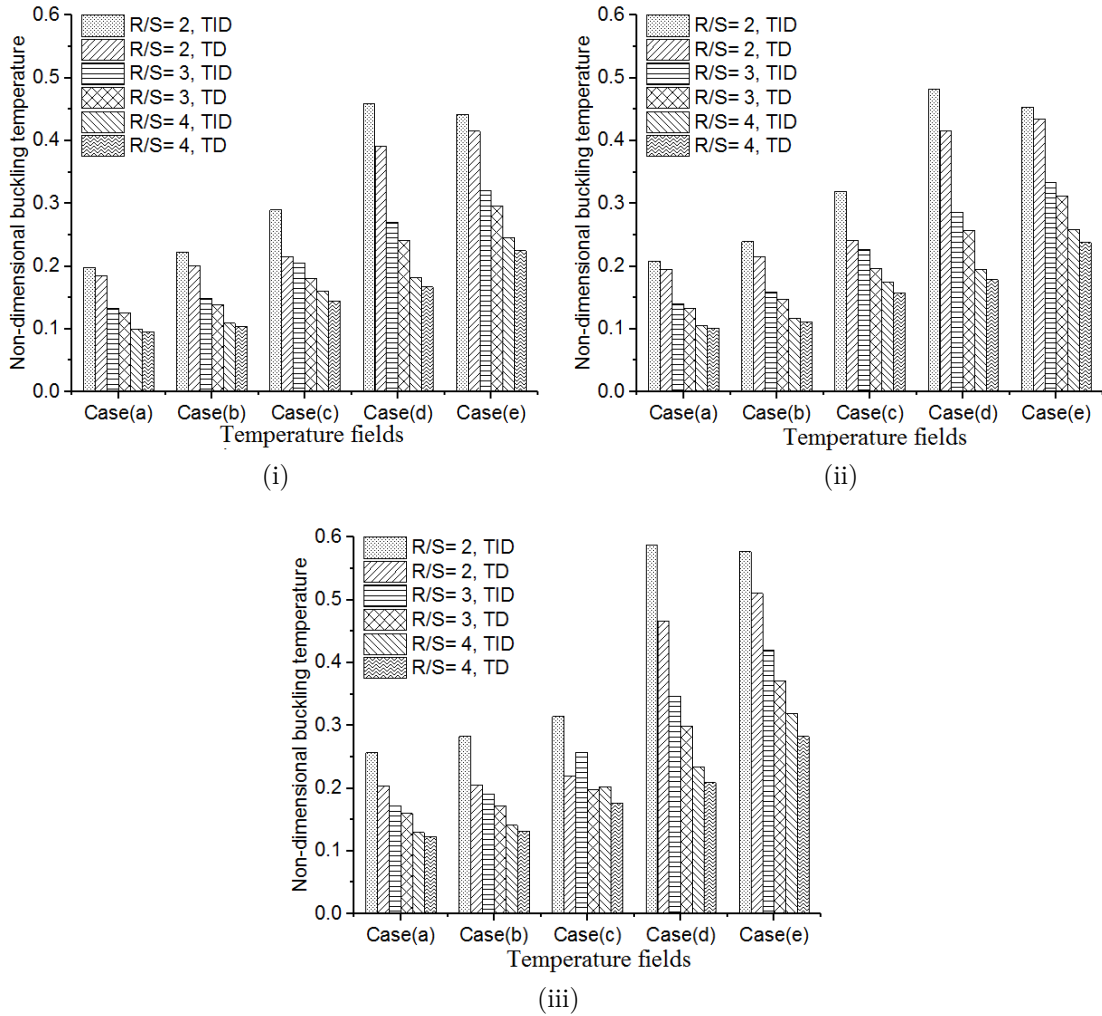


Figure 5.8: Effect of curvature ratio and temperature fields on buckling strength of CCCC cylindrical panel with CNTs volume fraction (i) 0.12, (ii) 0.17, and (iii) 0.28

The percentage difference of the buckling temperature is highly influenced by the CNTs grading pattern, thus FG-X pattern is observed to have a high-temperature difference compared to UD, FG-V and FG-O, pattern.

Influence of structural boundary constraints and CNTs grading patterns on the thermal buckling strength of the panel with different temperature fields are shown in Table 5.11. As expected, CCCC panel is observed to have lowest buckling strength compared to others. This is due to the fact that panel under CCCC boundary constraint does not allow any rotation and translation motion from any of its edges, thus free thermal expansion is completely restricted which leads to the development of high thermal stresses. However, the panel under CCFC boundary constraint allows free expansion from one of its edges and the amount of stress developed due to thermal load is partly released from the free edge making panel to buckle at a higher temperature. Whereas, the panel under SSCC boundary constraints shows the highest buckling temperature due to the relaxed degree of freedom associated with the simply supported edges. As observed in earlier, a panel with the FG-X pattern has the highest buckling temperature irrespective of boundary constraints.

To know the influence of CNTs volume fraction and CNTs grading patterns on the fundamental buckling mode shape, CCCC cylindrical panel with  $S/h=100$ ,  $R/S=5$ , and  $L/S=1$  has been analyzed. Effects of CNTs grading patterns and CNTs volume fraction on the buckling modes of the CCCC cylindrical panel is shown in Table 5.12 and Table 5.13 respectively. It is seen that the buckling mode shapes are significantly influenced by the in-plane temperature fields. It is clearly observed that there is not much variation in the buckling mode shapes and its bending amplitude with the CNTs grading patterns and CNTs volume fraction. For different temperature fields, it is seen that the maximum bending amplitude of buckling modes occurs nearer to the heating source, thus for Case(b) temperature field maximum bending amplitude of buckling modes occurs at forefront curved

Table 5.10: Influence of CNTs volume fraction, CNTs grading patterns and temperature fields on the buckling temperature

CNTs volume fraction	CNTs grading patterns	Temperature fields																	
		Case(a)			Case(b)			Case(c)			Case(d)			Case(e)					
		TID	TD	% Diff.	TID	TD	% Diff.	TID	TD	% Diff.	TID	TD	% Diff.	TID	TD	% Diff.	TID	TD	% Diff.
0.120	UD	0.172	0.161	6.40	0.191	0.174	8.90	0.244	0.208	14.75	0.415	0.370	10.84	0.403	0.391	2.98			
	FG-X	0.198	0.185	6.57	0.223	0.200	10.31	0.290	0.215	25.86	0.459	0.392	14.60	0.443	0.415	6.32			
	FG-O	0.141	0.133	5.67	0.154	0.143	7.14	0.194	0.172	11.34	0.353	0.327	7.37	0.337	0.331	1.78			
	FG-V	0.155	0.146	5.72	0.171	0.157	8.08	0.217	0.188	12.95	0.381	0.349	8.47	0.370	0.369	0.31			
0.170	UD	0.179	0.168	6.15	0.200	0.183	8.50	0.262	0.224	14.50	0.427	0.385	9.84	0.405	0.400	1.23			
	FG-X	0.208	0.195	6.25	0.239	0.215	10.04	0.319	0.241	24.45	0.482	0.416	13.69	0.454	0.435	4.19			
	FG-O	0.147	0.140	4.76	0.164	0.152	7.32	0.212	0.187	11.79	0.363	0.339	6.61	0.334	0.330	1.20			
	FGV	0.162	0.154	5.35	0.182	0.168	7.68	0.237	0.206	13.34	0.398	0.366	7.85	0.381	0.376	1.30			
0.280	UD	0.207	0.189	8.70	0.226	0.196	13.27	0.281	0.210	25.27	0.501	0.430	14.17	0.493	0.469	4.87			
	FG-X	0.257	0.204	20.62	0.283	0.205	27.56	0.315	0.219	30.48	0.588	0.466	20.75	0.578	0.511	11.59			
	FG-O	0.176	0.165	6.25	0.195	0.177	9.23	0.244	0.210	13.93	0.443	0.410	7.45	0.400	0.397	3.17			
	FG-V	0.198	0.183	7.42	0.218	0.195	10.72	0.273	0.221	18.90	0.496	0.443	10.69	0.485	0.438	9.61			

Note: TID-Temperature independent; TD-Temperature dependent; Diff.: Difference

Table 5.11: Influence of structural boundary constraints, CNTs grading patterns and temperature fields on the buckling temperature

CNTs grading pattern	BC	Temperature fields																																												
		Case(a)						Case(b)						Case(c)						Case(d)						Case(e)																				
		TID	TD	% Diff.	TID	TD	% Diff.	TID	TD	% Diff.	TID	TD	% Diff.	TID	TD	% Diff.	TID	TD	% Diff.	TID	TD	% Diff.	TID	TD	% Diff.																					
UD	CCCC	0.172	0.161	6.40	0.191	0.174	8.90	0.244	0.208	14.80	0.415	0.370	10.80	0.403	0.391	3.00	0.246	0.225	8.50	0.328	0.252	23.20	0.311	0.236	24.10	0.515	0.487	5.40	0.564	0.554	1.80	0.199	0.179	10.10	0.205	0.183	10.70	0.252	0.208	17.50	0.528	0.432	18.20	0.676	0.543	19.70
	CCCC	0.198	0.185	6.60	0.223	0.200	10.30	0.290	0.215	25.90	0.459	0.392	14.60	0.443	0.415	6.30	0.278	0.236	15.10	0.376	0.259	31.10	0.351	0.245	30.20	0.581	0.543	6.50	0.637	0.614	3.60	0.233	0.200	14.20	0.243	0.201	17.30	0.300	0.216	28.00	0.578	0.443	23.40	0.725	0.465	35.90
	FG-X	CCCC	0.141	0.133	5.70	0.154	0.143	7.10	0.194	0.172	11.30	0.353	0.327	7.40	0.337	0.331	1.80	0.199	0.184	7.50	0.265	0.225	15.10	0.245	0.212	13.50	0.430	0.410	4.70	0.485	0.471	2.90	0.159	0.146	8.20	0.164	0.149	9.10	0.199	0.175	12.10	0.465	0.405	12.90	0.587	0.570
FG-O	CCCC	0.155	0.146	5.80	0.171	0.157	8.20	0.217	0.189	12.90	0.381	0.349	8.40	0.371	0.370	0.30	0.220	0.204	7.30	0.299	0.243	18.70	0.276	0.225	18.50	0.491	0.477	2.90	0.576	0.536	6.90	0.177	0.161	9.00	0.183	0.165	9.80	0.223	0.192	13.90	0.497	0.423	14.90	0.645	0.620	3.90
	SSCC	0.155	0.146	5.80	0.171	0.157	8.20	0.217	0.189	12.90	0.381	0.349	8.40	0.371	0.370	0.30	0.220	0.204	7.30	0.299	0.243	18.70	0.276	0.225	18.50	0.491	0.477	2.90	0.576	0.536	6.90	0.177	0.161	9.00	0.183	0.165	9.80	0.223	0.192	13.90	0.497	0.423	14.90	0.645	0.620	3.90
	CCFC	0.177	0.161	9.00	0.183	0.165	9.80	0.223	0.192	13.90	0.497	0.423	14.90	0.645	0.620	3.90	0.177	0.161	9.00	0.183	0.165	9.80	0.223	0.192	13.90	0.497	0.423	14.90	0.645	0.620	3.90	0.177	0.161	9.00	0.183	0.165	9.80	0.223	0.192	13.90	0.497	0.423	14.90	0.645	0.620	3.90

Note: TID-Temperature independent; TD-Temperature dependent; Diff-Difference, BC- Boundary constraints

Table 5.12: Influence of CNTs grading patterns on the fundamental buckling mode of CCCC cylindrical panel

CNTs grading patterns	Temperature fields				
	Case(a)	Case(b)	Case(c)	Case(d)	Case(e)
UD					
FG-X					
FG-O					
FG-V					

Note: Red- max. displacement, Blue- min. displacement and others-inbetween

Table 5.13: Influence of CNTs volume fraction on the fundamental buckling mode of CCCC cylindrical panel

CNTs volume fraction	Temperature fields				
	Case(a)	Case(b)	Case(c)	Case(d)	Case(e)
0.12					
0.17					
0.28					

Note: Red- max. displacement, Blue- min. displacement and others-inbetween

edge. Whereas for Case(d) and Case(e) temperature fields it occurs at the central location and for Case(c) temperature field it is observed on the extreme edges. A similar observation is noted for different CNTs volume fractions also.

### Free vibration characteristics under thermal load

In order to analyze the influence of thermal load, CNTs volume fraction and TD properties on the fundamental frequencies, a panel with three different CNTs volume fraction and five different temperature fields with a peak elevated the tem-

perature of 150K is considered. Fig. 5.9 shows the effect of temperature fields, CNTs volume fraction and TD properties on the natural frequencies. It is noted from Fig. 5.9 those fundamental frequencies of the panel can be increased by CNTs volume fraction, thus volume fraction of 0.28 shows higher values of fundamental frequencies. It is noticed, that the fundamental frequencies are significantly influenced by the thermal stress developed due to temperature fields and change in stiffness due to TD properties. Influence of TD properties on the frequencies is more significant at higher modes. Further, it is observed that reduction in natural frequency due to thermal load is more significant for the panel under Case(a) temperature field and less significant under Case(e). This is due to the fact that thermal stress developed in a panel with Case(a) is high and Case(e) it is low, compared to other temperature fields. Through thickness CNTs, grading patterns also influences the fundamental frequencies of the panel and the same is shown in Fig. 5.10. CNTs distribution is more effective when it is more at the extreme layers of the panel and less at the center, Therefore the panel with FG-X pattern provides better stiffness compared to other patterns. Panel with FG-X pattern gives higher fundamental frequencies. It is also seen that a reduction in the frequency due to thermal stress is more in Case(a) temperature field compared to others. Compare to non-uniform temperature fields, reduction in fundamental frequencies is higher in Case(b) temperature field. Effect of functional grading pattern, TD properties, and temperature fields is observed for all the frequencies modes analyzed. Table 5.14 indicates the influence of thermal load on the fundamental frequencies of the panel with TID properties exposed to five different temperature fields. Thermal load is considered to be a function of critical buckling temperature as analyzed in the preceding chapter. Irrespective of CNTs grading pattern, fundamental frequencies tends to decrease with the increase in temperature due to a reduction in structural stiffness of the panel. It is also seen that the CNTs grading patterns enhances the fundamental frequencies of the panel and the FG-X pattern is observed to high fundamental frequencies compared to FG-O and



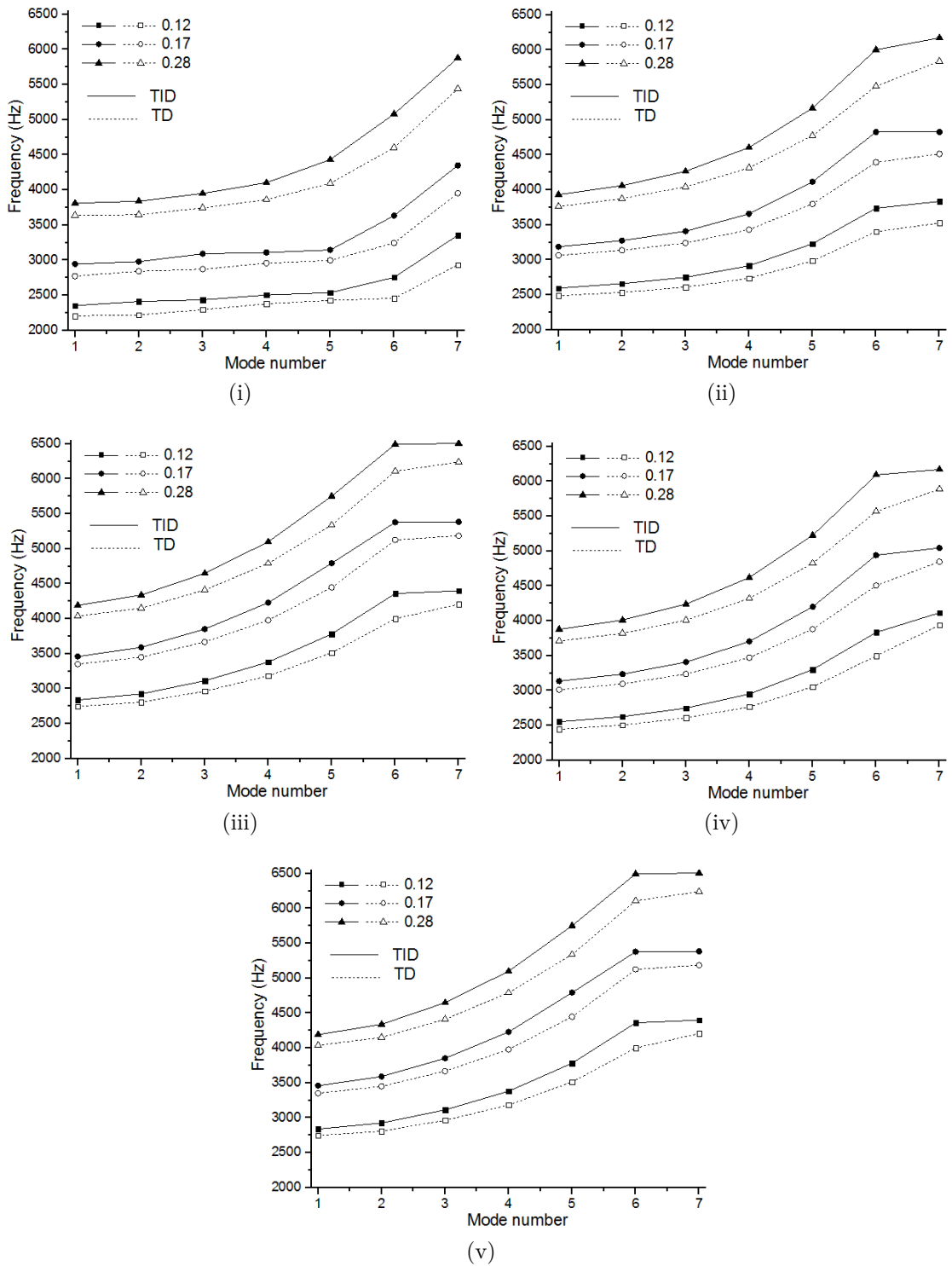


Figure 5.9: Effect of CNTs volume fraction on fundamental frequencies of CCCC cylindrical panel with temperature fields (i) Case(a), (ii) Case(b), (iii) Case(c), (iv) Case(d) and (v) Case(e)

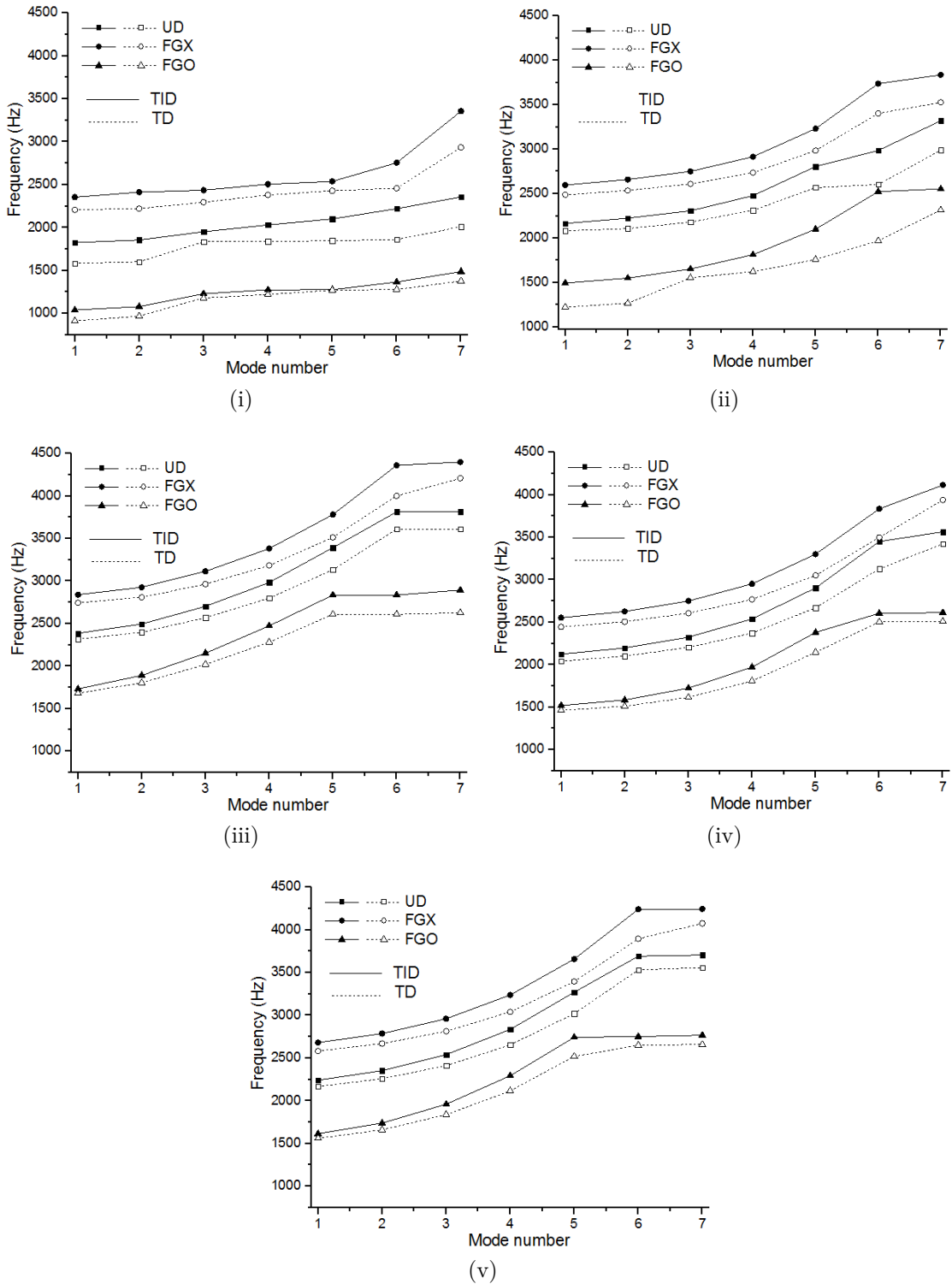


Figure 5.10: Effect of CNTs grading patterns on fundamental frequencies of CCCC cylindrical panel with temperature fields (i) Case(a), (ii) Case(b), (iii) Case(c), (iv) Case(d) and (v) Case(e)

FG-V CNTs distribution. Effect of TD properties on the fundamental frequencies when exposed to five different temperature field is analyzed and results are given in Table 5.15. Effect of TD properties of the panel on fundamental frequencies is significant and can be noticed under all the temperature fields irrespective of CNTs functional grading. Further, it is noticed from Table 5.15 that reduction in fundamental frequencies of the panel with TD properties is more compared to the panel with TID properties. This behavior of the panel is due to change in stiffness of the panel by thermal stress along with a change in elastic properties with temperature.

Influence of TD and TID properties on free vibration modes of the panel with different temperature fields are shown in Table 5.16. It is observed that the free vibration mode shapes are significantly influenced by the rise in temperature under different temperature fields analyzed. It is also found that modes tend to shift along with the change in nodal and anti-nodal positions under different temperature fields. For example, mode 1 of CCCC panel having modal indices of (1,2) at ambient temperature changes to (3,2) at 95% of the critical buckling temperature under Case(a) temperature field whereas the change in amplitude and nodal positions can be observed under Case(b) temperature field. Panel with TD properties is also analyzed for the change in mode shapes. As expected even with TD properties mode shapes and nodal position of free vibration modes changes with the temperature and its effect is more significant at 95% of critical buckling temperature.

## 5.5 Closure

This chapter deals with the investigation of buckling and free vibration behavior of laminated composite and functionally graded carbon nanotubes(FGCNT) reinforced composites cylindrical panels with TD properties exposed to different

Table 5.14: Influence of thermal load and CNTs grading patterns on the fundamental frequencies(Hz) of cylindrical panel with TID properties

CNTs grading patterns	Modes	At ambient temp.	Temperature fields														
			Case(a)			Case(b)			Case(c)			Case(d)			Case(e)		
			50% $T_{cr}$	95% $T_{cr}$	50% $T_{cr}$	95% $T_{cr}$	50% $T_{cr}$	95% $T_{cr}$	50% $T_{cr}$	95% $T_{cr}$	50% $T_{cr}$	95% $T_{cr}$	50% $T_{cr}$	95% $T_{cr}$			
UD	1	2428	2230	1752	2274	2083	2397	2370	1948	877	2145	1181					
	2	2627	2303	1757	2391	2128	2529	2436	1973	919	2210	1203					
	3	2967	2444	1921	2589	2214	2775	2570	2071	964	2328	1694					
	4	3437	2655	1990	2884	2358	3110	2759	2155	1011	2527	1706					
FG-X	1	2883	2635	1817	2686	2272	2849	2819	2316	1251	2553	1567					
	2	3059	2681	1866	2784	2482	2956	2863	2335	1349	2614	1583					
	3	3367	2782	2113	2941	2548	3174	2986	2455	1642	2721	2076					
	4	3807	2938	2184	3190	2669	3484	3169	2530	1654	2894	2078					
FG-O	1	1773	1635	1450	1669	1581	1748	1728	1443	898	1575	891					
	2	2033	1757	1467	1834	1666	1948	1875	1467	1035	1665	900					
	3	2446	1975	1576	2113	1795	2275	2115	1552	1232	1836	1269					
	4	2924	2283	1586	2497	2003	2693	2402	1706	1502	2115	1327					
FG-V	1	2043	1899	1545	1933	1811	2018	1992	1710	294	1871	881					
	2	2269	2003	1624	2076	1858	2187	2097	1743	843	1943	912					
	3	2640	2193	1649	2320	1924	2475	2275	1828	1082	2085	1420					
	4	3143	2476	1739	2675	2099	2863	2505	1986	1432	2338	1459					

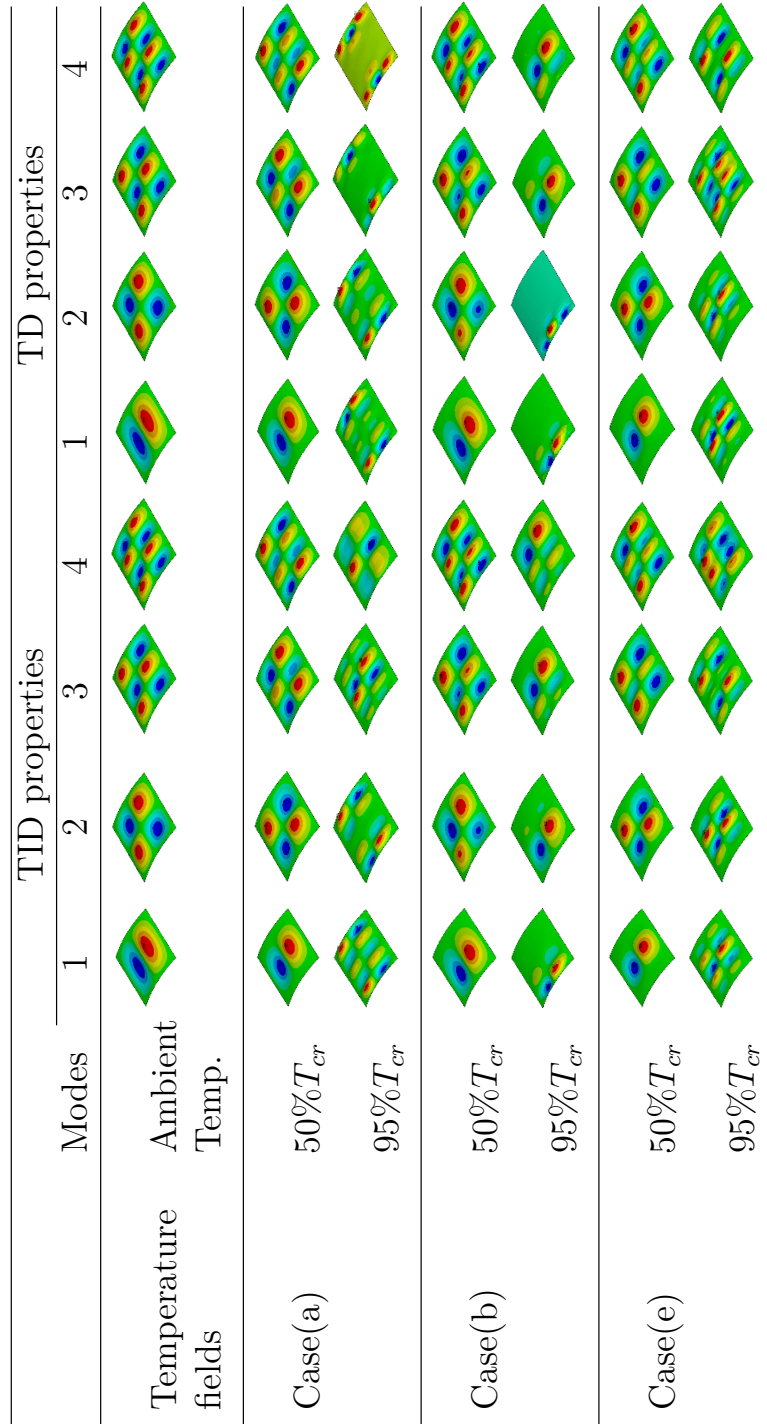
Note:  $T_{cr}$ - Critical buckling temperature associated with the temperature field

Table 5.15: Influence of thermal load and CNTs grading patterns on the fundamental frequencies(Hz) of cylindrical panel with TD properties

CNTs grading patterns	Modes	At ambient temp.	Temperature fields														
			Case(a)			Case(b)			Case(c)			Case(d)			Case(e)		
			50% $T_{cr}$	95% $T_{cr}$	50% $T_{cr}$	95% $T_{cr}$	50% $T_{cr}$	95% $T_{cr}$	50% $T_{cr}$	95% $T_{cr}$	50% $T_{cr}$	95% $T_{cr}$	50% $T_{cr}$	95% $T_{cr}$			
UD	1	2428	2185	1425	2225	1716	2343	2262	1804	500	2029	832					
	2	2627	2246	1442	2330	1744	2454	2269	1812	1050	2077	837					
	3	2967	2371	1573	2503	2031	2669	2331	1932	1214	2165	1388					
	4	3437	2557	1575	2766	2094	2964	2438	1993	1389	2303	1410					
FG-X	1	2883	2566	1392	2611	1776	2775	2681	2110	1246	2383	964					
	2	3059	2602	1395	2699	1902	2863	2692	2112	1499	2428	970					
	3	3367	2689	1736	2834	2322	3053	2772	2255	1542	2515	1611					
	4	3807	2821	1736	3047	2369	3323	2888	2327	1598	2633	1614					
FG-O	1	1773	1608	1312	1640	1530	1714	1672	1358	364	1511	670					
	2	2033	1716	1332	1789	1583	1891	1780	1374	955	1575	690					
	3	2446	1915	1332	2043	1625	2188	1961	1453	1128	1701	1114					
	4	2924	2198	1354	2397	1630	2570	2149	1543	1283	1915	1114					
FG-V	1	2043	1868	1351	1899	1634	1979	1920	1620	467	1794	723					
	2	2269	1960	1353	2029	1658	2128	1982	1642	690	1845	731					
	3	2640	2133	1423	2250	1742	2388	2086	1719	1050	1948	1206					
	4	3143	2392	1426	2576	1804	2740	2209	1822	1142	2139	1266					

Note:  $T_{cr}$ - Critical buckling temperature associated with the temperature field

Table 5.16: Influence of thermal load on the free vibration modes of cylindrical panel with TD and TID properties



Note: Red- max. displacement, Blue- min. displacement and others-inbetween

temperature fields using finite element method. Influence of geometrical parameters, in-plane temperature fields, lamination schemes, CNTs grading pattern, the CNTs volume fraction and boundary constraints on the buckling and free vibration behavior of the panel are investigated in detail. It is found from the analysis that, thermal buckling strength of the panel is significantly influenced by the TD properties and variation of the temperature fields. It is also found that the effect of TD properties on the buckling strength is more significant on a panel at lower thickness and curvature ratio i.e. on the stiffer panel. Further, CNTs grading pattern of type FG-X gives better buckling strength than the other pattern analyzed, irrespective of temperature fields. Further, fundamental buckling mode shapes are sensitive to the variation of temperature fields and geometric parameters. It is also found that fundamental frequencies of the laminated composites and FG-CNT reinforced composites panel decreases with increase in temperature due to thermal stress and also due to TD properties. As expected free vibration mode shapes are also sensitive to the variation of temperature fields.

# CHAPTER 6

## OPTIMIZATION STUDIES

### 6.1 Introduction

As reported in preceding chapters for a laminated panel, buckling strength and free vibration characteristics changes with the laminate orientation and thus can be maximized by optimizing the laminate orientation. Present chapter focuses on optimization of buckling strength and the fundamental frequency of non-uniformly heated laminated cylindrical panels. Two different case studies are carried out in this chapter. The first case study focuses on the optimization of buckling strength of laminated cylindrical panels, whereas second case study deals with the optimization both buckling strength and the fundamental frequency of the panels exposed to five different heating conditions( including uniform temperature rise). Five cases of temperature fields discussed in chapter 4 are used in the present study for the analysis. They are as follows; Case(a)-uniform temperature field; Case(b)-decreasing trend in temperature field; Case(c)- decreasing and increasing trend in temperature field; Case(d)-increasing and decreasing trend in temperature field and Case(e)-Camel hump trend in temperature field. Four boundary constraints (CCCC, SSCC, SSSS and CCFC) used in preceding chapters are also considered for the investigation.



## 6.2 Optimization studies on buckling strength

### 6.2.1 Problem Formulation

Study on optimal buckling strength problem has been divided into two parts: Part-1 deals with the single objective optimization problem wherein thermal buckling strength is maximized for a known temperature field from the various temperature fields considered in the analysis. Whereas, Part-2 deals with multi-objective optimization problem wherein thermal buckling strength is maximized for an unknown temperature field. In both the optimization problem critical buckling temperature is taken as an objective function which needs to be maximized with laminate orientation as a design variable. Mathematical formulation of the problem is as follows:

Part 1: Single objective optimization problem

Determine the laminate orientation( $\theta^\circ$ ) of the panel exposed to known temperature field in order to maximize the critical buckling temperature( $T_{cr}$ ).

$$(T_{cr})_{\max} = \max \left[ T_{cr} (\theta^\circ)_{\text{case}(j)} \right] \quad j = a, b, c, d, e. \quad (6.1)$$
$$0^\circ \leq \theta^\circ \leq 90^\circ$$

where case(j) represent the different temperature fields considered.

Part 2: Multi-objective optimization problem

Determine the laminate orientation( $\theta^\circ$ ) of the panel exposed to unknown temperature field in order to maximize the critical buckling temperature( $T_{cr}$ ).

$$(T_{cr})_{\max} = \max \left[ T_{cr} (\theta^\circ)_{\text{Case}(a)}, T_{cr} (\theta^\circ)_{\text{Case}(b)}, T_{cr} (\theta^\circ)_{\text{Case}(c)}, \right. \\ \left. T_{cr} (\theta^\circ)_{\text{Case}(d)}, T_{cr} (\theta^\circ)_{\text{Case}(e)} \right] \quad (6.2)$$

$$0^\circ \leq \theta^\circ \leq 90^\circ$$

where case(j) represent the different temperature fields.

Multi-objective optimization problem is converted to single objective optimization problem by using the weighted sum method. This method converts multiple objective function into an aggregated objective function by incorporating each objective function with a weighting factor( $w$ ) and summing up all weighted objective functions.

$$(T_{cr})_{\max} = \max \left[ w_1 * T_{cr}(\theta^\circ)_{Case(a)} + w_2 * T_{cr}(\theta^\circ)_{Case(b)} + w_3 * T_{cr}(\theta^\circ)_{Case(c)}, \right. \\ \left. + w_4 * T_{cr}(\theta^\circ)_{Case(d)} + w_5 * T_{cr}(\theta^\circ)_{Case(e)} \right] \quad (6.3)$$

$$\sum_{i=1}^5 w_i = 1; \quad 0 \leq w_i \leq 1$$

In the present study all the objective functions are assumed to have equal weightage, thus equal weights are considered and the resulting objective function is as given below.

$$(T_{cr})_{\max} = \max \left[ 0.2 * T_{cr}(\theta^\circ)_{Case(a)} + 0.2 * T_{cr}(\theta^\circ)_{Case(b)} + 0.2 * T_{cr}(\theta^\circ)_{Case(c)}, \right. \\ \left. + 0.2 * T_{cr}(\theta^\circ)_{Case(d)} + 0.2 * T_{cr}(\theta^\circ)_{Case(e)} \right] \quad (6.4)$$

$$0^\circ \leq \theta^\circ \leq 90^\circ$$

## 6.2.2 Validation of optimum thermal buckling strength

A CCCC laminated plate investigated by Topal and Uzman (2008) for optimizing the buckling strength under uniform temperature rise has been considered for the validation. The dimensions of the plate considered by Topal and Uzman (2008) are  $S/h=100$ ,  $R/S=1000$  and  $L/S=1$  with following properties;  $E_{11}=181\text{GPa}$ ,  $E_{22}=E_{33}=10.3\text{GPa}$ ,  $G_{12}=G_{13}=7.17\text{GPa}$ ,  $G_{23}=2.39\text{GPa}$ ,  $\nu_{12}=\nu_{13}=\nu_{23}=0.28$ ,  $\rho=1603\text{ kg/m}^3$ ,  $\alpha_1=0.02\times 10^{-6}/^\circ\text{C}$ ,  $\alpha_2=22.5\times 10^{-6}/^\circ\text{C}$ ; Wherein, they used modified feasible direction (MFD) method for optimization, while particle swarm optimization method is used in the present study. Based on the present approach, the optimum laminate orientation recorded as shown in Table 6.1 agrees very well with that of the value reported by Topal and Uzman (2008).

Table 6.1: Comparison of optimum laminate orientation with Topal and Uzman (2008)

Optimum laminate orientation, $\theta_{opt}^\circ$		%diff.
Topal and Uzman (2008)	Present study	
54	54.025	0.05

## 6.2.3 Results and discussion

In this study, an investigation is carried out on a cylindrical panel with thickness ( $h$ ), width ( $S$ ), length ( $L$ ) and radius ( $R$ ) with following geometrical parameters: thickness ( $h$ ) =1mm, aspect ratio ( $L/S$ ) = 1, thickness ratio ( $S/h$ ) =100 and curvature ratio ( $R/S$ ) =5. Cylindrical panel analyzed is made up of T300/5208 Graphite/Epoxy material with following material properties;  $E_{11}=181\text{GPa}$ ,  $E_{22}=E_{33}=10.3\text{GPa}$ ,  $G_{12}=G_{13}=7.17\text{GPa}$ ,  $G_{23}=2.39\text{GPa}$ ,  $\nu_{12}=\nu_{13}=\nu_{23}=0.28$ ,  $\rho=1603\text{ kg/m}^3$ ,  $\alpha_1=0.02\times 10^{-6}/^\circ\text{C}$ ,  $\alpha_2=22.5\times 10^{-6}/^\circ\text{C}$ ,  $K_1/K_2=4.62/0.72$ . where  $E$ ,  $G$ ,  $\nu$ ,  $\alpha$  and  $K$  denote Young's modulus, Shear modulus, Poisson's ratio, coefficient of thermal expansion and thermal conductivity, respectively. The subscripts 1, 2, and 3 denotes the on-axis material coordinates. Two different laminate schemes

analyzed are symmetric angle ply [ $\theta^\circ/-\theta^\circ/-\theta^\circ/\theta^\circ$ ] and un-symmetric angle ply [ $\theta^\circ/-\theta^\circ/\theta^\circ/-\theta^\circ$ ]. Panel investigated is assumed to have temperature independent material properties.

The non-dimensional critical buckling temperature is of the form

$$T_{cr}^* = \alpha_1 \times T_{cr} \times 10^3 \quad (6.5)$$

The optimization approach involves the stages of determining the critical buckling temperature,  $T_{cr}$  for a given laminate orientation,  $\theta^\circ$  and then maximizing it by optimizing the laminate orientation. Thus, the computational method involves repeated stages of determination and optimization of laminate orientation correspond to buckling strength until the optimum laminate orientation,  $\theta_{opt}^\circ$  is found.

### **Single objective maximization**

Optimization of thermal buckling strength of CCCC cylindrical panel exposed to a known temperature field is analyzed and presented in this section. Laminate orientation is used as a design parameter for this purpose. The influence of geometrical parameters, lamination schemes, different temperature fields and structural boundary constraints on the optimum design, has been investigated.

To analyze the influence of curvature ratio on optimum buckling strength and associated laminate orientation, three different curvature ratio (2.5, 5 and 10) are considered. Variations in optimum buckling strength of the CCCC panel with different curvature ratio and temperature fields are presented in Fig. 6.1. It can be observed from Fig. 6.1 that optimum buckling strength of the panel decreases with the increase in curvature ratio. It is the known fact that moment of inertia of the cylindrical panel changes with the curvature ratio, thus affecting the stiffness of the panel. This decreasing trend of buckling strength is observed for all

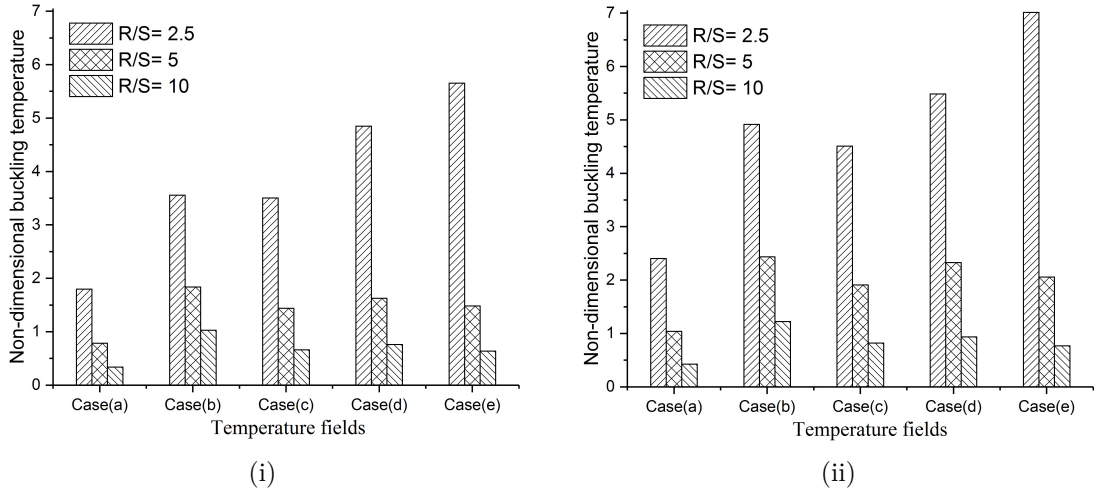


Figure 6.1: Effect of curvature ratio on the optimum buckling strength of CCCC laminated panel with (i) Symmetric and (ii) Un-symmetric

in-plane temperature fields. It can also be noted from Fig. 6.1, that the symmetric laminated panel has higher buckling strength compared to the un-symmetric panel under uniform temperature field (Case(a)). Whereas, the panel under non-uniform temperature field, the maximum buckling strength is observed for the un-symmetric laminate scheme. This is due to the fact that influence of bending and membrane coupling under un-symmetric is more for Case(a) temperature field compared to other temperature fields. The panel, under Case(a) and Case(b) temperature field, exhibits lowest and highest optimum buckling strength respectively. Due to the fact that under Case(a), the total area of the panel is exposed to temperature field, thus develops more membrane forces, whereas the panel under Case(b) produce fewer membrane forces due to the location of heat source at the clamped edge of the panel. It is also seen that influence of different temperature fields on the buckling strength of the panel is more significant at lower curvature ratio and becomes negligible at higher curvature ratio.

Table 6.2 shows the effect of curvature ratio and different temperature fields on the optimum laminate orientation obtained for CCCC laminated cylindrical panel. It can be seen from Table 6.2 that there is not much variation in the

Table 6.2: Effect of curvature ratio on the optimum laminate orientation( $\theta_{opt}^\circ$ ) of CCCC panel

Lamination scheme	$R/S$	Temperature fields				
		Case(a)	Case(b)	Case(c)	Case(d)	Case(e)
Symmetric	2.5	48.569	49.264	49.625	47.236	49.707
	5	47.061	47.613	48.564	45.904	47.613
	10	42.674	46.378	43.737	42.340	44.543
Un-symmetric	2.5	47.378	47.784	48.415	47.328	48.748
	5	46.709	47.592	48.190	45.274	46.617
	10	42.384	47.517	43.799	41.252	43.692

optimum laminate orientation of the panel with different temperature fields when the curvature ratio is less than 5. Optimum laminate orientation obtained for curvature ratio of 10 is in the range of  $42^\circ$  to  $46^\circ$  which is comparatively lesser than the values obtained for a curvature ratio of 2.5 and 5. Thus it can be concluded that the effects of curvature ratio on the optimum results are significant at larger curvature ratio. Results in Table 6.2 indicates that the optimum laminate orientation is not sensitive to the nature of temperature fields for a given curvature ratio. This is due to the fact that, the material properties of the panel depends only on the laminate orientation due to temperature independent elastic properties assumptions.

In order to study the effect of thickness ratio on the optimum buckling strength, a panel with three different thickness ratios (100, 150 and 200) has been analyzed. Fig. 6.2 shows the effect of thickness ratio on the optimum buckling strength of the CCCC panel with different temperature fields. It can be observed from Fig. 6.2 that the buckling strength of the panel is significantly influenced by the thickness ratio. This is due to the fact that the width of the panel increases with the thickness ratio, which decreases the bending stiffness of the panel. Case(b) temperature field is found to have maximum buckling strength whereas Case(a) recorded with minimum buckling strength. Decreasing trend of buckling strength is observed for both symmetric and un-symmetric laminated panel irrespective of

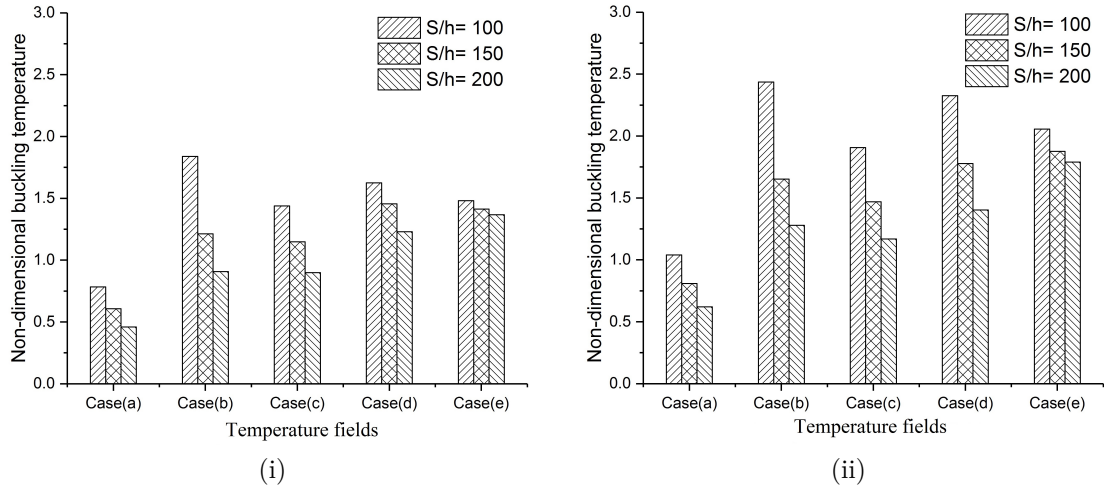


Figure 6.2: Effect of thickness ratio on the optimum buckling strength of CCCC laminated panel with (i) Symmetric and (ii) Un-symmetric

Table 6.3: Effect of thickness ratio on the optimum laminate orientation( $\theta_{opt}^\circ$ ) of CCCC panel

Lamination scheme	$S/h$	Temperature fields				
		Case(a)	Case(b)	Case(c)	Case(d)	Case(e)
Symmetric	100	47.062	47.613	48.581	45.878	47.612
	150	48.480	48.869	49.403	46.880	48.754
	200	49.058	49.881	50.562	47.612	49.826
Un-symmetric	100	46.710	47.765	48.417	45.253	46.631
	150	47.649	47.792	48.838	46.654	47.603
	200	47.684	48.495	49.134	47.508	49.617

the temperature fields. Table 6.3 depicts the influence of thickness ratio on the optimum laminate orientation of the CCCC laminated panel exposed to different temperature fields. It is observed that there are no significant variations in the optimum laminate orientation under different temperature fields analyzed. However, it increases marginally with the increase in thickness ratio.

Stress developed in the cylindrical panel due to thermal load is highly influenced by the boundary constraints. To analyze this, a panel subjected to four different boundary constraints is investigated. Table 6.4 shows the influence of boundary constraints on the optimum buckling strength of panel with different

Table 6.4: Effect of boundary constraints on the optimum buckling strength of CCCC panel

Lamination scheme	Boundary constraint	Temperature fields				
		Case(a)	Case(b)	Case(c)	Case(d)	Case(e)
Symmetric	CCCC	0.783	1.838	1.438	1.625	1.481
	SSCC	0.875	4.561	1.688	1.821	1.743
	SSSS	1.863	6.074	3.938	2.684	2.570
	CCFC	0.885	1.840	1.701	1.806	1.686
Un-symmetric	CCCC	1.039	2.436	1.907	2.328	2.057
	SSCC	1.231	5.562	2.320	2.557	2.391
	SSSS	2.085	7.224	4.530	3.071	3.036
	CCFC	1.172	2.450	2.162	2.535	2.254

temperature fields. As expected, a panel with more boundary constraints is observed to have less optimum buckling strength compared to a panel with less constraint. Thus laminated panel with CCCC boundary constraint has lower optimum buckling strength, whereas SSSS panel has higher optimum buckling strength. This is mainly due to stiffness associated with the corresponding boundary constraints. It is also observed from Table 6.4 that the optimum buckling strength of the panel is significantly influenced by the free edge as seen with CCFC boundary constraint and this can be attributed to relaxation of the developed thermal stress from the free edge. SSCC panel is observed with higher optimum buckling strength than CCCC panel, but lower than the SSSS panel. A similar trend of optimum buckling strength is observed with un-symmetric laminated cylindrical panel also. Further, it is observed that un-symmetric panel has higher optimum buckling strength than the symmetric panel.

Fig. 6.3 shows the influence of aspect ratio on the optimum buckling strength of the panel with different temperature fields. It is observed from Fig. 6.3 that optimum buckling strength of CCCC panel decrease with the increase in aspect ratio. The stiffness of the panel and the membrane forces generated in the panel due to heat source has a combined effect on the buckling strength of the panel. The stiffness of the panel decreases with the increase in aspect ratio, but still



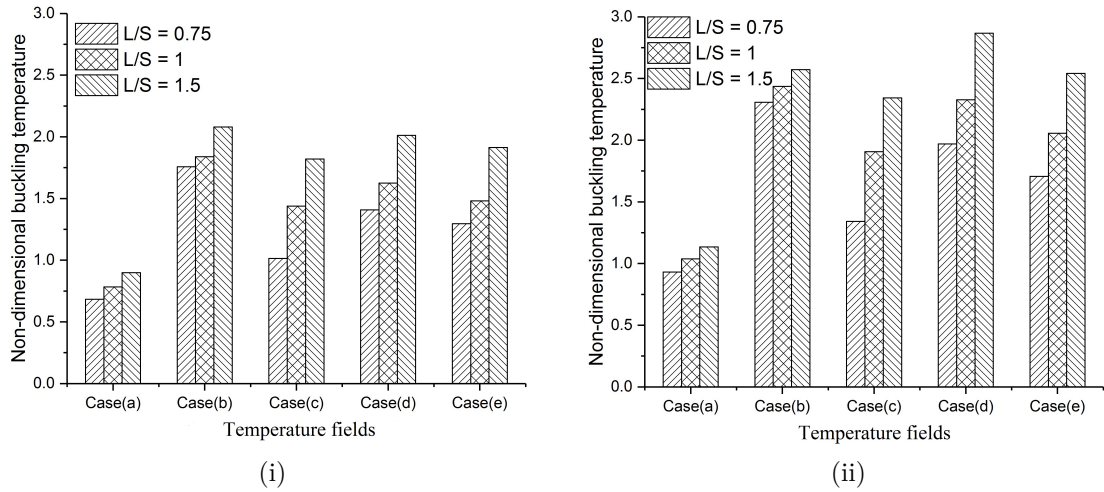


Figure 6.3: Effect of aspect ratio on the optimum buckling strength of CCCC laminated panel with (i) Symmetric, (ii) Un-symmetric

optimum buckling strength increases. It is due to the fact that membrane forces generated by heat source decrease with the increase in aspect ratio. Thus, it can be seen that buckling strength is dominated by the membrane forces generated in the panel compared to its stiffness. Both symmetric and un-symmetric laminated panel follows the similar behavioral trend in regards to aspect ratio. Influence of different aspect ratio on the optimum laminate orientation of symmetric and un-symmetric laminated panels with different temperature fields is given in Table 6.5. It is noted from Table 6.5 that there is not much variation in optimum laminate orientation for different temperature fields analyzed. This indicates that it is not so sensitive to the nature of temperature fields for a given aspect ratio.

### Multi-objective optimization

In the single objective optimization problem, the laminate orientation of the panel is optimized for a given temperature field to obtain maximum buckling strength in regards to that temperature field. However, if the same optimized panel is exposed to some other temperature field then it may not give the desired buckling strength. In order to solve this problem, a multi-objective optimization approach

Table 6.5: Effect of aspect ratio on the optimum laminate orientation( $\theta_{opt}^\circ$ ) of CCCC panel

Lamination scheme	Aspect ratio	Temperature fields				
		Case(a)	Case(b)	Case(c)	Case(d)	Case(e)
Symmetric	0.75	46.015	46.560	46.884	44.824	46.439
	1	47.060	47.649	48.569	45.902	47.611
	1.5	47.362	47.790	48.497	46.376	48.056
	2	47.982	47.780	47.866	46.601	48.150
Un-symmetric	0.75	45.603	47.740	47.007	44.558	46.653
	1	46.681	47.794	48.425	45.292	46.614
	1.5	46.551	47.699	47.902	45.369	46.706
	2	46.528	47.640	47.643	45.170	46.824

is carried out wherein optimum laminate orientation is obtained by considering all temperature fields together in other words all temperature fields are given equal importance.

In this section, results obtained from the multi-objective optimization approach are compared with the results of single objective optimization approach. From single objective optimization studies, a symmetric laminated panel with Case(d) temperature field is chosen for comparison due to symmetry associated with thermal boundary constraint and location of the heat source. The optimum laminate orientation obtained by single objective optimization approach is compared with the values obtained by the multi-objective optimization approach as shown in Table 6.6. In the multi-objective optimization approach, laminate orientation is optimized in such a way that it gives maximum buckling temperature for all in-plane temperature fields. Here equal weightage is given to all the temperature fields whereas single objective optimization approach considers one particular temperature field at a time. It can be observed from Table 6.6 that, for a thickness ratio of 100, the optimum laminate orientation obtained for a panel with Case(d) temperature field gives maximum buckling strength correspondence to that temperature field, whereas for other temperature fields it gives less buckling strength as compared to the values obtained through multi-objective optimization approach.

Table 6.6: Effect of thickness ratio on the optimum laminate orientation( $\theta_{opt}^\circ$ ) and the buckling strength, of CCCC panel.

Optimization approach	$S/h$	$\theta_{opt}^\circ$	Temperature fields				
			Case(a)	Case(b)	Case(c)	Case(d)	Case(e)
Single objective	100	45.877	0.769	1.806	1.334	1.625	1.425
	150	46.879	0.598	1.187	1.053	1.456	1.300
	200	46.551	0.432	0.868	0.779	1.229	1.139
	250	47.361	0.346	0.703	0.657	1.052	1.323
	300	47.612	0.287	0.587	0.559	0.925	1.312
Multi objective	100	47.410	0.782	1.838	1.412	1.585	1.480
	150	48.248	0.606	1.210	1.137	1.374	1.402
	200	48.731	0.455	0.906	0.869	1.162	1.417
	250	49.257	0.357	0.725	0.709	1.001	1.478
	300	49.561	0.291	0.606	0.593	0.862	1.573

For example, under single objective optimization approach, for laminate orientation of  $45.877^\circ$  the buckling strength observed for different temperature fields are 0.769, 1.806, 1.334, 1.625 and 1.425 corresponds to Case(a), Case(b), Case(c), Case(d) and Case(e) respectively. Whereas under multi-objective optimization approach, for optimum laminate orientation of  $47.41^\circ$  the buckling strength observed are 0.782, 1.838 1.412, 1.585 and 1.480 for a temperature field of Case(a), Case(b), Case(c), Case(d) and Case(e) respectively. It is clearly seen that under single objective optimization approach more importance has been given to Case(d) temperature field, whereas under multi-objective equal importance is given to all temperature fields, thus the laminate orientation of  $47.41^\circ$  gives better buckling strength under all in-plane temperature fields. It is also observed that buckling strength of the panel decreases with the increase in thickness ratio.

To study the influence of curvature ratio on the optimum laminate orientation obtained using multi-objective optimization approach, five different curvature ratio (1, 2, 2.5, 5 and 10) are considered. Table 6.7 shows the influence of curvature ratio on the maximum buckling strength of symmetric laminated panel obtained using multi-objective optimization approach. It is observed that buckling strength of

Table 6.7: Effect of curvature ratio on the optimum laminate orientation( $\theta_{opt}^\circ$ ) and the buckling strength, of CCCC panel

R/S	$\theta_{opt}^\circ$	Temperature fields				
		Case(a)	Case(b)	Case(c)	Case(d)	Case(e)
1	49.060	4.063	8.447	8.364	12.935	38.163
2	48.972	2.160	4.391	4.296	6.150	9.133
2.5	48.592	1.780	3.550	3.404	4.607	5.645
5	46.198	0.775	1.817	1.352	1.623	1.444
10	43.729	0.339	1.012	0.662	0.752	0.636

the panel decreases with the increase in curvature ratio irrespective of temperature fields. It is also observed that buckling strength of the panel decreases drastically when cylindrical panel changes to flat panel (R/S=10) which has the least moment of inertia thus offers less resistance to deflection. There is not much variation in optimum laminate orientation when the curvature ratio is less than 2.5 as seen in Table 6.7. Fig. 6.4 depicts the difference between two optimization approach used for optimizing the buckling strength of the panel. Irrespective of the curvature ratio, the multi-objective optimization approach as expected is found to give better buckling strength for most of the temperature fields. Fig. 6.4 also shows that under two different curvature ratio, a panel with only Case(d) temperature field is observed to have maximum buckling strength under single objective optimization approach. This is due to fact that laminate orientation is optimized considering Case(d) temperature field as a foremost objective. It is clear from Fig. 6.4 that multi-objective approach dominates the single-objective approach irrespective of curvature ratio of the panel.

Table 6.8 depicts the influence of aspect ratio on the buckling strength of symmetric and un-symmetric laminated cylindrical panel. With the increase in aspect ratio, the length of the panel increases, which decreases the stiffness of the panel and but also decreases the intensity of membrane forces generated due to thermal load. In most of the cases, membrane forces generated dominates the stiffness of the panel thus it can be seen from Table 6.8 that optimum buckling strength

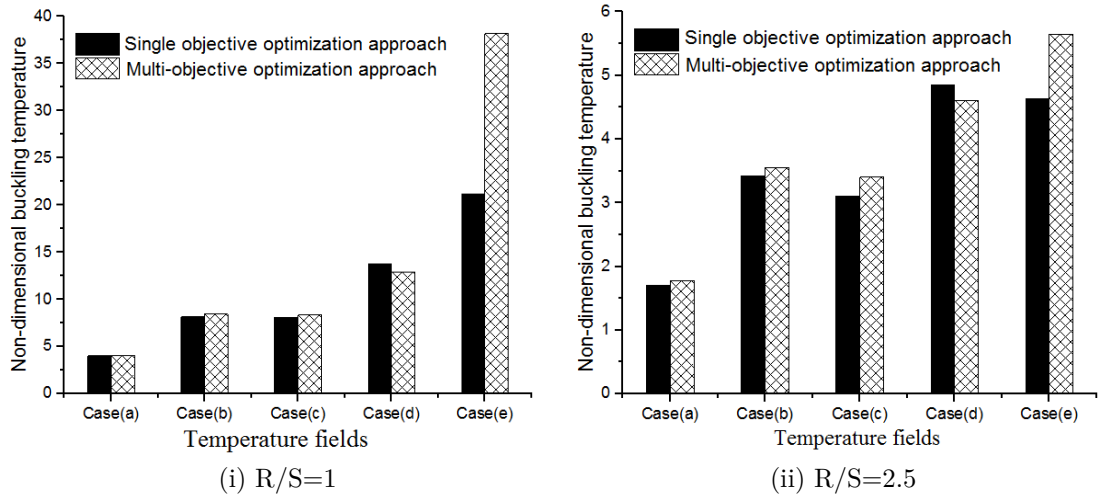


Figure 6.4: Comparison of buckling strength of panels using single and multi-objective optimization approach with curvature ratio, (i)  $R/S=1$  and (ii)  $R/S=2.5$

increases with the increase in aspect ratio. Similar behavior is observed for all in-plane temperature fields irrespective of the lamination scheme. Uniform temperature field (Case(a)) is observed to have minimum buckling strength compared to all other non-uniform temperature fields. This is due to fact that membrane forces generated due to thermal load under Case(a) temperature field are more compared to others. It can also be seen that un-symmetric lamination scheme has higher optimum buckling strength than the symmetric irrespective of aspect ratio. Optimum laminate orientation obtained for different aspect ratio for both the symmetric and un-symmetric CCCC panels is not varying significantly with respect to the aspect ratio.

Fig. 6.5 shows the comparison of optimum buckling strength obtained for a panel with two different aspect ratio using two optimization approaches. From Fig. 6.5 it is further clarified that multi-objective optimization approach is superior to the single objective optimization approach when all temperature fields are considered. It is also observed that superiority of multi-objective optimization method is irrespective of the aspect ratio of the panel. Single objective optimization approach has an upper hand when Case(d) temperature field is considered

Table 6.8: Effect of aspect ratio on the optimum laminate orientation( $\theta_{opt}^\circ$ ) and the buckling strength, of CCCC panel

Lamination scheme	$L/S$	$\theta_{opt}^\circ$	Temperature fields				
			Case(a)	Case(b)	Case(c)	Case(d)	Case(e)
Symmetric	0.75	46.085	0.683	1.756	1.011	1.392	1.295
	1	47.421	0.782	1.838	1.413	1.584	1.480
	1.5	47.594	0.899	1.838	1.805	1.970	1.904
	2	47.785	0.913	1.839	1.834	2.024	2.141
Un-symmetric	0.75	45.945	0.923	2.219	1.334	1.846	1.700
	1	46.745	1.039	2.350	1.715	2.138	2.054
	1.5	46.724	1.131	2.348	2.219	2.634	2.541
	2	46.847	1.152	2.362	2.338	2.661	2.760

alone.

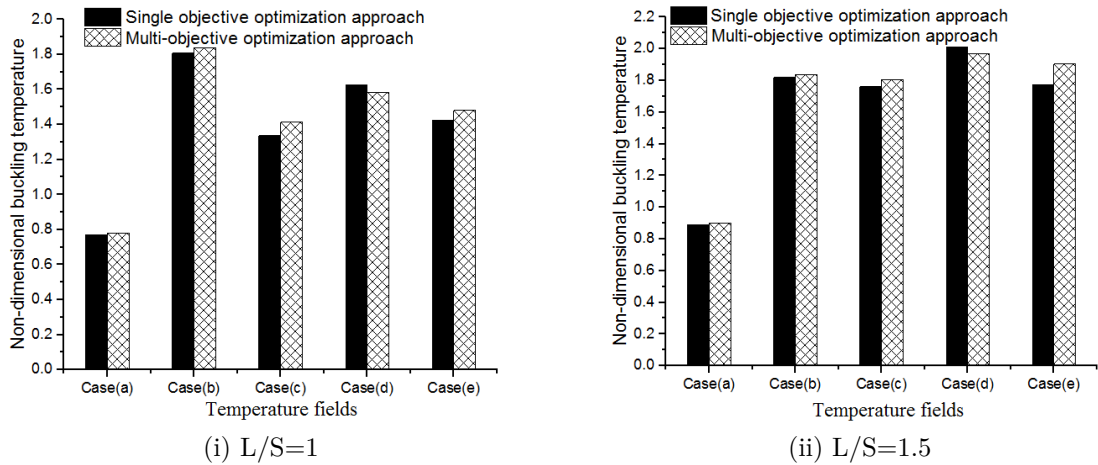


Figure 6.5: Comparison of optimum buckling strength using single and multi-objective optimization approach with aspect ratio, (i)  $L/S=1$  and (ii)  $L/S=1.5$

### 6.3 Optimization studies on buckling strength and fundamental frequency

The nature of temperature fields plays a significant role in the design of structural components exposed to heat during their operation. Knowing the importance of

non-uniform thermal load in structural design, the present study deals with the maximization of buckling strength and the fundamental frequency of laminated cylindrical panels under non-uniform thermal load. The normalized quantities used in the present study are given below:

Non-dimensional buckling temperature ( $T_{cr}^*$ )

$$T_{cr}^* = \frac{T_{cr}}{T_o} \quad (6.6)$$

Non-dimensional fundamental frequency ( $f^*$ )

$$f^* = \frac{f}{f_o}; \quad (6.7)$$

where  $T_o$  and  $f_o$  are the critical buckling temperature and fundamental frequency, respectively corresponding to a laminated cylindrical shell with following geometrical parameters  $L/S=1$ ,  $R/S=5$  and  $S/h=100$  with laminate orientation of ( $0^\circ/0^\circ/0^\circ/0^\circ$ )<sub>S</sub>.

### 6.3.1 Problem formulation

The present study deals with the maximization of thermal buckling strength ( $T_{cr}^*$ ) and fundamental frequency ( $f^*$ ) of the laminated cylindrical panel. Thus, considered to be multi-objective optimization problem with the laminate orientation of the panel as a design variable. Mathematical formulation of problem can be stated as follows:

Find laminate orientation ( $\theta^\circ$ )

Maximize the critical buckling temperature

$$(T_{cr}^*)_{\max} = \max T_{cr}(\theta^\circ)_{Case(j)} \quad j = a, b, c, d, e. \quad (6.8)$$

Maximize the fundamental frequency

$$(f^*)_{\max} = \max f^*(\theta^\circ) \quad (6.9)$$

$$0^\circ \leq \theta^\circ \leq 90^\circ$$

Well-known weighted sum method is implemented to convert multi-objective optimization problem into a single objective optimization problem. This method makes multiple objectives function into an aggregated objective function by allocating each objective function with a weighting factor and summing up all weighted objective functions. Throughout the analysis the aggregated objective function resulted from weighted sum method, called as multi-objective design index (MODI) is stated as follows:

$$MODI = \eta \times (T_{cr}^*)_{Case(j)} + \xi \times f^* \quad (6.10)$$

$$\eta + \xi = 1 \quad 0 \leq (\eta, \xi) \leq 1$$

where the weighting coefficient assigned for thermal buckling strength and fundamental frequency is given by  $\eta$  and  $\xi$  respectively. Thus, the resulting optimization problem is given by

Find laminate orientation ( $\theta^\circ$ ) to maximize MODI,

$$Max(MODI) = \max \left( \eta \times T_{cr}^*(\theta^\circ)_{Case(j)} + \xi \times f^*(\theta^\circ) \right) \quad (6.11)$$

$$0^\circ \leq \theta^\circ \leq 90^\circ$$

### 6.3.2 Results and discussion

A cylindrical panel with thickness ( $h$ ), width ( $S$ ), length ( $L$ ) and radius ( $R$ ) with following geometrical parameters: thickness ( $h$ )=1mm, aspect ratio ( $L/S$ ) =1,



thickness ratio  $(S/h) = 100$  and curvature ratio  $(R/S) = 5$  with lamination scheme of  $(\theta^\circ / -\theta^\circ / \theta^\circ / -\theta^\circ)_S$  is considered for the optimization studies presented in this section, if otherwise mentioned. The panel investigated is composed of T300/5208 Graphite/Epoxy material. Influence of different geometrical parameter and lamination scheme on the optimum buckling strength and the fundamental frequency of laminated cylindrical panel with different temperature fields are investigated.

Detailed investigations are carried out on the cylindrical panel to analyze the influence of weighting factor on the multi-objective design index (MODI) and to decide upon the weighting factor required for further calculation. Weighting factor basically shows the importance of one objective over the other. It is observed from Fig. 6.6 that trend of MODI changes with the weighting factor irrespective of temperature fields. Further, it is noted that for a cylindrical panel with different temperature fields, MODI varies with the laminate orientation. It is also found that MODI attains higher value at a particular laminate orientation which needs to be optimized. Panel with case(a) temperature field shows lower amplitude MODI curve whereas case(b) shows higher, irrespective of the weighting factor.

As discussed in preceded section behavior of MODI curve changes with laminate orientation and the weighting factor. To investigate the influence of weighting factor on  $MODI_{max}$  and optimum laminate orientation, a study has been carried out on CCCC cylindrical panel with five different temperature fields. Table 6.9 depicts the influence of weighting factor on  $MODI_{max}$  of the panel. As expected it is noted from Table 6.9 that  $MODI_{max}$  increases with the weighting factor which shows that, change of buckling temperature with laminate orientation is more significant compared to change in fundamental frequency with laminate orientation. Further, it is also seen that there is no significant change in optimum laminate orientation with the weighting factor. It has been observed from Table 6.9 that optimum laminate orientation ranges between  $45^\circ$  to  $50^\circ$  as properties of laminates in transverse and longitudinal direction is more effective in this range. Further,

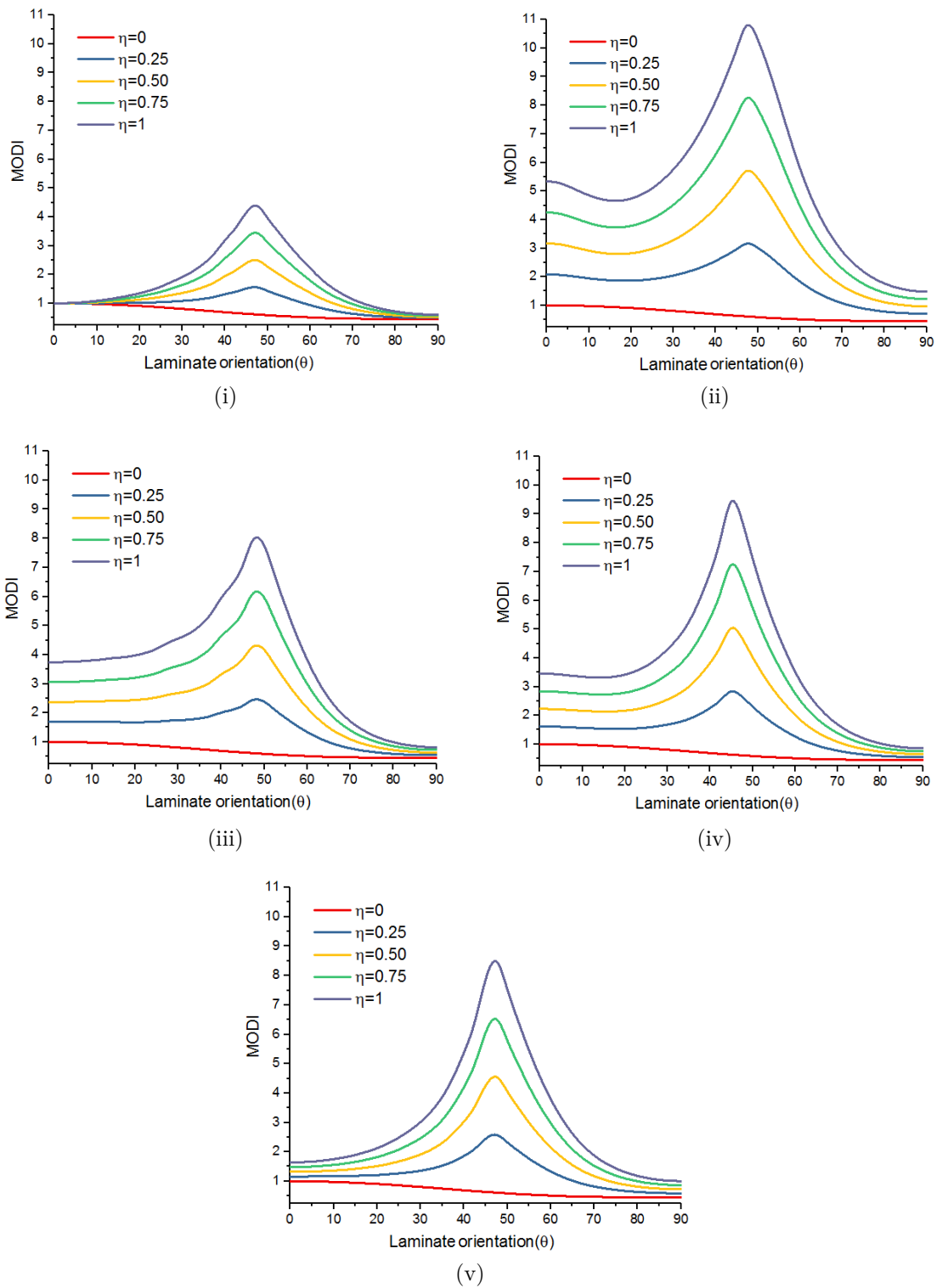


Figure 6.6: Influence of weighting factors on MODI of CCCC panel with temperature fields of type (i) Case(a), (ii) Case(b), (iii) Case(c) , (iv) Case(d) and (v) Case(e)

it is also found that optimum laminate orientation is not highly influenced by different temperature fields.

Table 6.9: Influence of weighting factor and temperature fields on  $MODI_{max}$

Weighting factor( $\eta$ )	Temperature fields				
	Case(a)	Case(b)	Case(c)	Case(d)	Case(e)
0.25	1.50	3.13	2.35	2.83	2.51
0.5	2.53	6.05	4.38	5.06	4.60
0.75	3.48	8.22	6.06	6.60	6.57

Table 6.10: Influence of weighting factor and temperature fields on the optimum laminate orientation( $\theta_{opt}^\circ$ )

Weighting factor( $\eta$ )	Temperature fieldss				
	Case(a)	Case(b)	Case(c)	Case(d)	Case(e)
0.25	45.94	48.00	49.12	45.54	47.28
0.5	46.90	45.19	48.42	45.30	46.87
0.75	46.58	47.21	49.66	47.86	47.16

Laminate orientation of panel with five different lamination schemes such as  $(\theta^\circ/-\theta^\circ/\theta^\circ/-\theta^\circ)_S$ ,  $(\theta^\circ/-\theta^\circ/90^\circ/0^\circ)_S$ ,  $(\theta^\circ/-\theta^\circ/0^\circ/90^\circ)_S$ ,  $(\theta^\circ/-\theta^\circ/90^\circ/90^\circ)_S$  and  $(\theta^\circ/-\theta^\circ/0^\circ/0^\circ)_S$  is also optimized in the present study. Fig. 6.7 shows the influence of lamination scheme on the MODI of the panel with temperature fields. It is observed from Fig. 6.7 that MODI varies with the laminate orientation with different laminate schemes. Table 6.11 and Table 6.12 shows the influence of different lamination scheme on the optimum laminate orientation and  $MODI_{max}$  respectively. It is observed from Table 6.11 that optimum laminate orientation of a panel changes with the lamination scheme. Panel with lamination scheme of  $(\theta^\circ/-\theta^\circ/90^\circ/90^\circ)_S$  shows optimum laminate orientation is in the range of  $35^\circ$  to  $40^\circ$ , whereas for a lamination scheme of  $(\theta^\circ/-\theta^\circ/0^\circ/0^\circ)_S$  it is in the range of  $55^\circ$  to  $88^\circ$  and for other lamination schemes it is observed  $45^\circ$  to  $55^\circ$ . Further, it is found from Table 6.12 that lamination scheme used in panel influences  $MODI_{max}$ .

Compared to all the lamination scheme used in the analysis  $(\theta^\circ/-\theta^\circ/\theta^\circ/-\theta^\circ)_S$  gives higher value of  $MODI_{max}$  thus considered to be the best lamination scheme.

Table 6.11: Influence of lamination schemes and temperature fields on the optimum laminate orientation( $\theta_{opt}^\circ$ )

Lamination scheme	Case(a)	Case(b)	Case(c)	Case(d)	Case(e)
$(\theta^\circ/-\theta^\circ/\theta^\circ/-\theta^\circ)_S$	46.90	45.19	48.42	45.30	46.87
$(\theta^\circ/-\theta^\circ/90^\circ/0^\circ)_S$	49.93	48.46	54.12	43.95	49.83
$(\theta^\circ/-\theta^\circ/0^\circ/90^\circ)_S$	53.93	53.52	57.82	48.49	53.62
$(\theta^\circ/-\theta^\circ/90^\circ/90^\circ)_S$	37.49	37.20	40.64	31.68	35.79
$(\theta^\circ/-\theta^\circ/0^\circ/0^\circ)_S$	88.29	62.47	58.66	56.28	64.73

Table 6.12: Influence of lamination schemes and temperature fields on  $MODI_{max}$

Lamination scheme	Case(a)	Case(b)	Case(c)	Case(d)	Case(e)
$(\theta^\circ/-\theta^\circ/\theta^\circ/-\theta^\circ)_S$	2.53	6.05	4.38	5.06	4.60
$(\theta^\circ/-\theta^\circ/90^\circ/0^\circ)_S$	2.37	5.77	3.58	4.50	3.96
$(\theta^\circ/-\theta^\circ/0^\circ/90^\circ)_S$	2.36	5.71	3.48	4.51	4.00
$(\theta^\circ/-\theta^\circ/90^\circ/90^\circ)_S$	2.36	5.21	3.48	4.26	4.14
$(\theta^\circ/-\theta^\circ/0^\circ/0^\circ)_S$	2.55	6.43	3.76	4.54	3.61

Table 6.13 and Table 6.14 depicts the influence of thickness ratio and temperature fields on the  $MODI_{max}$  and corresponding laminate orientation. The panel is analyzed for three different thickness ratio such as 75, 100 and 125 along with two different lamination scheme. It is observed that  $MODI_{max}$  decrease with the increase in thickness ratio and this is due to fact that stiffness of the panel decreases with the increase in thickness ratio. A Higher value of  $MODI_{max}$  is observed for a panel exposed to Case(b) temperature field whereas lower value is observed for Case(a). Laminate scheme analyzed are found to have a significant influence on the optimum laminate orientation for different thickness ratio. Panel with laminate scheme of  $(\theta^\circ/-\theta^\circ/\theta^\circ/-\theta^\circ)_S$  does have optimum laminate orientation varies from  $45^\circ$  to  $49^\circ$  whereas for laminate scheme of  $(\theta^\circ/-\theta^\circ/0^\circ/90^\circ)_S$  it varies from  $50^\circ$  to  $55^\circ$ . It is also noted that, for a given laminate scheme, the influence of

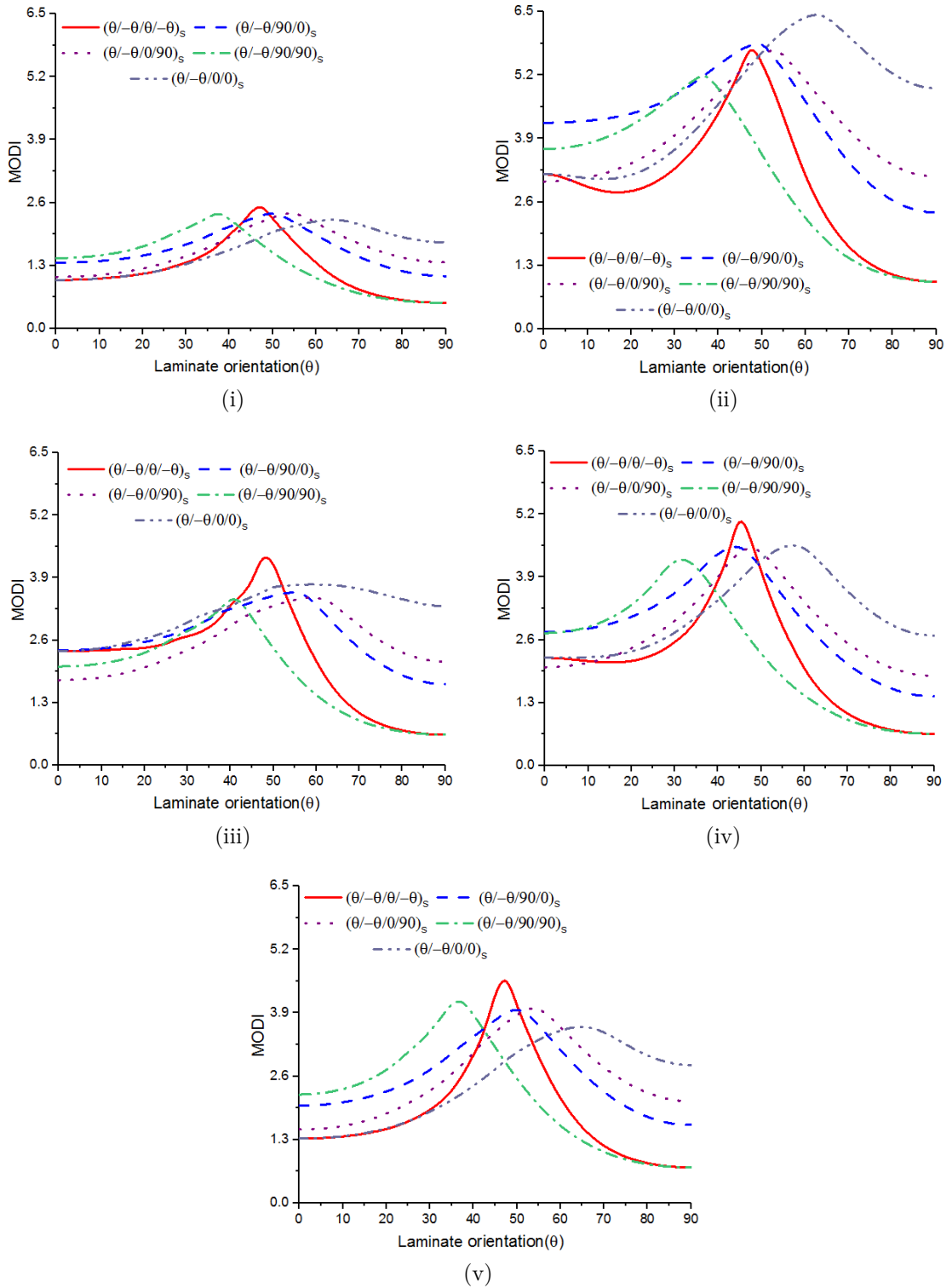


Figure 6.7: Influence of lamination schemes on MODI of CCCC panel with temperature fields of type (i) Case(a), (ii) Case(b), (iii) Case(c), (iv) Case(d) and (v) Case(e)

thickness ratio on the optimum laminate orientation is not significant irrespective of temperature fields.

Table 6.13: Influence of thickness ratio and temperature fields on  $MODI_{max}$

Temperature fields	$(\theta^\circ/-\theta^\circ/\theta^\circ/-\theta^\circ)_S$			$(\theta^\circ/-\theta^\circ/0^\circ/90^\circ)_S$		
	75	100	125	75	100	125
Case(a)	3.10	2.53	2.24	3.20	2.36	2.14
Case(b)	7.58	6.05	4.55	7.66	5.71	4.63
Case(c)	5.17	4.38	3.82	5.42	3.48	3.74
Case(d)	6.24	5.06	4.53	5.93	4.51	4.48
Case(e)	5.63	4.60	4.14	5.36	4.00	3.92

Table 6.14: Influence of thickness ratio and temperature fields on the optimum laminate orientation ( $\theta_{opt}^\circ$ )

Temperature fields	$(\theta^\circ/-\theta^\circ/\theta^\circ/-\theta^\circ)_S$			$(\theta^\circ/-\theta^\circ/0^\circ/90^\circ)_S$		
	75	100	125	75	100	125
Case(a)	44.93	46.90	47.59	51.71	53.93	55.62
Case(b)	47.07	45.19	48.53	53.29	53.52	52.11
Case(c)	47.64	48.42	48.39	56.65	57.82	58.51
Case(d)	44.09	45.30	46.02	46.62	48.49	49.15
Case(e)	46.95	46.87	44.14	51.03	53.62	55.33

Curvature ratio of a cylindrical panel plays a dominant role in deciding its buckling strength and the fundamental frequency. Influence of curvature ratio on  $MODI_{max}$  and the corresponding laminate orientation is investigated. It is clearly seen from Table 6.15 that as the curvature ratio increases, the  $MODI_{max}$  decreases irrespective of temperature fields. Further, this behavior of  $MODI_{max}$  is observed with both the lamination schemes. Variation of optimum laminate orientation with the curvature ratio is also investigated. Panel with different curvature ratio is found to have different optimum laminate orientation under different lamination scheme. Further it is observed that, for a lamination scheme of  $(\theta^\circ/-\theta^\circ/\theta^\circ/-\theta^\circ)_S$  optimum laminate orientation ranges from  $45^\circ$  to  $50^\circ$  whereas for  $(\theta^\circ/-\theta^\circ/0^\circ/90^\circ)_S$  it varies from  $50^\circ$  to  $60^\circ$ . Table 6.16 depicts the influence of curvature ratio on the

optimum laminate orientation of the panel exposed to different temperature fields. It is seen from the Table 6.16, that optimum laminate orientation varies with the curvature ratio irrespective of temperature fields. It is also observed that variation in optimum laminate orientation noted for two different lamination scheme is more significant at lower curvature ratio.

Table 6.15: Influence of curvature ratio and temperature fields on  $MODI_{max}$

Temperature fields	$(\theta^\circ/-\theta^\circ/\theta^\circ/-\theta^\circ)_S$			$(\theta^\circ/-\theta^\circ/0^\circ/90^\circ)_S$		
	2.5	5	10	2.5	5	10
Case(a)	5.76	2.53	1.18	4.56	2.36	1.26
Case(b)	11.15	6.05	3.06	10.10	5.71	3.34
Case(c)	10.32	4.38	2.10	6.30	3.48	2.06
Case(d)	11.44	5.06	2.36	9.39	4.51	2.31
Case(e)	4.81	4.60	1.97	8.55	4.00	2.02

Table 6.16: Influence of curvature ratio and temperature fields on the optimum laminate orientation( $\theta_{opt}^\circ$ )

Temperature fields	$(\theta^\circ/-\theta^\circ/\theta^\circ/-\theta^\circ)_S$			$(\theta^\circ/-\theta^\circ/0^\circ/90^\circ)_S$		
	2.5	5	10	2.5	5	10
Case(a)	48.05	46.90	43.02	57.41	53.93	45.40
Case(b)	48.20	45.19	45.97	52.20	53.52	50.88
Case(c)	50.12	48.42	43.13	58.27	57.82	49.78
Case(d)	49.83	45.30	41.37	52.24	48.49	40.76
Case(e)	49.12	46.87	43.05	60.81	53.62	44.92

Studies are carried out to investigate the influence of boundary constraints on the optimum laminate orientation and also on  $MODI_{max}$ . Four different boundary constraints (CCCC, SSCC, SSSS and CCFC ) are considered for investigation. Table 6.17 depicts the influence of different boundary constraints on  $MODI_{max}$  wherein it is found that  $MODI_{max}$  changes with boundary constraints. Panel with SSSS boundary constraints is observed to have a high value of  $MODI_{max}$  due to relaxation of some degree of freedom and as expected, a panel with CCCC boundary constraints have a low value of  $MODI_{max}$ . It is also noted that  $MODI_{max}$

of a panel with different boundary constraints also changes with temperature fields. Table 6.18 shows the influence of boundary constraints on the optimum laminate orientation. It is clearly seen that there is not much variation in the optimum laminate orientation with the boundary constraints which ranges from  $45^\circ$  to  $55^\circ$ .

Table 6.17: Influence of boundary constraints and temperature fields on  $MODI_{max}$

Boundary constraints	Temperature fields				
	Case(a)	Case(b)	Case(c)	Case(d)	Case(e)
CCCC	2.53	6.05	4.38	5.06	4.60
SSCC	2.83	12.65	5.15	5.52	5.22
SSSS	5.15	16.90	10.90	7.29	7.28
CCFC	2.76	5.66	5.09	5.53	4.94

Table 6.18: Influence of boundary constraints and temperature fields on the optimum laminate orientation( $\theta_{opt}^\circ$ )

Boundary constraints	Temperature fields				
	Case(a)	Case(b)	Case(c)	Case(d)	Case(e)
CCCC	46.90	45.19	48.42	45.30	46.87
SSCC	47.09	44.36	48.66	45.55	46.90
SSSS	45.92	41.78	44.14	42.11	44.50
CCFC	47.14	47.70	47.99	45.10	47.82

## 6.4 Closure

Studies carried out on optimization of buckling strength of laminated cylindrical panels with different temperature fields are presented. Buckling strength of the panel is obtained by using finite element method and is optimized by a particle swarm optimization (PSO) technique. The laminate orientation of the panel is taken as a design variable. Buckling strength of the panel with different temperature fields is optimized by two different optimization approach like single objective optimization approach and multi-objective optimization approach. In single objective optimization, the panel is exposed known temperature field whereas, in



multi-objective optimization, the panel is exposed to unknown temperature fields when in-service. Multi-objective optimization approach has proved to be superior to that of single objective optimization approach when all the temperature fields are taken together. Further, studies are also carried out on optimization of buckling strength and fundamental frequency. Buckling strength and the fundamental frequency are measured by using finite element method and to optimize it, PSO along with artificial neural network (ANN) are employed. ANSYS APDL code is integrated with ANN code and later with PSO code using MATLAB. It is observed that the MODI of the panel can be maximized by optimizing laminate orientations. It can be clearly seen from the outcomes of the analysis that, Multi-objective design index (MODI) of the cylindrical panels under thermal load is complex and significantly influenced by the temperature field, lamination scheme, in-plane boundary constraints, elevated temperature and geometric parameters. Further, it is observed that panel with lamination scheme of  $(\theta^\circ / -\theta^\circ / \theta^\circ / -\theta^\circ)_S$  gives higher value of  $\text{MODI}_{max}$  compared to other lamination schemes considered.

# CHAPTER 7

## SUMMARY AND CONCLUSIONS

### 7.1 Summary

Cylindrical panels form a backbone of many engineering structures which includes aerospace components, marine structures, turbine disks, oil storage tanks, piping systems, nuclear and pressure vessels. In most of the engineering applications, panels are exposed to the hostile thermal environment during their operation which gives rise to thermal stress. Stresses set up due to thermal load may lead to buckling failure and affects the dynamic behavior of the panel. So, it is very important to investigate the buckling and vibration behavior of panels under thermal load. Further, it is also seen that, in real life application, because of un-symmetric geometric variation and the nature of heat source, most of the panels are exposed to arbitrarily varying non-uniform temperature fields which are more susceptible to thermal buckling. Considering all the above factors, present work focuses on the buckling and free vibration behavior of non-uniformly heated cylindrical panel.

The in-house experimental set-up is developed to compute critical buckling temperature of a cylindrical panel with three different types of non-uniform temperature fields. Results obtained through experiments is then used to validate the numerically computed values. Finite element tool, ANSYS is employed for the numerical approach. Studies are further extended to investigate in detail the combined buckling and free vibration behavior of the non-uniformly heated cylindrical panel. Two different panels analyzed are made of isotropic and laminated composite material. The panel investigated with five different temperature fields along with four different structural boundary constraints. Influence of different

geometrical parameters, temperature variation fields and boundary constraints on the buckling and free vibration behavior of cylindrical panel is analyzed in detail.

Temperature-dependent properties of material play a significant role in deciding the buckling and dynamic strength of the heated panel. The study has been carried out to analyze the influence of temperature dependent properties on buckling and free vibration behavior of non-uniformly heated panel. Laminated composite and functionally graded carbon nanotubes reinforced composite are analyzed considering their importance in today's engineering applications. Influence of temperature dependent properties, different geometric parameters, structural boundary constraints and non-uniform temperature fields on buckling and free vibration behavior is non-uniformly heated cylindrical panels.

Further, optimization studies are carried out on maximizing the buckling strength and fundamental frequency of non-uniformly heated cylindrical panel. Two different cases are discussed, the first case focuses on optimization of buckling temperature using particle swarm optimization approach. Whereas the second case deals with multi-objective optimization of buckling temperature and fundamental frequency using particle swarm optimization approach in conjunction with artificial neural networks. laminate orientation is considered as a design variable for optimization. Influence of different geometric parameters, structural boundary constraints and non-uniform temperature fields on optimum laminate orientation and corresponding buckling temperature and frequency are also investigated

## 7.2 Conclusions

- Results obtained through experiments revealed that non-uniform temperature fields significantly influence the buckling behavior of the panel and play a significant role in deciding the buckling strength of the panel. Panel exposed to temperature field with a heat source at the center is observed to

have lowest buckling strength whereas panel exposed to temperature field with a heat source at extreme end is noted to have highest buckling strength. Buckling temperature noted for a panel with CCFC boundary constraints is higher than the CCCC boundary constraints. Numerically predicted values match very well with that of experimentation which ensures the fate of numerical approach.

- Further, it is found that buckling temperature of the non-uniformly heated cylindrical panel can be predicted using buckling temperature of the uniformly heated panel with the help of magnification factor which derives the relation between the two. It is also found that thickness and curvature ratio of the panel is inversely proportional to the buckling strength. Effect of non-uniform temperature fields on the buckling strength of the panel is more prominent on the stiffer panel.
- Free vibration frequencies of the panel are highly influenced by the stress setup due to thermal load and structural boundary constraints. It is noted that free vibration frequencies decrease drastically at a temperature close to buckling temperature. Shifting of nodal and anti-nodal lines and changing of modal indices with the elevated temperature has been observed. Non-uniform temperature fields significantly influence the free vibration frequencies. Further, free vibration frequencies and their associated mode shapes are highly influenced by the temperature close to the buckling temperature.
- Thermal buckling strength and free vibration frequencies of the panel are significantly influenced by the temperature dependent properties and variation of temperature fields. The effect of temperature dependent properties on the buckling strength is more significant for a panel with lower thickness, and curvature, ratio i.e. on the stiffer panel. Influence of temperature dependent properties on the buckling temperature is more significant for a panel with lamination scheme of  $(45/-45/45/-45)_2$ . Variation in buckling temper-

ature for a panel with TID and TD properties is more at higher buckling temperature.

- Studies on FG-CNT reinforced composite revealed that CNTs grading pattern of types FG-X gives better buckling strength than FG-O and FG-V, irrespective of temperature fields. It is also seen that high CNTs volume fraction provides better stiffness thus CNTs volume fraction of 0.28 gives higher buckling strength compared to 0.12 and 0.17. Variation in buckling temperature of the panel with TID and TD properties is more on stiffer panels thus the influence of TD properties is high for a panel with CNTs volume fraction of 0.28 with FG-X grading pattern.
- Further, it is also noticed that fundamental buckling mode shapes are sensitive to the variation of temperature fields and geometric parameters. It is also found that natural frequencies of the laminated composites and FG-CNT reinforced composite panel decreases with increase in temperature due to thermal stress and TD properties and reduction is more significant compared to panel with TID properties. Free vibration mode shapes are sensitive to the variation of temperature fields. With the temperature rise, shifting of nodal and anti-nodal lines and change of modal indices is commonly observed.
- Buckling strength of the heated panel is optimized by two different optimization approach, single objective, and multi-objective, optimization approach. In single objective optimization, the panel is exposed known temperature field whereas, in multi-objective optimization, the panel is exposed to unknown temperature field when in-service. Multi-objective optimization approach has proved to be superior to that of single objective optimization approach when all the temperature fields are taken together i.e. under unpredictable temperature fields.
- Studies carried out on optimization of both buckling strength and the fun-

damental frequency is taken together revealed that multi-objective design index (MODI) of the cylindrical panels under thermal load is complex and significantly influenced by the temperature fields, lamination scheme, in-plane boundary constraints, elevated temperature and geometric parameters. It is also observed that the MODI of the panel is inversely proportional to thickness, and curvature, ratio. MODI is maximized by optimizing laminate orientation. It is also observed that panel with lamination scheme of  $(\theta^\circ / -\theta^\circ / \theta^\circ / -\theta^\circ)_S$  gives higher value of MODI compared to other lamination schemes considered.

- Particle swarm optimization technique is found to be simple with fast convergence rate thus efficiently used in present optimization studies. Further, to reduce computing time artificial neural network in conjunction with particle swarm optimization has been used.

### 7.3 Scope for future research

In this research work, buckling and free vibration behavior of isotropic, laminated composite, and FG-CNTs reinforced composite, of non-uniformly heated cylindrical panels with TD and TID properties has been investigated. Following research work can be carried out in future:

- Experimental investigation work can be extended further to investigate FG-CNT reinforced composite cylindrical panels.
- Numerical investigation on buckling and free vibration behavior of cylindrical panels with a hole.
- Buckling strength and free vibration frequency can be optimized by Layer-wise optimization technique.

## REFERENCES

- Abouhamze, M.** and **M. Shakeri** (2007). Multi-objective stacking sequence optimization of laminated cylindrical panels using a genetic algorithm and neural networks. *Composite Structures*, **81**(2), 253–263.
- Adali, S.** and **K. Duffy** (1990). Optimal design of antisymmetric hybrid laminates against thermal buckling. *Journal of Thermal Stresses*, **13**(1), 57–71.
- Ahmadi, S. A.** and **H. Pourshahsavari** (2016). Three-dimensional thermal buckling analysis of functionally graded cylindrical panels using differential quadrature method (dqm). *Journal of Theoretical and Applied Mechanics*, **54**(1), 135–147.
- Al-Khaleefi, A. M.** (2004). Thermal buckling of clamped cylindrical panels based on first-order shear deformation theory. *International Journal of Structural Stability and Dynamics*, **4**(03), 313–336.
- Alibeigloo, A.** (2013). Static analysis of functionally graded carbon nanotube-reinforced composite plate embedded in piezoelectric layers by using theory of elasticity. *Composite Structures*, **95**, 612–622.
- Asadi, H., Y. Kiani, M. Aghdam,** and **M. Shakeri** (2016). Enhanced thermal buckling of laminated composite cylindrical shells with shape memory alloy. *Journal of Composite Materials*, **50**(2), 243–256.
- Au, F.** and **Y. Cheung** (1996). Free vibration and stability analysis of shells by the isoparametric spline finite strip method. *Thin-walled structures*, **24**(1), 53–82.
- AU Shi, D.-L., X.-Q. Feng, Y. Y. Huang, K.-C. Hwang,** and **H. Gao** (2004). The effect of nanotube waviness and agglomeration on the elastic property of carbon nanotube-reinforced composites. *Journal of Engineering Materials and Technology*, **126**(03), 250–257.
- Aubad, M. J.** (2014). Thermal buckling of laminate composite spheroidal spherical shell. *International Journal of Current Engineering and Technology*, **4**, 933–938.
- Bai, Q.** (2010). Analysis of particle swarm optimization algorithm. *Computers and Information Science*, **3**(1), 180–184.

- Balaji, A., B. Karthikeyan, and C. S. Raj** (2014). Bagasse fiber—the future biocomposite material: a review. *International Journal of Cemtech Research*, **7**(1), 223–233.
- Beni, Y. T., F. Mehralian, and H. Razavi** (2015). Free vibration analysis of size-dependent shear deformable functionally graded cylindrical shell on the basis of modified couple stress theory. *Composite Structures*, **120**, 65–78.
- Bhimaraddi, A. and K. Chandrashekhara** (1993). Nonlinear vibrations of heated antisymmetric angle-ply laminated plates. *International journal of solids and structures*, **30**(9), 1255–1268.
- Birman, V. and C. W. Bert** (1993). Buckling and post-buckling of composite plates and shells subjected to elevated temperature. *Journal of Applied Mechanics*, **60**(2), 514–519.
- Boroujerdy, M. S., R. Naj, and Y. Kiani** (2014). Buckling of heated temperature dependent fgm cylindrical shell surrounded by elastic medium. *Journal of theoretical and applied mechanics*, **52**(4), 869–881.
- Brischetto, S., F. Tornabene, N. Fantuzzi, and E. Viola** (2016). 3d exact and 2d generalized differential quadrature models for free vibration analysis of functionally graded plates and cylinders. *Meccanica*, **51**(9), 2059–2098.
- Buchanan, G. R. and B. S. Rich** (2002). Effect of boundary conditions on free vibration of thick isotropic spherical shells. *Modal Analysis*, **8**(3), 389–403.
- Chakravorty, D., J. Bandyopadhyay, and P. Sinha** (1995). Finite element free vibration analysis of point supported laminated composite cylindrical shells. *Journal of Sound and Vibration*, **181**(1), 43–52.
- Chen, L.-W. and L.-Y. Chen** (1987). Thermal buckling of laminated cylindrical plates. *Composite structures*, **8**(3), 189–205.
- Czapski, P. and T. Kubiak** (2015). Numerical and experimental investigations of the post-buckling behaviour of square cross-section composite tubes. *Composite Structures*, **132**, 1160–1167.
- Darvizeh, M., A. Darvizeh, A. Shaterzadeh, and R. Ansari** (2010). Thermal buckling of spherical shells with cut-out. *Journal of Thermal Stresses*, **33**(5), 441–458.



- Dasgupta, A.** and **K. Huang** (1997). "a layer-wise analysis for free vibrations of thick composite spherical panels". *Journal of Composite Materials*, **31**(7), 658–671.
- Dhanaraj, R.** *et al.* (1990). Free vibration of initially stressed composite laminates. *Journal of sound and vibration*, **142**(3), 365–378.
- Eberhart, R.** and **J. Kennedy**, A new optimizer using particle swarm theory. In *Micro Machine and Human Science, 1995. MHS'95., Proceedings of the Sixth International Symposium on.* IEEE, 1995.
- Einde, L. V. D., L. Zhao,** and **F. Seible** (2003). Use of frp composites in civil structural applications. *Construction and Building Materials*, **17**(6), 389 – 403. Fibre-reinforced polymer composites in construction.
- Eslami, M.** and **R. Javaheri** (1999). Buckling of composite cylindrical shells under mechanical and thermal loads. *Journal of thermal stresses*, **22**(6), 527–545.
- Fantuzzi, N., S. Brischetto, F. Tornabene,** and **E. Viola** (2016). 2d and 3d shell models for the free vibration investigation of functionally graded cylindrical and spherical panels. *Composite Structures*, **154**, 573–590.
- Fares, M., Y. Youssif,** and **M. Hafiz** (2005). Multiobjective design and control optimization for minimum thermal postbuckling dynamic response and maximum buckling temperature of composite laminates. *Structural and Multidisciplinary Optimization*, **30**(2), 89–100.
- Fidelus, J., E. Wiesel, F. Gojny, K. Schulte,** and **H. Wagner** (2005). Thermo-mechanical properties of randomly oriented carbon/epoxy nanocomposites. *Composites Part A: Applied Science and Manufacturing*, **36**(11), 1555 – 1561.
- Ganapathi, M., B. Patel,** and **D. Pawargi** (2002). Dynamic analysis of laminated cross-ply composite non-circular thick cylindrical shells using higher-order theory. *International journal of solids and structures*, **39**(24), 5945–5962.
- Ganesan, N.** and **V. Pradeep** (2005). Buckling and vibration of circular cylindrical shells containing hot liquid. *Journal of sound and vibration*, **287**(4), 845–863.
- George, N., P. Jeyaraj,** and **S. Murigendrappa** (2016). Buckling of non-uniformly heated isotropic beam: Experimental and theoretical investigations. *Thin-Walled Structures*, **108**, 245 – 255.

- Ghadiri, M.** and **H. Safarpour** (2017). Free vibration analysis of size-dependent functionally graded porous cylindrical microshells in thermal environment. *Journal of Thermal Stresses*, **40**(1), 55–71.
- Gharib, A.** and **M. Shakeri**, Stacking sequence optimization of laminated cylindrical shells for buckling and free vibration using genetic algorithm and neural networks. *In 2nd International Conference on Engineering Optimization*. 2010.
- Gotsis, P.** and **J. Guptill** (1994). Fiber composite thin shells subjected to thermal buckling loads. *Computers & structures*, **53**(6), 1263–1274.
- Hafezalkotob, A.** and **M. Eslami** (2010). "thermomechanical buckling of simply supported shallow fgm spherical shell with temperature dependent material". *Iranian journal of Mechanical engineering*, **11**(02), 39–65.
- Han, Q., Z. Wang, D. H. Nash,** and **P. Liu** (2017). Thermal buckling analysis of cylindrical shell with functionally graded material coating. *Composite Structures*, **181**(Supplement C), 171 – 182.
- Han, Y.** and **J. Elliott** (2007). Molecular dynamics simulations of the elastic properties of polymer/carbon nanotube composites. *Computational Materials Science*, **39**, 315–323.
- Hirano, T., T. Yamada, J. Teraki, M. Niini,** and **A. Kumakawa**, A study on a functionally gradient material design system for a thrust chamber. *In International Symposium on Space Technology and Science, 16 th, Sapporo, Japan*. 1988.
- Hosseini-Hashemi, S., S. R. Atashipour, M. Fadaee,** and **U. Girhammar** (2012). An exact closed-form procedure for free vibration analysis of laminated spherical shell panels based on sanders theory. *Archive of Applied Mechanics*, **82**(7), 985–1002.
- Jahanbakhsh, J., M. Eslami,** and **P. Ghaedi** (2012). Thermal buckling of imperfect deep functionally graded spherical shell. *Journal of Thermal Stresses*, **35**(10), 921–946.
- Jeng-Shian, C.** and **C. Wei-Chong** (1991). Thermal buckling analysis of antisymmetric laminated cylindrical shell panels. *International Journal of Solids and Structures*, **27**(10), 1295–1309.
- Jeyaraj, P.** (2013). Buckling and free vibration behavior of an isotropic plate under nonuniform thermal load. *International Journal of Structural Stability and Dynamics*, **13**(03), 1250071.

- Jin, G., X. Xie, and Z. Liu** (2014a). The haar wavelet method for free vibration analysis of functionally graded cylindrical shells based on the shear deformation theory. *Composite Structures*, **108**, 435–448.
- Jin, T., N. Ha, and N. Goo** (2014b). A study of the thermal buckling behavior of a circular aluminum plate using the digital image correlation technique and finite element analysis. *Thin-Walled Structures*, **77**, 187–197.
- Jin, T., N. San Ha, V. T. Le, N. S. Goo, and H. C. Jeon** (2015). Thermal buckling measurement of a laminated composite plate under a uniform temperature distribution using the digital image correlation method. *Composite Structures*, **123**, 420–429.
- Jones, R., J. Mazumdar, and Y. Cheung** (1980). Vibration and buckling of plates at elevated temperatures. *International Journal of Solids and Structures*, **16**(1), 61–70.
- Jooybar, N., P. Malekzadeh, A. Fiouz, and M. Vaghefi** (2016). Thermal effect on free vibration of functionally graded truncated conical shell panels. *Thin-Walled Structures*, **103**, 45–61.
- Kamarian, S., M. Shakeri, and M. Yas** (2016). Thermal buckling optimisation of composite plates using firefly algorithm. *Journal of Experimental & Theoretical Artificial Intelligence*, 1–8.
- Kandasamy, R., R. Dimitri, and F. Tornabene** (2016a). Numerical study on the free vibration and thermal buckling behavior of moderately thick functionally graded structures in thermal environments. *Composite Structures*, **157**(Supplement C), 207 – 221.
- Kandasamy, R., R. Dimitri, and F. Tornabene** (2016b). Numerical study on the free vibration and thermal buckling behavior of moderately thick functionally graded structures in thermal environments. *Composite Structures*, **157**, 207–221.
- Kar, V. R. and S. K. Panda**, Thermal buckling of temperature dependent functionally graded cylindrical panel. *In AIMTDR 2014*. 2014.
- Kar, V. R. and S. K. Panda** (2015). Free vibration responses of temperature dependent functionally graded curved panels under thermal environment. *Latin American Journal of Solids and Structures*, **12**, 2006 – 2024.

- Katariya, P. V. and S. K. Panda** (2016a). Thermal buckling and vibration analysis of laminated composite curved shell panel. *Aircraft Engineering and Aerospace Technology: An International Journal*, **88**(1), 97–107.
- Katariya, P. V. and S. K. Panda** (2016b). Thermal buckling and vibration analysis of laminated composite curved shell panel. *Aircraft Engineering and Aerospace Technology*, **88**(1), 97–107.
- Khdeir, A.** (2012). Thermoelastic response of cross-ply laminated shells based on a rigorous shell theory. *Journal of Thermal Stresses*, **35**(11), 1000–1017.
- Ko, W. I.** (2004). Thermal buckling analysis of rectangular panels subjected to humped temperature profile heating.
- Koronis, G., A. Silva, and M. Fontul** (2013). Green composites: A review of adequate materials for automotive applications. *Composites Part B: Engineering*, **44**(1), 120 – 127. ISSN 1359-8368.
- Kurpa, L., T. Shmatko, and G. Timchenko** (2010). Free vibration analysis of laminated shallow shells with complex shape using the r-functions method. *Composite Structures*, **93**(1), 225–233.
- Lam, K. and C. Loy** (1995). Analysis of rotating laminated cylindrical shells by different thin shell theories. *Journal of Sound and Vibration*, **186**(1), 23 – 35.
- Lam, K. and W. Qian** (2000). Free vibration of symmetric angle-ply thick laminated composite cylindrical shells. *Composites Part B: Engineering*, **31**(4), 345–354.
- Lee, D.-M. and I. Lee** (1997). Vibration behaviors of thermally postbuckled anisotropic plates using first-order shear deformable plate theory. *Computers & structures*, **63**(3), 371–378.
- Lee, J.** (2009). The application of the pseudospectral method to the analysis of helical springs of arbitrary shape. *Journal of Mechanical Science and Technology*, **23**(1), 81–88.
- Lei, Z., L. Zhang, K. Liew, and J. Yu** (2014). Dynamic stability analysis of carbon nanotube-reinforced functionally graded cylindrical panels using the element-free kp-ritz method. *Composite Structures*, **113**, 328–338.
- Loy, C. and K. Lam** (1999). Vibration of thick cylindrical shells on the basis of three-dimensional theory of elasticity. *Journal of sound and vibration*, **226**(4), 719–737.

- Ma, S.-F.** and **M. Wilcox** (1991). Thermal buckling of antisymmetric angle-ply laminated cylindrical shells. *Composites Engineering*, **1**(3), 183–192.
- Malekzadeh, P., A. R. Vosoughi, M. Sadeghpour, and H. R. Vosoughi** (2012*a*). Thermal buckling optimization of temperature-dependent laminated composite skew plates. *Journal of Aerospace Engineering*, **27**(1), 64–75.
- Malekzadeh, P., A. R. Vosoughi, M. Sadeghpour, and H. R. Vosoughi** (2012*b*). Thermal buckling optimization of temperature-dependent laminated composite skew plates. *Journal of Aerospace Engineering*, **27**(1), 64–75.
- Matsunaga, H.** (2007). Thermal buckling of cross-ply laminated composite shallow shells according to a global higher-order deformation theory. *Composite structures*, **81**(2), 210–221.
- Mead, D.** (2003). Vibration and buckling of flat free–free plates under non-uniform in-plane thermal stresses. *Journal of sound and vibration*, **260**(1), 141–165.
- Mehar, K. and S. Kumar Panda** (2017). Thermal free vibration behavior of fg-cnt reinforced sandwich curved panel using finite element method. *Polymer Composites*, n/a–n/a. ISSN 1548-0569.
- Mehar, K. and S. K. Panda** (2017). Elastic bending and stress analysis of carbon nanotube-reinforced composite plate: Experimental, numerical, and simulation. *Advances in Polymer Technology*, n/a–n/a. ISSN 1098-2329.
- Meistring, R., S. Beyer, S. Schmidt, F. Maidl, M. Bouchez, and P. Peres**, Advanced composite materials for current and future propulsion and industrial applications. In *Advanced Inorganic Fibrous Composites V*, volume 50 of *Advances in Science and Technology*. 2006.
- Mirzaei, M. and Y. Kiani** (2015). Thermal buckling of temperature dependent fg-cnt reinforced composite conical shells. *Aerospace Science and Technology*, **47**, 42–53.
- Mirzaei, M. and Y. Kiani** (2016*a*). Free vibration of functionally graded carbon nanotube reinforced composite cylindrical panels. *Composite Structures*, **142**, 45–56.
- Mirzaei, M. and Y. Kiani** (2016*b*). Thermal buckling of temperature dependent fg-cnt reinforced composite plates. *Meccanica*, **51**(9), 2185–2201.

- Mochida, Y., S. Ilanko, M. Duke, and Y. Narita** (2012). Free vibration analysis of doubly curved shallow shells using the superposition-galerkin method. *Journal of Sound and Vibration*, **331**(6), 1413–1425.
- Murphy, K. D. and D. Ferreira** (2001). Thermal buckling of rectangular plates. *International Journal of Solids and Structures*, **38**(22), 3979–3994.
- Narita, Y., Y. Ohta, and M. Saito** (1993). Finite element study for natural frequencies of cross-ply laminated cylindrical shells. *Composite structures*, **26**(1-2), 55–62.
- Nguyen-Van, H., N. Mai-Duy, and T. Tran-Cong** (2008). Free vibration analysis of laminated plate/shell structures based on fsdt with a stabilized nodal-integrated quadrilateral element. *Journal of Sound and Vibration*, **313**(1), 205–223.
- Niino, M., A. Suzuki, T. Hirai, R. Watanabe, T. Hirano, and N. Kuroishi** (1988). Method of producing a functionally gradient material.
- Panda, S. and B. Singh** (2009). Nonlinear free vibration of spherical shell panel using higher order shear deformation theory—a finite element approach. *International Journal of Pressure Vessels and Piping*, **86**(6), 373–383.
- Panda, S. and B. N. Singh** (2013). Thermal postbuckling behavior of laminated composite spherical shell panel using nfem#. *Mechanics Based Design of Structures and Machines*, **41**(4), 468–488.
- Panda, S. K. and T. R. Mahapatra** (2014). Nonlinear finite element analysis of laminated composite spherical shell vibration under uniform thermal loading. *Meccanica*, **49**(1), 191–213.
- Park, J.-S., J.-H. Kim, and S.-H. Moon** (2004). Vibration of thermally post-buckled composite plates embedded with shape memory alloy fibers. *Composite Structures*, **63**(2), 179–188.
- Patel, B., Y. Nath, and K. Shukla** (2007). Thermo-elastic buckling characteristics of angle-ply laminated elliptical cylindrical shells. *Composite structures*, **77**(1), 120–124.
- Patel, B., K. Shukla, and Y. Nath** (2004). Thermal buckling of laminated cross-ply oval cylindrical shells. *Composite structures*, **65**(2), 217–229.

- Ram, K. S.** and **T. S. Babu** (2002). Free vibration of composite spherical shell cap with and without a cutout. *Computers & structures*, **80**(23), 1749–1756.
- Ram, K. S.** and **P. Sinha** (1992). Hygrothermal effects on the free vibration of laminated composite plates. *Journal of Sound and Vibration*, **158**(1), 133–148.
- Ramakrishna, S., J. Mayer, E. Wintermantel,** and **K. W. Leong** (2001). Biomedical applications of polymer-composite materials: a review. *Composites Science and Technology*, **61**(9), 1189 – 1224. ISSN 0266-3538.
- Rao, S. N.** and **N. Ganesan** (1985). Vibration of plates immersed in hot fluids. *Computers & structures*, **21**(4), 777–787.
- Reddy, J.** and **C. Liu** (1985). A higher-order shear deformation theory of laminated elastic shells. *International Journal of Engineering Science*, **23**(3), 319 – 330.
- Rini, D. P., S. M. Shamsuddin,** and **S. S. Yuhaniz** (2011). Particle swarm optimization: technique, system and challenges. *International Journal of Computer Applications*, **14**(1), 19–26.
- Rogers, C. W.** (1968). Advanced-composite-material application to aircraft structures. *Journal of Aircraft*, **5**(3), 311–316.
- Roh, J.-H., J.-H. Woo,** and **I. Lee** (2008). Thermal post-buckling and vibration analysis of composite conical shell structures using layerwise theory. *Journal of Thermal Stresses*, **32**(1-2), 41–64.
- Sahoo, S. S., S. K. Panda,** and **T. R. Mahapatra** (2016). Static, free vibration and transient response of laminated composite curved shallow panel – an experimental approach. *European Journal of Mechanics - A/Solids*, **59**(Supplement C), 95 – 113. ISSN 0997-7538.
- Sahoo, S. S., S. K. Panda,** and **V. K. Singh** (2017). Experimental and numerical investigation of static and free vibration responses of woven glass/epoxy laminated composite plate. *Proceedings of the Institution of Mechanical Engineers, Part L: Journal of Materials: Design and Applications*, **231**(5), 463–478.
- Sahu, S.** and **P. Datta** (2002). Dynamic stability of curved panels with cutouts. *Journal of Sound and Vibration*, **251**(4), 683 – 696.
- Sasaki, M., Y. Wang, T. Hirano,** and **T. Hiral** (1989). Design of sic/c functionally gradient material and its preparation by chemical

vapor deposition. *Journal of the Ceramic Society of Japan*, **97**(1125), 539–543.

**Shahsiah, R.** and **M. Eslami** (2003). Thermal buckling of functionally graded cylindrical shell. *Journal of Thermal Stresses*, **26**(3), 277–294.

**Shariyat, M.** (2007). Thermal buckling analysis of rectangular composite plates with temperature-dependent properties based on a layer-wise theory. *Thin-Walled Structures*, **45**(4), 439–452.

**Shen, H.-S.** (2011). Postbuckling of nanotube-reinforced composite cylindrical shells in thermal environments, part i: Axially-loaded shells. *Composite Structures*, **93**(8), 2096 – 2108.

**Shen, H.-S.** (2012). Thermal buckling and postbuckling behavior of functionally graded carbon nanotube-reinforced composite cylindrical shells. *Composites Part B: Engineering*, **43**(3), 1030 – 1038.

**Shen, H.-S.** and **C.-L. Zhang** (2010). Thermal buckling and postbuckling behavior of functionally graded carbon nanotube-reinforced composite plates. *Materials & Design*, **31**(7), 3403–3411.

**Shi, Y.** and **R. C. Eberhart**, Parameter selection in particle swarm optimization. *In International Conference on Evolutionary Programming*. Springer, 1998.

**Shiau, L.-C.** and **S.-Y. Kuo** (2006). Free vibration of thermally buckled composite sandwich plates. *Journal of vibration and acoustics*, **128**(1), 1–7.

**Singh, A.** (1999). Free vibration analysis of deep doubly curved sandwich panels. *Computers Structures*, **73**(15), 385 – 394.

**Singha, M. K., L. Ramachandra,** and **J. Bandyopadhyay** (2000). Optimum design of laminated composite plates for maximum thermal buckling loads. *Journal of Composite Materials*, **34**(23), 1982–1997.

**Singha, M. K., L. Ramachandra,** and **J. Bandyopadhyay** (2006). Vibration behavior of thermally stressed composite skew plate. *Journal of sound and vibration*, **296**(4), 1093–1102.

**Sk, L.** and **P. Sinha** (2005). Improved finite element analysis of multilayered, doubly curved composite shells. *Journal of reinforced plastics and composites*, **24**(4), 385–404.



- Soldatos, K. P.** (1984). A comparison of some shell theories used for the dynamic analysis of cross-ply laminated circular cylindrical panels. *Journal of Sound and Vibration*, **97**(2), 305 – 319.
- Song, Z., L. Zhang, and K. Liew** (2016). Vibration analysis of cnt-reinforced functionally graded composite cylindrical shells in thermal environments. *International Journal of Mechanical Sciences*, **115**, 339–347.
- Spallino, R. and G. Thierauf** (2000). Thermal buckling optimization of composite laminates by evolution strategies. *Computers Structures*, **78**(5), 691 – 697.
- Sreehari, V. and D. Maiti** (2016). Buckling load enhancement of damaged composite plates under hygrothermal environment using unified particle swarm optimization. *Structural and Multidisciplinary Optimization*, 1–11.
- Sun, J., X. Xu, C. Lim, and W. Qiao** (2015). Accurate buckling analysis for shear deformable fgm cylindrical shells under axial compression and thermal loads. *Composite Structures*, **123**(Supplement C), 246 – 256.
- Tang, D. Z.**, The application of carbon fiber materials in sports equipment. In *Computer-Aided Design, Manufacturing, Modeling and Simulation III*, volume 443 of *Applied Mechanics and Materials*. Trans Tech Publications, 2014.
- Thangaratnam, K. R., Palaninathan, and J. Ramachandran** (1989). Thermal buckling of composite laminated plates. *Computers & Structures*, **32**(5), 1117–1124.
- Topal, U.** (2009). Multiobjective optimization of laminated composite cylindrical shells for maximum frequency and buckling load. *Materials & Design*, **30**(7), 2584–2594.
- Topal, U.** (2013). Application of a new extended layerwise approach to thermal buckling load optimization of laminated composite plates. *Steel and Composite Structures*, **14**(03), 283–293.
- Topal, U. and U. Uzman** (2007). Optimum design of laminated composite plates to maximize buckling load using mfd method. *Thin-Walled Structures*, **45**(7), 660–669.
- Topal, U. and U. Uzman** (2008). Thermal buckling load optimization of laminated composite plates. *Thin-Walled Structures*, **46**(6), 667–675.

- Topal, U.** and **U. Uzman** (2009). Frequency optimization of laminated folded composite plates. *Materials Design*, **30**(3), 494 – 501.
- Tornabene, F., S. Brischetto, N. Fantuzzi,** and **E. Viola** (2015). Numerical and exact models for free vibration analysis of cylindrical and spherical shell panels. *Composites Part B: Engineering*, **81**(Supplement C), 231 – 250.
- Vangipuram, P.** and **N. Ganesan** (2007). Buckling and vibration of rectangular composite viscoelastic sandwich plates under thermal loads. *Composite Structures*, **77**(4), 419–429.
- Vosoughi, A.** and **M. Nikoo** (2015). Maximum fundamental frequency and thermal buckling temperature of laminated composite plates by a new hybrid multi-objective optimization technique. *Thin-Walled Structures*, **95**, 408–415.
- Walker, M., T. Reiss, S. Adali,** and **V. E. Verijenko** (1997). Optimal design of symmetrically laminated plates for maximum buckling temperature. *Journal of thermal stresses*, **20**(1), 21–33.
- Wang, W., S. Guo, N. Chang, F. Zhao,** and **W. Yang** (2010). A modified ant colony algorithm for the stacking sequence optimisation of a rectangular laminate. *Structural and Multidisciplinary Optimization*, **41**(5), 711–720.
- Wu, L., Z. Jiang,** and **J. Liu** (2005). Thermoelastic stability of functionally graded cylindrical shells. *Composite Structures*, **70**(1), 60–68.
- Yang, J.** and **H.-S. Shen** (2003). Nonlinear bending analysis of shear deformable functionally graded plates subjected to thermo-mechanical loads under various boundary conditions. *Composites Part B: Engineering*, **34**(2), 103–115.
- Yas, M., A. Pourasghar, S. Kamarian,** and **M. Heshmati** (2013). Three-dimensional free vibration analysis of functionally graded nanocomposite cylindrical panels reinforced by carbon nanotube. *Materials & Design*, **49**, 583–590.
- Zhang, L., Z. Lei, K. Liew,** and **J. Yu** (2014a). Static and dynamic of carbon nanotube reinforced functionally graded cylindrical panels. *Composite Structures*, **111**, 205 – 212.
- Zhang, L., P. Zhu,** and **K. Liew** (2014b). Thermal buckling of functionally graded plates using a local kriging meshless method. *Composite Structures*, **108**, 472–492.

**Zhao, X.** and **K. M. Liew** (2010). A mesh-free method for analysis of the thermal and mechanical buckling of functionally graded cylindrical shell panels. *Computational Mechanics*, **45**(4), 297–310.

**Zhao, X.**, **T. Ng**, and **K. Liew** (2004). Free vibration of two-side simply-supported laminated cylindrical panels via the mesh-free kp-ritz method. *International Journal of Mechanical Sciences*, **46**(1), 123–142.

**Zhu, P.**, **Z. Lei**, and **K. Liew** (2012). Static and free vibration analyses of carbon nanotube-reinforced composite plates using finite element method with first order shear deformation plate theory. *Composite Structures*, **94**(4), 1450 – 1460.

# CURRICULUM VITAE

1. Name: **Vinod Suresh Bhagat**
2. Date of Birth: 03/06/1984
3. Permanent Address: Montipio police qtrs.,  
Room No. 13, Comba  
Margao, Goa  
Pincode-403601
4. Educational Qualification:
  - 2005 **Bachelor of Engineering**  
Institution: Padre Conceicao college of Engineering  
Goa, India  
Specialization: Mechanical Engineering
  - 2012 **Master of Engineering**  
Institution: Goa college of Engineering  
Goa, India  
Specialization: Industrial Engineering
  - 2017 **Doctor of Philosophy**  
Institution: National Institute of Technology Karnataka  
Mangalore, India  
Registration Date: 15/07/2014  
Thesis Submission Date: 10/04/2017  
Viva-Voce Date: 08/12/2017